ISSN 1173-5996

STABILITY OF PRECAST CONCRETE TILT PANELS IN FIRE

BY

Linus C S Lim

Supervised by
Associate Professor Andrew H Buchanan

Fire Engineering Research Report 00/8

March 2000

This report was presented as a project report
as part of the M.E. (Fire) degree at the University of Canterbury

School of Engineering
University of Canterbury
Private Bag 4800
Christchurch, New Zealand

Phone 643 364-2250
Fax 643 364-2758

ACKNOWLEDGEMENTS

I would like to thank the following people who have helped me with my project:

- Associate Professor Andrew Buchanan, who has provided invaluable advice and guidance throughout the course of this project.

- Dr. Jean-Marc Franssen of the University of Liege in Belgium and Nathalie Robert for their guidance in using SAFIR.

- Esli Forrest, for his technical advice on tilt-up construction.

- The staff of the Engineering Library for obtaining the reference materials.

- Melody Callahan who helped prepare the pictures in this report.

- And finally, to my parents and sisters for their unwavering support and guidance over the years.

ABSTRACT

This report investigates the behaviour of slender cantilever concrete panels and concrete panels in steel frames exposed to elevated temperatures. This report also provides recommendations for the design of slender tilt-up wall panels for fire resistance.

The current trend of tilt-up construction in industrial buildings utilises very tall and thin concrete wall panels that are reinforced with a single layer of reinforcing in the middle. These wall panels are cantilevered from the base and are not connected to a column or a portal frame. The panels are connected directly to the steel frame by a steel rafter or indirectly to the eaves tie.

The analysis of this project was conducted using SAFIR, a non-linear finite element programme developed in the University of Liege, Belgium. Reinforced concrete walls subjected to a fire on one side will undergo non-uniform thermal expansion, causing the walls to bow. Free-standing concrete cantilever walls with slenderness ratios (Height to thickness ratio) in excess of 50 experience very large deflections when exposed to a fire on one side. The analyses have shown that these large deflections will lead to outward collapse of the walls onto the neighbouring property.

Concrete cantilever walls connected to unbraced steel frames are dangerous as they cause the frame to sway and fall out onto the neighbouring property during a fire. Braced steel frames connected to the walls enhance the behaviour of the walls by preventing the large outward deflections of the panels. If bracing is available from the steel roof to prevent sway, the wall panels can be constructed up to 12 metres and slenderness ratios up to 96, without outward collapse or buckling failure of the wall panels. For the partially braced frames conducted in this study, the height of the wall panels should not exceed 9.0 metres and the slenderness ratios should not exceed 65.

It is concluded that the deflections of the free standing cantilever walls should be controlled. Slender cantilever walls should be connected to a braced steel frame with well designed connections to the rafter and the eaves tie.

Table of Contents

LIST OF FIGURES

LIST OF TABLES

GLOSSARY OF TERMS

Latin Symbols

Symbol	Description	Units
a_c	Thermal diffusivity	m^2/s
A_f	Floor area of firecell	m^2
A_g	Gross area of section	m^2
A_h	Area of horizontal openings in the roof	m^2
A_s	Area of steel	m^2
A_v	Area of vertical window and door openings	m^2
c_p	Specific heat	J/kg K
e_f	Fire load	MJ/m^2
E_c	Elastic modulus of concrete	*GPa*
E_s	Elastic modulus of steel	*GPa*
E_{eff}	Effective elastic modulus	*GPa*
f'_c	Specified compressive strength of concrete	*MPa*
f_y	Yield strength of steel	*Mpa*
H_{we}	Effective height of a wall	*m*
H_{wu}	Unsupported height of a wall	*m*
I	Moments of inertia	m^4
I_{eff}	Effective moments of inertia	m^4
jd	Internal lever arm	*mm*
k_c	Strength reduction coefficient	
L	Length of member	*m*
M_b	Moments at the base of the wall	*kNm*
M_p	Plastic moment	*kNm*
N^*	Applied axial load	*kN*
p	Steel ratio	
t_e	Equivalent time	minutes
t_w	Thickness of wall	*m*
ΔT	Temperature difference	°C
T_f	Fire temperature	°C
w_f	Ventilation factor	

Greek Symbols

Symbol	Description	Units
α	Coefficient of thermal expansion	$^{o}C^{-1}$
Δ_c	Deflection at the free end of a cantilever	m
Δ_m	Deflection at midspan of an element	m
ε_T	Total strain	
ϕ	Curvature	m^{-1}
λ	Slenderness ratio	
ν_c	Concrete Poisson's ratio	
ν_s	Steel Poisson's ratio	

1. INTRODUCTION

1.1. Tilt-up wall construction in New Zealand

Tilt-up precast concrete construction is a popular form of construction in New Zealand. Its fast erection method and on-site fabrication of the panels makes it preferred over other construction methods.

Traditional industrial buildings comprise a steel portal frame with precast concrete panels attached to the portal frames. The precast panels are pinned to the frame or cantilevered at the base of the wall. There is a recent trend for modern industrial buildings in New Zealand to have tall and slender tilt-up precast concrete wall panels which are cantilevered from the ground and directly support the roof steelwork. The concrete wall panels do not have any columns attached to them and the steel rafter or truss is typically attached to alternate wall panels. The wall panels are connected to each other with a steel eaves tie at the top.

These cantilever tilt panels have been constructed with very high slenderness ratios. The slenderness ratios H_{wu}/t_w (the unsupported height of the wall, H_{wu}, relative to the thickness of the wall, t_w), typically range from 50 to in excess of 80 (Bull, 1998). The stability of these tilt panels is a major concern from seismic (Brown, 1997) and fire resistance (Clifton, 1996) perspectives.

From a fire resistance perspective, these walls pose an important stability issue as the concrete panels will be exposed to very high temperatures on one side in the event of a fire in an industrial building. This would result in non-uniform thermal expansion of the wall, causing the wall to deflect away from the heat source. This phenomenon, known as thermal bowing, poses stability issues if the lateral deflections of the wall become large enough to cause the wall collapse onto firefighters or neighbouring property.

1.2. Impetus for the research

Tilt panel industrial buildings were built primarily to achieve maximum storage space at the lowest possible financial expense. While this is economically gratifying to the developers, the possibility of outward collapse of these slender wall panels under a fire situation has raised a pressing concern amongst the owners of adjacent property. Fire fighters are more concerned about their safety, should one of these panels fall outwards onto them, when attending a fire in one of these buildings.

This project is initiated to determine the performance of slender concrete walls under a fire situation and to investigate the limits of slenderness of these walls so that life safety is not threatened.

1.3. Objective of this research

- The primary objective of this research project is to investigate the behaviour of slender concrete cantilever walls subjected to elevated temperatures and to propose design recommendations.

- The scope of this research covers the behaviour of:

1. Free-standing cantilever walls; this represents the lower bound of the performance of concrete walls. These wall panels are not laterally restrained to a steel rafter or an eaves tie. Therefore, the wall panels are assumed to behave as free-stranding cantilever walls.

2. Propped cantilever walls; this represents the upper bound of the performance of concrete wall panels. A fire-protected steel rafter is assumed to be attached to the top of the wall panels and restrains the lateral deflection at the top of the wall during a fire.

3. Cantilever walls in a steel frame; this represents the behaviour of the walls between the lower and upper bounds. The wall panels in some cases will be attached to an unprotected steel rafter which will allow some lateral displacement in the event of a fire. The behaviour of the cantilever panels will be dependent on the behaviour of the steel rafter attached.

The structural analysis in this project is conducted with a non-linear finite element programme, SAFIR, developed by Jean-Marc Franssen from the University of Liege, Belgium.

1.4. Organisation of this report

This report consists of nine chapters. Chapter 2 provides a review of the literature from various design code provisions and a summary of the properties of materials at elevated temperatures. It also summarises the performance of buildings and concrete walls under elevated temperatures and available analysis methods to quantify their behaviour.

Chapter 3 describes the behaviour of concrete and steel under elevated temperatures in detail. Chapter 4 describes the behaviour of concrete cantilever walls and industrial buildings when subjected to elevated temperatures. Chapter 5 describes the method of analysis of the concrete walls and frames for this project. It also covers other available analysis methods in detail.

Chapter 6 discusses the analysis results of free standing cantilever walls subjected to elevated temperatures. Chapter 7 covers the results of propped cantilever walls; Chapter 8 describes the analysis and results of concrete cantilever walls in a steel frame subjected to two types of time-temperatures curves. Chapter 9 investigates the behaviour of steel frames with different wall slenderness ratios and levels of bracing.

Chapter 10 describes the conclusions and design recommendations available for design and for future research.

2. LITERATURE REVIEW

2.1. Introduction

This chapter provides an overview of the literature relevant to this project. This literature review covers extracts of various design codes, properties of concrete and steel at elevated temperatures, experimental studies and computer programmes.

2.2. Review of Design Codes

2.2.1. The New Zealand Building Code

The New Zealand Building Code has several important objectives with regard to fire safety. Its aim is to ensure that the occupants can escape a burning building safely and that the firefighters can conduct their fire-fighting operations safely. The building code also requires that the adjacent household units and other property be protected from horizontal fire spread by thermal radiation or structural collapse.

In the case of the industrial buildings, the concrete wall panels attached to the side of an industrial building must not deform in a manner which will threaten the stability of the building by falling outwards. If the wall panels collapse outwards, it will endanger the lives of firefighters and damage adjacent property. Apart from that, it could allow the fire to spread to adjacent buildings.

In the event of the inward collapse of the walls, they must remain connected to each other so that they act as an effective barrier against the spread of the fire to adjacent property. The inwards collapse of the walls can increase the fire separation to the adjacent property. The adjacent property can be protected by utilising one or a combination of the following:

i) building separation;
ii) providing adequate fire resistance for primary and secondary elements;
iii) restricting the use of combustible surface finishes; and
iv) installing sprinklers.

The required fire resistance of the elements in a building can be determined according to the New Zealand Building Code. The Building Code specifies the fire resistance ratings of any element by three criteria: stability, integrity and insulation. Not all these criteria apply to all types of elements.

- The stability criterion applies to primary elements: e.g.: columns, beams, floors and load bearing walls. It requires the elements to maintain its load bearing capacity during a fire.
- The integrity criterion applies to secondary elements such as fire separations and floors. These elements are required to prevent the penetration of flame or hot gases during a fire.
- The insulation criterion applies to both primary and secondary elements. This criterion requires elements to prevent the average temperature rise of 140°C or a local maximum of 180°C on the unexposed face.

Fire Resistance Ratings

The fire resistance rating of a primary or secondary element depends also on the risk exposed to the elements. Two ratings are used to classify the elements (Table 2-1).

Nature of risk	Term used	Symbol
Internal spread of fire	Firecell rating	F
Structural collapse close to a relevant boundary and fire spread through external walls	Structural fire endurance rating	S

Table 2-1: Classification of F and S ratings (Section 3.1.2 BIA Approved Documents, 1992)

In the case of concrete cantilever walls, the structural fire endurance rating, the *S rating*, for external walls must be determined as they pose a threat of fire spread to the adjacent property.

The S rating an be determined from the following formula:

$S = kt_e$ (Section 3.2.4 BIA Approved Documents, 1992)

Where t_e = Equivalent time of fire exposure in minutes (determined from Table C3/AS1 of the BIA Approved Documents, 1992) or from the equivalent fire formula from EC1 (1994).

k = 1.0 for unsprinklered firecells, or

= 0.5 for sprinklered firecells.

The New Zealand Building Code categorises different hazard categories to buildings with different fuel loads. Hazard categories 1, 2 and 3 (from Table 1 of the BIA Approved Documents, 1992) represent fuel load densities of a building with 400, 800 and 1200 MJ/m^2 floor area, respectively. Fire hazard category 4 applies to buildings that require specific fire engineering design. The equation above is applicable to hazard categories 1, 2 and 3.

	Fire Hazard Category 1 (FLED = 400 MJ/m^2)					Fire Hazard Category 2 (FLED = 800 MJ/m^2)					Fire Hazard Category 3 (FLED = 1200 MJ/m^2)				
	A_h/A_f					A_h/A_f					A_h/A_f				
A_v/A_f	0.00	0.05	0.10	0.15	0.20	00	0.05	0.10	0.15	0.20	0.00	0.05	0.10	0.15	0.20
0.05 or less	65	43	36	32	30	130	87	72	64	60	195	130	108	96	90
0.06	60	40	34	30	28	120	81	67	61	57	180	121	101	91	85
0.07	56	38	32	29	27	111	75	63	58	54	167	113	95	87	82
0.08	52	35	30	28	26	103	70	60	55	52	155	105	90	83	78
0.09	48	33	29	26	25	96	66	57	53	50	144	99	86	79	76
0.10	45	31	27	26	24	89	62	55	51	49	134	94	82	77	73
0.11	41	30	26	25	24	83	59	53	49	48	124	89	79	74	72
0.12	39	28	25	24	23	77	56	51	48	47	116	85	76	72	70
0.13	36	27	25	23	23	72	54	49	47	46	109	81	74	70	68
0.14	34	26	24	23	22	68	52	48	46	45	102	78	72	69	67
0.15	32	25	23	23	22	64	50	47	45	44	91	75	70	68	66
0.16	30	24	23	22	22	61	48	46	44	44	86	73	68	66	65
0.17	29	24	22	22	22	58	47	45	44	43	86	71	67	66	65
0.18	27	23	22	22	21	55	46	44	43	43	82	69	66	65	64
0.19	26	23	22	21	21	52	45	43	43	42	79	68	65	64	63
0.20	25	22	21	21	21	50	44	43	42	42	76	66	64	64	63
0.25 or greater	22	21	21	21	21	44	42	41	41	41	66	63	62	62	62

Table 2-2: Values of equivalent fire severity for the S ratings for fire hazard categories 1, 2 and 3 (from C3/AS1, BIA 1992)

The table above shows the equivalent fire severity for the S ratings. The table is for a firecell ceiling height of 3.0 meters and lined with cellulosic materials.

The expression required to determine the equivalent fire severity t_e (minutes) according to the Eurocode (EC1, 1994) is:

$t_e = e_f k_b w_f$

Where e_f = fire load (MJ/m^2 floor area)

k_b = conversion factor

w_f = ventilation factor.

$(\lambda\rho c)^{0.5}$ (J/m^{2}Ks$^{0.5}$)	Typical construction	k_b (min m$^{2.3}$/MJ)
<720	Insulating material	0.090
720 to 2500	Concrete or plasterboard	0.055
> 2500	Thin Steel	0.045

Where λ = thermal conductivity W/m.K

ρ = density kg/m^3

c = specific heat J/kg.K

Table 2-3: Conversion factors for ventilation, k_b.

If the properties of the lining material are not known, a value of k_b=0.067 can be used (Buchanan, 1994). This formula is based on cellulosic-type fuels.

The ventilation factor w_f is given as:

$$w_f = \left(\frac{6.0}{H}\right)^{0.3}\left[0.62 + \frac{90(0.4-\alpha_v)^4}{1+b_v\alpha_h}\right] \rangle 0.5$$

Where $\alpha_v = A_v/A_f$ $\quad 0.05 \leq \alpha_v \leq 0.25$

$\alpha_h = A_h/A_f$ $\quad \alpha_h \leq 0.20$

$b_v = 12.5(1+10\alpha_v-\alpha_v^2)$

A_f = Floor area of firecell (m^2)

A_v = Area of vertical window and door openings (m^2)

A_h = Area of horizontal openings in the roof (m^2)

H = height of the firecell (m)

2.2.2. Concrete Structures Standard NZS 3101: 1995

Fire resistance ratings for walls

The tilt-up cantilever walls in the industrial buildings are required to fulfil three criteria to satisfy the fire resistance requirements. These criteria are stability, integrity and insulation. The stability criterion is required in this case as the wall performs a load-bearing role.

i) Insulation

In order to satisfy the insulation criteria, the local maximum temperature on the unexposed side of the wall must not exceed 180°C and not have an average maximum temperature rise of 140°C. The minimum effective thickness of a wall for fire resistance ratings for insulation according to the *Concrete Structures Standard NZS 3101:1995* are shown in Table 2-4. The effective thickness for solid walls are taken as its actual thickness.

ii) Integrity

The standard specifies that the wall has a fire resistance rating for integrity if the requirements for both insulation and stability are met.

iii) Stability

In order to satisfy the stability criterion according to *NZS 3101: 1995*, the minimum thickness of load bearing walls have to comply with *section 6.7.4* of the standard which states the following criteria:

i) The effective thickness of the wall shall not be less than 100mm thick and not less than 1/30 the distance between supporting or enclosing members;

ii) The effective thickness of the walls have to satisfy the insulation criteria;

iii) If $N^* \leq 0.03f'_cA_g$, h_{we}/t_w shall not be greater than 50 (h_{we}/t_w is the Effective height/ wall thickness ratio);

iv) If $N^* > 0.03f'_cA_g$,

- h_{we}/t_w shall not be greater than 20; and
- The cover from the fire-exposed face to the vertical reinforcement or tendons shall not be less than specified in Table 2-5.

Fire resistance rating (minutes)	Effective thickness (mm) for different aggregate type		
	Type A aggregate	Type B Aggregate	Type C aggregate
30	50	45	40
60	75	70	55
90	95	90	70
120	110	105	80
180	140	135	105
240	165	160	120
Aggregate types: A – quartz, greywacke, basalt and all others not listed B – dacite, phonolite, andesite, rhyolite, limestone C- pumice & selected lightweight aggregates			

Table 2-4: Minimum effective slab and wall thickness for fire resistance ratings for insulation (Table 6.1 of NZS 3101: 1995).

Fire resistance rating	Concrete cover, c (mm)	
	To reinforcement	To tendons
30	20	30
60	20	30
90	35	30
120	40	30
180	45	35
240	50	50

Table 2-5: Minimum cover to vertical reinforcement and tendons for the stability of walls (Table 6.4 of NZS 3101: 1995)

2.2.3. Loadings Standard NZS 4203: 1992

The Loadings Standard gives guidance on the performance of structures subjected to elevated temperatures. Clause 2.4.3.4 of the standard states:

"*2.4.3.4.*
Strength and stability in fire emergency conditions and afterwards shall comply with (a) and (b) following:

(a) For that period of time during fire emergency conditions when the structure is subject to elevated temperatures and designated members are required to remain stable, the affected members shall be designed for the following combination of factored load:

(7) G & Q_u

(b) The stability of elements which could collapse onto adjacent household units or other properties shall be ensured:

Either by designing the element and supporting structure to resist the loads in combination (7) above, using a detailed stress analysis which considers elevated temperatures and appropriate structural deformations throughout the fire.

Or, as an approximation, by designing the element and an appropriately fire rated supporting structure so that after a fire the residual structure at ambient temperatures is able to resist the loads in combination (7) above, plus a uniformly distributed face load on the residual structure of 0.5 kPa."

During a fire, the cantilever walls must be proven capable of supporting their own weight, taking account of any thermal deformations and not collapse onto adjacent property. If detailed stress analysis is not available, then as an approximation, they must be able to resist load combinations (7) stated above and a uniformly distributed face load on the residual structure of 0.5kPa after the fire.

2.2.4. Building Code of Australia 1996

A clause has been added to the Building Code of Australia because fires have occurred in single storey warehouses and the external wall panels have become detached during the fire and fallen outwards. This detaching of the panels is due to poor design and detailing of the connections between the supporting structure and the panels. This clause describes the measures to be taken to reduce the likelihood of external wall panels detaching from the supporting elements and collapsing onto the adjacent property.

Clause C1.11 of the *Building Code of Australia* states:

"*C1.11 Performance of external walls in fire*

1. Scope

This Specification contains measures to minimise, in the event of fire, the likelihood of external walls covered by Clause 2 collapsing outwards as complete panels and the likelihood of panels separating from supporting members.

2. Application

This Specification applies to buildings having a rise in storeys of not more than 2 with concrete external walls that could collapse as complete panels (eg. Tilt-up and precast concrete) which-

- *(a) consists of either single or multiple panels attached by steel connections to lateral supporting members; and*
- *(b) depend on those connections to resist outward movement of the panels relative to the supporting members and*
- *(c) have height to thickness ratio not greater than 50.*

3. General requirements for external wall panels

- *(a) Cast-in inserts and fixings must be anchored into the panel with welded bars or be fixed to the panel reinforcement.*
- *(b) Cast-in inserts for top connections and fixings acting together must be able to resist an ultimate load of two times the larger of the forces required to develop:*
  - *(i) the ultimate bending moment capacity of the panels at its base; or*

(ii) the overturning moment at the base of the panel arising from an outwards lateral displacement at the top of the panel equal to one tenth of the panel height.

(c) Top connections of the panel exposed to fire, such as clips and drilled-in insets, acting together must be able to resist an ultimate load of six times the larger of the forces required to develop the moment specified in (b)(i) or (ii).

(d) Lateral supporting members and their connections must be designed to resist the connection forces specified in (b) and (c) and in the case of an eaves tie member the force in the member must be determined assuming that it deforms in a manner compatible with the lateral displacement of the wall panels, and that it acts in tension only.

(e) External wall panels that span vertically must have at least two upper connections per panel to the supporting member, except that where a number of panels are designed to act as one unit, (eg. Tongue and groove hollow-core panels), only two upper connections are required for each unit.

(f) External wall panels that span horizontally between columns must have at least two connections at each column."

2.2.5. Eurocode

The Eurocode (EC2, 1995) provides details on the thermal and mechanical properties of concrete and reinforcing steel when they are subjected to elevated temperatures. EC3 (1995) describes the behaviour of structural steel when it is subjected to elevated temperatures. The details of the material properties of steel and concrete from the Eurocode are explained in detail in Section 3 and will be used in the analyses of this project.

2.3. Properties of materials at elevated temperatures

This section summarises the various sources of research on the behaviour of concrete and steel under elevated temperatures. The details of the investigations on the behaviour of concrete and steel are described in section 3.

2.3.1. Concrete

Thermal properties

Harmathy (1970), Harmathy and Allen (1973) and Schneider (1985) performed most of the investigations of the thermal properties of concrete at elevated temperatures. Other investigators have found similar trends of the thermal properties with some slight discrepancies, due to the variations in the materials used and the experimental methods. Bažant and Kaplan (1996) have provided a summary of the thermal and mechanical properties of concrete under elevated temperatures from various investigators.

Thermal deformation

Browne (1972) has investigated the effect of silica on the thermal expansion of the aggregates. Schneider (1985) and Harmathy (1993) have investigated the thermal expansion of concretes with different types of aggregates. Anderberg and Thelandersson (1976) have shown that the total thermal strain exhibited by heated concrete consists of four components, which are thermal strain, stress related strain, creep strain and transient strain. The phenomenon of transient strain has been investigated in detail by Khoury, Grainger and Sullivan (1985a, 1985b and 1986).

Spalling

Malhotra (1984) has described the phenomenon of spalling of concrete under transient heating condition. He has described the effects of spalling of concrete, the influencing factors and methods to prevent spalling.

Stress-strain relationship

Anderberg and Thelandersson (1976) and Schneider (1985) have investigated the stress-strain relations of concrete when it is heated.

Elasticity

Schneider (1985) has investigated the thermal effects of elasticity in great detail. Bažant and Kaplan (1996) have summarised the thermal effects on the modulus of elasticity of concrete from various researchers.

Strength

The degradation of the strength of concrete at high temperatures is important as it is relied on to resist compressive stresses. Schneider (1985) has investigated the effect of temperatures on the behaviour of concrete under different stress levels and for different aggregates.

2.3.2. Steel

The thermal properties of steel at elevated temperatures are given by Harmathy (1993). The total strain in steel (Anderberg and Thelandersson, 1976) constitutes of the thermal strain, stress related strain and creep strain. The transient strain is absent in steel.

Harmathy and Stanzak (1970) have investigated the stress-strain relations of structural and prestressing steel under high temperatures. Kirby and Preston (1988) have shown that the creep strain of steel is very sensitive to high temperatures. At high temperatures, the creep strain of steel increases very markedly. The reduction of the elastic modulus and strength of steel is given by Harmathy (1993).

2.4. Behaviour of concrete walls and industrial buildings subjected to elevated temperatures

2.4.1. Concrete walls

Cooke (1987) and Cooke and Morgan (1988) have investigated the behaviour of concrete cantilever walls subjected to elevated temperatures. The phenomenon of thermal bowing of concrete walls is significant particularly for tall fire separating walls subjected to fires on one side. Details of the investigations are discussed in section 4.4.

2.4.2. Industrial buildings

O'Meagher, Bennetts, Dayawansa, Thomas, BHPR-ML (1992), O'Meagher (1994) and O'Meagher and Bennetts (1997) have investigated the behaviour of industrial buildings when a fire occurs. They have also provided design recommendations to prevent undesirable collapse of the structure onto the neighbouring property. Details of their investigations are discussed in section 4.5.

2.5. Analysis methods

This section summarises the available methods of analysing the behaviour of concrete walls and steel frames. The details of these methods are described in Section 5.

2.5.1. Computer programmes

Thermal analysis

Munukutla (1989) has developed a computer programme, HEAT, to calculate the thermal distribution through concrete walls during an ISO standard fire test. Wickström (1979) has developed a finite element thermal analysis programme, TASEF-2, capable of determining the thermal distribution in the concrete walls.

Structural analysis

O'Meagher and Bennetts (1991) have developed a programme (FIREWALLS) to analyse the structural behaviour of concrete walls with pin supports at both ends, exposed to a fire on one

side. FIREWALLS takes into account the variation of material properties with temperature. This programme was modified by Munukutla (1989) to investigate concrete walls with different end supports to suit the construction practices in New Zealand. Both O'Meagher and Bennetts (1991) and Munukutla (1989) performed the analyses only for walls with low slenderness ratios. O'Meagher (1994) has analysed the behaviour of concrete walls and industrial buildings using FIREWALLS.

Cooke, Virdi and Jeyarupalingam (1997) have developed a computer programme to numerically simulate the structural response of brick walls with different thicknesses subjected to a fire on one side. The programme assumes that the material properties are independent of temperature, resulting in inconsistent results.

2.5.2. Simple formulas for hand calculations

The temperatures in a concrete section can be determined from a simple hand method developed by Wickström (1986). Cooke (1987) has derived some simple formulas to predict the horizontal deflection of structural elements due to thermal bowing. This formula has been validated for steel elements with both linear and curvilinear thermal distributions. Cooke *et al* (1997) has also derived a simple formula to predict the deflections of a wall, based on test results of a wall of a different height. Details of these hand methods are described in section 5.4.

2.6. Experimental Studies

The only experiment conducted to investigate thermal bowing of walls was reported by Cooke and Morgan (1988). The brick walls were subjected to a fire on one side and the horizontal deflections at the top of the walls were measured. The results showed that the deflections were significant.

Cooke and Morgan (1988) has also reported tests to determine the amount of thermal bowing of simply supported reinforced concrete slabs. Woodside, de Ruiter and Wade (1991) have conducted fire resistance tests of one meter square concrete slabs with different types of aggregates available in New Zealand. Inwood (1999) repeated those tests with lightweight aggregate concrete.

3. PROPERTIES OF MATERIALS AT HIGH TEMPERATURES

3.1. Introduction

The materials that are used in the construction of tilt-up walls are concrete and steel. This chapter describes the thermal and mechanical properties of concrete and steel when they are subjected to elevated temperatures. More detailed attention will be given to describe the properties of concrete with siliceous aggregates as they are commonly used in construction. The sources of this review are from various researchers and from the Eurocode (EC2 and EC3, 1995).

3.2. Thermal properties of concrete

3.2.1. Thermal conductivity

Thermal conductivity is the ability of a material to conduct heat and is defined as the ratio of heat flux to the temperature gradient. It represents the uniform flow of heat through concrete of unit thickness over a unit area subjected to a unit temperature difference between the two opposite faces (Bažant and Kaplan, 1996).

Cement Paste

The thermal conductivity of oven-dried hardened cement paste does not show much variation when subjected to temperatures up to 1000°C. Harmathy (1970) performed these tests with different cement pastes of different water-cement ratios, shown in Figure 3.1. Pastes 1, 2 and 3 represent water-cement ratios of 0.25, 0.33, and 0.5 respectively.

Aggregates

Harmathy (1970) has shown that highly crystalline rocks have relatively high thermal conductivities at room temperature. As the temperatures increase, their thermal conductivities gradually decrease. Lightweight aggregates, which have amorphous structures and high porosities, have low thermal conductivities. Harmathy (1970) has plotted the effects of increasing temperature on the thermal conductivities on quartzitic sandstone, anorthosite, two dense shales and two lightweight expanded shale aggregates (refer to Figure 3.2).

The quartzitic sandstone, which has high silica contents, has the highest thermal conductivity at room temperature of about 6.7 $Wm^{-1}°C^{-1}$, which decreases to 2.5 $Wm^{-1}°C^{-1}$ at 1000°C. The lightweight expanded shale aggregates, however, has a thermal conductivity of 0.4 $Wm^{-1}°C^{-1}$ at room temperature and remained approximately constant up to 1000°C.

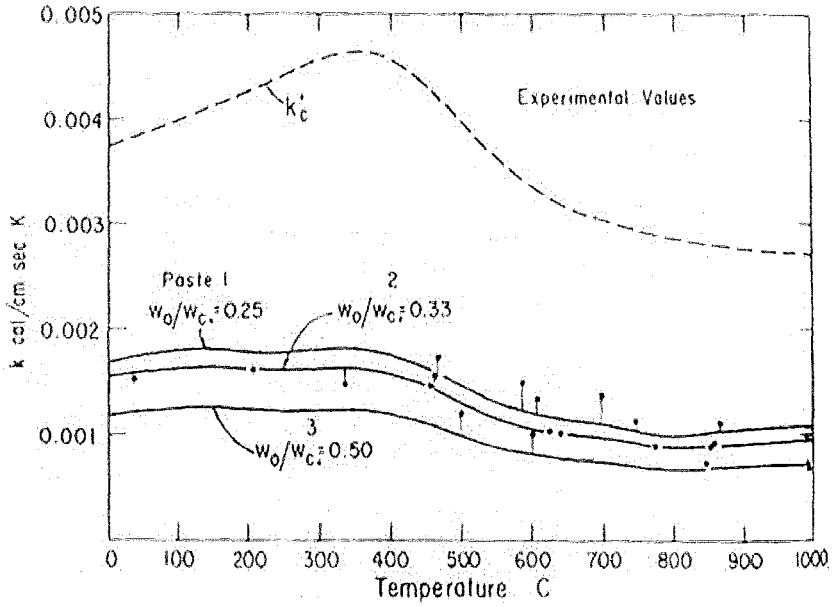

Figure 3.1: Thermal conductivity of cement paste (Harmathy, 1970).

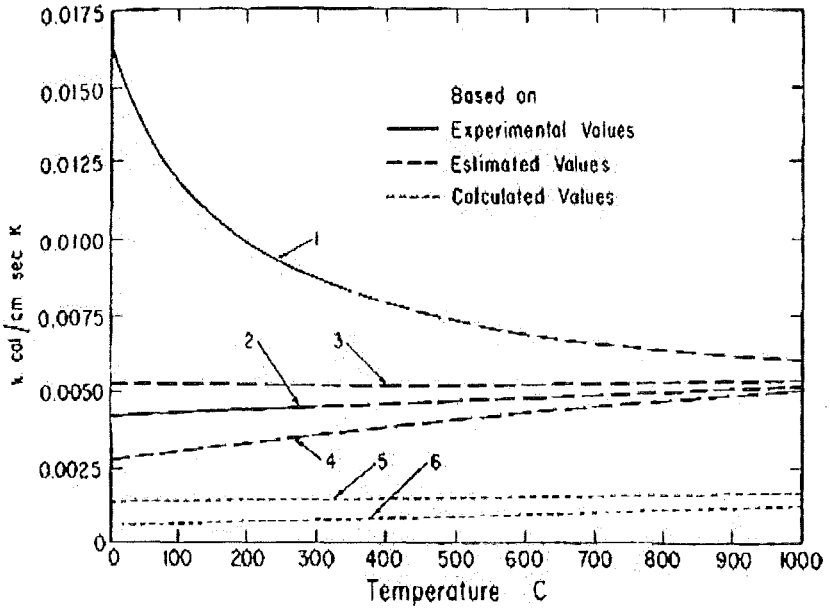

Figure 3.2: Thermal conductivity of different aggregates: 1 quartz, 2 anorthosite, 3 & 4 Dense shale, 5 & 6 expanded shale (Harmathy, 1970).

Concrete

Harmathy (1970) has calculated the thermal conductivities of four concretes in oven-dry conditions. They are referred to as Concretes 1, 2, 3 and 4 which were assumed to contain quartz, anorthosite and two lightweight shales respectively. The results of the variation of the calculations are shown in Figure 3.3. The thermal conductivity of normal weight concrete with siliceous and calcareous aggregates has been shown to lie between the theoretical lines of Concrete 1 and 2 in the above figure (Harmathy and Allen 1973). For lightweight concrete, the results lie in between the lines of Concrete 3 and 4.

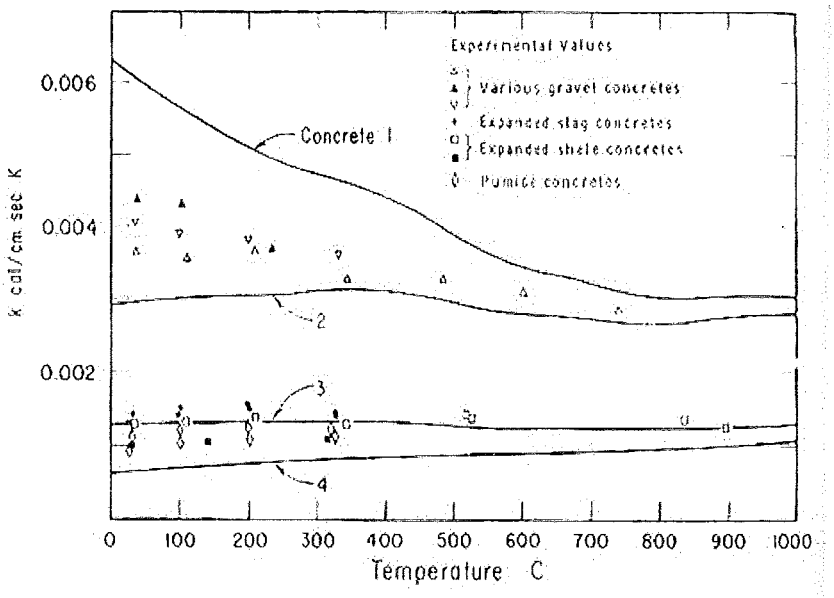

Figure 3.3: Thermal conductivities of various concretes (Harmathy, 1970).

The thermal conductivity of concrete with siliceous aggregates is shown in Figure 3.4 and may be taken as:

For $20°C < T \leq 1200°C$

$$\lambda = 2 - 0.24\ T/120 + 0.012\ (T/120)^2\ (W/mK)$$

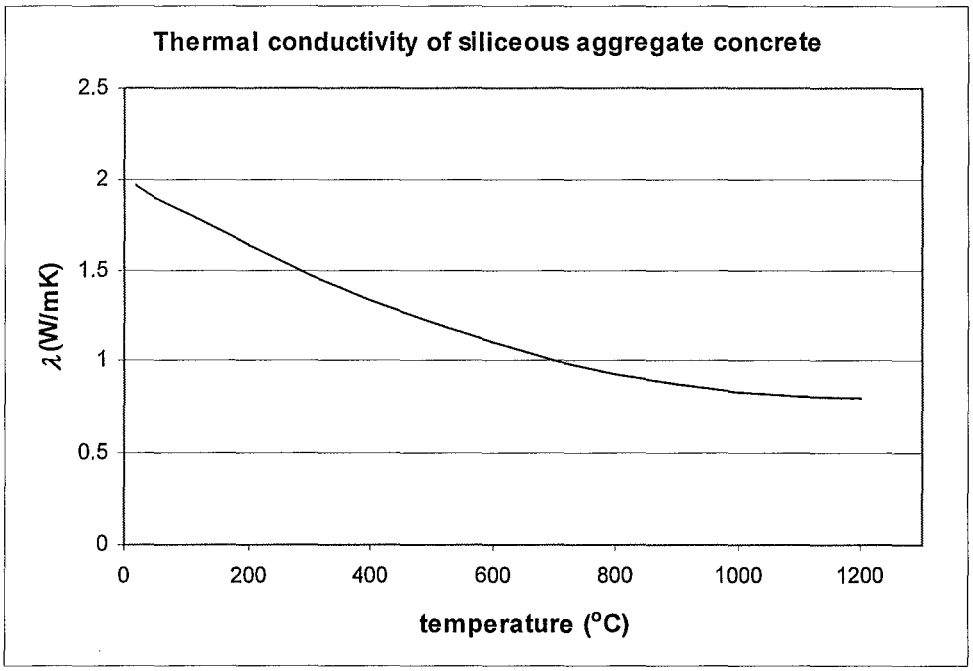

Figure 3.4: Thermal conductivity of siliceous aggregate concrete according to EC2 (1995).

3.2.2. Thermal diffusivity

Thermal diffusivity represents the rate of temperature change in a material. It is used to calculate temperature distributions under transient conditions. Thermal diffusivity is expressed as $k/(\rho c_p)$, where k is the thermal conductivity, ρ is the material density and c_p is the specific heat of the material.

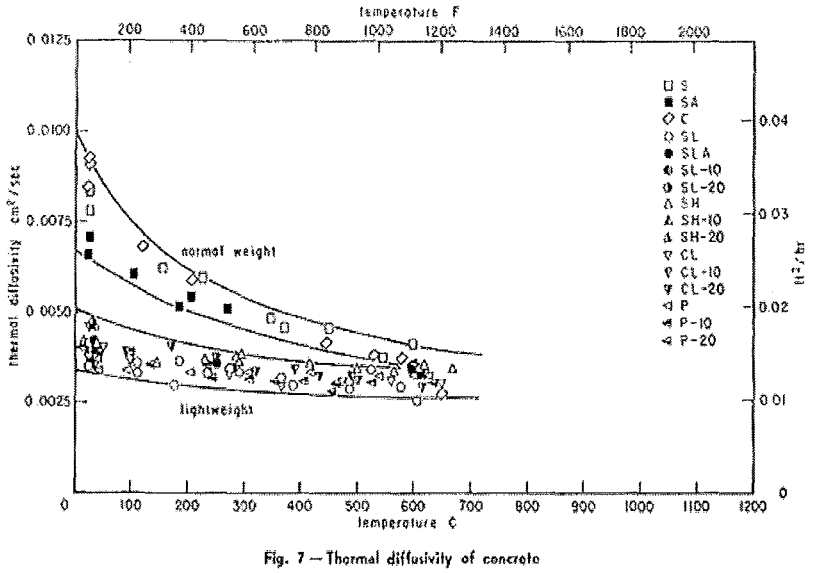

Fig. 7 — Thermal diffusivity of concrete

Figure 3-5: Thermal diffusivity of concrete (Harmathy and Allen, 1973).

The thermal diffusivity of normal and lightweight concrete is shown in Figure 3-5. The graph shows that the thermal diffusivity of the normal-weight concrete by approximately 50 percent when the temperatures were increased from normal to 650°C. The reduction is approximately 25 percent for lightweight concrete.

The thermal diffusivity of concrete a_c (m^2/s) according to EC2 is considered to be independent of the concrete temperature and is taken as

$a_c = 0.69 \times 10^{-6}\ m^2/s$ (for concrete with siliceous aggregates).

3.2.3. Specific heat

The specific heat of a material is the amount of heat per unit mass which is required to change the temperature of the material by one degree. It is defined as (Harmathy and Allen, 1973):

$$c_p = \frac{\partial H}{\partial T}_p$$

where H= enthalpy, T= temperature and P=pressure. If the heating of the solid is accompanied by chemical reactions, the enthalpy is a function of the degree of conversion from the reactants into the products, $\xi(0 \leq \xi \leq 1)$, and temperature. Therefore, the specific heat is then defined as

$$c_p = \frac{\partial H}{\partial T}_{P,\xi} + \frac{\partial H}{\partial \xi}_{P,T} \frac{\partial \xi}{\partial T}$$

The apparent specific heat c_p, as a function of temperature for an idealised Portland cement paste with a water-cement ratio 0.50 (Figure 3.6).

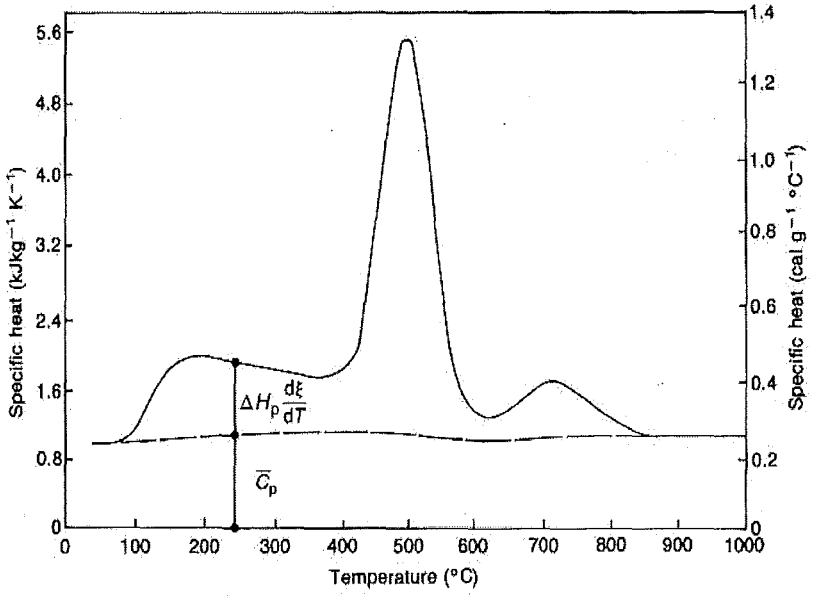

Figure 3.6: Apparent specific heat of idealised Portland cement paste of water-cement ratio 0.5 as a function of temperature (Harmathy and Allen, 1970).

The figure indicates that at temperatures between 100°C and 850°C, the latent heat contribution to the specific heat is very significant and the effective value of the specific heat may be several times higher than the "sensible heat capacity". This is due to the absorption of

heat in the dehydration reactions. The highest peak shown in the curve at approximately 500°C, is due to the dehydration of calcium hydroxide.

The specific heat of concrete is not very sensitive to either the aggregate type or the mix proportions but is very dependent on the moisture content. The effects of temperature on experimentally determined specific heats of various concretes are shown in Figure 3.7. The specific heat c_p of concrete with siliceous aggregates as a function of temperature according to EC2 (Figure 3.8) follows the equation below:

For $20°C < T \leq 1200°C$

$$c_p = 900 + 80\ T/120 - 4(T/120)^2\ (J/kgK)$$

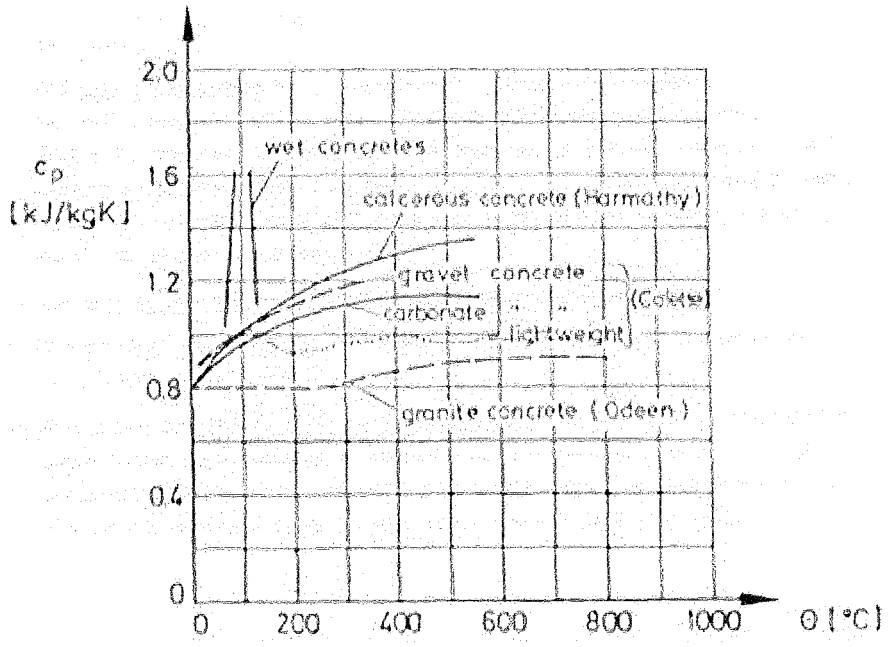

Figure 3.7: Effect of temperature on specific heats of different concretes. (Schneider, 1985)

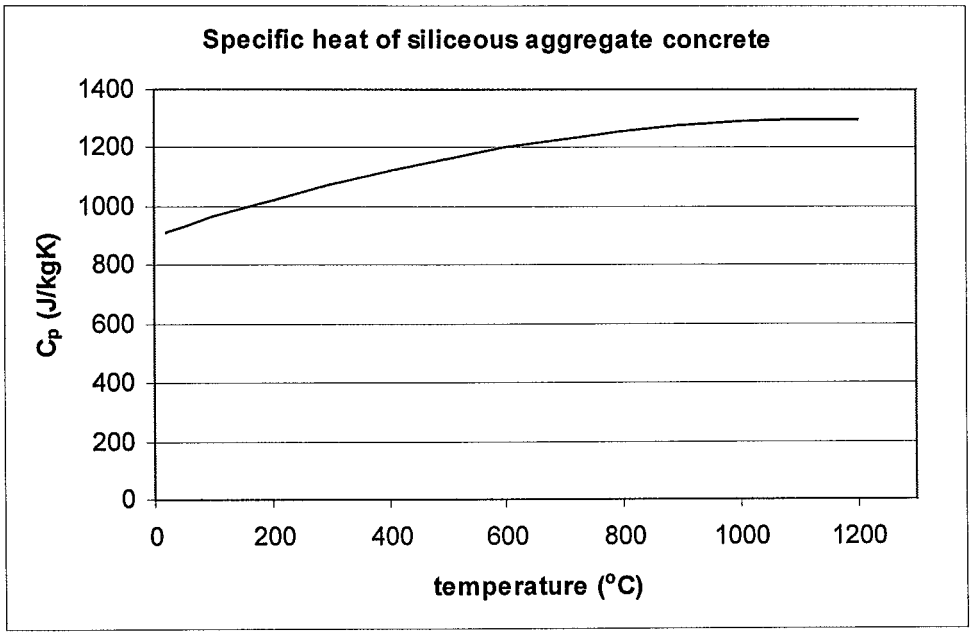

Figure 3.8: Specific heat of siliceous aggregate concrete according to EC2 (1995).

3.2.4. Thermal expansion of concrete

Concrete is an isotropic material and exhibits thermal expansion when it is subjected to a temperature change. Since it is an isotropic material, the thermal strain is the same in all directions. Stresses develop on concrete structures to the non-uniform thermal expansion, which in turn leads to cracking and large scale spalling (Bažant and Kaplan, 1996).

i) Thermal expansion of aggregates

The thermal expansion of aggregates has a very important effect on the changes in the volume of concrete as they normally occupy between 65 percent and 80 percent of the total volume (Bažant and Kaplan, 1996). The main factor affecting the coefficient of thermal expansion of the aggregates is the percentage of silica present in them. Rocks with high contents of silica, such as quartzite and sandstone, have high coefficients of thermal expansion, ranging from 9×10^{-6} and 10×10^{-6} $°C^{-1}$ (Browne, 1972).

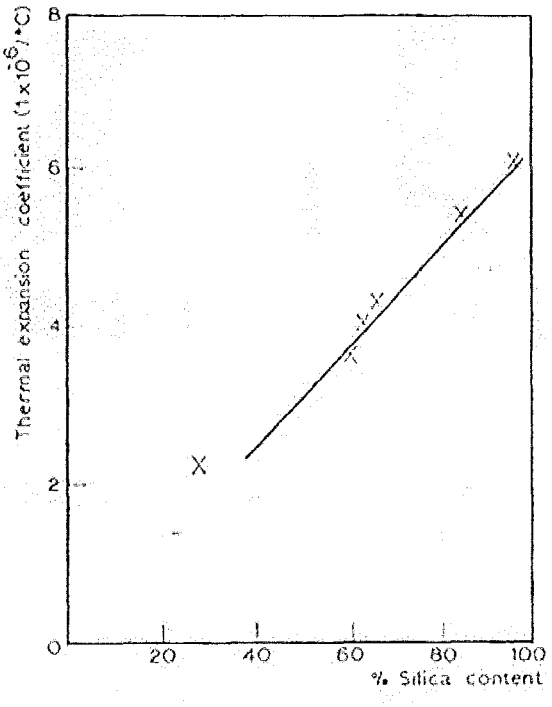

Figure 3.9: Effect of silica content on aggregate thermal expansion (Browne, 1972).

Rock Group	General silica content (% by wt)	Thermal Expansion Coefficient $1 \times 10\text{-}6°C\text{-}1$			
		Rock		Concrete	
		Range	Average	Range	Average
Chert	94	7.4-13.0	11.8	11.4-12.2	13.2
Quartzite	94	7.0-13.2	10.3	11.7-14.6	12.1
Sandstone	84	4.3-12.1	9.3	9.2-13.3	11.4
Marble	Negligible	2.2-16.0	8.3	4.1-17.4	10.7
Siliceous limestone	45	3.6-9.7	8.3	8.1-11.0	10.7
Granite	66	1.8-11.9	6.8	8.1-10.3	9.6
Dolerite	50	4.5-8.5	6.8	-	9.6
Basalt	51	4.0-9.7	6.4	7.9-10.4	9.3
Limestone	Negligible	1.8-11.7	5.5	4.3-10.3	8.6
Lightweight Aggregate	-	-	-	5.0-11	8.0

Table 3-1: Coefficients of thermal expansion of different rocks and concretes at normal temperatures (Browne, 1972)

The mineral composition of the rocks also plays an important part in their thermal expansion. The thermal expansion of siliceous aggregates for example, is considered to be affected by the conversion of the α-quartz to the β-quartz that occurs at 573°C and is followed by a significant volume expansion which flattens out at 600°C (Harmathy and Allen, 1973).

ii) Thermal expansion of hardened cement paste

The results of the thermal expansion of hardened cement paste from several investigators are shown in Figure 3.10. At temperatures up to about 300°C, thermal shrinkage competes with thermal expansion to give a net expansion. At temperatures greater than 300°C, the thermal shrinkage exceeds the expansion and gives a net shrinkage. This competition of expansion and contraction affects the microstructure of the paste and its physical and mechanical properties (Bažant and Kaplan, 1996). The shrinkage at elevated temperatures has been attributed to the loss of moisture from the cement paste. When the cement paste is heated, the free pore water is driven out and if the temperatures are severe enough, the solid paste matrix will be dehydrated (Cruz and Gillen, 1980).

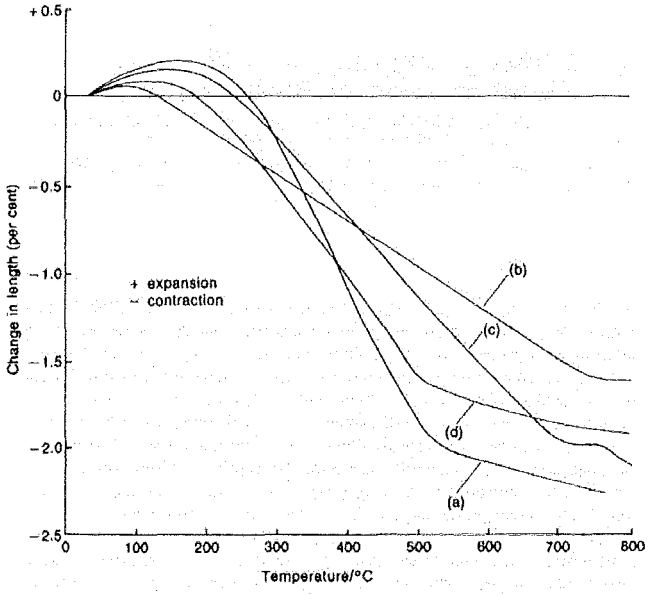

Figure 3.10: Length change of Portland cement paste specimens at various temperatures (a) Philleo (1958); (b) Harada *et al.* (1972); (c) Cruz and Gillen (1980); (d) Crowley (1956). (Bažant and Kaplan, 1996)

iii) Thermal expansion of concrete

There is almost a linear relationship between the thermal expansion of the aggregates and the concretes made from them (Cruz et al 1980; Bažant and Kaplan, 1996). This is shown in Table 3-1 and in Figure 3.11.

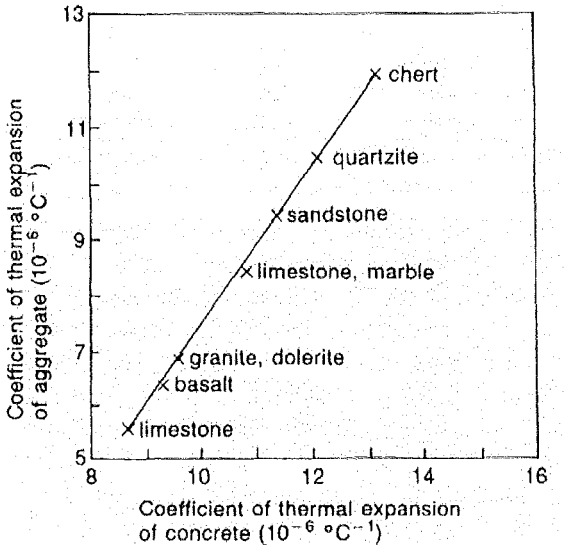

Figure 3.11: Correlation between the coefficient of thermal expansion of aggregate and of concrete. (Bažant and Kaplan, 1996)

Figure 3.12 shows the thermal expansion for different types of concrete (Harmathy, 1993). Their data labels as shown in the diagram below are summarised in Table 3-2. Generally, expansion increases with temperature at temperatures greater than about 150°C to 300°C. Concretes made with siliceous aggregates show the highest expansion coefficients.

Data label	Aggregate
LI	Limestone
SI	Siliceous rock
AD	Andesite
SG	Expanded slag
CL	Expanded clay
PU	Pumice

Table 3-2

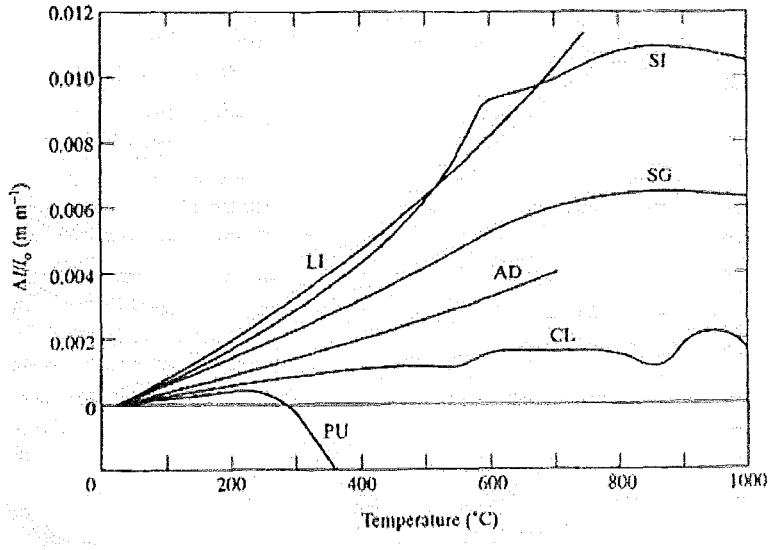

Figure 3.12 : Dilatometric curves for three normal weight concretes and three lightweight concretes (Harmathy, 1993).

Khoury, Grainger and Sullivan (1985a, 1985b and 1986) have showed that there is considerable contraction for concrete under load compared with the free thermal strains (FTS). These contractions are referred to as "load-induced thermal strain" (LITS). The total thermal strain under load, expressed as a function of temperature (T) and stress (s) is the difference between the FTS and the LITS.

$$\text{i.e.: Total thermal strain} = FTS(T,0) - LITS(T,s)$$

The FTS of concrete is a non-linear function of temperature dominated by the aggregate type and content. The main contributor to LITS was is the interaction with transient phenomena in drying creep. The equation above is valid only at low temperatures. At higher temperatures, there is a rapid increase in the rate of thermal expansion. This is due to the transformation of the aggregates and the failure of the bond between aggregate and cement paste (Blundell, Diamond and Browne, 1976).

Schneider (1985) has discussed the dimensional and volumetric changes in concrete. Calcareous aggregate concrete expands progressively up to about 900°C. At higher temperatures, the decarbonation of limestone increases and causes a decrease in the rate of expansion of the concrete.

Concrete made of siliceous aggregates expand progressively up to about 700°C. There is a marked rate of expansion at about 570°C due to the conversion of α-quartz to β-quartz. This will cause micro-cracking with failure of the bond between the cement and the aggregate. At temperatures greater than 700°C, the concrete starts to contract. This contraction is due to the contraction of hardened cement paste and the dehydration and decomposition of the calcium silicate hydrates in the cement paste.

The coefficient of thermal elongation of concrete with siliceous aggregates according to EC2 is expressed as:

For $20°C < T \leq 700°C$

$$\Delta l/l_c = (-1.8 \times 10^{-4}) + (9 \times 10^{-6} T) + (2.3 \times 10^{-11} T^3)$$

For $700°C < T \leq 1200°C$

$$\Delta l/l_c = (-14 \times 10^{-3})$$

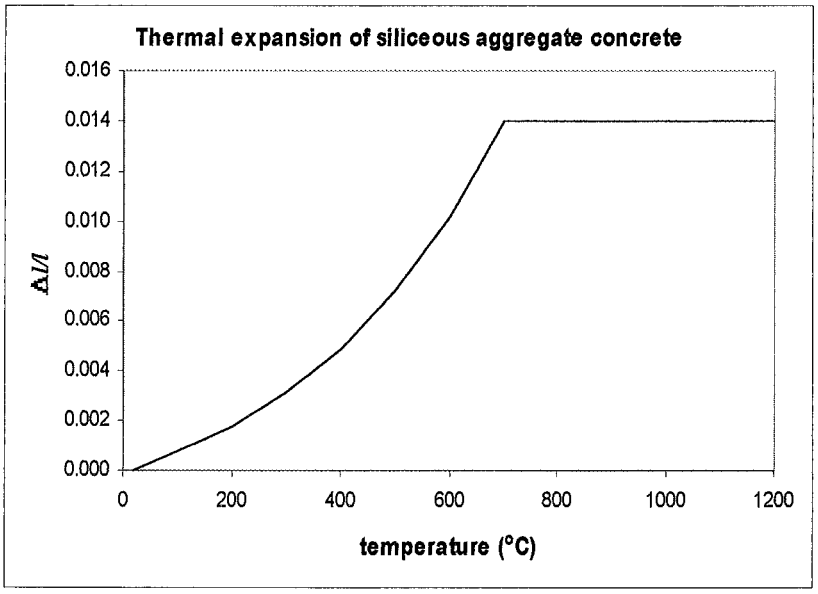

Figure 3.13: Thermal elongation of siliceous aggregate concrete according to EC2 (1995).

3.2.5. Spalling

Spalling is the separation of concrete from the surface in concrete structures when they are exposed to high temperatures. This phenomenon can seriously affect the fire resistance and stability of the structure and has been categorised into three categories (Institution of Structural Engineers, 1975):

i) General or destructive spalling: This form of spalling is violent which usually occurs during the early stages of heating. It can result in extensive damage or complete destruction of the concrete element.

ii) Local spalling: This consists of surface pitting, aggregate splitting or corner break-off.

iii) Sloughing off: This is a progressive form of breakdown of the concrete elements after prolonged heating. Surface layers of concrete are separated from the main body of the member by long irregular cracks and cavities.

The factors that influence the occurrence of spalling are (Malhotra, 1984):

i) The moisture content of the concrete.

ii) The number of faces exposed to heating.

iii) The level of stress in the concrete. High compressive stresses increase the probability of spalling and promote explosive spalling.

iv) The quantity of reinforcement in the member and the thickness of the member.

iii) The rate of heating of the structure. Rapid heating encourages spalling more than slow rates of heating.

vi) Cracking due to aggregate expansion, internal cracks or reinforcement expansion can also cause spalling.

Spalling can be prevented by:

i) Reducing the moisture content.

ii) Reducing the compressive stresses.

iv) Constructing with lightweight concrete.

v) Providing additional reinforcement.

vi) Incorporating polypropylene fibres into the concrete.

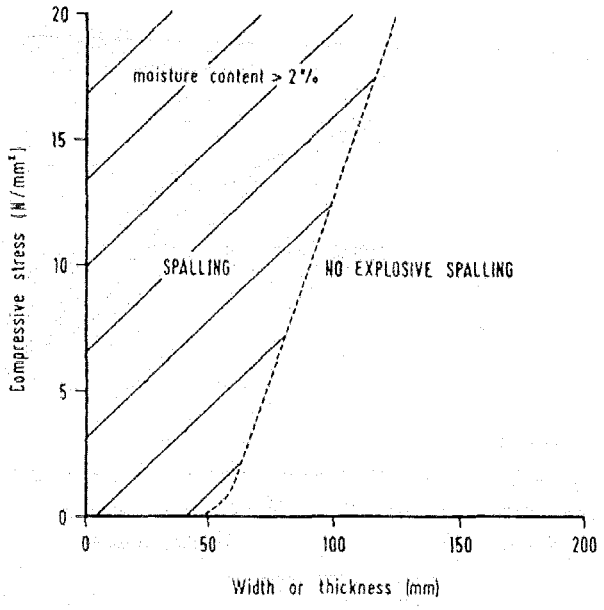

Figure 3.14: Approximate boundary between explosive and non-explosive spalling (Malhotra, 1984).

3.3. Thermal properties of steel

3.3.1. Thermal conductivity

The thermal conductivity of steel depends mainly on the amount of alloying elements and on the heat treatment. The thermal conductivity of steel λ_a for EC3 (1995) is determined from the following equations:

For $20°C \leq T < 800°C$

$\lambda_a = 54 - 3.33 \times 10^{-2} T$ (W/mK)

For $800°C \leq T < 1200°C$

$\lambda_a = 27.3$(W/mK)

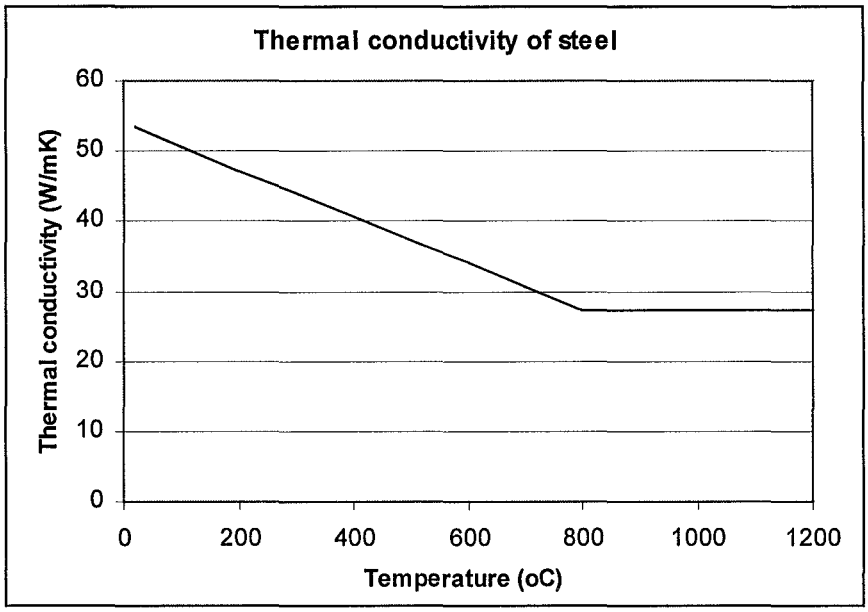

Figure 3.15: Thermal conductivity of steel as a function of temperature according to EC3 (1995).

3.3.2. Specific heat

The Eurocode (EC3, 1995) expresses the specific heat of steel c_a according to the following equations and is shown graphically in Figure 3-16.

For $20°C \leq T < 600°C$

$c_a = 425 + 7.73 \times 10^{-1}T - 1.69 \times 10^{-3}T^2 + 2.22 \times 10^{-6} T^3$ (J/kgK)

or $600°C \leq T < 735°C$

$c_a = 666 + 13002/(738-T) \times 9$ (J/kgK)

For $735°C \leq T < 900°C$

$c_a = 545 + 17820(T-731) \times 10$ (J/kgK)

For $900°C \leq T < 1200°C$

$c_a = 650$ (J/kgK)

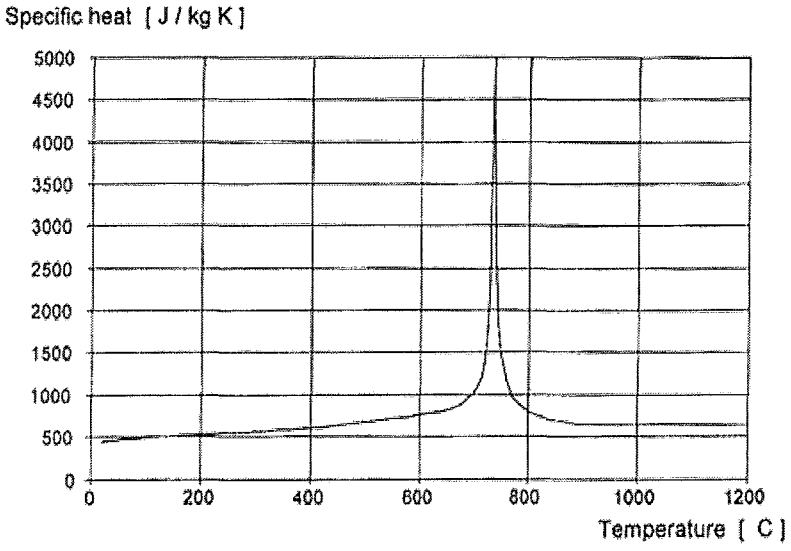

Figure 3-16: Specific heat of steel according to EC3 (1995).

3.3.3. Thermal expansion

The coefficient of thermal expansion of steel at room temperatures is about 11.4×10^{-6}. $m^{-1}K^{-1}$ (Harmathy, 1993). The thermal expansion of various carbon and low- alloy steels depends on the carbon content and the heat treatment.

The thermal elongation of structural and reinforcing steel according to EC3 (1995) is taken as:

For $20°C < T \leq 750°C$

$$\Delta l/l_s = (-2.416 \times 10^{-4}) + (1.2 \times 10^{-5} T) + (0.4 \times 10^{-8} T^2)$$

For $750°C < T \leq 860°C$

$$\Delta l/l_s = 11 \times 10^{-3}$$

For $T \geq 860°C$

$$\Delta l/l_s = (-6.2 \times 10^{-4}) + (2 \times 10^{-5} T)$$

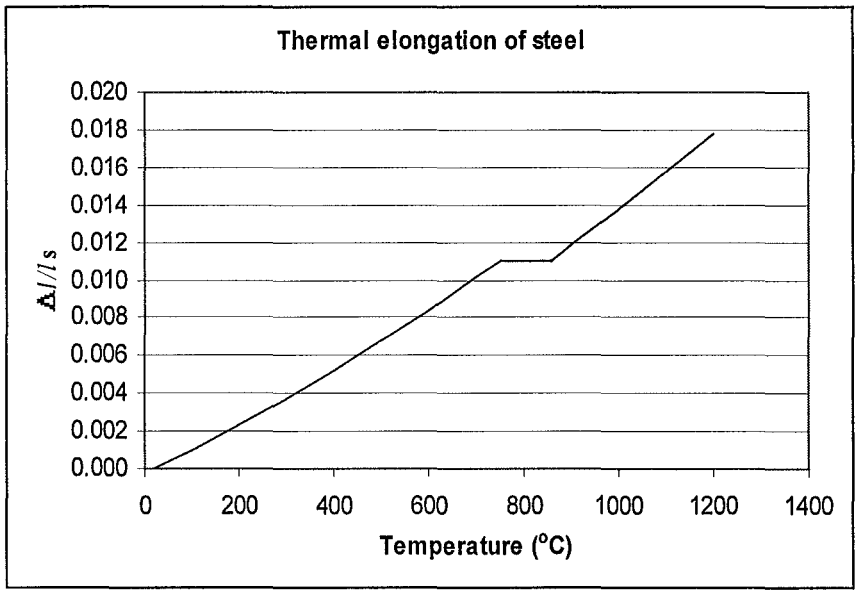

Figure 3.17: Thermal elongation of structural and reinforcing steel according to EC3 (1995).

3.4. Mechanical properties of concrete

3.4.1. Determination of concrete properties by different test methods

The material properties of concrete are closely related to the specific test method employed. The properties of concrete under elevated temperatures can be defined from several viewpoints. The properties of concrete when it is subjected to transient temperature conditions need to be distinguished from those derived from steady state conditions. The different types of test methods for determining the mechanical properties on concrete when subjected to elevated temperatures are (Schneider, 1985):

i) Steady state tests; and
ii) Transient tests.

These tests can be summarised in Figure 3.18.

3.4.2. Constitutive Law

Anderberg and Thelandersson (1976) proposed the constitutive law for concrete under transient high temperature conditions. The following equations in this section have been extracted from Anderberg and Thelandersson (1976), unless stated otherwise.

The constitutive law for concrete under high temperatures may be expressed as follows:

$$\varepsilon_T = \varepsilon_{th}\, T + \varepsilon_\sigma(\tilde{\sigma},\sigma,T) + \varepsilon_{cr}(\sigma,T,t) + \varepsilon_{tr}(\sigma,T)$$

where ε_T = Total strain

ε_{th} = Thermal strain

ε_σ = Instantaneous, stress-related strain

ε_{cr} = Creep strain

ε_{tr} = Transient strain

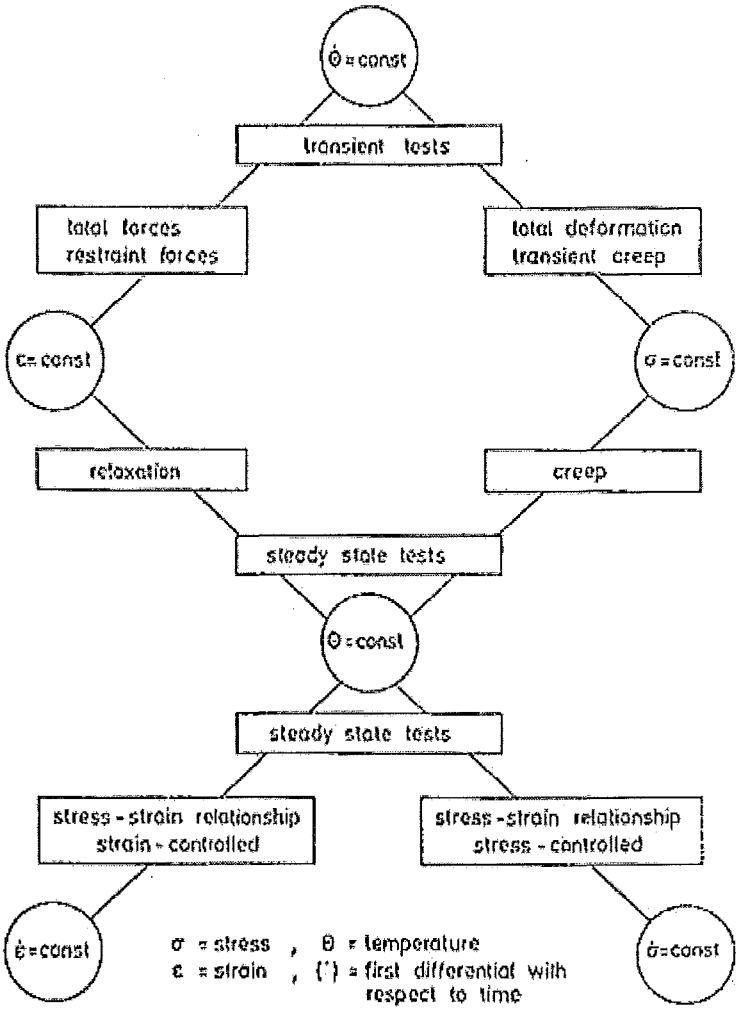

Figure 3-18: Different testing regimes for determining mechanical properties (Schneider, 1985).

3.4.3. Total strain, ε_{th}

The total strains of concrete in compression and under heating are illustrated in Figure 3-19. It shows the strains of specimens being stressed at different levels and heated to failure at a constant rate of 5°C/min. The thermal expansion is significantly reduced under stress and for a stress equal to about 40 percent of the ambient temperature strength, the thermal expansion is fully compensated by the stress induced deformation. As the temperature approaches a critical value, the compressive strain increases rapidly and finally failure occurs.

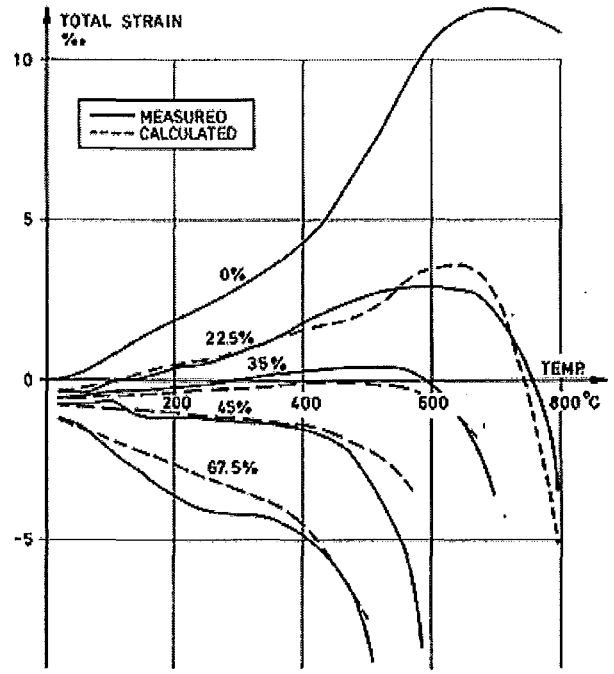

Figure 3-19: Deformation upon heating (5°C.min-1) for different levels of compressive stress (percent of strength at ambient conditions) (Anderberg and Thelandersson, 1978).

3.4.4. Thermal strain, ε_{th}

The thermal strain is the unrestrained thermal expansion of concrete. This component of the total strain has been explained in 3.2.4.

3.4.5. Instantaneous, stress-related strain, ε_{σ}

The stress-related strain is based on the concept that at every state, a specified stress-strain relation is valid for the material. The stress-strain behaviour is affected by two main factors: the current temperature and the prehistory of the stress. Anderberg and Thelandersson (1976) and Schneider (1985) have investigated the stress-strain relationships of concrete under elevated temperatures. The influence of temperature on the stress-strain curve is shown in Figure 3-20.

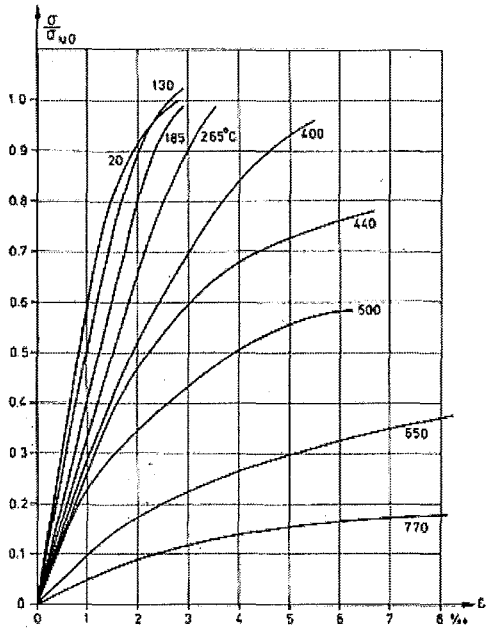

Figure 3-20: Stress-strain relations at different temperatures. The stress is given relative to the strength at ambient conditions. Rate of heating $5^{0}C.min^{-1}$. Rate of loading 14MPa Min^{-1}. (Anderberg and Thelandersson, 1976)

The high-temperature stress-strain relationship will be considerably different if the concrete is subjected to stress during the period of heating. Its deformability will be smaller and a slight increase in strength is observed. The general description of the stress-strain relation is shown in Figure 3-21.

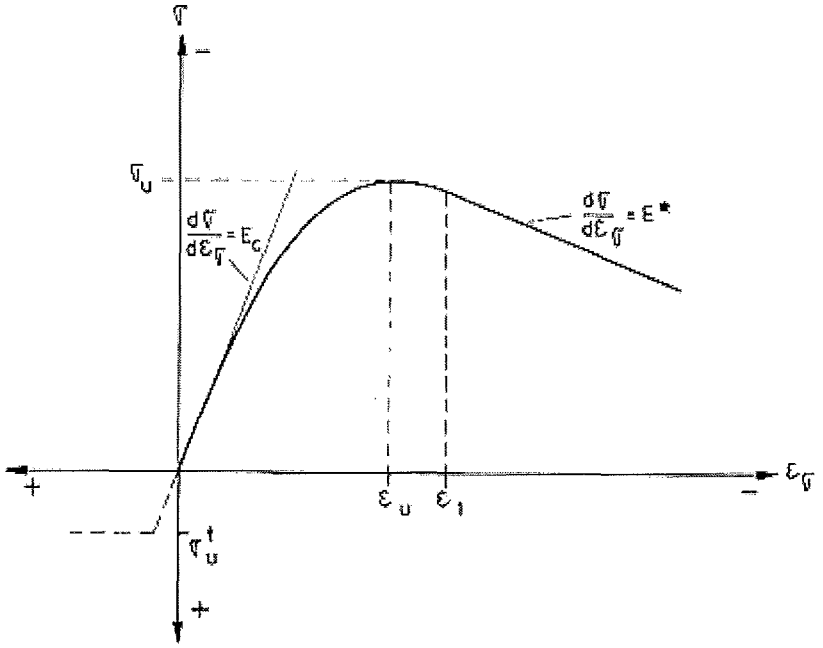

Figure 3-21: Stress strain relation of concrete (Anderberg and Thelandersson, 1976).

The three parameters used to describe the envelope in Figure 3-21 are:

σ_u = compressive strength at the current state

ε_u = strain at maximum stress, the ultimate strain

E^* = slope of descending branch

(The following equations in this page and the following page have been taken from Anderberg and Thelandersson, 1976.) The boundary conditions of the parabolic curve in the figure are:

$$\sigma = 0 \qquad \text{when} \quad \varepsilon_\sigma = 0$$

$$\sigma = \sigma_u \qquad \text{when} \quad \varepsilon_\sigma = \varepsilon_u$$

$$\frac{\delta\sigma}{\delta\varepsilon_\sigma} = 0 \qquad \text{when} \quad \varepsilon_\sigma = \varepsilon_u$$

These boundary conditions yield the following equations for the parabolic branch:

$$\sigma = \sigma_u \frac{\varepsilon_\sigma}{\varepsilon_u}(2 - \frac{\varepsilon_\sigma}{\varepsilon_u}) \qquad 0 \geq \varepsilon_\sigma \geq \varepsilon_1$$

where $\varepsilon_1 < \varepsilon_u$ is the strain at transition between the parabolic branch and the linear descending branch. The initial fictitious elastic modulus E_c (when $\varepsilon \rightarrow 0$) is obtained from the previous equation.

$$E_c = 2.\frac{\sigma_u}{\varepsilon_u}$$

The linear descending portion of the stress-strain envelope in compression is given by:

$$\sigma = E^*.\varepsilon_\sigma + \sigma^* \qquad \varepsilon_1 > \varepsilon_\sigma$$

where: $$\sigma^* = \sigma_u(1 - \frac{E^*}{E_c})^2$$

The transition point ε_1, between the two portions is obtained from:

$$\varepsilon^* = (1 - \frac{E^*}{E_c})\varepsilon_u$$

Therefore, the stress-strain relations is uniquely defined if the three parameters σ_u, ε_u and E^* are known. The difficulty lies in expressing these parameters as functions of temperature and stress history. The description of the material model in this general context is made for the case when the stresses are negative during the whole history.

The Eurocode (EC2, 1995) specifies the strength of uniaxial stressed concrete by a set of stress-strain relationships with a shape specified in Figure 3.22.

Range I of the model is expressed as

$$\sigma_c(\theta) = f_c(\theta) = \left[\frac{\varepsilon_c(\theta)}{\varepsilon_{c1}(\theta)} \times \frac{3}{2 + \left(\frac{\varepsilon_c(\theta)}{\varepsilon_{c1}(\theta)}\right)^3} \right];$$

$\frac{f_c(\theta)}{f_c(20°C)}$ *and* $\varepsilon_{c1}(\theta)$ to be chosen according to table A.1 of EC2 (1995)

Range II: For numerical purposes a descending branch should be adopted. Linear and non-linear models are permitted.

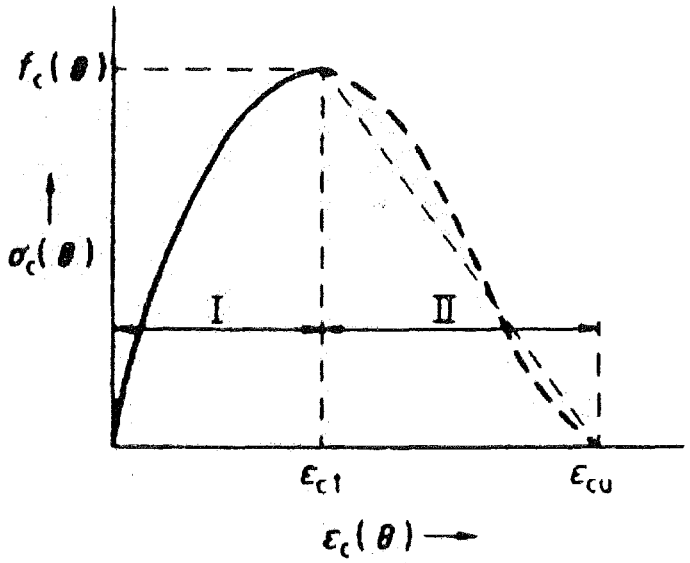

Figure 3.22: Model for compression stress-strain relationships for siliceous and calcareous concrete at elevated temperatures (EC2, 1995).

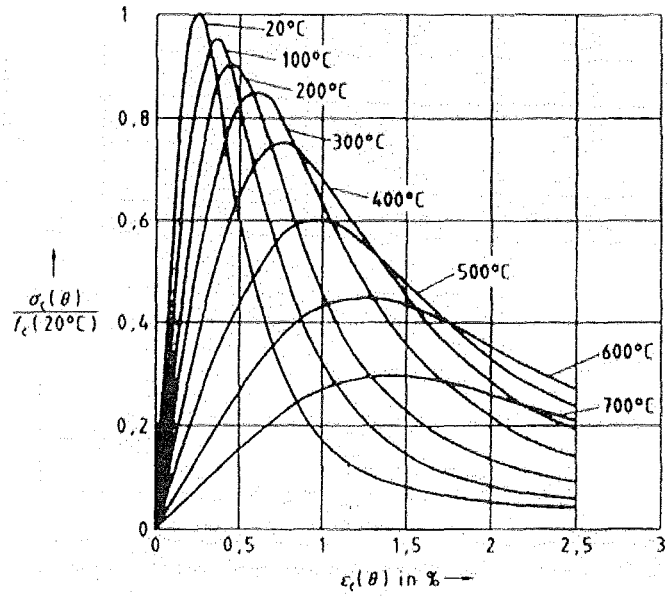

Figure 3.23: Stress strain relationships of siliceous aggregate concrete under elevated temperatures according to EC2 (1995).

3.4.6. Creep Strain, ε_{cr}

The basic creep ε_{cr} at constant temperature and constant stress is given by (Anderberg and Thelandersson, 1976):

$$\varepsilon_{cr} = \beta_o \frac{\sigma}{\sigma_u T}\left(\frac{t}{t_r}\right)^p e^{k(T-2)_1}$$

where: β_o $= -0.53.10^{-3}$

σ = stress

$\sigma_u(T)$ = ultimate stress at current temperature

t = time

t_r = 3 hours

p = 0.5

k_1 $= 3.04.10^{-3}°C^{-1}$

T = temperature

The equation above expresses the creep versus time for any given combination of temperature and stress. Figure 3.24 shows that when the temperature and stress vary with time, the evaluation of the creep strain is based according to the strain hardening principle.

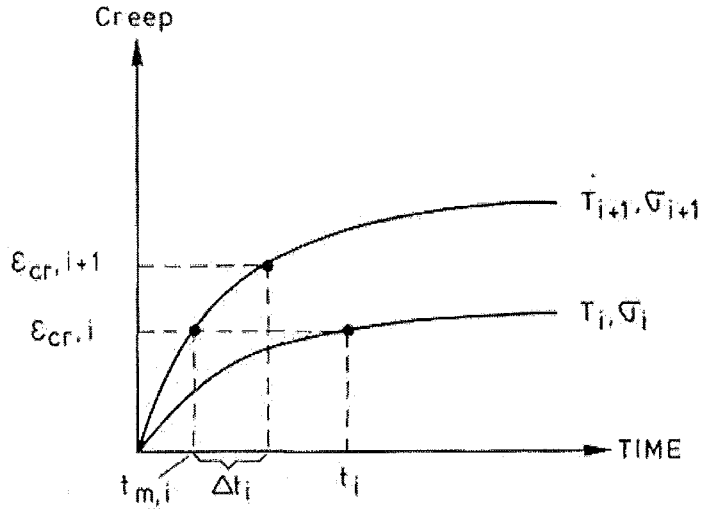

Figure 3.24: The principle of strain hardening for creep (Anderberg and Thelandersson, 1976).

3.4.7. Transient strain, ε_{tr}

Anderberg and Thelandersson (1976) discovered that transient effects were important when they performed tests under constant stress and varying temperature and measured the resultant strain. Transient strain develops under stress when the temperature is increased. This strain has been shown to be irrecoverable and occurs only on the first heating of concrete.

Khoury, Grainger and Sullivan (1985a, 1985b and 1986) have explained the phenomenon of transient strain more clearly. Transient creep originates in the cement paste and is restrained by the aggregates. It provides the concrete some thermal stability by accommodating the considerable thermal incompatibility that develops between the aggregate and the cement paste during first heating. Transient creep causes a significant relaxation and redistribution of thermal stresses.

Transient strain cannot be measured and must be determined from the remaining four strain components (Anderberg and Thelandersson, 1976).

$$\varepsilon_{tr} = \varepsilon_T - \varepsilon_{th} - \varepsilon_\sigma - \varepsilon_{cr}$$

Anderberg and Thelandersson (1976) have found that for siliceous aggregate concrete, the transient strain is of opposite sign to the thermal strain at temperatures below 500°C (which is the temperature at which the quartz phase change occurs). It is modelled as:

$$\varepsilon_{tr} = -2.35.\frac{\sigma_{i-1}}{\sigma_u}\varepsilon_{th} \qquad \text{T<500°C}$$

$$\varepsilon_{tr} = -0.0001.T.\frac{\sigma_{i-1}}{\sigma_u} \qquad \text{500°C<T<800°C}$$

where: σ_{i-1}. = stress in the element for the previous time step

σ_u. = compressive strength of the concrete at the current element temperature

T = element temperature

ε_{th} = thermal strain.

The transient strain is a very important component and Figure 3-25 below shows the relative order of magnitude for the different components.

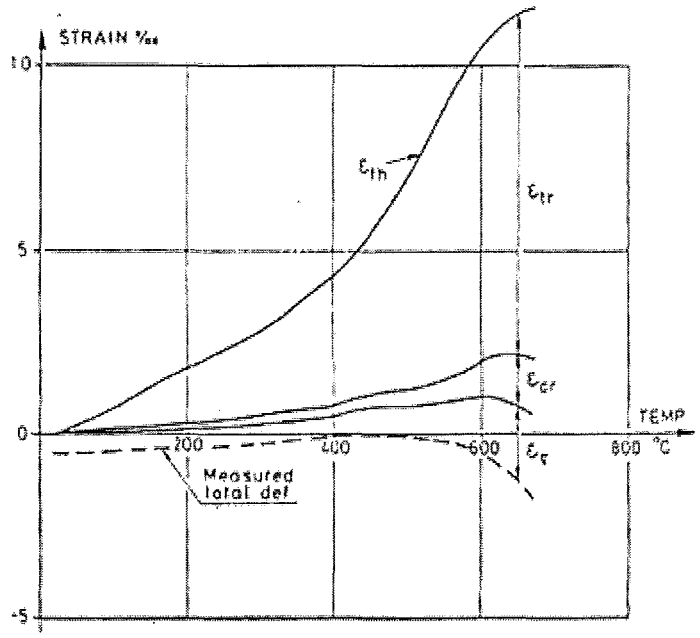

Figure 3-25: Relation between different strain components (Anderberg and Thelandersson, 1976).

3.4.8. Modulus of Elasticity

The reduction of modulus of elasticity with temperature for various types of aggregates is shown in the figure below. The reduction of the modulus of elasticity is due to the breakage of bonds in the microstructure of the cement paste when the temperatures increase. Another cause of the reduction of the elastic modulus is the increase of rapid short-time creep.

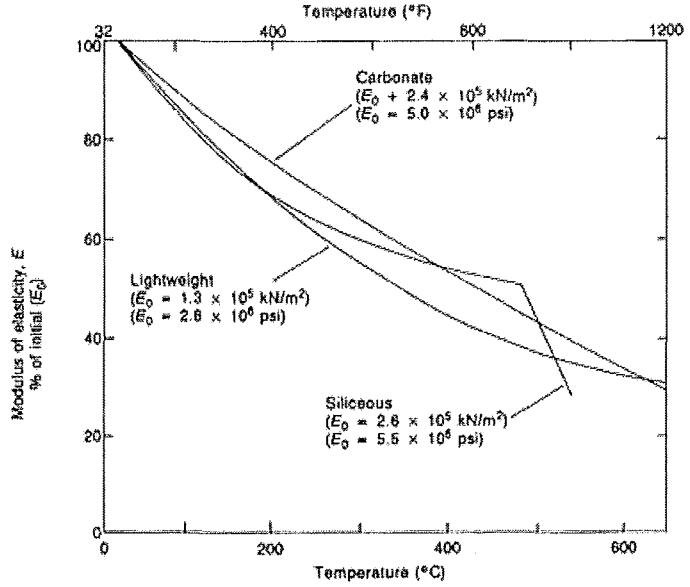

Figure 3-26: Reduction of modulus of elasticity for various types of aggregates with temperature (Bažant and Kaplan, 1996).

The type of aggregate used in the concrete has a strong influence on the reduction of the elastic modulus (Schneider, 1985). Although the data obtained from various investigators vary significantly, generally it is found that aggregates that are more compatible and chemically stable such as limestone exhibit a lower reduction (refer to Figure 3-26). Siliceous aggregates show a significant drop in the elastic modulus at temperatures above 500°C.

3.4.9. Compressive strength

The compressive strength of concrete is a function of temperature. The effects of the type of aggregate on the compressive strength of specimens that were unstressed during heating are shown in Figure 3.27.

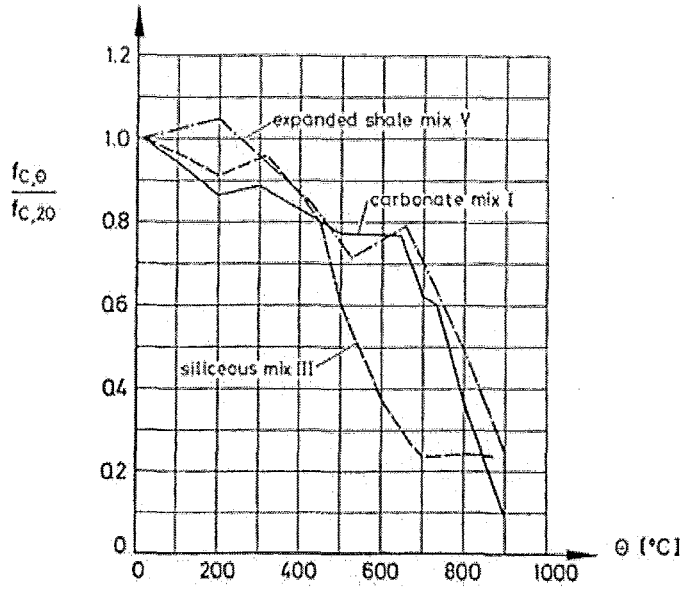

Figure 3.27: Variation of concrete compressive stress for different aggregates (Schneider, 1985).

The Eurocode (EC2, 1995) expresses the reduction of the characteristic compressive strength of concrete by the coefficient $k_c(T)$.

$$f_{ck}(T) = k_c(T).f_{ck}(20°C)$$

The strength reduction coefficient $k_c(T)$ for siliceous aggregate concrete as obtained from EC2 is shown in Figure 3.28 and follows the equations:

$k_c(T) = 1.0$ for $20°C \leq T \leq 100°C$

$k_c(T) = (1600-T)/1500$ for $100°C \leq T \leq 400°C$

$k_c(T) = (900-T)/625$ for $400°C \leq T \leq 900°C$

$k_c(T) = 0$ for $900°C \leq T \leq 1200°C$

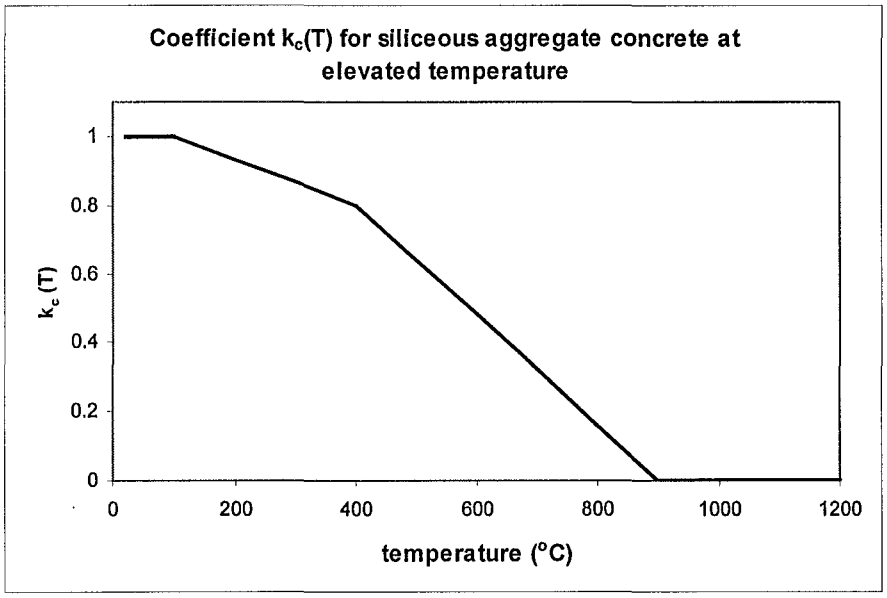

Figure 3.28: Coefficient $k_c(T)$ accounting for the decrease of compressive strength (f_{ck}) for siliceous aggregate concrete at elevated temperatures according to EC2 (1995).

One of the main factors that affect the compressive strength of the concrete is the type of aggregate used in the concrete. Figure 3.27 shows that from 450°C, the concrete with siliceous aggregates exhibited the greatest amount of strength reduction compared with that of calcareous or lightweight aggregates (Schneider, 1985). This trend was also observed when the concrete was stressed to $0.4\sigma_c$ and tested hot and to unstressed residual strengths. This was considered to be due to the abrupt volume change due to the inversion of the α-quartz to the β-quartz at about 570°C.

The concrete compressive strength is also very dependent on the stress level (Schneider, 1985). The "stressed strength" of concrete is evidently higher than the "unstressed strength" (Figure 3.29). The stress level itself has little effect on the ultimate strength as long as $\alpha > 0.20$. It becomes significant once $\alpha < 0.20$.

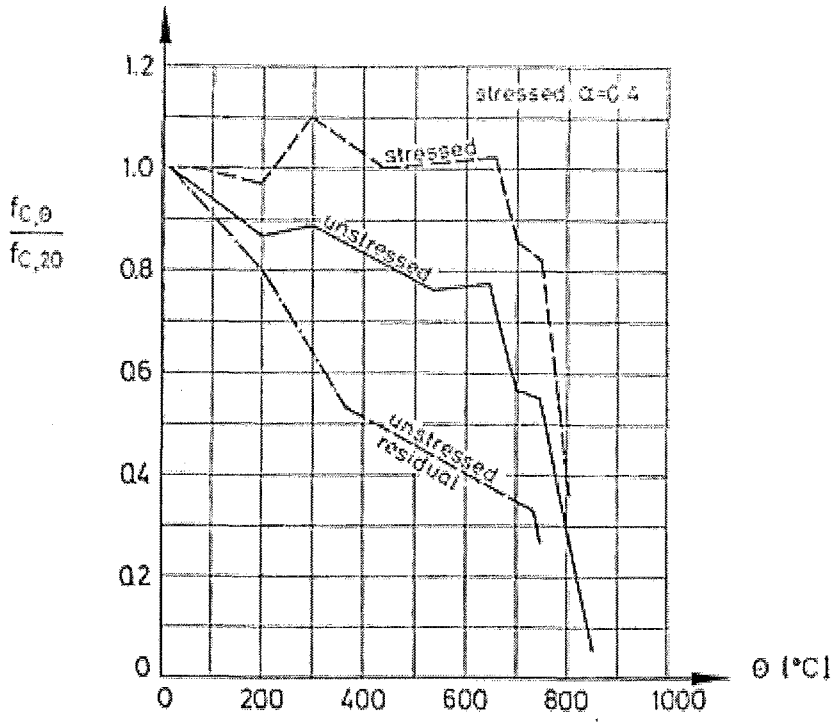

Figure 3-29: Stressed and unstressed concrete during heating (Schneider, 1985).

The compressive strength of concrete is highly dependant on the micro-cracks that develop at the paste-aggregate interfaces and in the paste itself. Therefore, the strength of the concrete is highly dependant on the strength of the cement paste and largely independent of the strength of the aggregates.

Another significant factor that affects the reduction of the concrete compressive strength when it is subjected to elevated temperatures is the aggregate-cement ratio (Malhotra, 1956). Leaner mixes (concrete with high aggregate-cement ratio) undergo a smaller proportional reduction in strength when heated to any given temperature, compared with the richer mixes (concrete with low aggregate-cement ratio).

3.4.10. Tensile Strength

The ultimate tensile strength of concrete is normally assumed to be absent, which is on the safe side. However, if the tensile strength of concrete is required, EC2 (1993) allows for the variation of the tensile strength of concrete with temperature as shown in Figure 3.30.

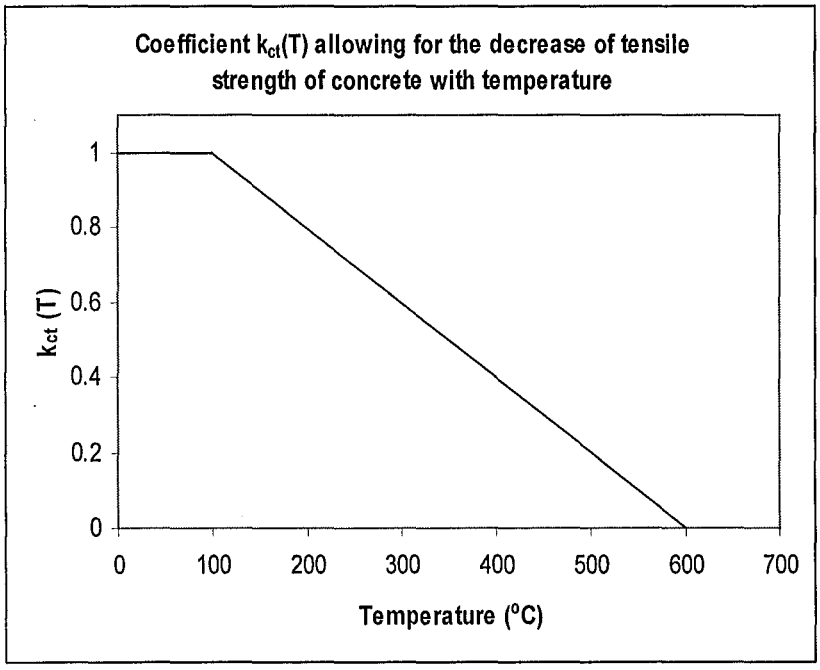

Figure 3.30: Coefficient $k_{ct}(T)$ allowing for the decrease in tensile strength of concrete at elevated temperatures. (EC2, 1995)

3.5. Mechanical properties of steel

For steel sections, the thickness is such that their temperatures across the section may be considered uniform. Therefore, the problem encountered with concrete on heating rates is not as important.

3.5.1. Components of strain

The deformation of steel at elevated temperatures is given by the total strain as shown below. The transient strain component does not exist for steel.

$$\varepsilon_T = \varepsilon_{th}\, T + \varepsilon_\sigma(\tilde{\sigma},\sigma,T) + \varepsilon_{cr}(\sigma,T,t)$$

where ε_{th} = Thermal strain

ε_σ = Instantaneous, stress-related strain

ε_{cr} = Creep strain

3.5.2. Thermal strain, ε_{th}

The thermal strain of steel is the thermal expansion of steel when it is heated up. Its behaviour under elevated temperatures is explained in section 3.3.3.

3.5.3. Stress-related strain, ε_σ

Typical stress–strain curves for structural steel elements at elevated temperatures at various temperatures as obtained by Harmathy and Stanzak (1970) are shown in Figure 3-31.

The graph shows that the yield plateau becomes less noticeable with temperature rise and disappears at about 300°C. After a slight decline at moderately elevated temperatures, the ultimate strength of the steel increases in the temperature range of 180°C to 370°C. Upon further temperature increase, the yield strength of the steel declines steadily.

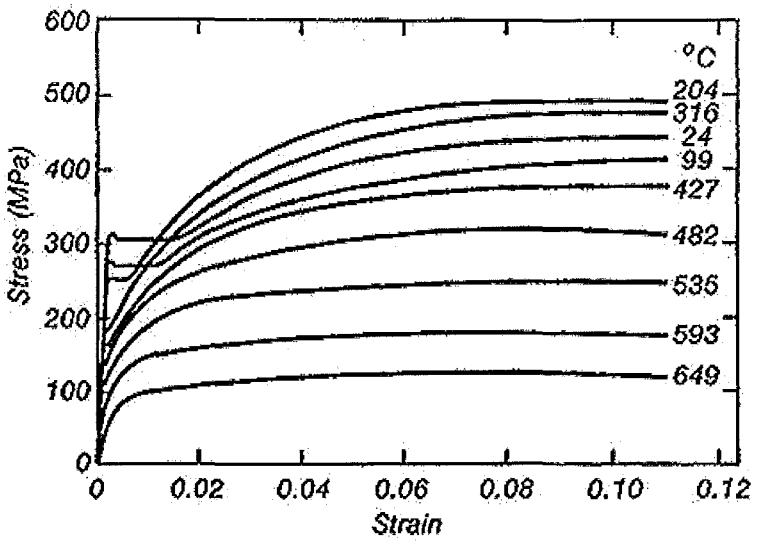

Figure 3-31: Stress strain curves at various temperatures for structural steel (Harmathy and Stanzak, 1970).

The stress-strain curve of steel according to EC3 (1995) at a given temperature is defined by three parameters.

i) The slope of the linear elastic range E_s(T),

ii) The proportional limit σ_{spr}(T), and

iii) The maximum stress level f_y(T).

Figure 3-32 describes the stress-strain relationships of hot-rolled structural and reinforcing steels at elevated temperatures.

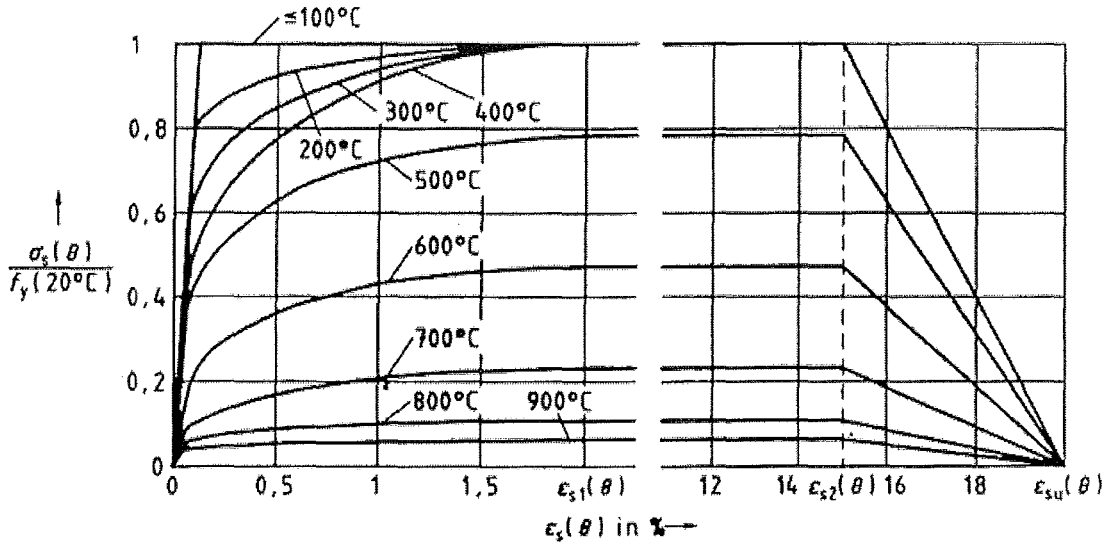

Figure 3-32: Stress strain relationships of hot rolled steel at elevated temperatures according to EC2 (1995).

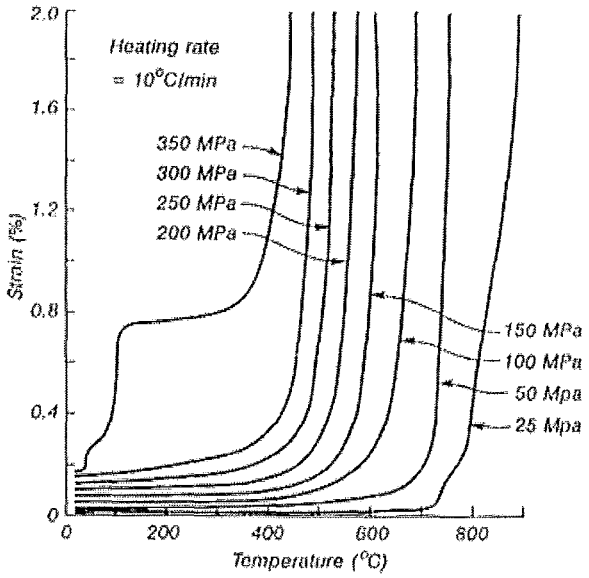

Figure 3-33: Variation of creep strain with temperature (Kirby and Preston, 1988).

3.5.4. Creep strain, ε_{cr}

Creep strain in structural steel elements only become significant at temperatures over 400-500°C. Kirby and Preston (1988) have shown that the creep is highly dependant on the temperature and stress level of the steel. When the steel section attains a certain temperature as shown in the graph below, the creep strain curve becomes almost vertical. Therefore, if the steel member of a particular stress level reaches a certain temperature, the member becomes plastic and runaway failure occurs.

3.5.5. Modulus of Elasticity

The reduction of the modulus of elasticity with temperature for various types of steel is shown in Figure 3-34 below. Its reduction trend is similar to that of the yield strength. Harmathy (1993) has made a comparison by various researchers on the effect of temperature on various types of steel.

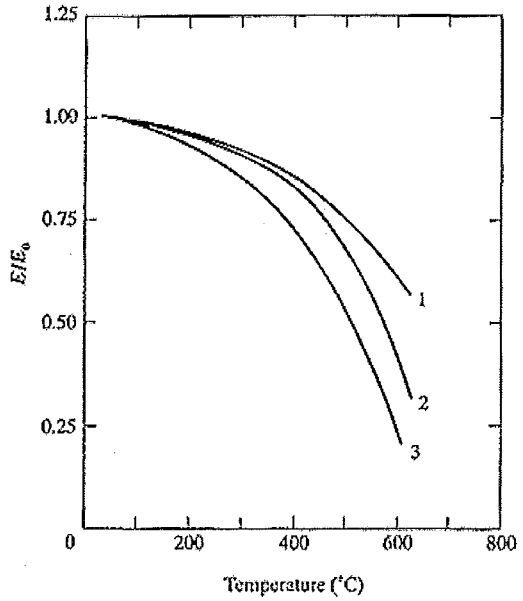

Figure 3-34: Variation of modulus of elasticity of steel with temperature. 1) Structural steel, 2) Prestressing steel, 3) Reinforcing steel (Harmathy, 1993)

3.5.6. Ultimate and yield strengths

Most normal construction steels utilise a well-defined yield strength at normal temperatures. However, this yield point disappears at elevated temperatures (Buchanan, 1999). The reduction of the ultimate and yield strengths of steel is shown in Figure 3-35 below. There is a significant amount of scatter shown with various curves recommended by various researchers. The vertically hatched and the horizontally hatched area represent the ultimate strength and yield strength of the steel. Curve *a* is the curve recommended by The Institution of Structural Engineers for both yield strength and ultimate strength.

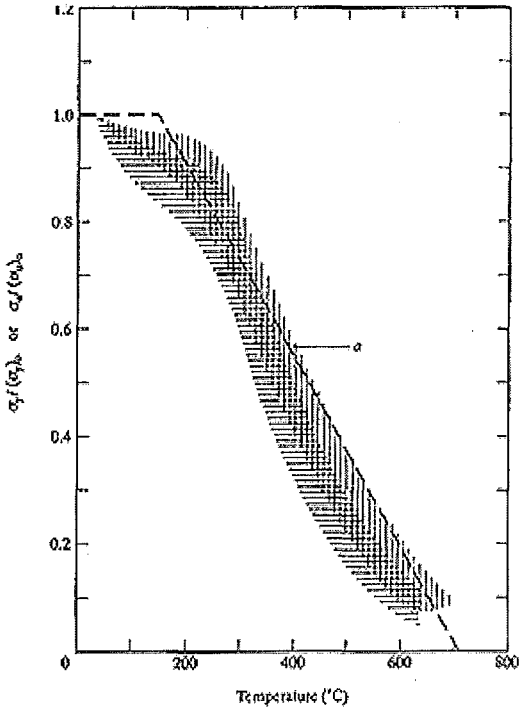

Figure 3-35: Ultimate and yield strengths of hot-rolled steel (Harmathy, 1993).

The variation of the elastic modulus, proportional limit and yield strength of steel as a function of temperature according to EC2 (1995) is shown in Figure 3-36. The stress strain relationships may be applied to the steel in both tension and in compression. The stress-strain relationships account in an approximate manner the effect of high temperature creep. The material model is applicable only for heating rates similar to those appearing under standard fire conditions.

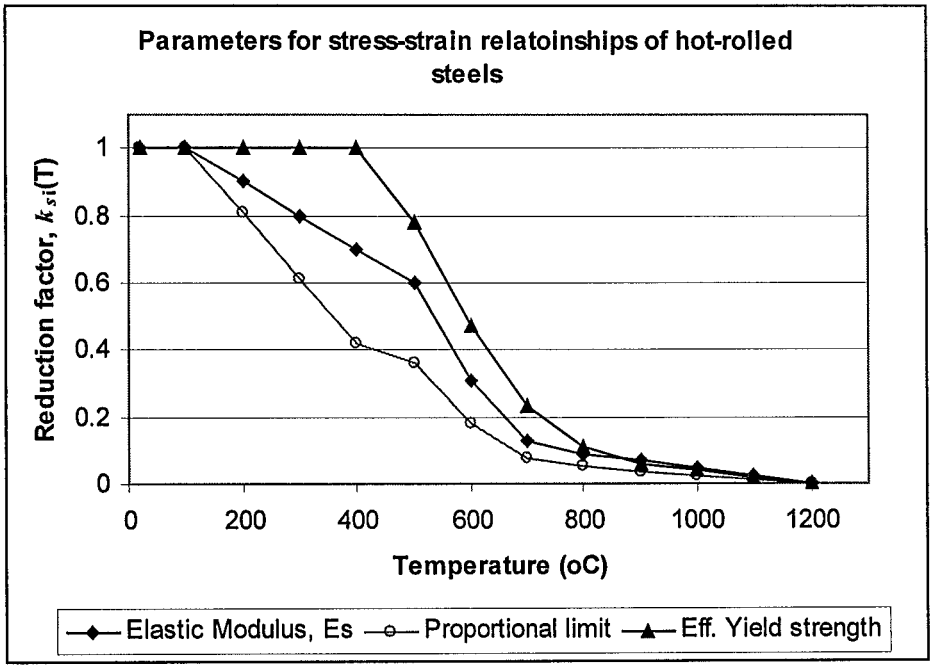

Figure 3.36: Parameters of stress-strain relationships of hot-rolled steels at elevated temperatures according to EC2 (1995).

4. Behaviour of Concrete Walls and Industrial Buildings under Elevated Temperatures

4.1. General

This chapter describes the construction forms of industrial buildings in New Zealand. It also describes the behaviour of isolated cantilever walls and cantilever walls in industrial buildings when they are subjected to elevated temperatures. Special emphasis is placed on buildings with slender cantilever precast panels. Included in this chapter are the results of analyses done by previous researchers on the behaviour of concrete wall panels and industrial buildings.

4.2. Industrial buildings in New Zealand

Single storey industrial buildings and warehouse complexes in New Zealand are used for manufacturing and storage purposes. They are used to store materials with low fuel loads such as vehicles to high fuel loads, such as petroleum products and wood and paper products (Cosgrove, 1996). Industrial buildings have large spans and high ceilings to meet handling requirements for material processing and storage purposes.

Figure 4.1: A typical industrial building in New Zealand.

4.2.1. Construction forms

Traditional industrial buildings

Traditional industrial buildings in New Zealand comprise a steel portal frame formed by a rafter spanning between steel columns. The steel columns are fixed (or partially fixed) at the base. The portal frames are typically spaced at 5 to 10 meters apart. The roof normally comprises thin steel sheeting with translucent plastic sheeting, supported on timber or steel purlins. Precast concrete panels are attached to the portal frames and are sometimes connected to each other by an eaves tie.

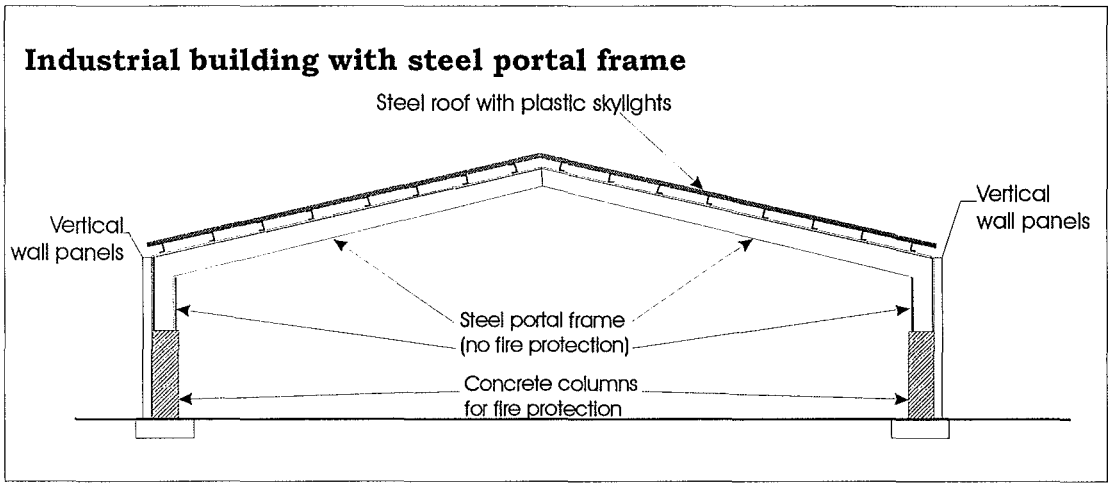

Figure 4.2: Traditional industrial building

The portal frames are sometimes fire protected by:

i) Encasing the full height or part height of the steel portal leg in concrete or lightweight protection; or

ii) Sitting the steel portals, with shortened legs, on top of concrete columns (refer to Figure 4.2).

In the event of a fire, the roof will collapse and the wall panels will cantilever above the concrete columns or protected steel columns (Figure 4.3). In some cases, the steel portal has no protection and the panels cantilever from ground level (Figure 4.4). However, if the wall panels are connected to the portals at the knee joint, the steel rafter will push the panels outwards when it expands. When the portal collapses, it will drag the panels inward.

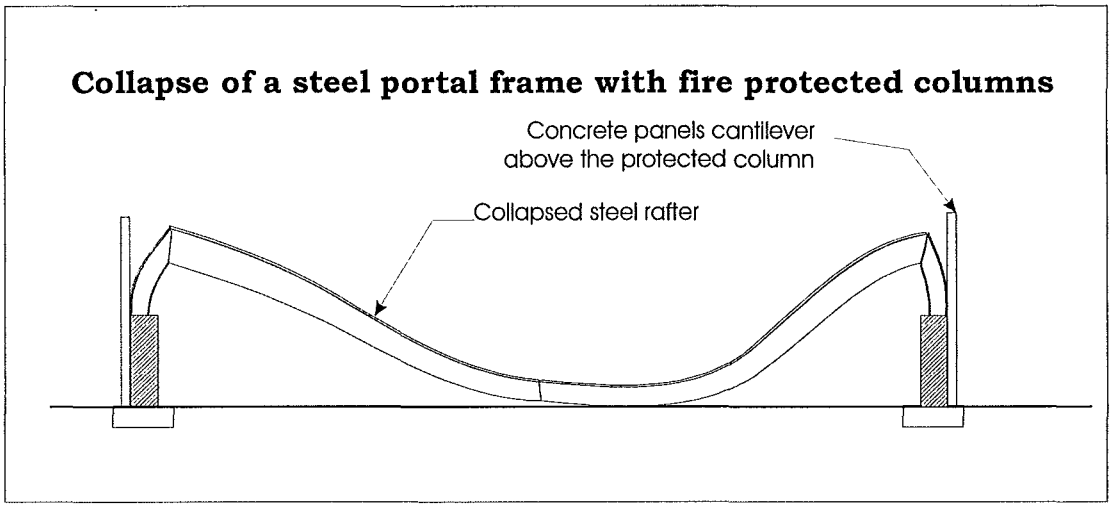

Figure 4.3: Collapse of a steel portal frame with fire protected columns.

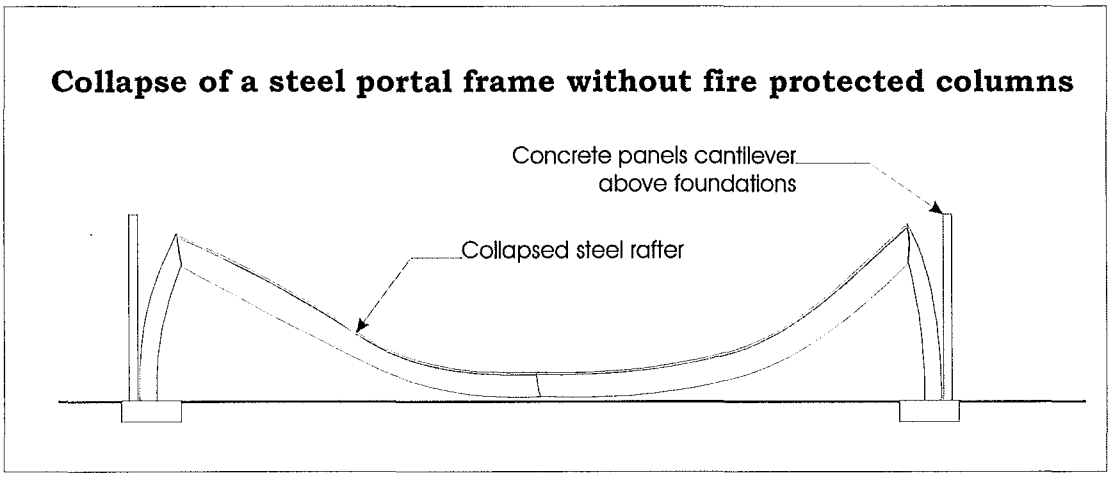

Figure 4.4: Collapse of a steel portal frame without fire protected columns.

Modern industrial buildings

Modern industrial buildings comprise a steel frame supported on internal columns and tilt-up precast panels at the perimeter of the building. The precast panels do not have columns attached to them. The industrial buildings are built with long span beams and high ceilings. The clear spans of the rafter range between 15 to 30 meters and the rafters are spaced at 6 to 12 metre centres.

The precast concrete panels are cantilevered at the base and act as fire separating walls at the boundary of the building. They act in unison with the internal steel columns to support the rafter and the roof. These panels also provide in-plane resistance to lateral loads (earthquake forces and wind pressure) with the roof bracing acting as a diaphragm.

There is a pressing concern regarding the stability of the tall and slender cantilever wall panels that have been built with slenderness ratios (Height/thickness ratio) ranging from 50 to in excess of 80. Some of these wall panels are very thin, in the range of 125mm to 150mm (Brown, 1999) and are only reinforced with one central layer of reinforcing steel. The slenderness ratios of these walls exceed the maximum allowable slenderness limits as stated in the *Concrete Structures Standard of New Zealand NZS3101: 1995* (Refer section 2.2.2). These wall panels have no intermediate lateral support and are connected to each other at the top by an eaves tie (Bull, 1998).

These slender walls pose important stability issues from fire resistance and seismic stability perspectives. This project is aimed at investigating the behaviour of these slender column-free wall panels when they are subjected to a fire.

The typical geometric details and construction forms of the industrial buildings are shown in Figure 4-6. Figure 4-5 shows the sequence of construction of the tilt slabs for a typical industrial building (Brown, 1999).

(1) Setting of reinforcing and formwork.

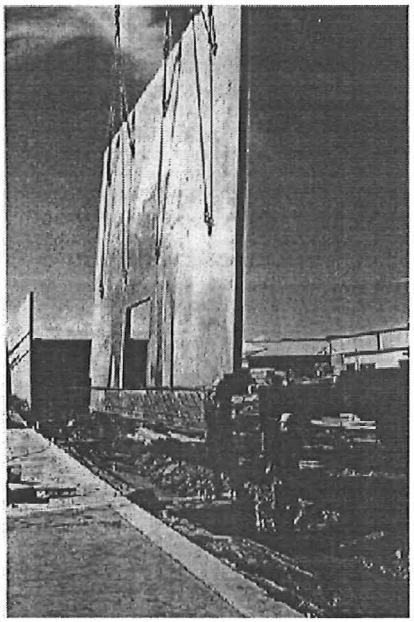

(3) Lifting of tilt panels before fixing them to the base.

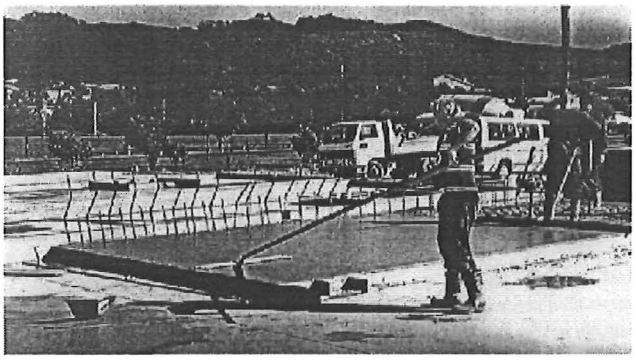

(2)Pouring of concrete

Figure 4.5: On-site fabrication of tilt panels (Brown, 1999).

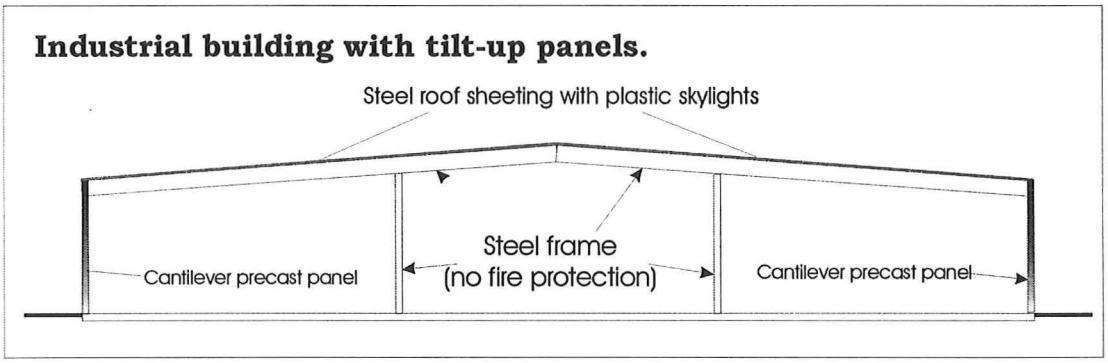

Figure 4.6: Cross section of a typical modern industrial building in New Zealand.

Figure 4.7: Layout of a typical industrial building with its contents.

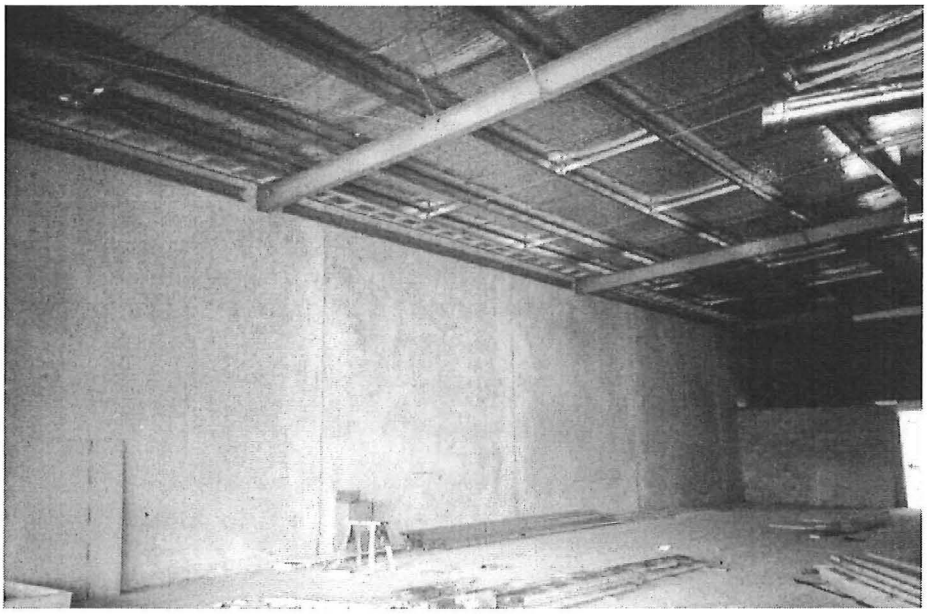

Figure 4.8: Typical construction of a modern industrial building with load bearing cantilever walls.

4.2.2. Typical details of the construction of modern industrial buildings

Typical construction details of these tilt-up panels obtained through personal communications (Forrest, E.) and McMenamin (1999) are as follows:

Wall dimensions:

Height, H_{wu}:	8.0m to 12.0m
Length, l_w:	2.5m – 3.0m
Thickness, t_w:	125mm – 200mm
Aspect ratio, A_r (H_{wu}/ l_w):	4.0 - 4.8
Slenderness ratio, λ (H_{wu}/t_w):	60–80

Reinforcing steel:

Yield strength, f_y:	430 MPa
Bar diameter, d_b:	12mm – 16mm
Placement:	Single layer of vertical and horizontal reinforcing in the middle of the section.
Spacing, s:	200mm – 250mm centres
Reinforcing ratio, p (A_{st}/A_g):	~0.5%

Concrete:

Compressive strength, f'_c:	25-30 MPa
Aggregates:	Normal weight concrete, Greywacke aggregates (Siliceous)

The larger diameter bars can be lapped with smaller bars higher up the walls. Walls thicker than or equal to 200mm have the reinforcing bars placed in two layers to prevent spalling of the concrete. In some cases, the reinforcing of the wall has been substituted with welded mesh consisting of 9.5mm diameter bars placed at 150mm centres.

Roof details

The roof sheeting typically comprises steel sheeting and plastic translucent skylights. The roof panels are support by steel purlins which in turn, are supported by steel rafters or steel trusses. The steel rafters are typically attached to every second or third wall panel. Eaves ties attached at the top of the wall panels are used to connect these wall panels together. The eaves channels are connected to the wall panels with steel clips or bolted to cast-in inserts. Figure 4.9 and Figure 4.10 show the typical details of the eaves tie and rafter connections at the wall. Figure 4.11 shows the different types of steel embedments available for connecting structural steel elements to reinforced concrete elements.

Figure 4.9: Typical details of eaves tie and connecting rafter supported by the wall panel.

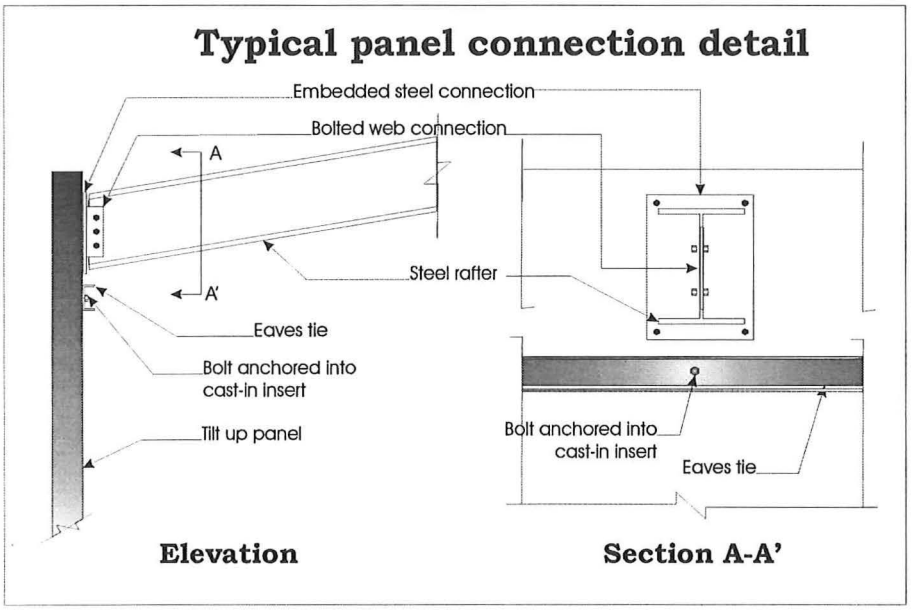

Figure 4.10: Section of wall showing eaves connection.

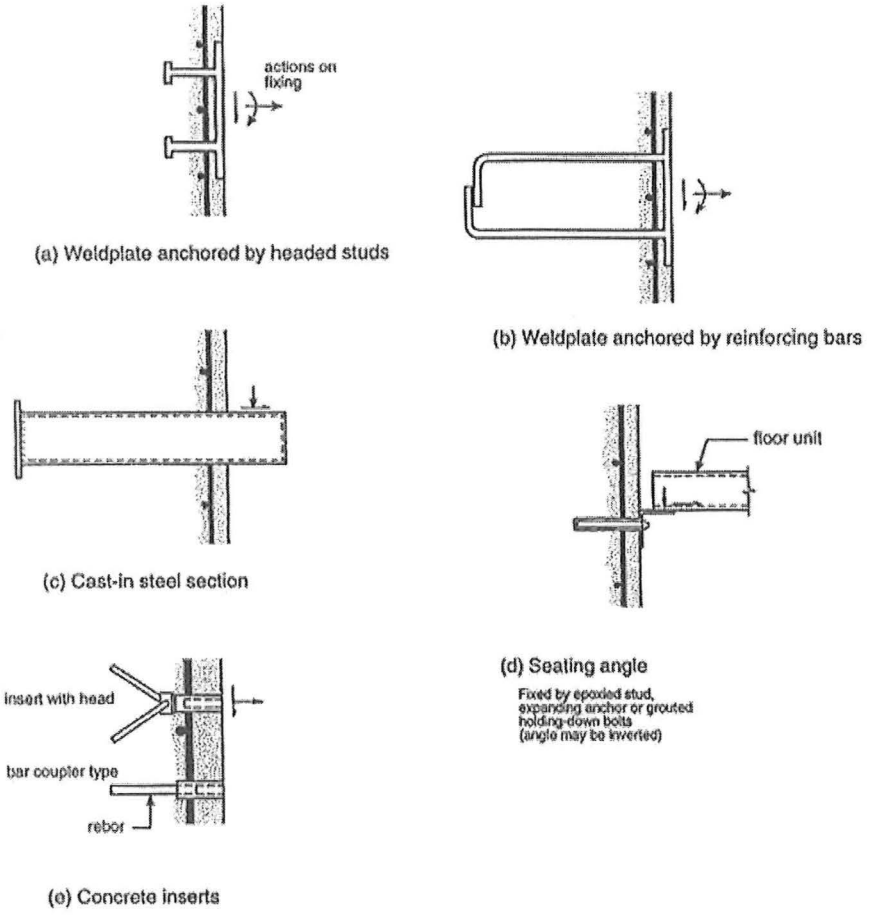

Figure 4.11: Different types of steel embedments (NZCS & NZNSEE, 1991).

Foundation details

The cantilever wall panels are attached at the base to the foundation beam and the floor slab by various types of connections. A survey was conducted to review the details of tilt-up construction (Restrepo, Crisafulli, Park, 1996). The typical details used in practice are shown in Figure 4-12. These connections provide full fixity at the base so that the walls resist overturning moments by cantilever action. The connection methods at the base range from simple reinforcing steel connections to proprietary connection methods, such as corrugated ducts filled with non-shrinkage grout and starter bars screwed into threaded inserts.

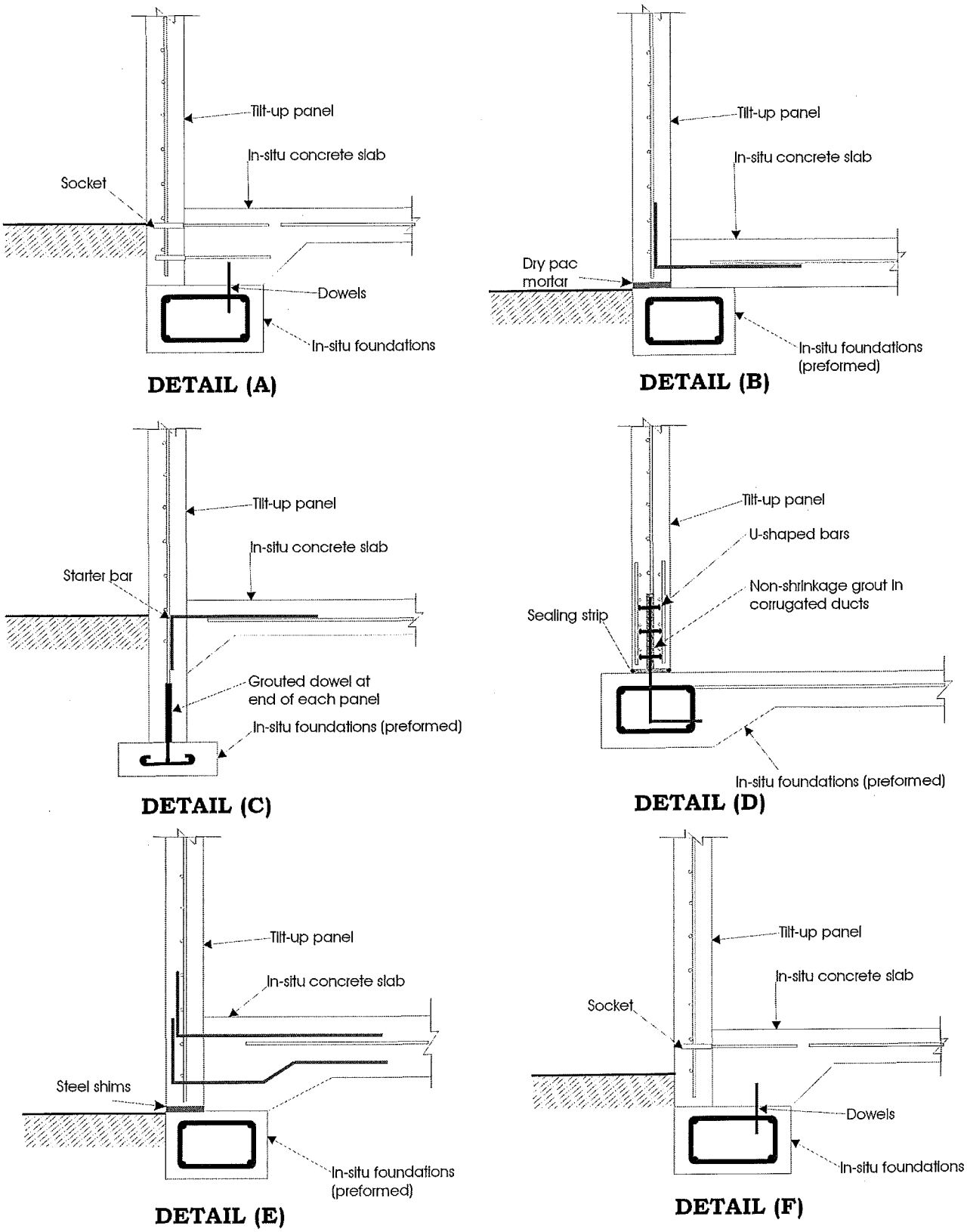

Figure 4-12: Typical base connections for cantilever walls.

4.3. Fires in industrial buildings

4.3.1. A typical room fire

In a typical room fire, the fire will form a convective plume of hot gas which will rise and reach the ceiling. It will then spread horizontally, in the form of a ceiling jet, to form a hot upper layer. As the burning continues, the volume of smoke and hot gases in the hot upper layer will increase. If the fire continues to grow and assuming sufficient fuel, the temperatures in the hot upper layer increase. This will increase the heat flux to the objects in the room. Once a critical level of heat flux is reached, flashover will occur where all exposed combustible items in the room will burn.

4.3.2. Large compartment fire

The behaviour of a fire in a large compartment, such as a warehouse, is not the same as in a small enclosure. The ceiling of these industrial buildings are high, and due to large open space available in these structures, the hot gases will continue to spread and not be able to accumulate. Therefore, the radiant heat flux from the hot layer may not reach the critical ignition level for flashover to occur.

The fire in this large compartment would be a fuel-controlled fire. The temperatures of the fire may get sufficiently hot at local areas in the building which may cause local structural failure such as local buckling of the purlins and rafters. It may also cause collapse of the roof and melting of the sky lights which in turn would cause venting of the fire, and release the accumulated hot gases to the atmosphere. Therefore, the temperatures of the fire in the building may be equivalent to an external fire.

Cosgrove (1996) has shown that the typical fire development sequence in an industrial building is shown in Figure 4-13. The figure shows that there are three main stages of fire development in an unprotected single storey industrial building:

i) Fire growth: This will take place until flashover occurs or until the maximum fuel surface is burning.

ii) Steady state condition: This condition can be ventilation or fuel controlled, depending on whether the burning rate of the involved fuel is greater or less than the relative burning rate possible due to the available ventilation openings. The collapse of the roof and melting of the plastic skylights will increase the available ventilation. This will consequently alter the heat release rate.

iii) Decay: Once the available fuel surface area has been decreased and depleted, the heat release rate will decrease.

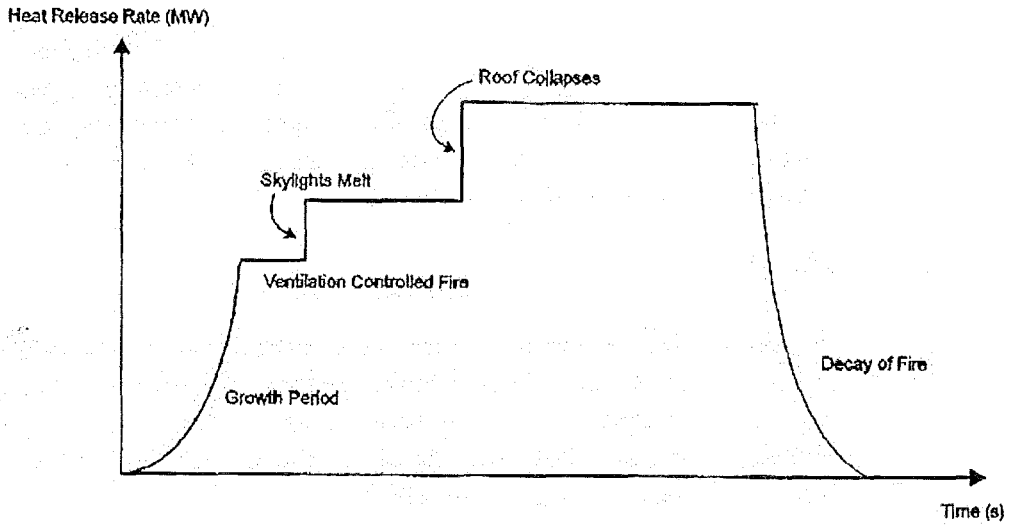

Figure 4.13: A typical fire development profile for a single storey building (Cosgrove, 1996)

4.3.3. Migrating fire

O'Meagher et al (1992) and Clifton (1996) have suggested a migrating fire model. A migrating fire begins at a particular location, and spreads out to other parts of the building. In the migrating fire, the heating is non-uniform throughout the building at any one time. Some parts of the building may be exposed to severe heating while other parts of the building are exposed to low heat levels that do not threaten its structural performance.

It will spread and cause an increasing number of structural elements to be affected. As the fire at the point of origin decays due to the consumption of the fuel, the fire would have spread to other areas and continue to develop in those areas. At any given time in a fully developed fire, the peak intensity of the fire occurs only over a relatively small floor plan area. This is due to the movement of the fire front and the zone of peak heat intensity as the material is consumed.

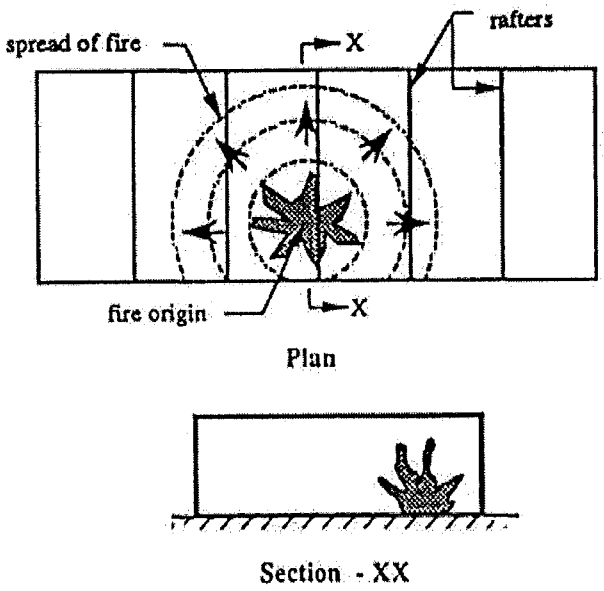

Figure 4.14: Migrating fire concept in single storey large enclosures (O'Meagher *et al*, 1992).

4.3.4. Reports of fires in industrial buildings

In a survey done by Cosgrove (1996) on industrial fire accidents in New Zealand from 1988 to 1994, 505 of the 626 reported fires were related to manufacturing complexes. The remaining 121 incidents were related to warehouse facilities. The highest number of fires occurring in the manufacturing complexes were wood and paper manufacturing facilities (42%), followed by furniture manufacturing facilities (11%). In warehouse storage facilities, general storage facilities had the highest number of fire incident reports (27%), followed by wood and paper products (21%).

Plastics Factory (Christchurch, 1993)

A plastics factory burnt down in Christchurch on the 25th October 1993. The factory was involved in the production of polyethylene foam products. The fire resulted in total demolition of the structure. Thirty fire service personnel and fourteen appliances were involved in controlling and extinguishing the fire over a period of five hours.

The construction form of the single storey factory featured a column-free, steel frame spanning between load bearing walls. The walls were approximately 5 meters high and were constructed of reinforced masonry. The fuel load of the building was very high (in excess of 1200 MJ/m^2) as most of the contents were plastic products.

After the fire, the plastic skylights had melted and the roof had collapsed. The purlins and the rafter sagged and collapsed into the building. There was slight deformation of the walls due to thermal bowing. Although the walls did not collapse in this case (due to its low slenderness ratio, H_{wu}/t_w, of approximately 30), this fire serves to show the potential of a large and destructive fire occurring in industrial buildings.

Figure 4-15: Remains of the plastics factory after the fire.

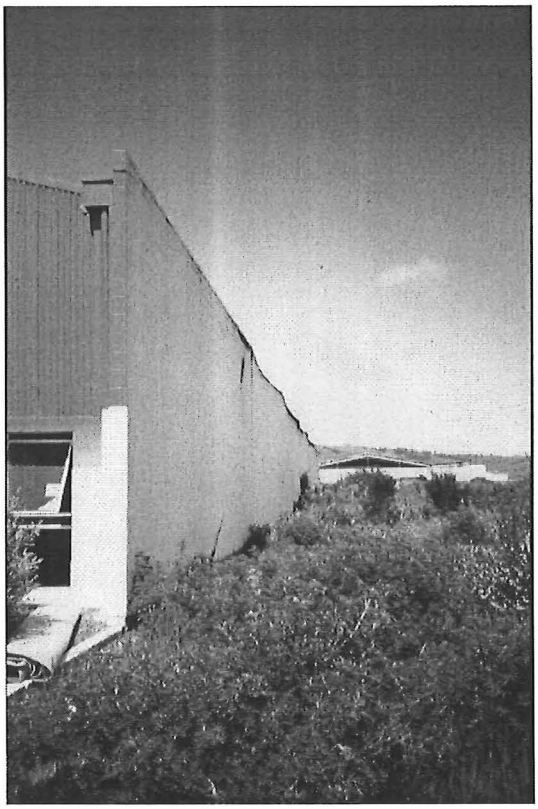

Figure 4-16: Slight deformation of the stocky reinforced masonry walls.

Other fires:

Figure 4.17: Remains of a warehouse after a fire.

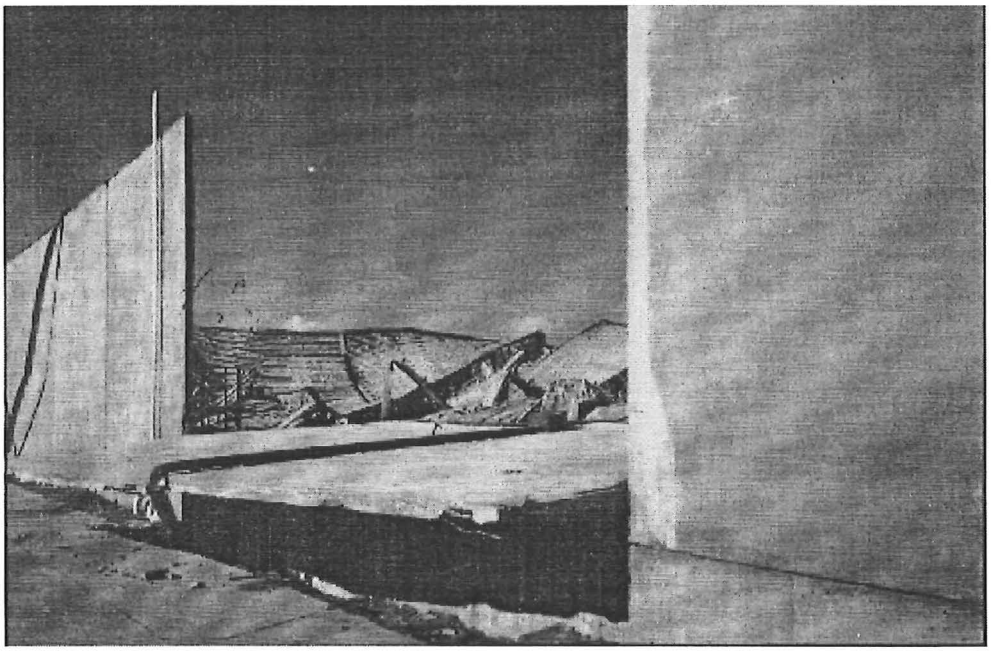

Figure 4.18: Inward collapse of a precast panel.

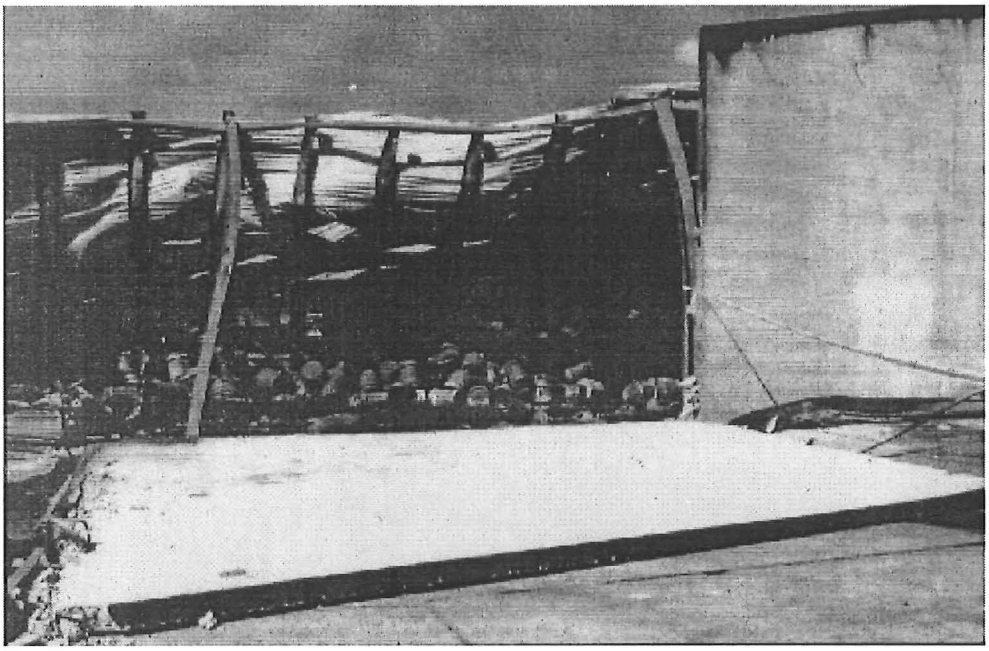

Figure 4.19: Outward collapse of a precast panel onto the neighbouring property.

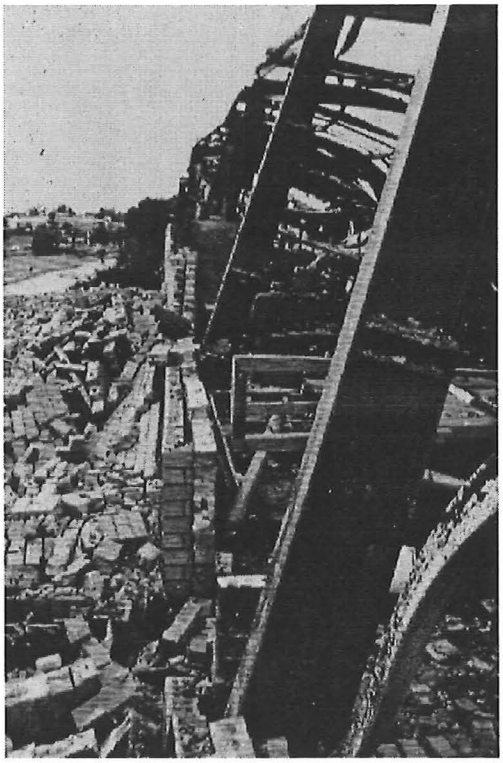

Figure 4.20: Outward collapse of brick walls due to thermal bowing.

4.4. Concrete Cantilever Walls

When a fire breaks out inside a building, the walls will be subjected to various types of forces apart from the heat-induced stresses. Apart from the thermal effects of the fire, the wall may also be subjected to wind forces occurring simultaneously. Forces may also arise from the collapse of an adjoining structure. During the initial stages of the fire, the steel-framed roof heated by fire can exert compressive forces at the top of the walls. During the later stages of the fire, the rafter will sag and will impose catenary forces. The contents inside the building may impose forces on the walls: high steel rack could collapse on the walls and gas bottles explosions can cause missile impact on the walls.

4.4.1. Thermal bowing

When one side of a structural element is heated, temperature differences will form across the thickness of the element. This will cause non-uniform thermal expansion across the section of the element, causing the wall to bow.

The theory of thermal bowing

Cooke (1987) has developed a simple theory of unrestrained thermal bowing which has been validated for metallic elements at elevated temperatures. When an unloaded and unrestrained structural element, such as a wall or slab, is exposed to a fire on one side of the wall, a temperature difference will emerge across the cross section of the element. This will cause the member to bow into a circular arc.

However, materials such as concrete and brickwork have low thermal conductivity. When a concrete or brick wall is heated on one side, the low thermal conductivity causes the thermal distribution across the section to become markedly curvilinear. The thermal gradient at the heated face of the element is steep. Hence, the selection of the temperature for calculation of thermal bowing of such elements is difficult.

Cooke (1987) has shown that the lateral deflections at the free end of a cantilever wall are four times greater than the midspan deflections of a wall pinned at both ends (refer to section 5.4). O'Meagher *et al* (1992) have stressed that cantilever walls have much lower fire

resistance than walls pinned at both ends due to the larger deflections that will develop in the cantilever walls. They have recommended that thicker sections for a cantilever wall be required to achieve the same fire resistance as a wall pinned at both ends.

Unfortunately, there is still very little information about this phenomenon, relating to the magnitude of the bowing in a building on fire. The standard fire resistance test BS 476: Part8: 1972, does not predict the thermal bowing of tall fire separating walls.

4.4.2. Experimental data

The only experiments conducted to determine the thermal bowing magnitude of walls was at the Building Research Establishment in the United Kingdom (Cooke and Morgan, 1988). Two brick wall specimens were been built into a standard furnace wall test. The walls acted as vertical cantilevers so that the tops of walls were free to move vertically and horizontally when they were subjected to elevated temperatures. Both of the walls measured 1m wide by 3m high. The thickness of the wall elements are 225mm and 337mm. The walls were heated according to the British Standard Procedure. The tests have shown that the deflections at the top of the walls can be very significant. The deflections measured 55mm for the thinner wall and 70mm for the thicker wall after being exposed to a 30-minute fire. From these tests, careful consideration should be given for thermal bowing especially in tall and slender walls.

Tests on concrete slabs have also showed that the deflections in specimens made of lightweight concrete are about one-half to two-thirds of the normal weight concrete slabs. This is due to the different coefficients of linear thermal expansion in the aggregates used.

Based on these experiments, Cooke and Morgan (1988) have made some recommendations to alleviate the thermal bowing deflections:

- Utilise construction materials with low coefficients of thermal expansion.
- Increase the thicknesses of the elements exposed to the temperatures.
- Transforming a cantilever member to simply supported elements.

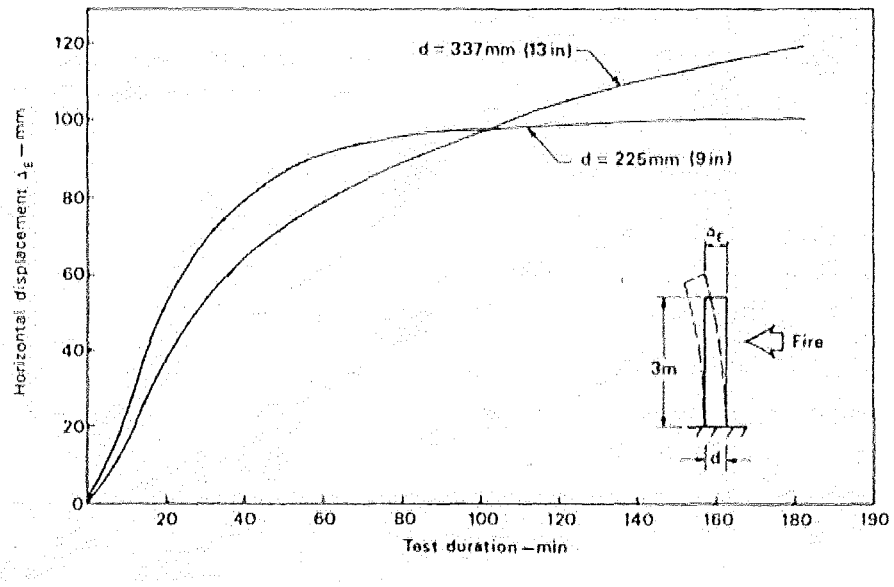

Figure 4.21: Thermal bowing of solid masonry walls (Cooke and Morgan, 1988).

4.4.3. Existing Analysis Methods of Concrete Cantilever Walls

4.4.3.1.Hand Calculation methods

Cooke (1987) has developed some simple hand methods to predict the thermal bowing deflections of elements with various support conditions. The theory has been validated for metallic elements but not for materials with low thermal conductivity such as concrete and brickwork. The details of these hand methods are described in Section 5.

4.4.3.2.Computer analysis

O'Meagher and Bennetts (1991) have developed a programme, FIREWALLS (FIre REsponse of reinforced concrete WALLS) to predict the structural performance of reinforced concrete walls subjected to fires. This programme performs the structural analysis on the wall based on the temperature history in the concrete wall, obtained from a thermal analysis programme such as TASEF-2 (Wickström, 1979). Munukutla (1988) modified FIREWALLS in order to model different restraint conditions of the walls to suit the construction practices done in New Zealand. This programme is described in detail in section **5.3**.

O'Meagher and Bennetts (1991) have performed structural analysis, using FIREWALLS, on walls that are pinned at the base and the top of the walls. These are the typical restraints found in concrete panels which are attached to steel portal frames. Munukutla (1988) has also studied the behaviour of propped cantilever walls, to simulate a wall attached to a fire resistant rafter.

O'Meagher (1994) has performed comprehensive structural analyses on walls with pinned and fixed restraints. His analyses also took into consideration the presence and absence of concrete tensile strength and P-delta effects. Apart from that, he has also performed structural analyses on portal frames with pinned and fixed restraints and different heating conditions.

There is a shortcoming of the analyses performed by Munukutla (1989) and O'Meagher (1994). The walls that they analysed have small slenderness ratios, ranging from 20 to 40, and cannot be used to accurately predict the behaviour of the tall tilt-up panels for this project.

4.4.4. Results of existing analysis methods

Cantilever walls

Munukulta (1989) has found that the deflections at the top of the cantilever walls are very sensitive to the heights and the thicknesses of the walls, i.e.: the slenderness ratio of the wall. As the slenderness ratio of the wall increases, the maximum deflections at the top of the walls increase at any given time. The time to the failure of the wall decreases with increasing slenderness of the wall. O'Meagher (1994) has performed an analysis for an isolated cantilever wall using FIREWALLS. The wall is subjected to an ISO standard fire on one face. The results of his analysis are shown in Figure 4-24. This graph emphasises the effect of the height and region of heating on the displacements of the wall. If the full height of the wall is heated, the deflections of the wall are much larger than a wall heated at the top two-thirds.

Munukutla (1989) has proposed the use of intermediate columns to reduce the effective length of the wall panels and to reduce the deflections at the top.

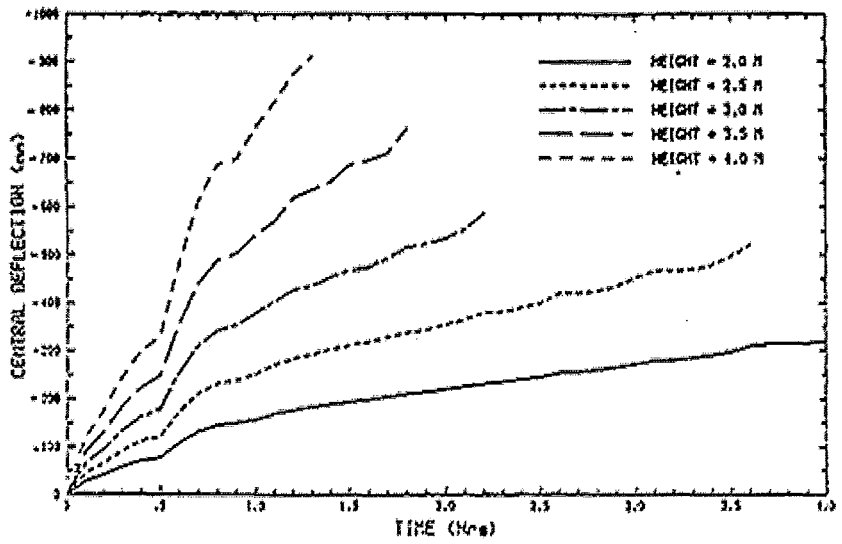

Figure 4-22: Effect of height on the performance of a 125mm thick cantilever wall (Munukutla, 1989).

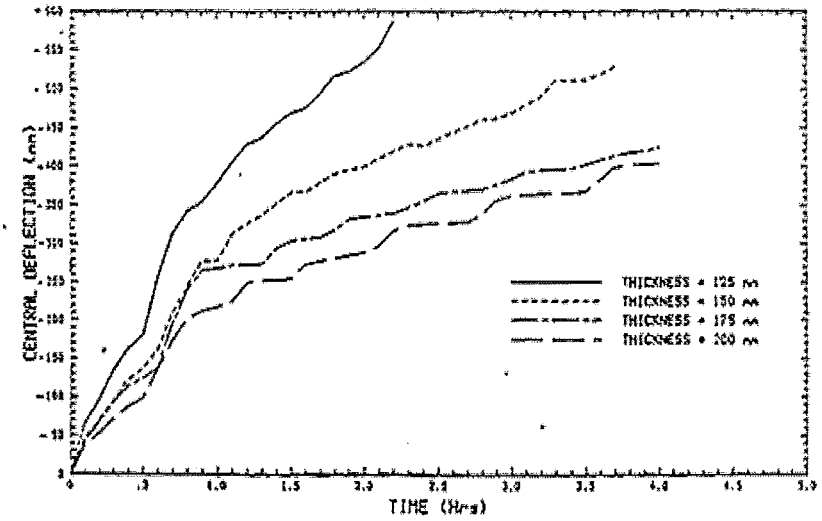

Figure 4-23: Effect of thickness on the performance of a 3000mm cantilever wall (Munukutla, 1989).

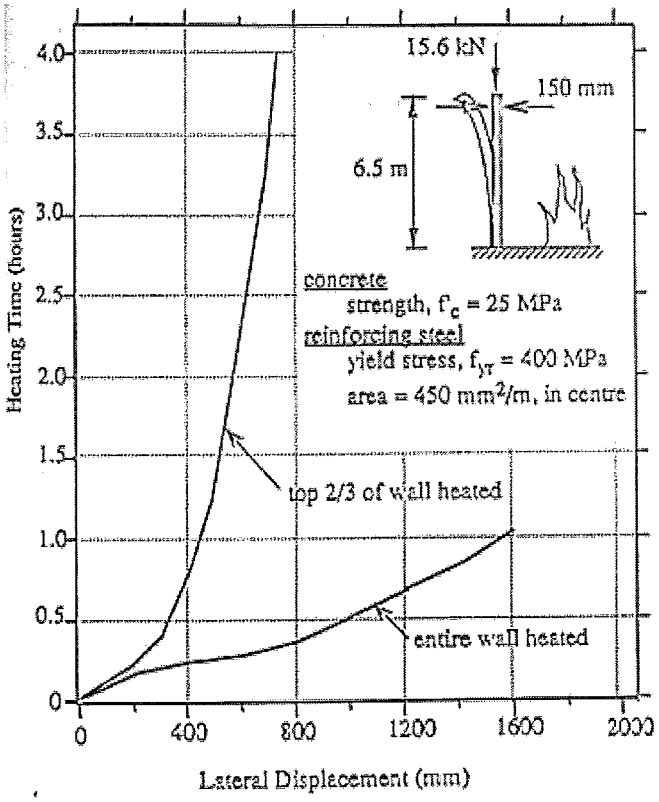

Figure 4-24: Results of analysis from O'Meagher (1994)

O'Meagher and Bennetts (1991) and Munukutla (1989) were able to derive the distributions of the different strain components in the concrete wall from their computer analysis. Figure 4-25 shows the summary of the strain distribution in the wall and the resulting actions.

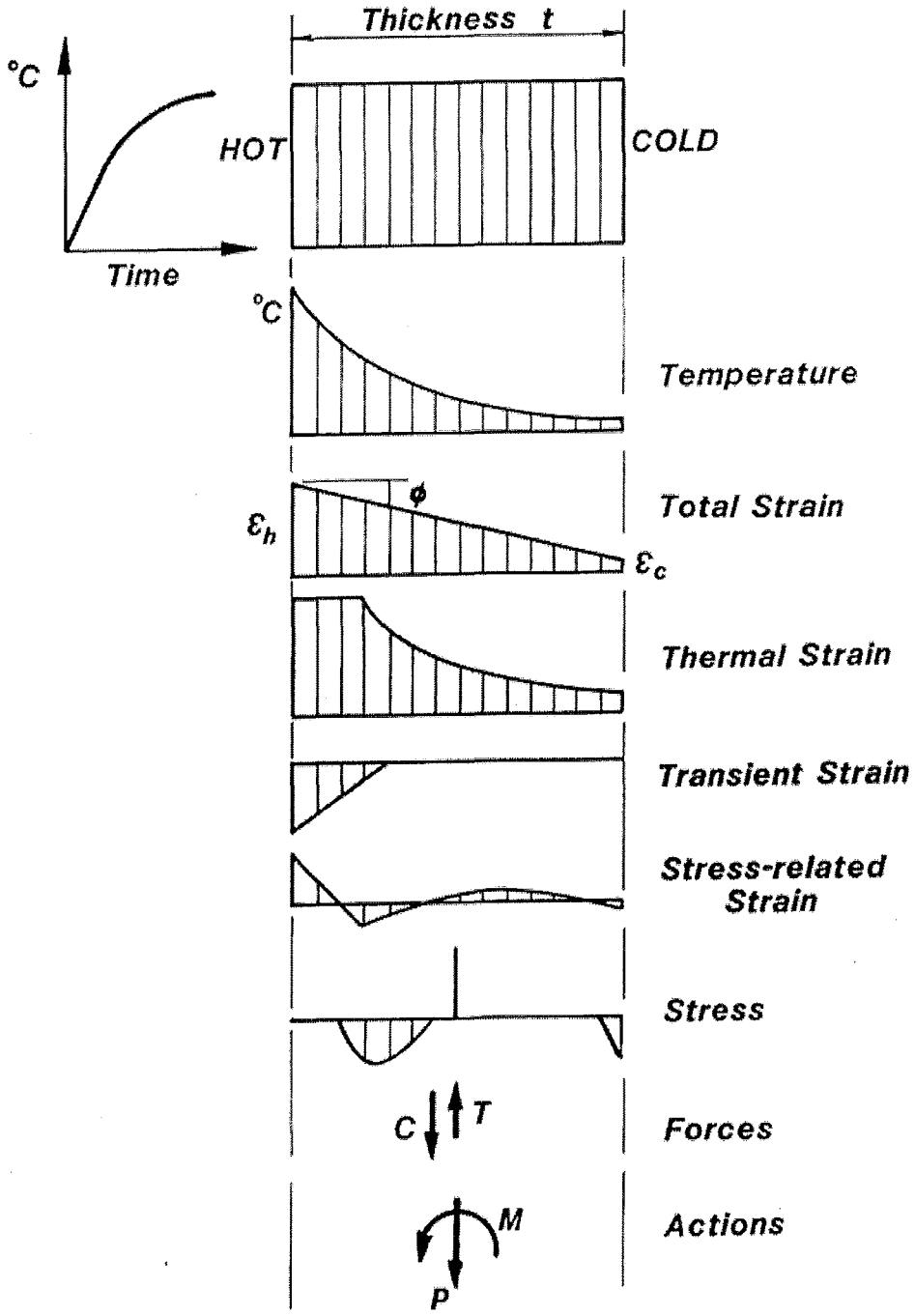

Figure 4-25: Strain components and resulting forces in a concrete wall subjected to a fire on one side (Munukutla, 1989).

Propped cantilever walls

Munukutla (1989) has also investigated the behaviour of propped cantilever walls. He has investigated the effect of the height of the wall and axial load on the horizontal reaction at the top of the wall.

As the axial load on the wall increases, the horizontal reaction of the wall increases. The increase in the axial load increases the moment capacity of the wall. Therefore, the reinforcing steel will yield at a higher moment, increasing the required horizontal reaction. The horizontal reaction of the wall decreases proportionately to the height of the wall.

The increase in thickness increases the moment capacity of the wall. Therefore, the required horizontal reaction at the top of the wall increases in order for the reinforcing steel at the base to yield.

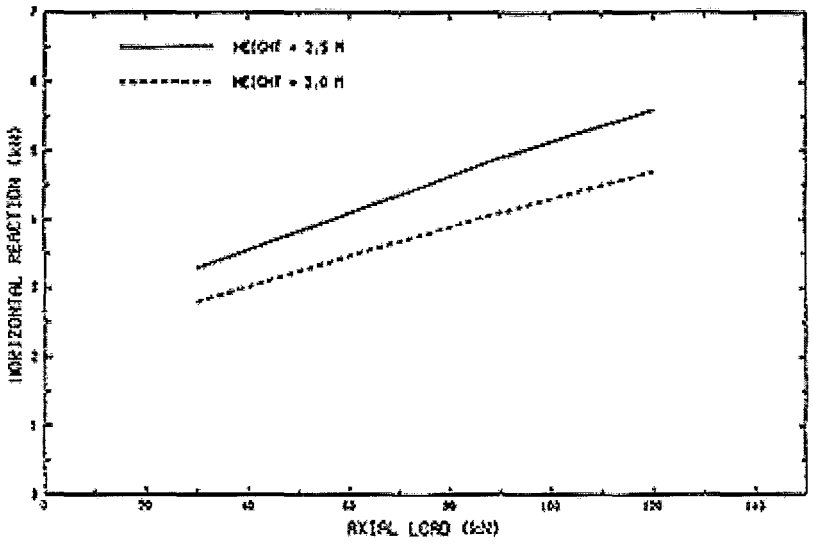

Figure 4-26: Effect of height of wall and axial load on horizontal reaction (Munukutla, 1989)

4.5. Industrial Buildings with Concrete Cantilever Walls

4.5.1. Behaviour of a frame in a fire

The behaviour of industrial buildings in fires is much harder to predict than small compartment fires. Given the nature of the migrating fire (refer to section 4.3) in a large open space building, the applicability of the ISO standard fire to the entire building may not be realistic as different parts of the building would be exposed to different heat intensities.

In a two-dimensional frame exposed to a migrating fire, one of the walls may be exposed to a severe fire, while the other wall may remain relatively cool. Thermal bowing of the heated cantilever wall will cause the frame to deform outwards. At the same time, the rafter will heat rapidly and sag. The sway of the frame, due to thermal bowing of the heated wall, is resisted by the frame components which are cooler and less affected by the fire.

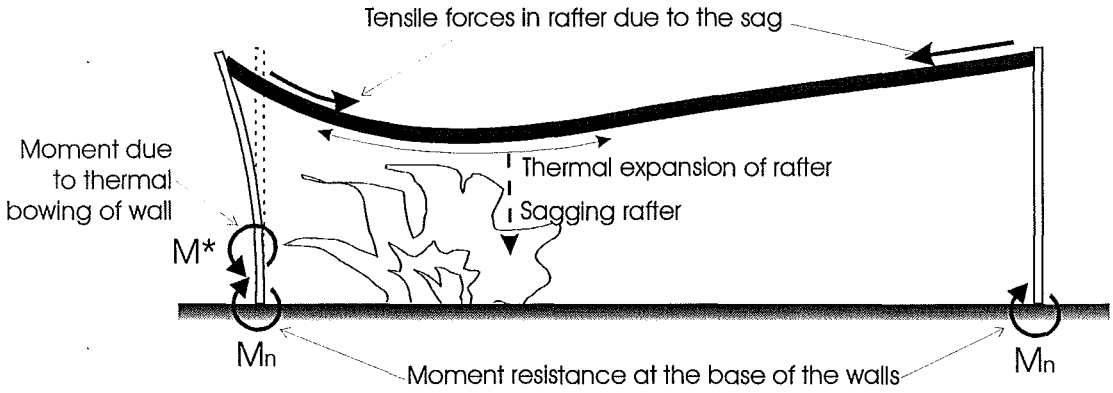

Figure 4.27: Actions and reactions on the frame at high temperatures.

During the initial stages, resistance to sway in an industrial building is provided by the "stressed skin" action of the roof. At the later stages, the P-delta effects may become too large to be resisted by stressed skin action of the roof. The cooler purlins and eaves tie members will resist these larger forces and act as catenary members between the cooler sections of the roof structure. These lateral forces will be transferred, by diaphragm action of the roof, to the side-walls acting in shear. The cooler walls can also resist the lateral deformation by out-of-plane bending.

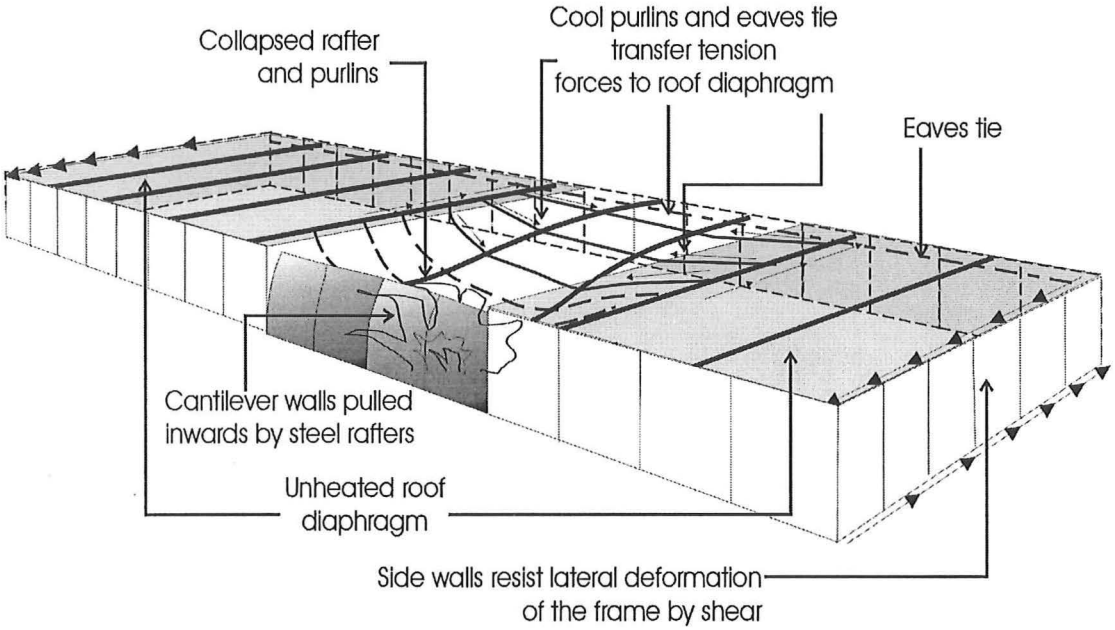

Figure 4.28: Behaviour of a frame subjected to a migrating fire.

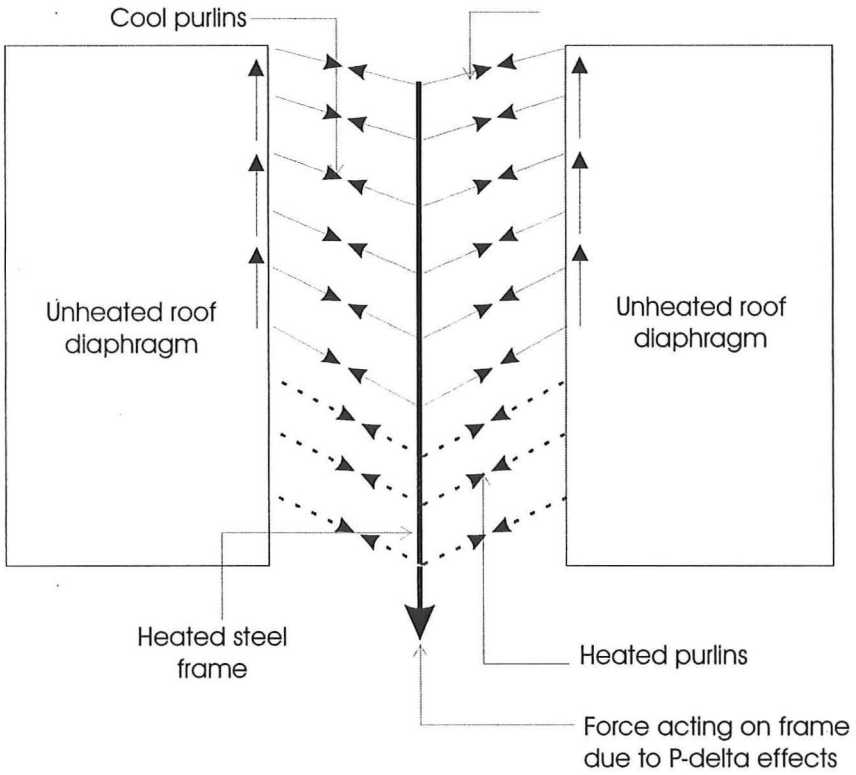

Figure 4.29: Plan view of the applied loads and reactions on part of the building (O'Meagher et al, 1992).

If there is insufficient lateral restraint from the roof and the unheated wall, the frame will collapse outwards. However, if there is sufficient lateral restraint from the roof and the unheated wall, the heated rafter would collapse, pulling the walls inwards. The latter mode of structural failure is desirable over the former, as it prevents the heated wall and rafter from collapsing outwards, damaging adjacent property and injuring people standing outside the building. O'Meagher *et al* (1992) have expressed that it is crucial that the rafter deforms downwards as quickly as possible to allow the desirable mode of failure to occur.

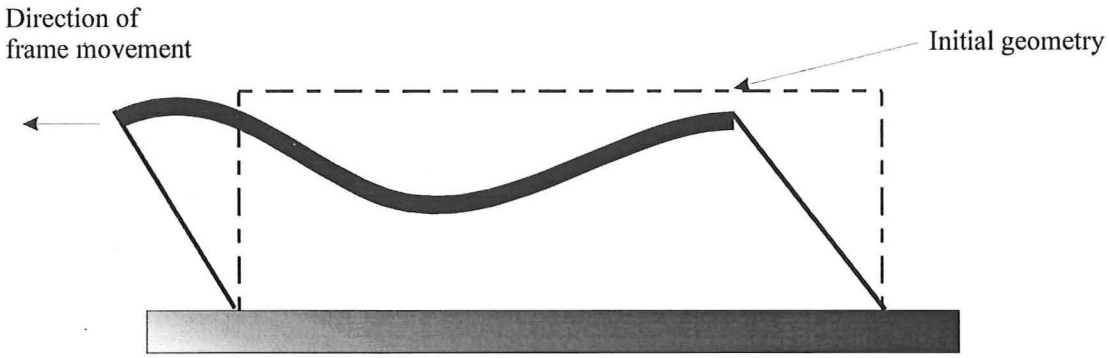

Figure 4.30: Unacceptable mode of failure of frame (O'Meagher *et al*, 1992).

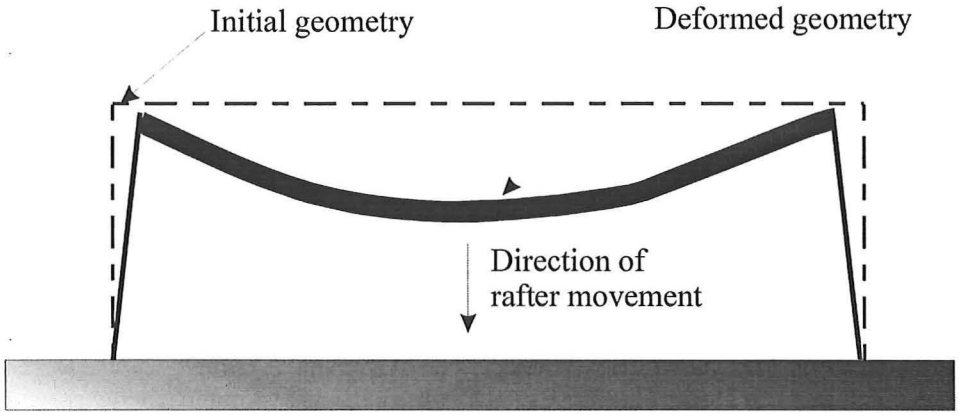

Figure 4.31: Acceptable mode of failure (O'Meagher *et al*, 1992).

As the fire spreads out from its point of origin, it will begin to affect increasing numbers of structural elements and frames. If the desirable mode of failure occurred in the first frame, then it would act as an anchor to the rest of the frames to constrain them to fail in the desirable mode. In order for this mode of failure to occur to the other frames, the steel frames

must be adequately tied together. This is achieved by providing an eaves tie to connect the wall panels together, acting together with the collapsing rafter.

In the event of a fire, the strength and stiffness of the eaves tie may be compromised. If the eaves tie fail to provide lateral restraint, these walls would behave as isolated cantilevers. The isolated cantilever walls would undergo thermal bowing when heated on one side, which could lead to the outwards collapse onto adjacent property and people.

4.5.2. Frame analyses from other researchers

O'Meagher *et al* (1992) and O'Meagher (1994) have done extensive investigations on the behaviour of two-dimensional frames subjected to fires at various locations in the structure. Their analyses were conducted using a finite element programme, ABAQUS, and FIREWALLS, which will be discussed in detail in section 5.3. Their investigations covered steel portal frames (Figure 4.2) and frames utilising concrete load-bearing walls. Their frames had concrete walls that were fixed at the base and walls that were pinned at both ends.

Their investigations have found that cantilevering the walls in a building will not ensure a desirable structural collapse and will not improve the fire resistance of the frame. The frame will collapse outwards unless there is sufficient restraint provided by the roof. When one wall in the frame is heated, the cooler wall will attract more force and subsequently crack at the base. Therefore, the stability of the structure is dependent on the heated wall. O'Meagher *et al* (1992) have emphasised the need for lateral restraint from the cooler parts of the building to ensure that the building will behave in an acceptable manner.

O'Meagher *et al* (1992) have suggested that there is no need for fire protecting the eaves members as the forces that develop in the purlins and tie members during the collapse are small. They have also suggested careful connection details between the rafter and the supporting cantilever wall. This is to avoid sudden roof collapse and to ensure that the desirable mode of failure occurs.

5. ANALYSIS METHODS

5.1. General

This chapter describes the available methods of analysis, ranging from simple hand calculation methods to computer programmes. More attention will be paid to the programme used for the analysis of this project, SAFIR.

5.2. SAFIR

5.2.1. Introduction

The structural and thermal analysis for this project was performed using a finite element computer programme, SAFIR, developed by Jean-Marc Franssen at the University of Liege, Belgium. This chapter summarises the contents of the *User Manual for SAFIR* (Nwosu, Kodur, Franssen and Hum, 1999). SAFIR is a general purpose, non-linear finite element program. It is the second generation of the structural fire models developed in the 1990's which follows an earlier program called CEFICOSS (Computer Engineering of the FIre resistance of Composite and Steel Structures) which was also developed in the 1980's at the University of Liege.

SAFIR utilises various elements for different idealisations, calculation procedures and various material models for incorporating stress-strain behaviour. The stress-strain material laws that are used include multi-linear or linear-elliptic for steel and non-linear for concrete.

SAFIR uses a step-by-step simulation to analyse the behaviour of structures. Although it was developed specifically for the analysis under fire conditions, it can also perform analysis under ambient temperatures.

5.2.2. Analysis procedure

The computer program SAFIR consists of two analysis components, which are the thermal analysis and structural analysis. The structural analysis can include torsional analysis for three dimensional beam elements whereby a section may be subjected to warping and its torsional stiffness may not be available. The behaviour of the structure is simulated as a function of time using the temperature distribution evaluated from the thermal analysis.

Step 1: Thermal analysis

The thermal analysis is performed independently of the structural analysis and needs to be carried out before performing the structural analysis. In the thermal analysis component, plane sections and three-dimensional structures can be analysed.

In the thermal analysis, heat transfer in the plane section or solid is by conduction. Heat transfer between the fire and the surface of the structure is by convection and radiation. The evaporation of moisture in the material can be modelled by modifying the thermal properties of the materials. Radiation in internal cavities of the section can also be considered in the thermal analysis.

To perform the thermal analysis, the cross-section of the element is first defined along with its material properties. This is done with a pre-processor, *SAFIR Pre-Processor Wizard98,* written by J-M. Franssen. Another pre-processor, *SAFIR Pre-Processor v0.9,* written by J. Mason is also available to perform the same function. Plane sections are discretized by triangular or quadrilateral (rectangular and non-rectangular) elements. In three-dimensional structures, they are discretized by solid elements (prismatic or non-prismatic) with six or eight nodes. The materials in the section can vary from element to element and their properties are temperature dependent. The materials such as steel, reinforced concrete and composite steel-concrete sections can be utilised to define the section. Figure 5.1 shows the pre-processor interface developed by J-M. Franssen.

In the thermal analysis, two-dimensional SOLID elements are used to define the cross section of BEAM, SHELL or TRUSS elements. At this stage, thermal calculations performed on a

three dimensional SOLID elements cannot be utilised to perform three-dimensional structural analysis.

The cross section of the element is then subjected to a time-temperature profile and analysed with *SAFIR98* to determine the thermal distribution across the cross section. The time-temperature profile applied to the thermal analysis can utilise either fire curves built into the programme (ISO 834, ASTM E119 or ULC S-101) or user-defined fire curves with decay phases. The results of the thermal analysis are stored in a data file. The results of the thermal analysis can be viewed with a post-processor, *Diamond 2000,* written by J-M. Franssen (Figure 5-2).

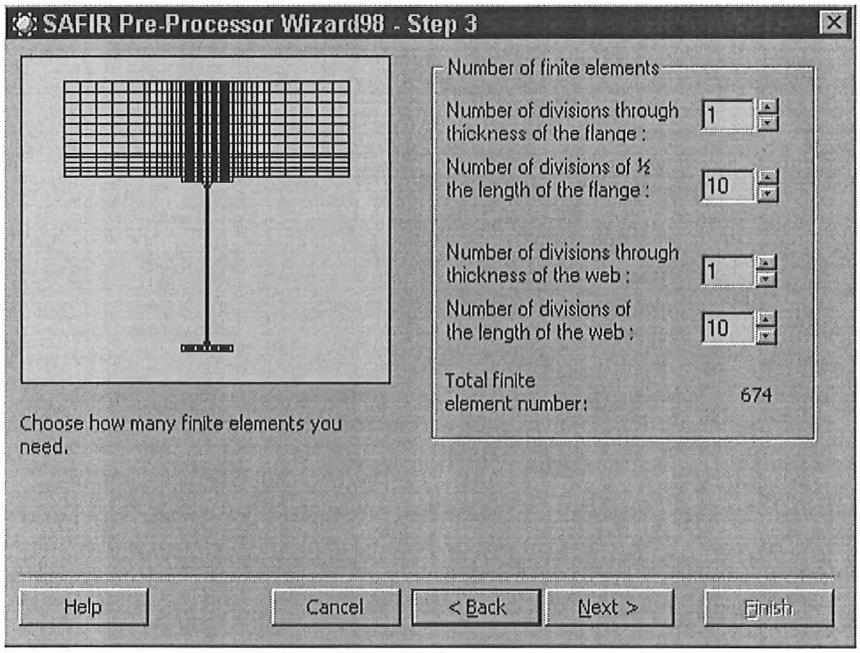

Figure 5-1: SAFIR Pre-Processor Wizard98 interface.

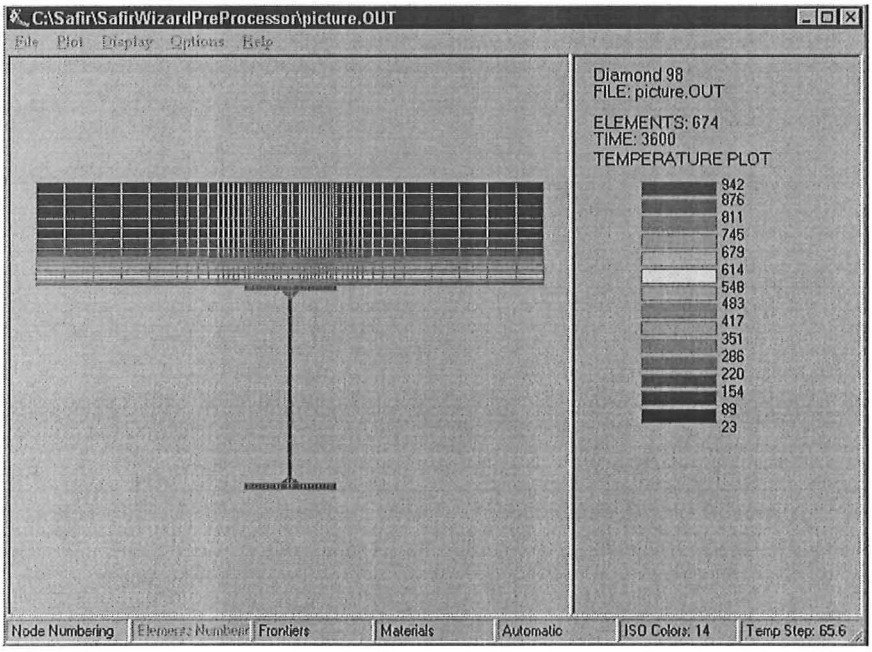

Figure 5-2: Diamond 2000 Post-processor.

Step 2: Structural analysis

In the structural analysis component of SAFIR, plane structures or three-dimensional structures can be analysed. When the temperature history in the elements of the structure is defined, the structural analysis can then be carried out. The temperature history of the elements are read from the data files and used to analyse the structure. The discretization of the structure is done with different types of elements:

i) Truss elements, made of one type of material with a uniform temperature per element.
ii) Beam elements, made of steel, reinforced concrete or composite.
iii) Solid (Shell) elements.

An iterative technique is used to find the equilibrium between the external load and the internal stress at every time step. For each iteration, the tangent stiffness matrix is evaluated and the system of equations is solved using the Newton-Raphson method. The iterations are repeated for every time step until convergence is achieved. When convergence is achieved, the following data is computed:

i) Displacements of the structure at each node;

ii) Axial and bending moments at each integration point in each element;

iii) Stresses, strains and the tangent modulus of each element in each fibre and each longitudinal integration point.

The procedure repeats successive time steps and halts when the specified final time is reached or the failure of the structure occurs (whichever occurs first). Local failure of a structural member does not lead to overall structural failure. This is dealt with by the arc length technique. Automatic adaptation of time step is possible and the structural calculation continues until failure. This means that there is no deflection criterion to make the failure point.

In the analysis, large displacements, thermal strain effects and temperature dependant non-linear materials can be taken into account. The unloading of the material is parallel to the elastic-loading branch. The program also allows the application of imposed displacements and residual stresses by means of initial strains. External supports that are used may or may not be parallel to the global axes. Nodal co-ordinates are defined in Cartesian or cylindrical co-ordinate systems.

5.2.3. Structural elements

This section describes the beam element from SAFIR that is used in the analysis of this project. The other elements that are available in SAFIR will not be described. This section is extracted from the *User Manual for SAFIR* (Nwosu, Kodur, Franssen and Hum, 1999).

Beam Element

In its undeformed geometry, the beam is a straight element. Its position and displacement in space is defined by the position of three nodes: two end nodes with three degrees of freedom per node – two translation and one rotation – and one node at mid-length to support the non-linear component of longitudinal displacement. The longitudinal displacement of the node line is a second order power function of the longitudinal co-ordinate, while the transverse displacement of the node line is described by a third order power function of the longitudinal co-ordinate.

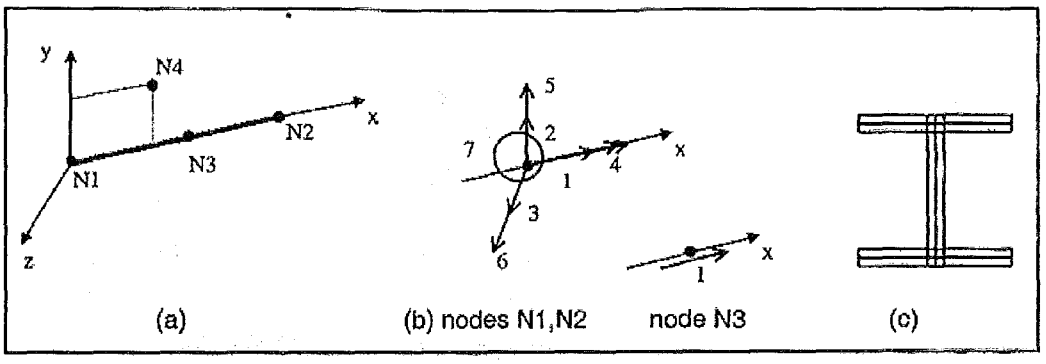

Figure 5.3: Beam element (a) Local axes (b) Degrees of freedom at nodes (c) Cross section (Nwosu, Kodur, Franssen and Hum, 1999).

The cross-section of the beam element is discretized by the fibre model, consisting of quadrilateral and/or triangular shaped elements. Each element has two or more longitudinal points of integration. At every longitudinal point of integration, all the variables such as temperature, strain and stress are uniform in each fibre. Each fibre in the beam can have its own material, allowing composite sections to be made and analysed.

There are several assumptions made in the beam element that were incorporated in the program:

i) Plane sections remain plane under bending.
ii) Shear energy is not considered as per Bernoulli's hypothesis.
iii) In the case of strain unloading, the material behaviour is elastic with the elastic modulus equal to the Young's modulus at the origin of the stress-strain curve.
iv) The plastic strain is not affected by the increase in temperature.
v) Residual stresses are considered by means of initial and constant strains.
vi) Plastifications are only considered in the longitudinal direction of the member; i.e.: uniaxial constitutive models.
vii) The non-linear portion of the strain is averaged on the length of the elements to avoid locking.
viii) Non-uniform torsion is considered in the beam element.

5.2.4. Material properties

The material models available in the SAFIR programme subroutines are available for analysis at elevated and ambient temperatures. Valid material names for the analyses at ambient temperatures are ELASTIC, BILIN and RAMBOSGOOD which represent elastic, bilinear and Ramberg-Osgood material properties, respectively. At elevated temperatures, steel materials, according to the Eurocode, are available for structural steel, reinforcing steel and prestressing steel. Concrete materials, taken according to the Eurocode and Schneider's model are available for calcareous and siliceous aggregate concrete.

Stress-strain relations of concrete and steel

The stress-strain relations for steel are multi-linear or linear-elliptic models, while the relations are non-linear for concrete. In structures exposed to fire loads, the materials are subjected to initial strains (ε_i), thermal strains (ε_{th}) and stress related strains (ε_σ). The difference between the total strain (ε_{total}) (obtained from nodal displacements and the initial and thermal strains) yield the stresses.

5.2.5. Sign Conventions

Global and local axes

The global axes are employed when defining a structure that is to be analysed with SAFIR using the Cartesian co-ordinate system. For two-dimensional (plane) problems, the axes a labelled G1 and G2, while the local axes are labelled L1 and L2. The applied force and displacements are positive in the direction of G1 and G2. The applied moments and rotations are positive in the counter-clockwise direction. (Refer to Figure 5.4)

For three-dimensional problems, the global axes are labelled G1, G2 and G3 and the local axes are labelled L1, L2 and L3. The movement is dextrorsum, the applied force and moments, displacements and rotations are all positive in the G1, G2 and G3 directions.

Stresses

The stresses are positive in tension. The axial forces are obtained as a summation of all the stresses, which are also positive in tension. The bending moments in the beam elements are obtained as the summation of $y_i\sigma_i$, with y_i measured on the local axis, L1. The moments are positive when the fibres in tension have a positive local co-ordinate.

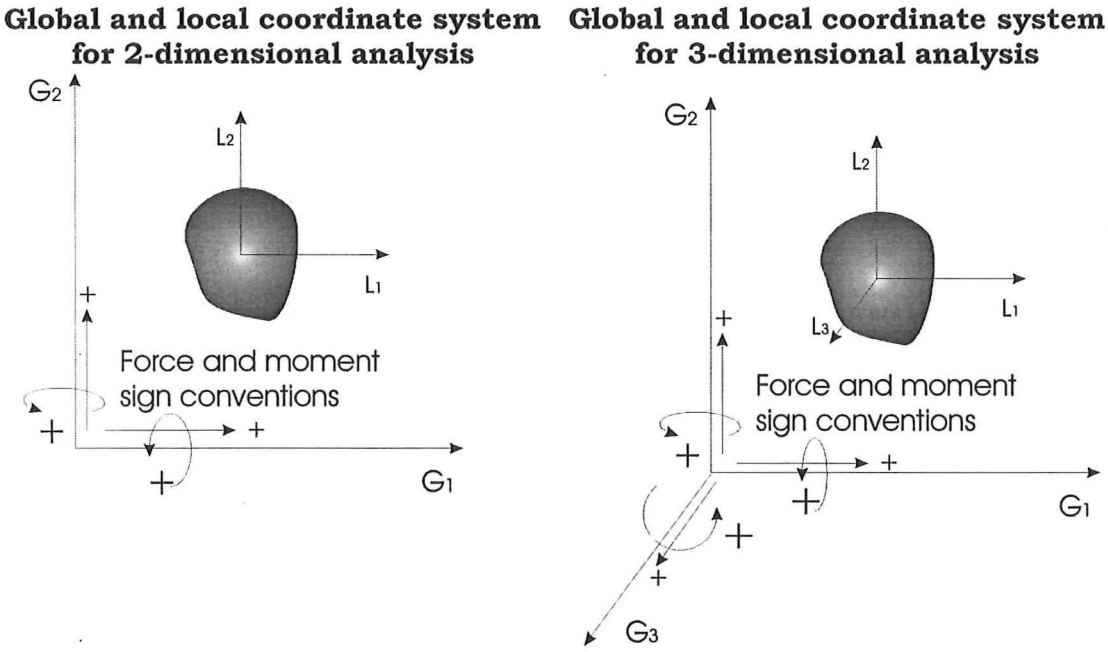

Figure 5.4: Global and local co-ordinate axes and positive sign conventions used in SAFIR

5.2.6. Common features in all analyses

In the all the different analyses, there are a few common features in all the computations.

i) Thermal and mechanical properties of steel and concrete in accordance to Eurocodes 2, 3 and 4 are embedded in the code and can be used directly.

ii) The matrix bandwidth is optimised to reduce the computer storage and calculation time. This is done by using an internal re-numbering of the system equations, which is transparent to the user.

iii) Mater-slave relations can be used to impose the same temperature or displacement at two different nodes.

iv) Graphical post-processing capabilities can be done by the post processor (DIAMOND98).

5.3. FIREWALLS

FIREWALLS is a structural analysis programme built to analyse the behaviour of concrete walls subjected to elevated temperatures. This programme was originally developed by O'Meagher and Bennetts (1991) and later modified by Munukutla (1989) to suit the wall construction practices in New Zealand. The original programme was written to read temperature data generated by the computer programme, TASEF-2, developed by Wickström (1979). The programme was modified to read the temperature data of the finite-difference computer programme, HEAT, developed by Munukutla (1989). The flow chart below describes the overall analysis procedure taken by Munukutla (1989).

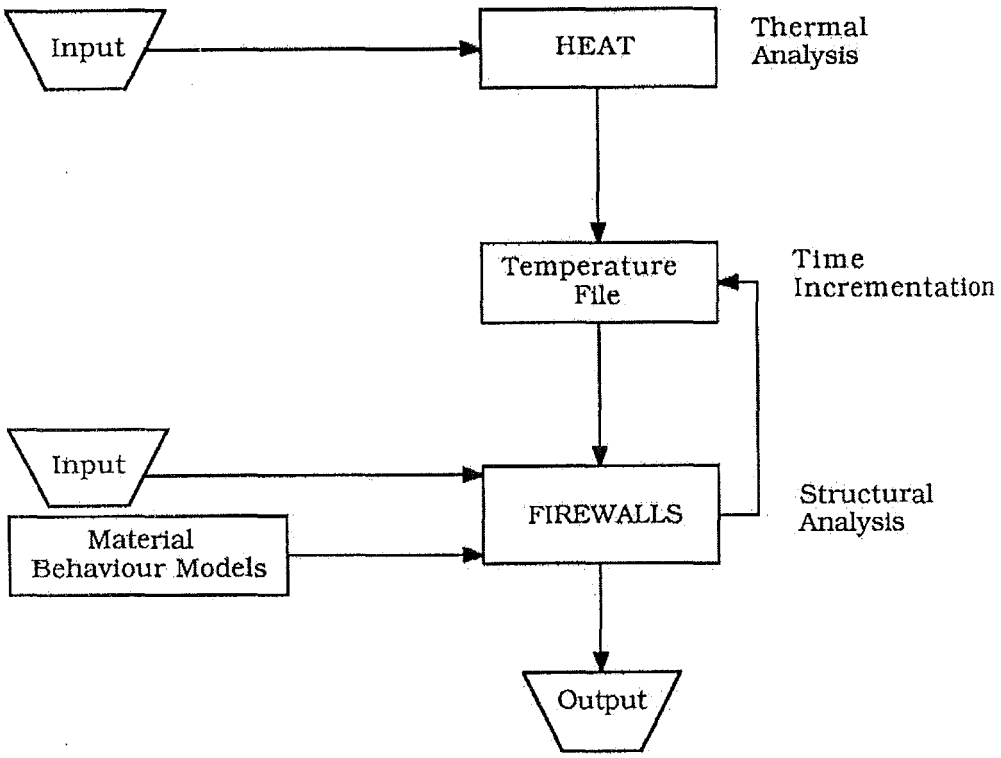

Figure 5.5: Macro flowchart of the overall analysis procedure (Munukutla, 1989)

5.3.1. Discretisation of wall

The wall of unit length is divided into a number of segments throughout its height. Each segment is then identically divided into a number of transverse elements across its thickness. This is shown in Figure 5-6.

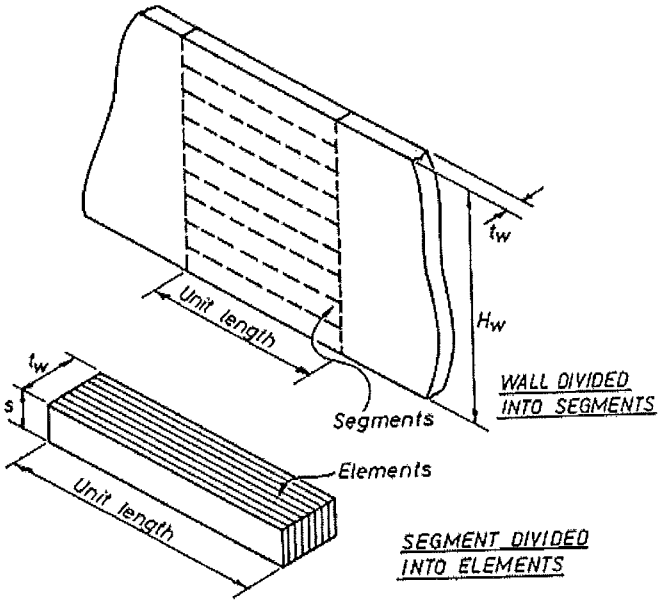

Figure 5-6: Discretisation of the wall (Munukutla, 1989).

5.3.2. Strain state in a segment

The strain state in a segment assumes that the deformations of the elements is such that plane sections remain plane. The deformation behaviour of the concrete and steel under elevated temperatures is derived from the constitutive equations derived by Anderberg and Thelandersson (1976).

5.3.3. P-delta effects

In order to allow for P-delta effects, it is necessary to calculate the lateral displacements of the wall at each segment boundary. From the curvatures of the wall at each segment boundary, the deflected shape of the wall can be determined (Refer to Figure 5-7).

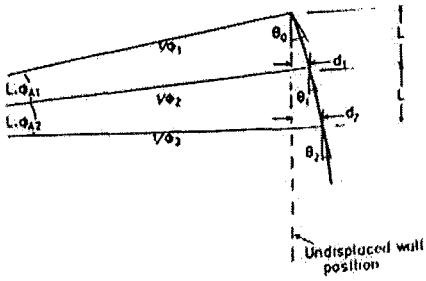

$$\left.\begin{aligned}\phi_{A1} &= \frac{1}{2}\left(\frac{1}{\phi_1}+\frac{1}{\phi_2}\right)\\ d_1 &= L\theta_0 - \frac{L^2\phi_{A1}}{2}\\ \theta_1 &= \theta_0 - L\phi_{A1}\end{aligned}\right\}\ \text{First segment}$$

$$\left.\begin{aligned}\phi_{A2} &= \frac{1}{2}\left(\frac{1}{\phi_2}+\frac{1}{\phi_3}\right)\\ d_2 &= d_1 + L\theta_1 - L\phi_{A2}\\ \theta_2 &= \theta_1 - L\phi_{A2}\end{aligned}\right\}\ \text{Second segment}$$

ϕ_n = curvature at segment boundary, n; L = segment length; and θ_n = slope at segment boundary, n.

Figure 5.7: Procedure for displacement calculation (O'Meagher *et al*, 1991)

5.3.4. Equilibrium requirements

Within a segment, the curvature is considered to be constant and a resultant strain (and therefore stress) state at a boundary can be determined by satisfying the following equilibrium conditions shown in Figure 5.8.

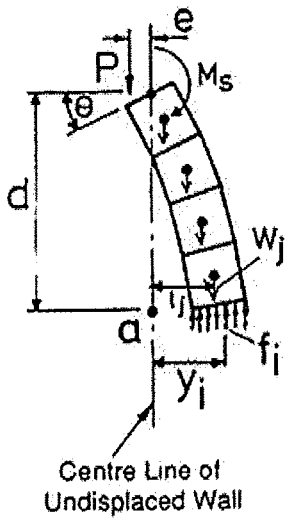

$$\sum f_i = P$$

$$\sum f_i y_i - \sum W_j I_j - M_s(H-d)/H + P.e = 0$$

Where:

P = applied vertical load

M_s = spring moment

$f_i y_i$ = element force x moment arm

H = height of wall

WjIj = self weight of wall x moment arm.

e = eccentricity of applied load

d = distance from *a* to location of spring

Figure 5.8: Equilibrium equations of the wall (O'Meagher *et al*, 1991)

5.3.5. Time steps

Since the material properties vary with temperature and time, an incremental analysis procedure is adopted to evaluate the structural behaviour. The time steps taken by both O'Meagher and Bennetts (1991) and Munukutla (1989) are shown below:

Time Range (Hr)	Time step increment (Hr)
0 to 1	0.01
1 to 4	0.1

5.3.6. Solution procedure

For each time step, each segment boundary down the wall is analysed in turn (refer to Figure 5.8). A set of total compatible strains is proposed for the concrete and the steel elements. The stress-related strains for the concrete and the steel elements are then obtained using the stress-strain laws modified for the element temperatures.

Equilibrium at the segment boundary is checked to determine whether the proposed strain state is valid. If equilibrium is achieved, then the next segment boundary down the wall is analysed for the current time step. If there is no equilibrium, a new set of total strains is proposed. When a set of proposed total strains which satisfy equilibrium cannot be found, then the wall is regard to have failed. Once a solution has been obtained satisfying both equilibrium and boundary conditions, the P-delta effects are considered and the calculations above are repeated.

5.4. Hand Calculation methods

Cooke (1987) has developed some simple equations to predict the thermal bowing deflections of elements with various support conditions. The theory has been validated for metallic elements but not for materials with low thermal conductivity such as concrete and brickwork.

Figure 5.9 shows the deflections due to thermal bowing for a simply supported beam. The deflection at the midspan of the beam is given as:

$$\Delta_M = \frac{\alpha \, H_{wu}^{\,2} (\Delta T)}{8 t_w}$$

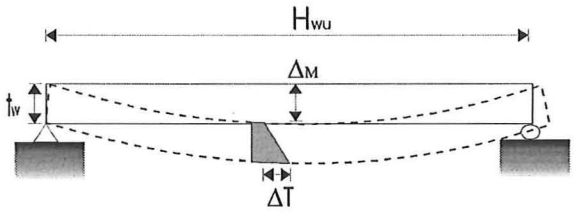

Where: ΔT = Temperature difference between heated face and unheated face

α = Coefficient of linear thermal expansion

t_w = Thickness of wall

H_{wu} = Unsupported length of member

Figure 5.9: Thermal bowing deflections of a simply supported beam (Cooke and Morgan, 1988)

The equation assumes that the coefficient of thermal expansion, α, does not vary greatly with temperature. This equation has been proven to be valid for steel members with both linear and curvilinear temperature profiles.

The deflection due to thermal bowing of a cantilever member is given as shown in Figure 5.10. The deflection at the free end of the cantilever member is given as:

$$\Delta_c = \frac{\alpha \, H_{wu}^{\,2} (\Delta T)}{2 t_w}$$

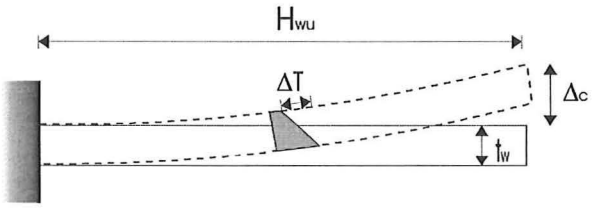

Figure 5.10: Thermal bowing deflections for a cantilever member (Cooke and Morgan, 1988).

An element that is fixed at both ends would deflect laterally when it is heated on one side, bowing into a circular arc. Cooke (1987) has shown that the deflection Δ_N, normal to the bar is given by:

$$\Delta_N = H_{wu}\sqrt{0.375\alpha(\Delta T)}$$

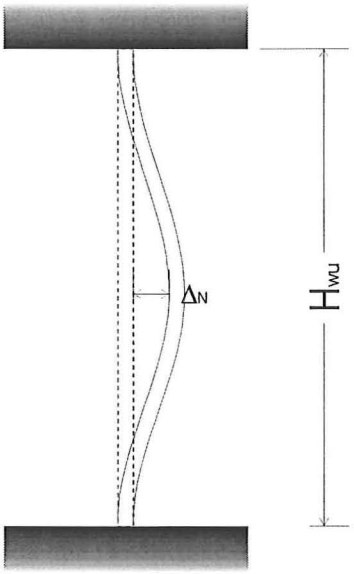

Figure 5.11: Thermal bowing deflections for an element fixed at both ends.

The comparison of Figure 5.9 and Figure 5.10 show that the deflection at the free end of a cantilever member is four times larger than the midspan deflection of a simply supported member of the same length.

Cooke (1987a) has suggested the possibility of using the above equations for materials such as concrete and bricks. This is provided the coefficient of thermal expansion is independent of temperature and the temperature at the heated face can be determined.

Cooke, Virdi and Jeyarupalingam (1996) have derived a simple theory to predict thermal bowing deflections for walls which are higher than test data. The predicted deflections Δ_P, of a wall with a height H_p, can be predicted from the measured deflections Δ_M, of a wall with height H_M.

$$\Delta_P = \Delta_M \left(\frac{H_P}{H_M} \right)^2$$

6. FREE STANDING CANTILEVER WALLS

6.1. Introduction

In this chapter, the behaviour of free-standing concrete cantilever walls will be analysed with SAFIR. Free-standing cantilever walls represent the lower bound performance of the wall panels as they are not horizontally restrained at the top. Particular attention will be paid to walls with slenderness ratios in excess of 50. The sensitivity of the quantity of reinforcing on the behaviour of the walls will also be investigated. The walls will also be exposed to different fire curves, with and without decay rates. The next chapter will describe the behaviour of propped cantilever walls.

6.2. Thermal and stress distribution

The thermal and stress distribution in a wall when it is subjected to a fire on one side is determined in this section.

Structural model

To determine the thermal and stress distribution, a 2 meter high wall with a 150mm thick section and 0.67 percent reinforcing is modelled. The wall is formed with beam elements and is subjected to the ISO standard fire on one side. The structural model and the section of the wall used for the analyses to represent the wall are shown in Figure 6.1 and Figure 6.2, respectively. The distribution of the temperatures and stresses are obtained from the output file from SAFIR. The stress distributions are analysed for different conditions and are summarised in Table 6-1.

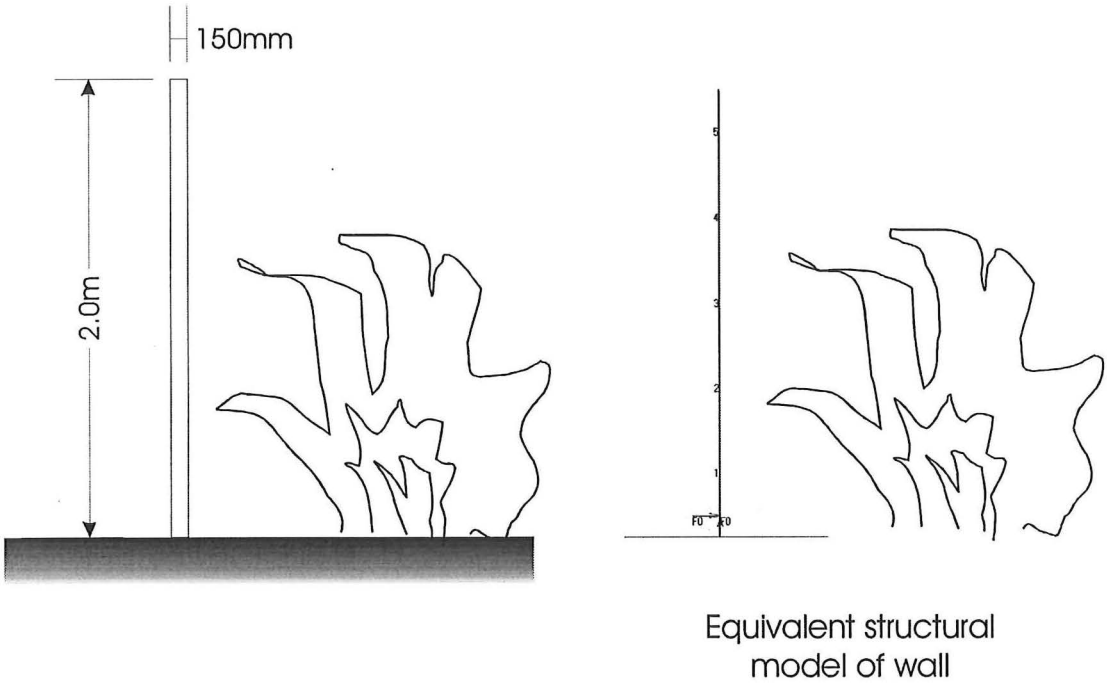

Figure 6.1: Representation of wall with SAFIR.

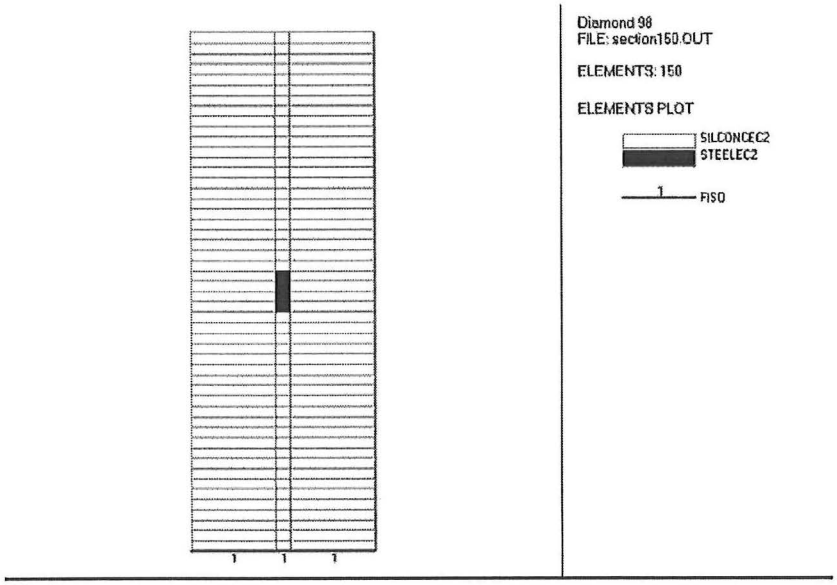

Figure 6.2: Section of the wall used in the structural modelling.

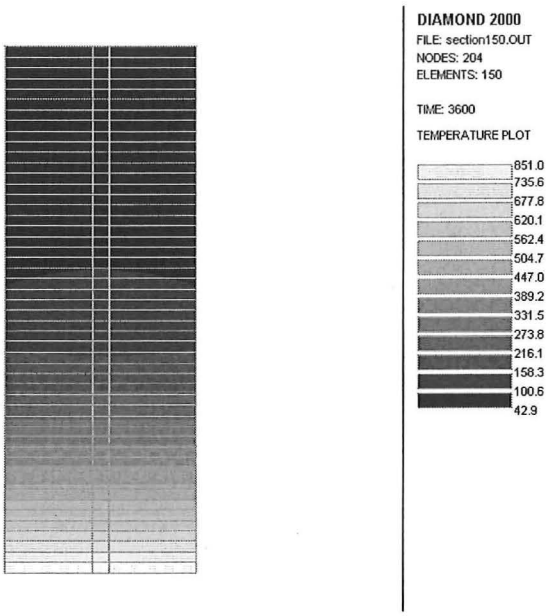

Figure 6-3: Thermal distribution of the wall after exposed to the ISO fire for 60 minutes.

Unless stated otherwise, the geometric and material properties used in the analyses are shown below:

Height of wall, H_w:	2.0m
Thickness of wall, t_w:	150mm
Unit width of wall, L_w:	55mm
End conditions:	Fixed at the base
Concrete model:	Siliceous aggregate concrete according to the Eurocode, EC2 (1995)
Concrete compressive strength, f'_c:	30.0 MPa
Concrete tensile strength, f'_t:	2.7 MPa
Concrete Poisson's ratio, ν_c:	0.15
Concrete density, ρ_c:	24.0 kN/m^3
Concrete elastic modulus, E_c:	18.0 GPa
Steel model:	Eurocode, EC2 (1995)
Reinforcing steel quantity:	1005mm^2/m, 0.67% in the middle of the section
Reinforcing steel elastic modulus, E_s:	210.0 GPa

Reinforcing steel yield strength, f_y: 430.0 MPa

Reinforcing steel Poisson's ratio, ν_s: 0.30

Steel density, ρ_s: 78.50 kN/m^3

Analysis	Reinforcing	Load
i)	Yes	Self-weight
ii)	No	Self-weight
iii)	No	Self-weight & $N^* = 0.1A_g f'_c$

Table 6-1: Stress analysis cases

6.2.1. Thermal distribution in concrete walls

Figure 6.4 shows the comparison of the results of the thermal analysis from SAFIR, with the results obtained from an experimental test performed by the Building Research Association of New Zealand, BRANZ, on siliceous aggregates (Wade, 1992). The concrete model for siliceous aggregates used in SAFIR is based on the Eurocode (EC2, 1995). The thermal analyses from SAFIR and BRANZ show that the temperature profiles across the section are in close agreement.

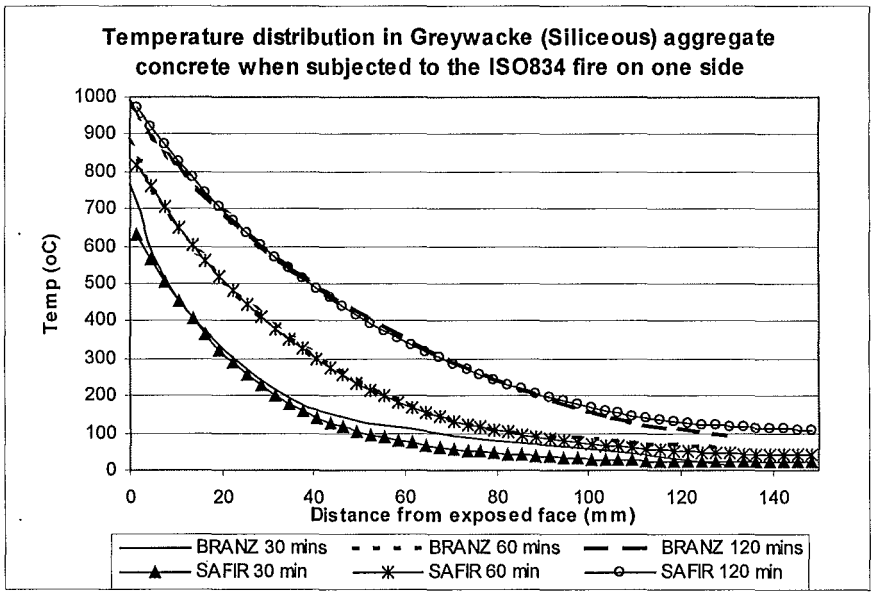

Figure 6.4: Comparison of thermal distribution across a concrete wall made with siliceous aggregates subjected to the ISO 834 standard fire.

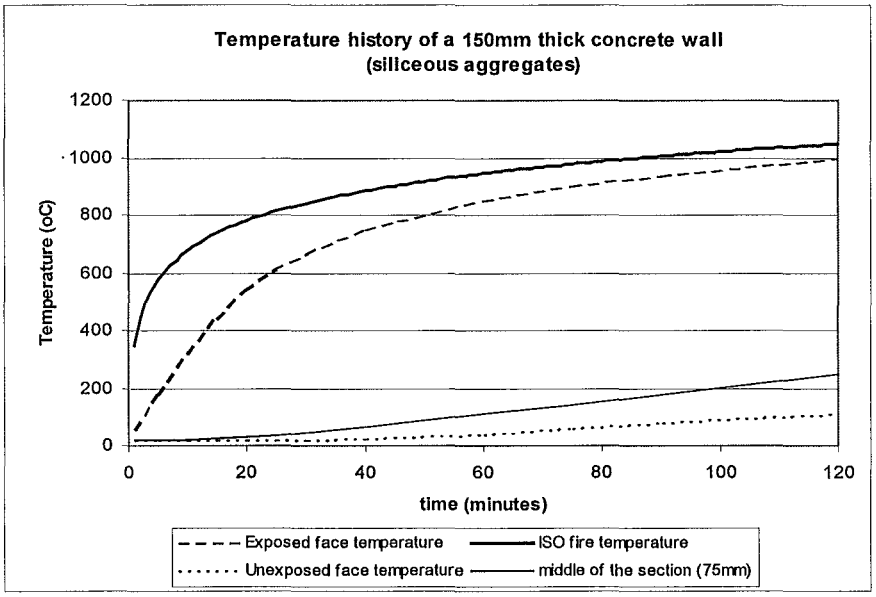

Figure 6.5: Variation of temperatures from the SAFIR thermal analysis of a 150mm concrete section subjected to the ISO fire.

6.2.2. Stress distribution in concrete walls

The following graphs illustrate the stress distribution in the concrete walls when it is exposed to the ISO standard fire on one side. The only loads applied to the wall is its self weight.

Case i): Wall with reinforcing and self weight only

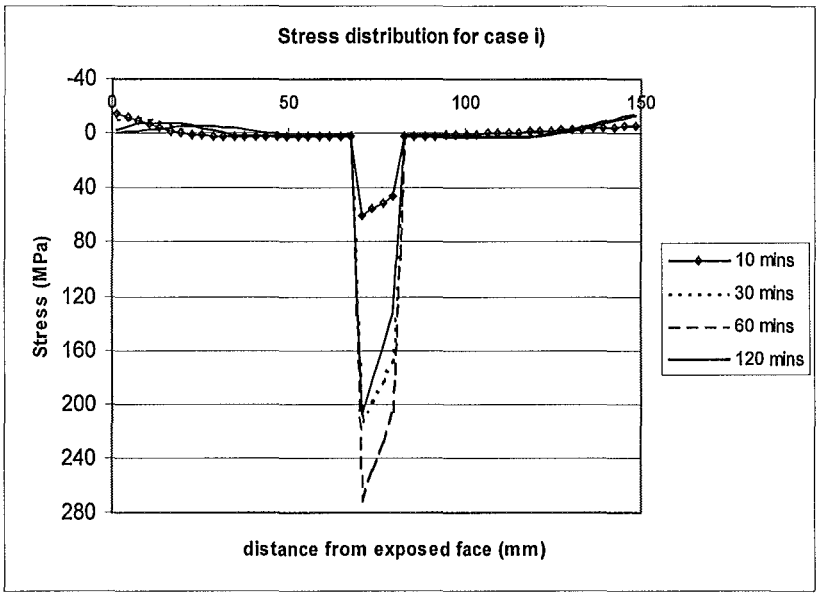

Figure 6.6: Stress distribution for case i)

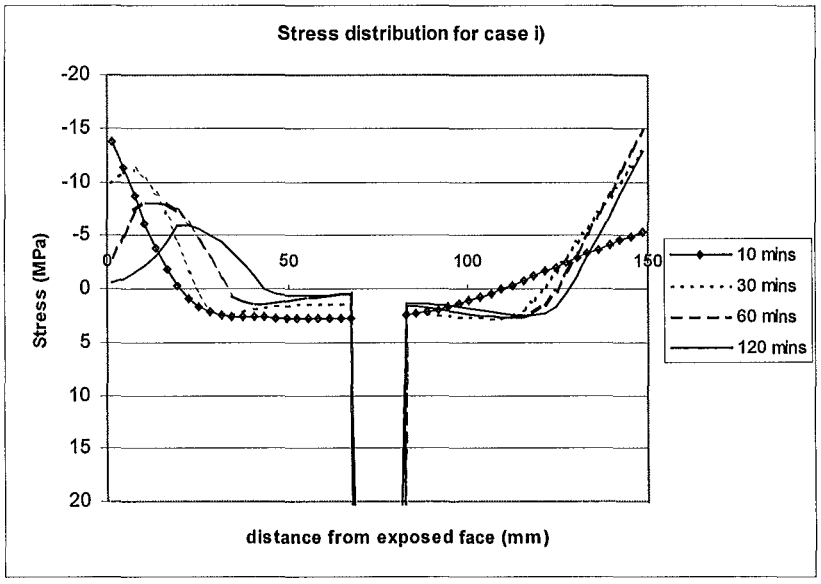

Figure 6.7: Stress distribution for case i)

Figure 6.6 and Figure 6.7 show the distribution of the stresses at the base of the wall, in both the steel and concrete, when the wall is heated on one side. Figure 6.6 shows the overall view of the stress distribution while Figure 6.7 shows the closer details of the stresses in the concrete. The tension stresses are positive and the compression stresses are negative.

Compressive stress

Figure 6.7 shows that during the initial stages (10 minutes – 30 minutes) of the fire, compressive stresses form at the heated (left) and cool (right) side of the wall. The compressive stresses at the heated face arise due to the thermal expansion of the concrete. The thermal expansion causes bending in the wall about the neutral axis. The bending is resisted by concrete tensile and compressive stresses at the cool side, and the reinforcing steel, which maintains internal equilibrium.

As the wall is progressively heated, the thermal stresses at the exposed surface of the wall decrease. However, further in from the face of the wall, the compressive stresses start to increase. At the same time, the distribution of the compressive stresses shifts inwards from the heated face and becomes broader. The redistribution of the concrete stresses is due to cracking of the concrete as the wall deforms due to bending. The reduction of the compressive stresses at the heated face is due to plastic deformation in the concrete and due to thermal effects on the concrete compressive stress. The reduction of the compressive stresses will cause a lesser deformation process.

At the cool face of the wall, the gradient of the reacting compressive stress increases and peaks at 60 minutes. At 120 minutes, the total compressive stresses reduce slightly but the gradient of the stress does not change. This slight reduction is due to the reduction of the compressive stresses at the heated face, thus reducing the resisting stresses.

Tensile stress

The tensile stresses at the heated portion of the wall grow to the limit permitted by the tensile strength of the concrete, and they subside as cracking occurs (Figure 6.7). At the unheated side of the wall, the tensile stresses in the concrete increase with time. This is due to the redistribution of the tensile stresses from the heated portion of the wall.

The stresses in the reinforcing steel (Figure 6.6) increase progressively as time increase. The tensile stress in the reinforcing steel contributes to the reaction forces from the concrete to resist the thermal stress at the heated face. At 60 minutes, the stresses in the steel peak and reduce by 120 minutes. This reduction is due to the thermal effects on the yield strength of the steel.

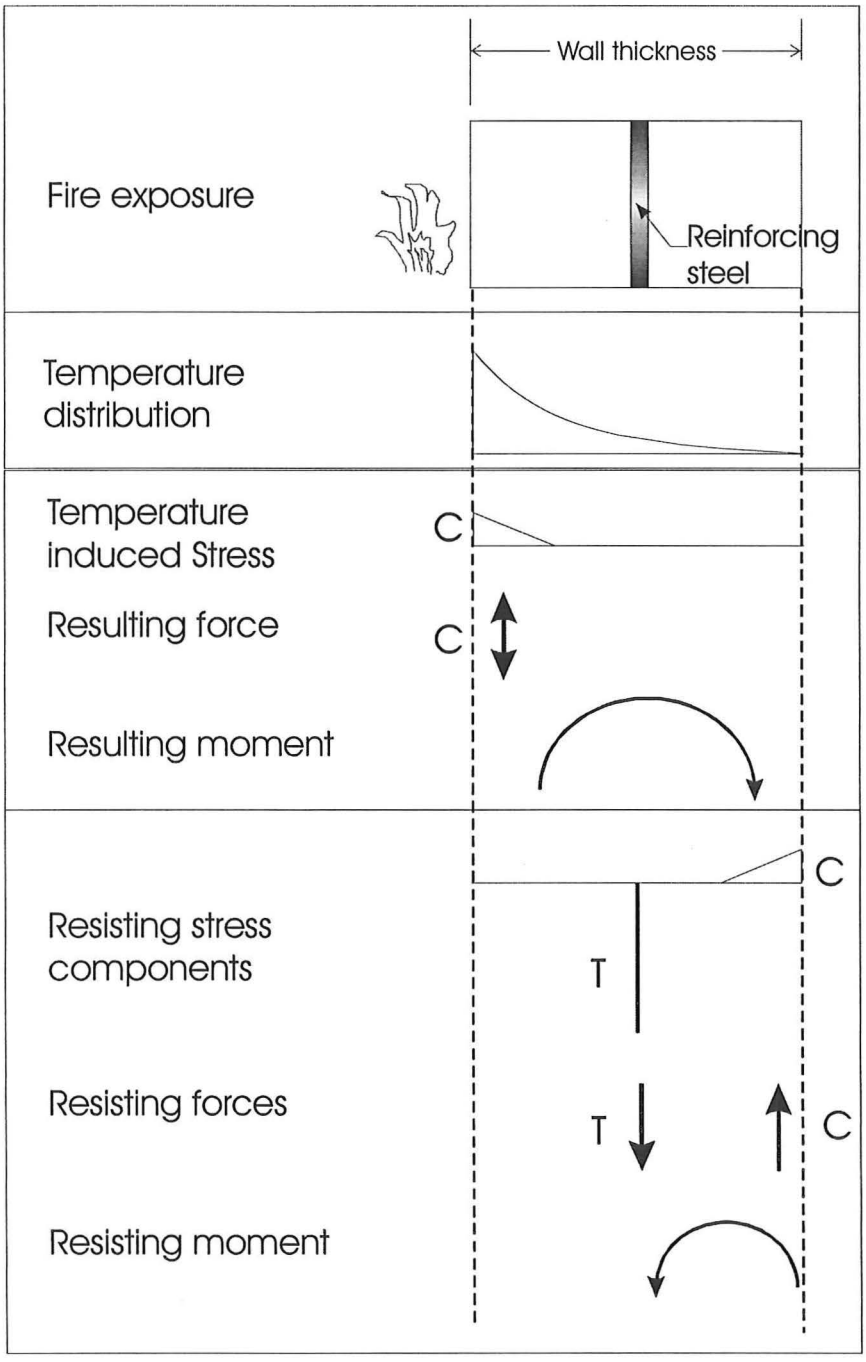

Figure 6.8: Actions and reactions due to heating on one side of a wall.

Case ii): Wall without reinforcing steel

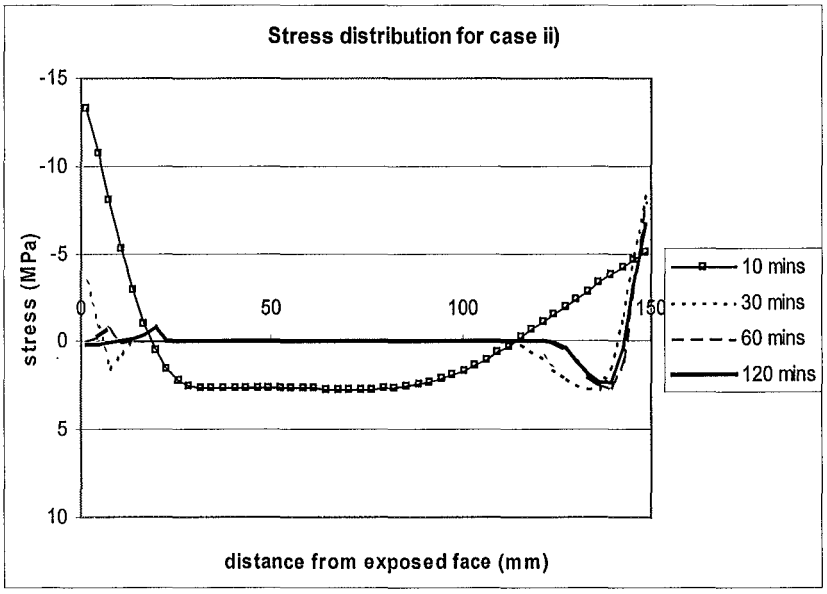

Figure 6.9: Stress distribution for case ii)

Figure 6.9 shows the distribution of the stresses in the section for an unreinforced concrete wall. As the wall is heated on one side (left side of the graph), compressive stresses build up due to the thermal expansion of the concrete. The thermal stresses cause bending in the wall element which is resisted by the concrete in compression on the cool side (right side) of the wall and the concrete in tension.

During the initial stage of the fire, the tensile stresses in the middle of the wall have reached their maximum. As the heating progresses from 30 minutes to 120 minutes, the compressive stresses at the heated face of the wall progressively decrease due to shrinkage and deformation. The strains across the thickness of the wall progressively increase as the curvature of the wall increases due to bending. As cracking in the section propagates from the left to right, the tensile stresses subside to zero. The tensile and compressive stresses at the cool side of the wall resist the bending moments imposed by the non-uniform thermal expansion across the section of the wall.

Case iii) Unreinforced wall with axial load $N^*=0.1A_gf'_c$

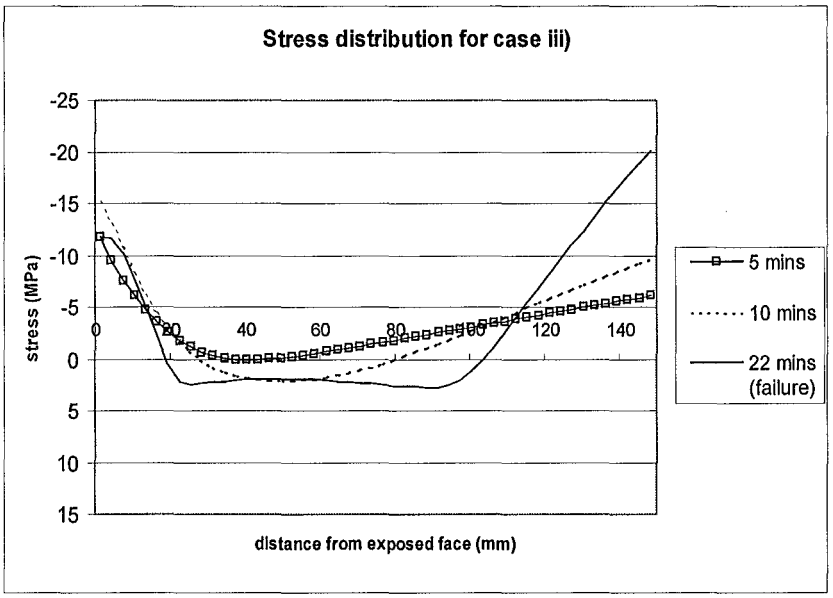

Figure 6.10: Stress distribution for case iii)

Figure 6.10 shows the distribution of the stresses in the wall when the wall is subjected to an axial load of $0.1A_gf'_c$. During the first 10 minutes, thermal stresses arise at the heated face of the wall due to thermal expansion of the concrete. The thermal stresses are resisted by compressive stresses at the cold side of the section and tensile stresses at the middle of the section. During this initial stage, the compressive stress gradient is low at the cold side and there is very little tensile resistance from the concrete. This is due to the effect of the applied axial load onto the concrete which causes the concrete to be more in compression than in tension.

As time progresses, the gradients of the compressive stresses at both the heated and the unheated sides of the wall increase. The tensile stress in the concrete also increases to resist the overturning moment caused by the thermal expansion at the heated face. At 22 minutes, failure occurs as the wall collapses due to the P-delta effect. The overturning moment due to thermal expansion and P-delta cannot be resisted by the compressive and tensile stresses in the wall, consequently it collapses.

6.3. Parameter study

This study investigates the effect of varying the parameters on the horizontal deflections at the top of the cantilever wall when it is subjected to the ISO standard fire. The parameters that will be varied are the height of the wall, the thickness of the wall and the quantity of reinforcing. The effects of P-delta and the concrete tensile strength will also be investigated.

Unless stated otherwise, the geometric and material properties adopted in the analysis are shown below. These properties are those of a typical wall that would normally be constructed in practice.

Height of wall, H_w:	10.0m
Thickness of wall, t_w:	150mm
Slenderness ratio, λ:	66.7
Unit width of wall, L_w:	55mm
End conditions:	Fixed at the base
Concrete model:	Siliceous aggregate concrete according to the Eurocode, EC2 (1995)
Concrete compressive strength, f'_c:	30.0 MPa
Concrete tensile strength, f'_t:	2.7 MPa
Concrete Poisson's ratio, ν_c:	0.15
Concrete density, ρ_c:	24.0 kN/m^3
Concrete elastic modulus, E_c:	18.0 GPa
Steel model:	Eurocode, EC2 (1995)
Reinforcing steel quantity:	1005mm^2/m, 0.67% in the middle of the section
Reinforcing steel elastic modulus, E_s:	210.0 GPa
Reinforcing steel yield strength, f_y:	430.0 MPa
Reinforcing steel Poisson's ratio, ν_s:	0.30
Steel density, ρ_s:	78.50 kN/m^3

Structural model

The section used to model the cross section of the wall is shown in Figure 6.1. Figure 6.11 shows the typical structural model used to analyse the walls in SAFIR. The model shown is for the standard 10 meter wall with a typical amount of reinforcing (0.67%) in the middle of the 150mm section. The wall is formed from beam elements and is fixed at the base. Figure 6.11 also shows the uniformly distributed self-weight of the wall. For the purpose of the parameter study, the ISO standard fire is used.

Assumptions made in the analysis

- The wall is fully fixed at the base.
- The wall is uniformly heated up its height.
- Spalling of concrete does not occur.
- There is no slippage between the concrete and the reinforcing steel.
- Failure does not occur at the foundations.
- There are no initial eccentricities in the wall due to precambering.

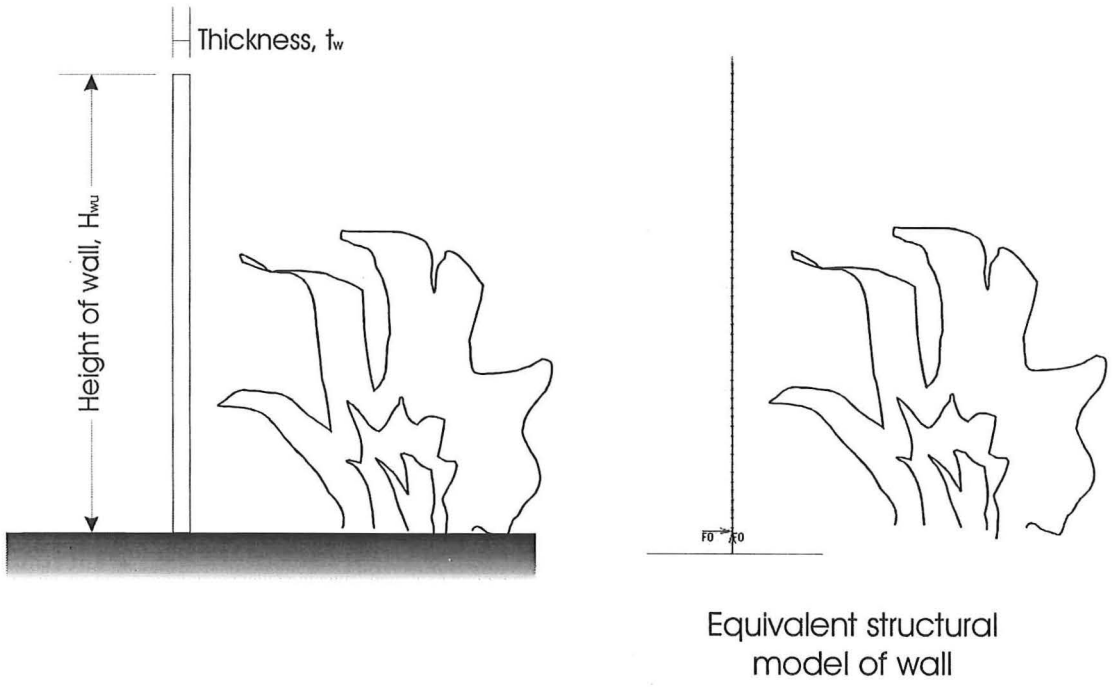

Figure 6.11: Structural model of wall used in SAFIR.

6.3.1. Height of wall

This part of the analysis investigates the behaviour of walls of different heights. Several walls of different heights and slenderness ratios, as shown in Table 6-2, are analysed. The other material and geometric properties are kept constant as stated in section 6.3. Walls with and without concrete tensile strength have also been analysed for comparison. Walls without P-delta effects are also analysed to determine the free thermal bowing of the walls.

Analysis case	Wall height	Slenderness ratio
i)	6m	40
ii)	8m	53.3
iii)	10m	67.7
iv)	12m	80

Table 6-2: Analysis cases with different wall heights

RESULTS OF ANALYSES

Figure 6.12 shows the deflected shape of a typical 10 meter wall just before collapse, after being exposed to the standard fire. The lateral deflection of the wall is due to the non-uniform thermal expansion of the wall. The corresponding bending moment diagram of the wall due to the P-delta effects is shown in Figure 6.13. It shows that the largest bending moment occurs at the base. This is the most likely location where a plastic hinge would form if flexural failure were to occur.

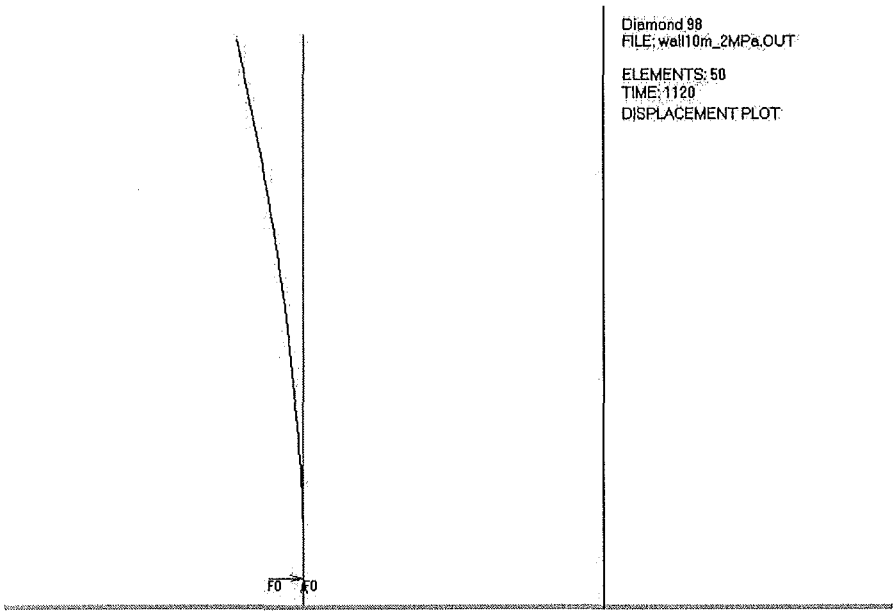

Figure 6.12: Deflected shape of the 10 m wall just before failure.

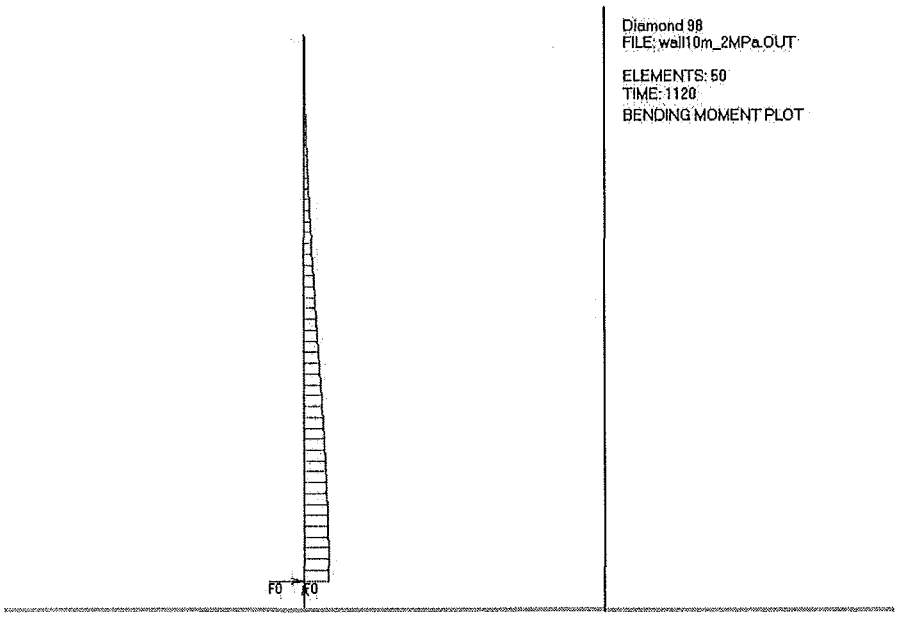

Figure 6.13: Bending moment diagram of the 10m wall.

- **Horizontal displacements at the top of the wall**

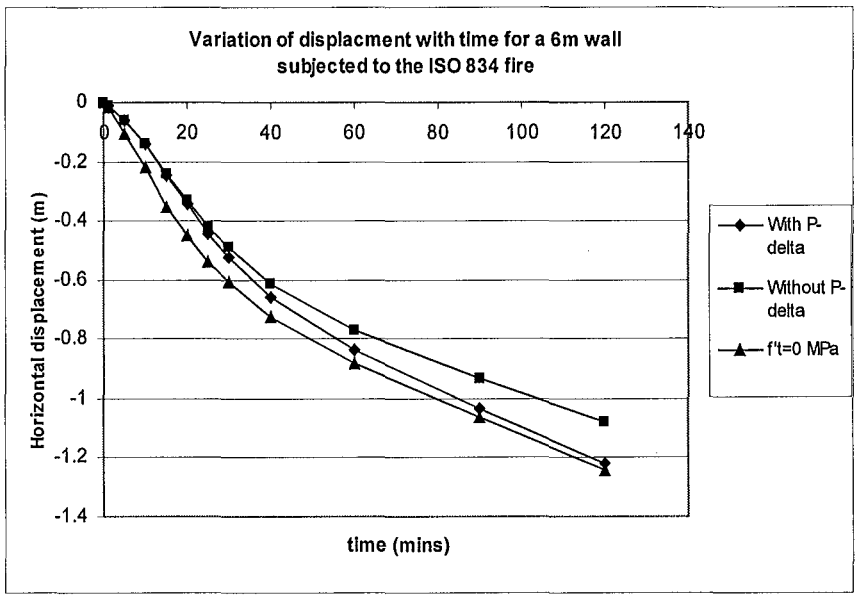

Figure 6.14: Horizontal displacement at the top of a 6m wall

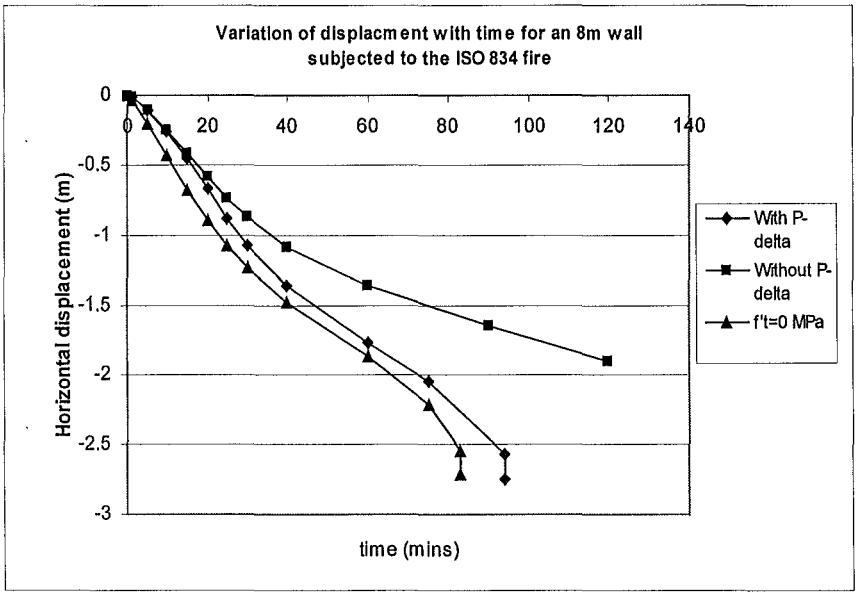

Figure 6.15: Horizontal displacement at the top of an 8m wall

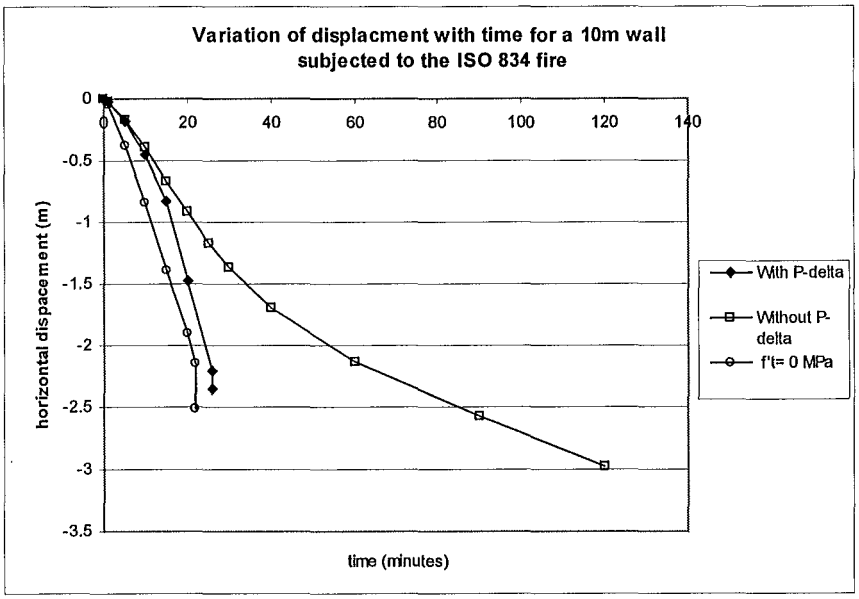

Figure 6.16: Horizontal displacement at the top of a 10m wall

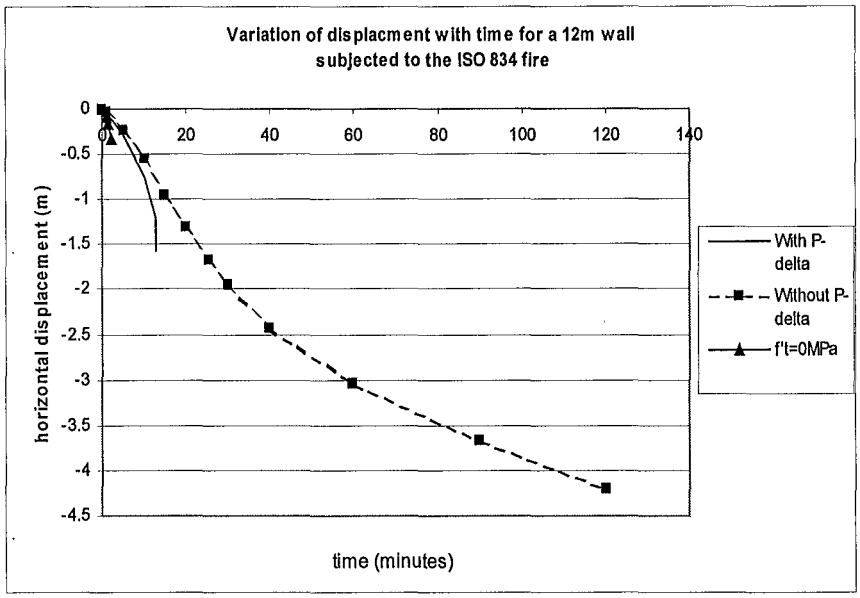

Figure 6.17: Horizontal displacement at the top of a 12m wall.

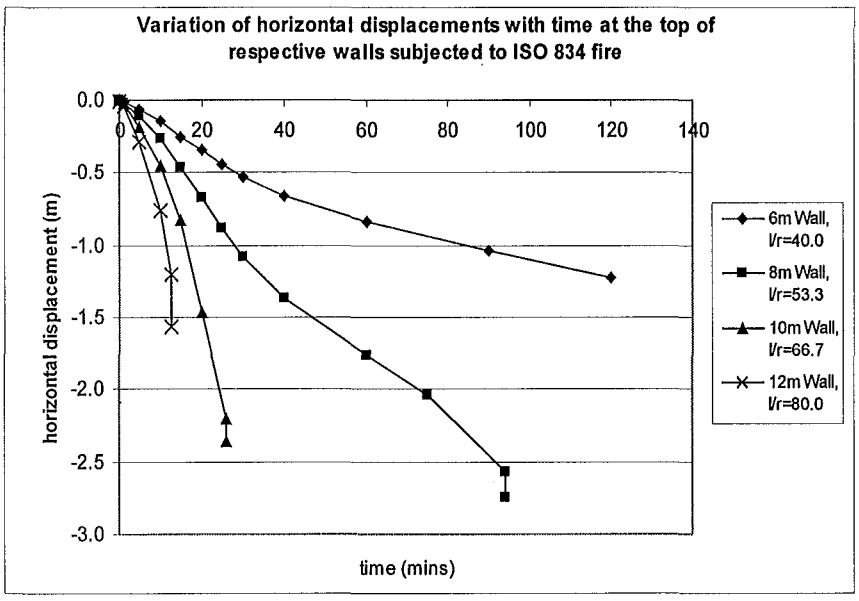

Figure 6.18: Comparison of displacements for walls of different heights.

The graphs in Figure 6.14 to Figure 6.18 show the displacements at the top of the walls with different heights. The horizontal displacements for the walls analysed without P-delta effects were solely due to the non-uniform thermal expansion of the wall. The absence of concrete tensile strength on the deflection of the walls is also investigated. The effects of both P-delta and zero concrete tensile strength are discussed in the following pages.

Figure 6.18 shows the comparison of walls with different heights subjected to the ISO standard fire. As the heights of the walls increase, the time to failure of the walls decreases. At any period of fire exposure, the displacements at the top of the walls increase with increasing wall height.

- **P-delta effects**

6 meter wall

Figure 6.14 shows that the displacements of the 6 meter wall with and without the P-delta effects are very similar. During the first 25 minutes, the displacement trends for both walls are exactly the same. From 25 minutes to 120 minutes, the P-delta effects cause the displacement trend to slowly digress from the wall without its self-weight. The displacements for both cases show that they are starting to asymptote towards a limiting displacement.

8 meter wall

The deflections of the 8 meter wall without its self weight asymptotes to approximately 1.90 meters by the end of the simulation and does not collapse. However, when the self-weight of the wall is included, the wall survives the fire only until 94 minutes when it eventually collapses. The wall deflected rapidly during the first 30 minutes of the fire, reaching 1.07 meters (Figure 6.15). Beyond this, the displacement rate becomes smaller. However, the wall collapses when the P-delta effects become too large.

10 meter wall

The wall without its self-weight managed to sustain very large displacements (approximately 3.0 meters) at the top of the wall without collapse. However, the wall analysed with its self-weight showed a runaway displacement trend and failed at about 26 minutes when the top of the wall had displaced 2.20 meters (Figure 6.16).

12 meter wall

As with the other walls, the 12 meter wall without its self weight managed to sustain very large deflections (4.2 meters at 120 minutes). However, when the self-weight of the wall is included, it collapsed very rapidly (13 minutes), shown by the sudden runaway displacement after it had bowed to 1.20 meters (Figure 6.17).

- **Concrete tensile stress**

Figure 6-14 to Figure 6-17 show the effect of the displacement of the wall when the concrete tensile strength is omitted from the analyses. If the tensile strength of concrete is omitted, the moment resistance is provided only from the steel in tension and the concrete in compression.

The presence of the concrete tensile strength reduces the deflection of the wall. The deflections are most noticeable during the initial stages of the fire. During the advanced stage of the fire (for the walls that survive), the displacements become more similar. Taking the 6 metre wall as an example (Figure 6-14), the displacements of the walls with and without concrete tensile strength become more similar as the fire exposure increases with time. For the 12 metre wall, the omission of the concrete tensile strength from the analysis is very noticeable as it fails after 2 minutes of fire exposure.

- **Bending moments at the base of the wall**

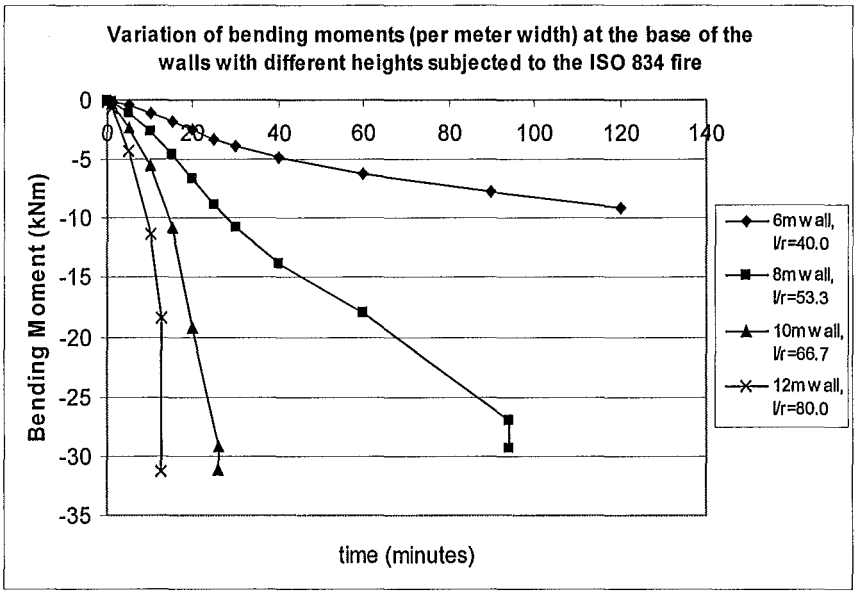

Figure 6.19: Variation of bending moments at the base of walls with different heights.

Figure 6.19 shows the variation of bending moments at the base of the walls. The trends of the bending moment with time are similar to the horizontal displacements at the top of the walls, shown in Figure 6.18. This is because of the direct relation of the displacements of the walls to the bending moments at the base of the wall.

The nominal moment of this wall section under ambient temperatures is approximately 28kNm per meter width. The diagram above shows that the bending moment at the base of the 6 meter wall does not approach anywhere near its yield moment. This means that the 6 meter wall with 0.67 percent reinforcing would not fail unless exposed to the fire for a much longer time. The 8 meter wall shows a gradual approach to its nominal moment and the wall collapses when the steel yields. The 10 meter walls shows a runaway bending moment trend until 26 minutes when the wall eventually collapses due to yielding of the reinforcing steel. The 12 meter wall shows the runaway bending moments when the wall buckles at approximately 13 minutes. The nominal moment of the section had not been reached for this wall but due to a different mode of failure, the wall collapsed as well.

DISCUSSION

This section discusses the behaviour of the walls with different heights and their modes of failure.

- **Behaviour of walls with different heights**

6 meter wall

During the initial stages, the deflections of the wall are due to thermal bowing. During the advanced stages, the P-delta effects slowly affect the displacements. The displacements for both cases asymptote towards a limiting value. The reason why the walls, with and without P-delta effects, do not collapse is due to the relatively high amount of reinforcing placed in the relatively short wall. Therefore, the flexural strength of the wall is much larger than the overturning moments due to P-delta. Consequently, the wall does not collapse.

8 meter wall

Unlike the 6 meter wall, this wall collapsed during the advanced stage of the fire. The collapse of the wall is due to a plastic hinge forming at the base of the wall when the reinforcing steel had yielded (Refer to Figure 6.19). The cause of the collapse is due to the moments from the P-delta effects. Apart from that, the flexural strength of the wall is reduced as the yield strength of the reinforcing steel is progressively reduced due to thermal effects.

When the plastic hinge formed at the base of the wall, SAFIR detected instability in the structure. This caused the stiffness matrix of the wall to became negative and SAFIR was unable to iterate to the next time step.

10 meter wall

The failure of this wall was due to a plastic hinge forming at the base when the reinforcing steel yielded (Refer to Figure 6.19). During the initial stages of the heating, the horizontal displacement was due to thermal bowing of the wall. The P-delta effects at the initial stages were small. Due to the runaway displacements, the P-delta effects increased very rapidly and caused the steel to yield. Consequently, the wall collapsed.

12 metre wall

The mode of failure of this wall is due to buckling. At the point of failure, the flexural rigidity at the base of the wall had been reduced (due to cracking of the concrete) to the point where the buckling load of the wall was reached. The reinforcing steel had not yielded at the point of failure.

The buckling of the 12m wall is verified by the calculations below:

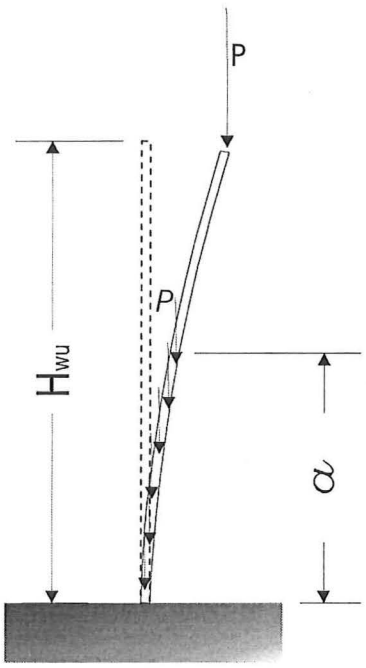

The buckling load of a cantilever can be determined as (Roark and Young, 1975):

$$(pa)' = K\frac{\pi^2 (EI)_{eff}}{H_{wu}^{\ 2}} \qquad \textbf{Equation 6-1}$$

For walls fixed at the base and free at the other end:

$P/pa = 0.0$ $\quad a/H_{wu} = 1.0$

H_{wu}= unsupported height of the wall.

a = length of uniformly distributed load

p = uniformly distributed load

P = Point load

From Table 34 of Roark and Young (1975), K=0.795

As the duration of the fire increases, the curvature of the wall increases due to thermal bowing, thus, causing the amount of cracking of the wall to increase. The flexural rigidity, *EI*, of the wall decreases due to cracking.

The following shows the calculation of the buckling load of the wall.

The left part of Equation 6-1 is the load of the wall:

$(pa)'$=3600N/m/m × 12m = 43200N/m (for a unit metre of wall)

The right part of the equation represents the buckling resistance of the wall:

$$K \times 3.142^2 \text{ x } (EI)_{eff} / (12\text{m})^2$$

The cracked moment of inertia of the section is given as (Park and Paulay, 1975):

$$I_{cr} = \frac{Mkd}{f'_c} = \frac{21429\text{Nm/m} \times 0.039\text{m}}{30 \times 10^6\ \text{N/m}^2} = 2.786 \times 10^{-5}\ \text{m}^4/\text{m}$$

$$(EI)_{eff} = E \times I_{cr} = 18 \times 10^9\ \text{N/m}^2 \times 2.786 \times 10^{-5}\ \text{m}^4/\text{m} = 501430\ \text{Nm}^2/\text{m}$$

The elastic modulus of the concrete in the wall is assumed to be not significantly affected by the temperatures because the unheated side of the wall provides the buckling resistance. Therefore, the value at ambient temperatures is taken. Therefore, the critical buckling load of the wall equals:

$$\frac{K\pi^2(EI)_{eff}}{H_{wu}^2} = \frac{0.795 \times 9.87 \times 501430}{12^2} = 27323\text{N/m}$$

Since the load of the wall (43200N/m) exceeds the critical buckling load of the wall (27323 N/m), the wall buckles and collapses.

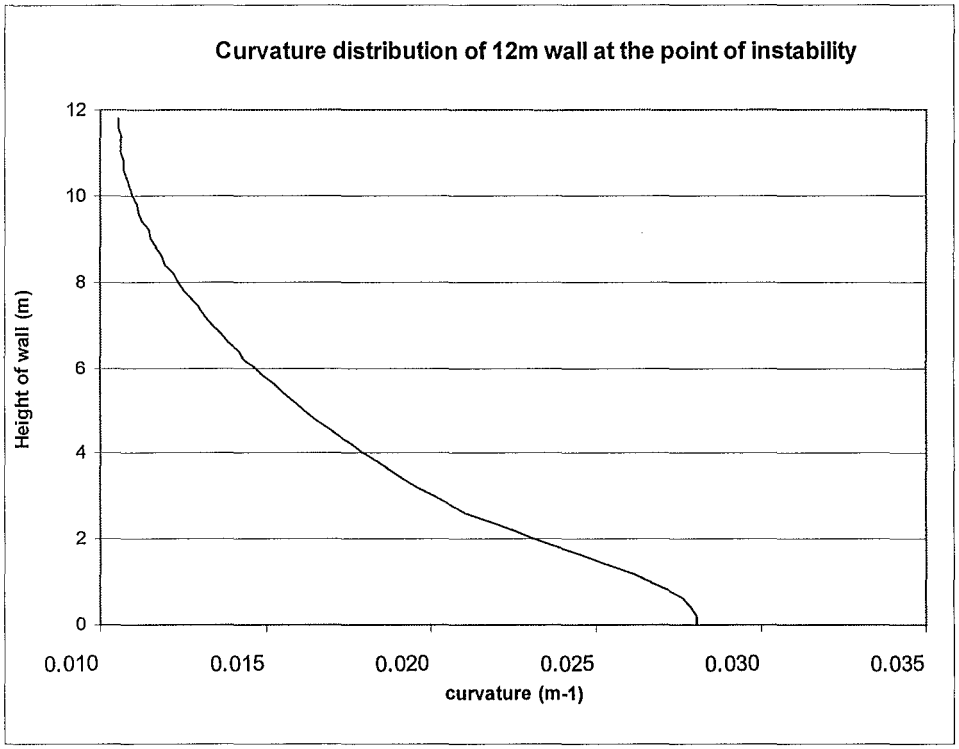

Figure 6-20: Curvature distribution of the 12 metre wall at the point of instability.

- **Concrete tensile stress**

During the initial stages of the fire, the absence of the concrete tensile stress is more significant than in the later stages. This is due to the cracking of concrete (for the wall with concrete tensile strength) during the advanced stages of the fire, which reduces the tensile stress contribution in the wall.

A wall without concrete tensile strength is assumed to be fully cracked, resulting in a lower flexural rigidity of the section. This is turn would increase the displacements of the wall for a given amount of imposed bending moment. The absence of the concrete tensile strength also becomes more noticeable as the heights of the walls increase. The possibility of temperature effects on the tensile strength is unlikely, as cracking would occur before the tensile stresses are sufficiently affected.

In the case of the 12 meter wall, the absence of the concrete tensile stress caused the flexural rigidity of the wall to be lower. Therefore, the critical buckling load of the wall was reached in the very early stages of the fire.

- **Base connections**

The analysis assumes that the wall is fully fixed at the base and failure does not occur at the base connections. In order for the walls to sustain the large displacements due to thermal bowing, the base connections must be well designed and possess sufficient strength. The moment capacity of the base connections must be greater than the plastic moment of the walls, else the walls will collapse before a plastic hinge has formed at the base of the wall.

- **Fire exposure of walls**

The analysis assumes that the wall is uniformly heated up its height. In reality, this is not the case as the walls will be exposed to different levels of heat intensity up their height. O'Meagher (1994) has conducted analysis on walls which were heated at the top two-thirds and found that the walls performed better (refer to Figure 4.24). Future analysis can be conducted on walls with variable heating patterns up the heights of the walls.

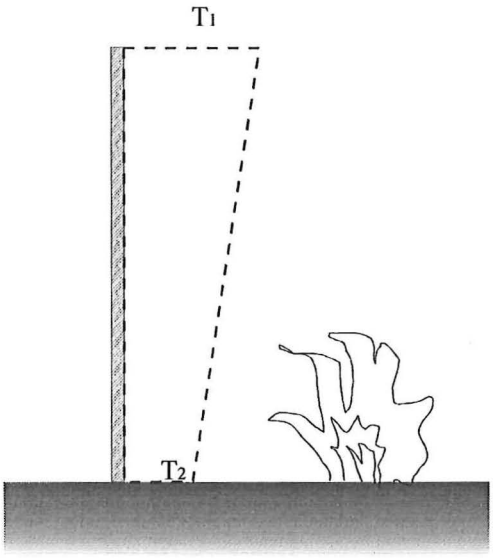

Figure 6.21: Variable temperature distributions along the height of the wall.

CONCLUSIONS

The analyses have shown that the walls experienced very large displacements when subjected to the ISO standard fire. The current quantity of reinforcing that is normally placed in these walls is inadequate for slenderness ratios in excess of 50 as they do not provide sufficient flexural rigidity to prevent large out-of-plane deflections. The large thermal bowing deflections generate very large moments at the base of the wall. Provided the supporting base connections do not fail, the large displacements will cause the wall to collapse by buckling or yielding of the reinforcement at the base.

6.3.2. Thickness of wall

This section investigates the behaviour of walls with different thicknesses. A 10 meter wall with different thicknesses is analysed. The thicknesses of the wall are chosen so that they will give the same slenderness ratios as those shown in Table 6-2. Table 6-3 shows the different wall thicknesses used in the analyses. The other variables are kept constant as stated in section 6.3.

Most of the walls would be constructed using the thicknesses shown in Table 6-3 except for case i), where the wall thickness is 250mm. This particular thickness was chosen just to obtain a slenderness ratio of 40 for comparison purposes with the results from section 6.3.1. In practice, a 250mm precast tilt slab would require two layers of reinforcing steel. For the purpose of the analysis, only one layer of reinforcing is used in this 250mm wall, as using two layers of reinforcing would cause the wall to behave differently due to the thinner amount of concrete cover to the reinforcing steel. The behaviour of concrete walls with two layers of reinforcing steel will be discussed in detail in section 6.3.4.

Analysis case	Wall thickness	Slenderness ratio
v)	250mm	40
vi)	185mm	53.3
vii)	150mm	67.7
viii)	125mm	80

Table 6-3 : Analysis cases with different thicknesses

RESULTS OF ANALYSES

▪ Horizontal displacements at the top of the wall

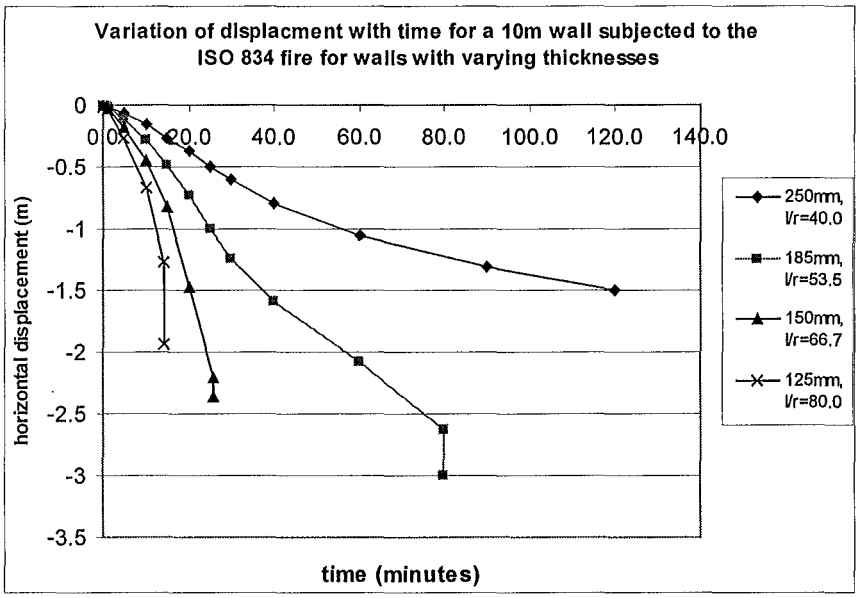

Figure 6.22: Variation of displacement for a 10m cantilever wall with different thickness.

Figure 6.22 shows the variation of horizontal displacements for a 10m wall with different thicknesses. Comparing the results shown for these slenderness ratios by varying the thicknesses with the results obtained in section 6.3.1, the results can be summarised in Figure 6.23

Slenderness ratio	Vary height			Vary thickness		
	Case	Wall height	Wall thickness	Case	Wall height	Wall thickness
40.0	i)	6m	150mm	v)	10m	250mm
53.3	ii)	8m	150mm	vi)	10m	185mm
66.7	iii)	10m	150mm	vii)	10m	150mm
80.0	iv)	12m	150mm	viii)	10m	125mm

Table 6-4 : Analysis cases to investigate the effects of different parameters

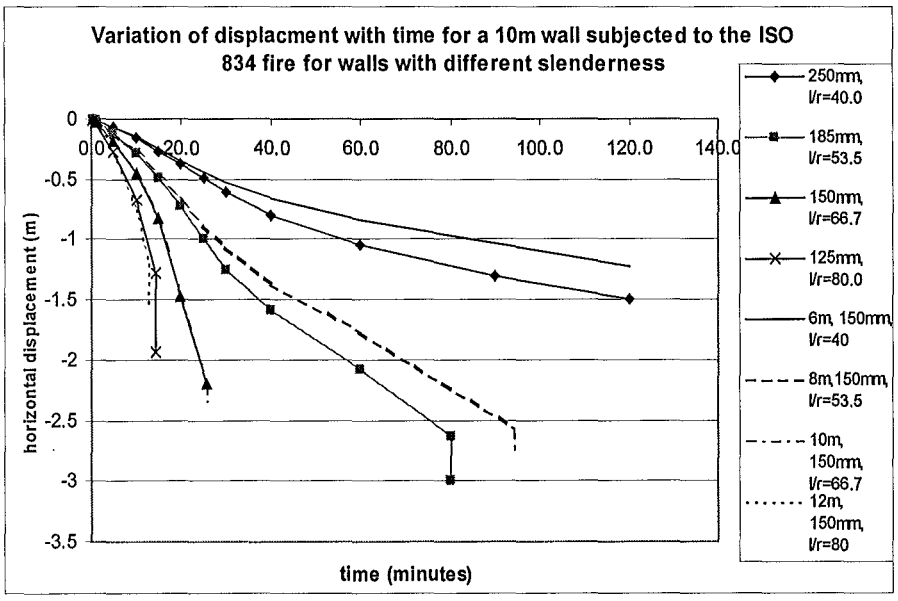

Figure 6.23: Comparison of different variables

Slenderness ratio, $\lambda = 40.0$

Two cases were analysed for the slenderness ratio of 40. Case i) is a 6 meter wall with a 150mm section and case v) is a 10 meter wall with a 250mm section. The displacement trends for cases i) and v) are similar. However, the displacement at a given time for the thicker and taller wall is larger compared to the thinner and shorter wall. The dissimilarity in the displacements increases from 3.5 percent during the initial stages to 25 percent at the end of the simulation.

Slenderness ratio, $\lambda = 53.3$

The displacement trend for the walls of this slenderness is also the same as for the slenderness of 40. The 10 meter wall deflected more than the 8 meter wall at any given time. The differences in the deflections ranged from 3 percent during the initial stages to 18 percent at the later stages of the fire. However, the 10 meter wall failed at an earlier time, 80 minutes, compared to the 8 meter wall, at 94 minutes.

Slenderness ratio, λ= 66.7

The heights and thicknesses of both walls (Case iii) and Case vii)) for this slenderness ratio are same, therefore, their results are the same.

Slenderness ratio, λ= 80.0

For this slenderness ratio, two cases were analysed. Case iv) is a 12 meter wall with a 150mm section and case viii) is a 10 meter wall with a 125mm section. Both walls showed very similar displacement trends. Although the 12 meter wall showed slightly larger displacements compared to the 10 meter wall, it managed to survive the fire slightly longer and sustain a larger displacement (1.2 meters compared with 0.67m).

▪ Bending moments at the base of the wall

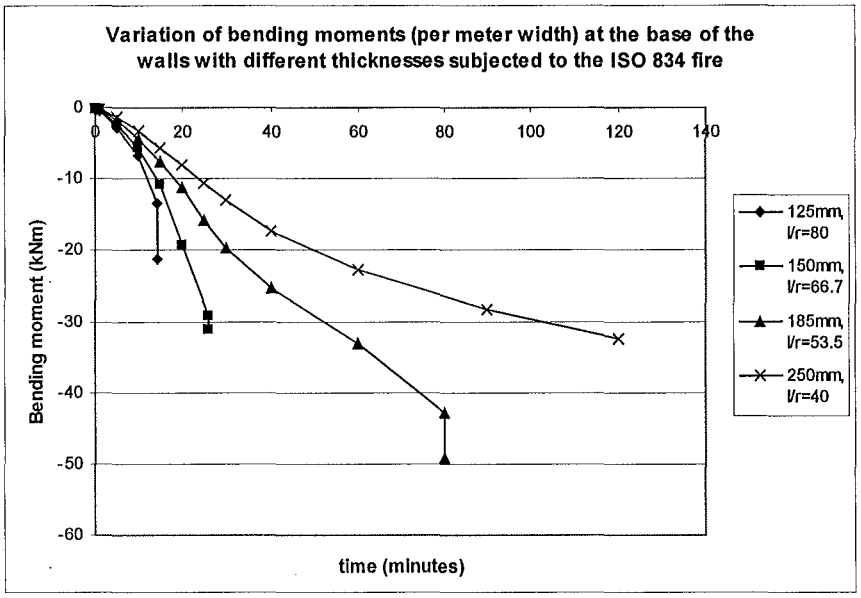

Figure 6.24: Variation of bending moments at the base of the walls with different thicknesses.

Figure 6.24 shows the variation of bending moment at the base of the wall with time. The trends of the bending moment are similar to the displacement trends in Figure 6.22. The flexural capacity increases as the thickness of the wall increases. The failure modes of the

wall with λ=66.7 and λ=53.3 are by flexural yielding of the reinforcement at the base. The walls with λ=80 fail due to buckling, before its nominal moment is reached.

DISCUSSION

Two types of behaviour are observed from the analyses:

i) For lower slenderness ratios (λ = 40.0 and λ = 53.3), the thicker and taller walls showed more deflections at the top of the walls despite having the same slenderness ratio as the shorter and thinner walls. This is due to the extra weight and height of the thicker and taller wall. This in turn causes them to fail earlier due to the larger P-delta effects. The failure mode of these walls is by yielding of the reinforcing steel.

ii) The mode of failure of the more slender walls (λ = 80.0) is due to buckling. The thicker and taller wall managed to survive the fire longer despite having a larger displacement at the top. The thicker wall had higher flexural rigidity, thus providing more resistance to buckling.

The analysis has shown that as the thickness of the walls increase, the horizontal deflections of the walls decrease. Therefore, walls should be built thicker to reduce the thermal bowing deflections. This will correspondingly reduce the moments due to P-delta at the base of the walls. A shortcoming of the computer analysis is that it does not consider spalling of concrete for thick walls with a single layer of reinforcement.

For walls with thicknesses greater than or equal to 200mm, the Concrete Structures Standard of New Zealand requires the wall to have two layers of reinforcement. Unfortunately, this will increase the time for fabrication and the overall cost of construction. The behaviour of walls with different layers of steel is discussed in 6.3.4.

CONCLUSIONS

The analyses have shown that the thermal bowing deflections of the walls can be decreased by increasing the thickness of the walls. The survival times of the walls also increased by increasing the thicknesses of the walls,

6.3.3. Quantity of reinforcing

To investigate the effect of varying the quantity of reinforcement on the deflection of the wall, the 10 meter wall with different quantities of reinforcing steel is analysed. The other variables of the wall are kept constant as stated in section 6.3. The quantity of reinforcing steel in the section is determined by the size of the reinforcing steel bars and their spacing, thus giving a steel ratio for a particular section. In order to model the equivalent steel ratio with SAFIR, the sizes of the reinforcing steel in the section are varied. The different quantities of reinforcing that were analysed are summarised in Table 6-5.

Case	Reinforcing bar size	Bar spacing	Equivalent steel ratio
ix)	12 mm	200mm c/c	0.38%
x)	16mm	200mm c/c	0.67%
xi)	16mm	125mm c/c	1.07%
xii)	16mm	100mm c/c	1.34%

Table 6-5: Cases analysed to investigate the effect of different amounts of reinforcing steel.

▪ Horizontal displacements at the top of the wall

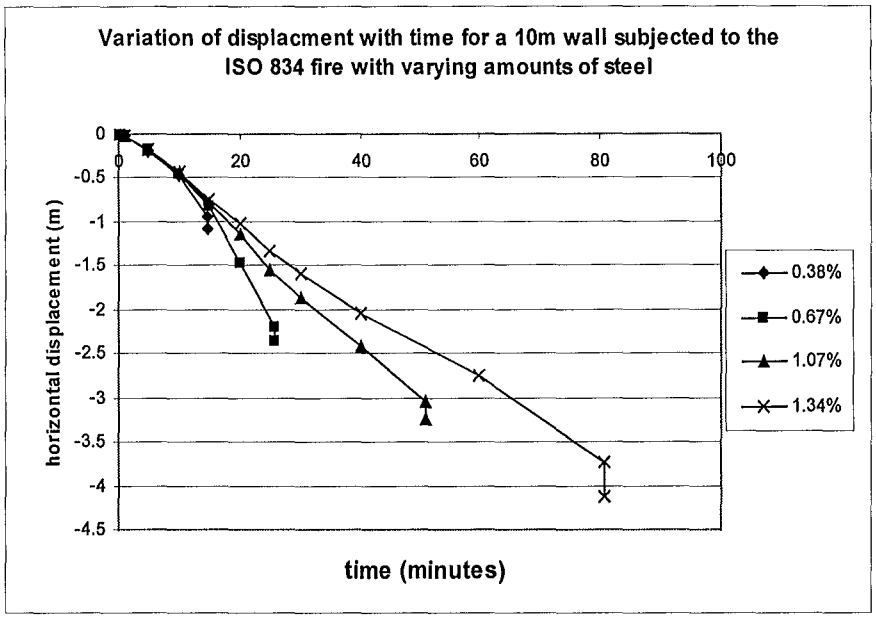

Figure 6.25: Variation of displacement for the 10 meter wall with different quantities of reinforcing steel.

Figure 6.25 shows the behaviour of walls with different quantities of reinforcement. Case x) shows that the typical wall with 0.67 percent reinforcing fails after 26 minutes of exposure to the fire. The displacement trend shows that the deflections tend to increase very rapidly when the wall reached its failure point.

By reducing the amount of reinforcing to 0.38 percent, a 45 percent decrease from 0.67 percent, the failure time reduces from 26 minutes to 15 minutes. The maximum deflection sustained by the wall before it fails is 0.95m, a 23 percent decrease. The displacement trend for 0.38 percent reinforcement is similar to 0.67 percent reinforcement, showing rapidly increasing displacement with time.

Increasing the reinforcement from 0.67 percent to 1.07 and 1.34 percent improves the performance of the wall significantly. The deflections of the walls are reduced, and the time to failure of the walls increase.

Steel ratio	0.38 %	0.67%	1.07%	1.34%
10 minutes	0.468m	0.449m	0.438m	0.424m
25 minutes	Failed	2.20m	1.543m	1.340m

Table 6-6: Comparison of horizontal displacements at the top of walls with different reinforcing steel ratios.

Table 6-6 shows the horizontal displacements at the top of the walls with different reinforcing steel ratios at different times. During the initial stage of the fire (10 minutes), the displacements are very similar and the quantities of reinforcement do not show any marked effect of the displacements.

As the fire progresses to 25 minutes, the wall with 0.38 percent reinforcing has collapsed while the wall with 0.67 percent reinforcing sustains a 2.20 meter deflection and is at the verge of collapse. The walls with 1.07 percent and 1.34 percent reinforcing show a thirty and forty percent reduction in the displacements, relative to the wall with 0.67 percent. Increasing the reinforcement from 0.67 percent to 1.07 percent shows the most significant reduction of the displacements.

- **Bending moments at the base of the wall**

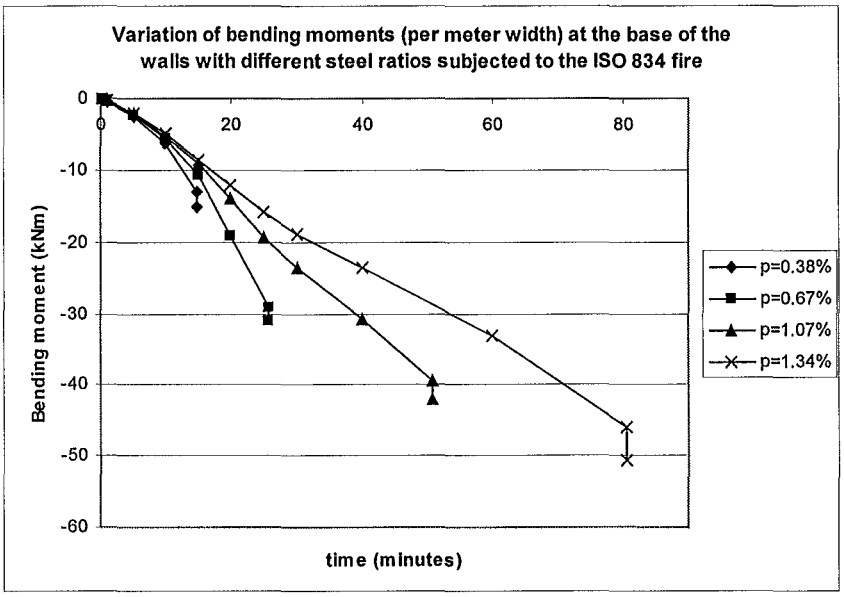

Figure 6.26: Variation of bending moments at the base of the walls with different steel ratios.

The figure above shows the variation of bending moments at the base of the walls with different amounts of reinforcement. The graph shows that as the quantity of reinforcing increases, the flexural strength of the wall increases. Therefore, the time required to form a plastic hinge at the base of the wall increases.

DISCUSSION

Mode of failure

The mode of failure of the wall with 0.38 percent reinforcing was due to buckling. The wall buckles when cracking at the base of the wall reduces the flexural rigidity to a point where it is unable to sustain the weight of the wall. When the wall buckled, neither the reinforcing nor the concrete had reached their yield and ultimate strengths, respectively. The analysis has shown that increasing the amount of reinforcing changes the mode of failure of the wall from lateral buckling, to yielding of the reinforcing steel.

Although the higher reinforcing steel quantity reduces the lateral displacements, the walls still collapse due to yielding at the base. Increasing the reinforcing steel correspondingly increases

the moment capacity of the wall. This means that the strength of the base connections must be built equally strong or else they will fail before the wall collapses.

CONCLUSIONS

This investigation shows that increasing the quantities of reinforcing reduce the deflections of the wall. The increase of reinforcing also increases the survivability of the wall despite undergoing very large deflections.

6.3.4. Steel arrangement

This section of the analysis investigates the effects of changing the reinforcement layout, from one layer in the middle of the section, to two layers. The cases that were analysed, comprising various quantities of reinforcing and arrangements, are summarised in Table 6-7. The structural model of the wall with two layers of reinforcing is shown in Figure 6.27.

Case	Wall thickness	Steel arrangement	Steel ratio
xiii)	150mm	1 layer x H16@200mm c/c	0.67%
xiv)	150mm	2 layers x H12@220mm c/c	0.67%
xv)	150mm	2 layers x H16@200mm c/c	1.34%
xvi)	200mm	2 layers x H16@300mm c/c	0.67%

Table 6-7: Cases analysed with different steel layouts

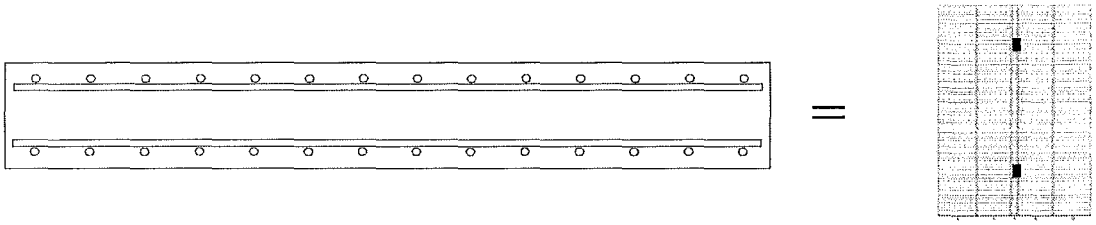

Figure 6.27: Structural model of wall section with two layers of reinforcing.

- **Horizontal displacements at the top of the wall**

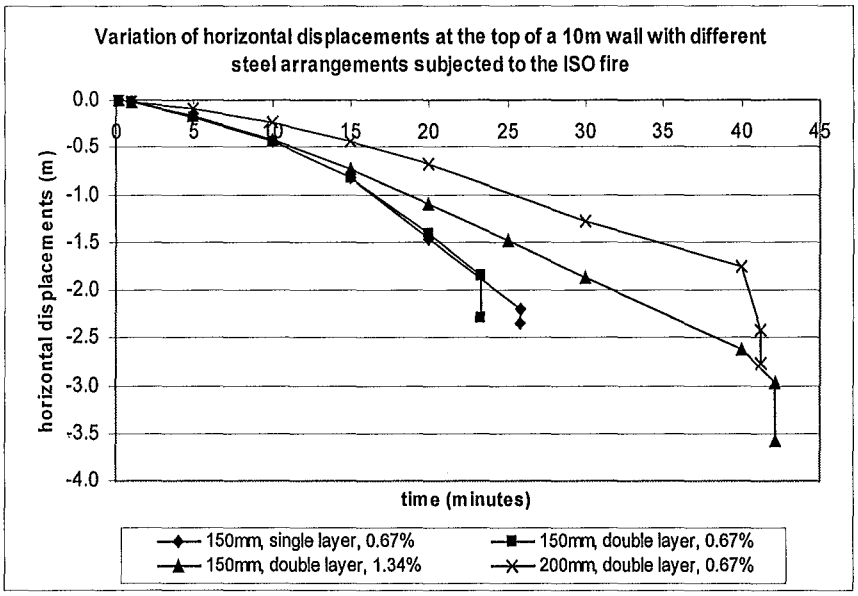

Figure 6.28: Variation of horizontal displacements at the top of a 10m wall with different steel arrangements subjected to the ISO fire.

Figure 6.28 shows the variation of horizontal displacements at the top of the 10 meter wall with different reinforcing arrangements. For the same amount of reinforcing, 0.67 percent, the wall with two layers of reinforcing (case xiv) collapses slightly earlier than the wall with a single layer of reinforcing (case xiii); 23 minutes compared to 26 minutes. The wall with two layers of reinforcing and 1.34 percent steel (case xv) managed to survive the fire for a longer duration, 42 minutes. By keeping the steel ratio constant at 0.67 percent, and increasing the thickness to 200mm, the wall experienced much smaller deflections compared to the other walls. However, it fails at 41 minutes when a plastic hinge forms at the base of the wall.

DISCUSSION

The collapse of all the walls is due to yielding of the reinforcing steel at the base. For the same amount of reinforcing, doubling the steel layers did not show any significant changes in the behaviour of the walls. Despite having a larger internal lever arm, case xiv) failed at about the same time as case xiii). This is due to the smaller amount of steel available to provide the moment resistance. The failure of wall is due to P-delta effects and not due to thermal effects on the reinforcing steel. The collapse of the wall occurred during the initial stages and the reinforcing steel had not lost its strength due to thermal effects.

When the reinforcing steel quantity is doubled (case xv), the wall survives the fire for a longer duration. The higher steel quantity is able to provide the flexural resistance for a longer period. Eventually the temperatures reduce the strength of the steel to a point where it cannot resist the temperature induced moments. Consequently, the steel yields and a plastic hinge forms at the base.

By increasing the thickness of the wall to 200 mm while maintaining the steel ratio at 0.67 percent, the wall is able to sustain much smaller displacements compared to the thinner walls. The lateral displacements of the wall are inversely proportionate to the thickness of the wall. However, this wall fails at about the same time as case xv) because the concrete cover for both walls are the same. The failure of this wall is due to the yielding of the reinforcement at the base.

The walls with lower amounts of reinforcing (0.67 percent) collapse very early regardless of whether the steel is arranged in single or double layers. The walls with higher quantities of reinforcing and thicker walls survive the fire for a longer duration. However, they collapse when the reinforcing steel loses its strength at the later stage of the fire.

CONCLUSIONS

This investigation shows that utilising two layers of reinforcement, while maintaining the steel quantity, does not improve the performance of the slender walls as they collapse due to P-delta effects and not due to thermal effects on the reinforcing steel. If the reinforcing quantity and steel layers are doubled, then the walls will perform better and collapse after a longer period of fire exposure.

6.4. Different fire curves

This section of the analysis serves to determine the behaviour of walls when it is subjected to different fire curves. The ISO standard fire used in the parameter study is a good representation of the temperatures in a small compartment. However, in a large compartment, such as a large industrial building, the temperatures may not be as severe as specified by the ISO fire curve. When a fire breaks out in one of these large compartments, the level of radiation may not be high enough to cause flashover.

As mentioned in the earlier chapters, a more realistic fire that could occur in these buildings is the migrating fire. In a migrating fire, the temperatures may be high at the area of the fire and structural damage may occur in the vicinity of the fire. Some of the likely damage that could occur is the melting of the plastic skylights and local collapse of the roof. This allows the fire to be vented and the temperatures inside the fire compartment to be reduced.

- **External fire curve**

A time temperature curve obtained from the Eurocode (EC1, 1994), for modelling temperatures of a well-ventilated fire, can be used as a more realistic representation of the temperatures which the structure would be exposed to. This Eurocode temperature curve was intended for the design of structural members located outside a burning compartment. The temperature of this external fire at a given time is given by the equation below:

$$T = 660(1 - 0.687e^{-0.32t'} - 0.313e^{-3.8t'}) + T_o$$

Where: t' = time in minutes

T_o =ambient temperature (°C)

- **Decay rates**

In this part of the analysis, the Eurocode external fire curve is applied to the walls and is compared with the ISO standard fire. Apart from that, temperature decay will be introduced to the Eurocode and ISO curves to simulate the decay phase of the fire. Buchanan (1999) has suggested using a temperature decay rate dT/dt of 625°C/hr modified for opening factor and thermal insulation:

$$\frac{dT}{dt} = 625\left(\frac{F_v}{0.04}\right)\Bigg/\left(\frac{\sqrt{k\rho c_p}}{1900}\right)$$

For the analysis of the walls, the temperature decay rate is simplified and taken as 625°C/hr.

- **Duration of fire**

Hand calculations can be used to determine the total burning time in a warehouse (Buchanan, 1994; Cosgrove, 1996). However, due to the high degree of variability in the size of the building and its fuel load, the burn times (before the decay phase) used for the purpose of the analysis are taken as 30, 60 and 90 minutes. These burn times will be applied to both the ISO standard fire and the Eurocode external fire. The Eurocode and ISO fire curves that are used for the structural analysis are shown in Figure 6-29.

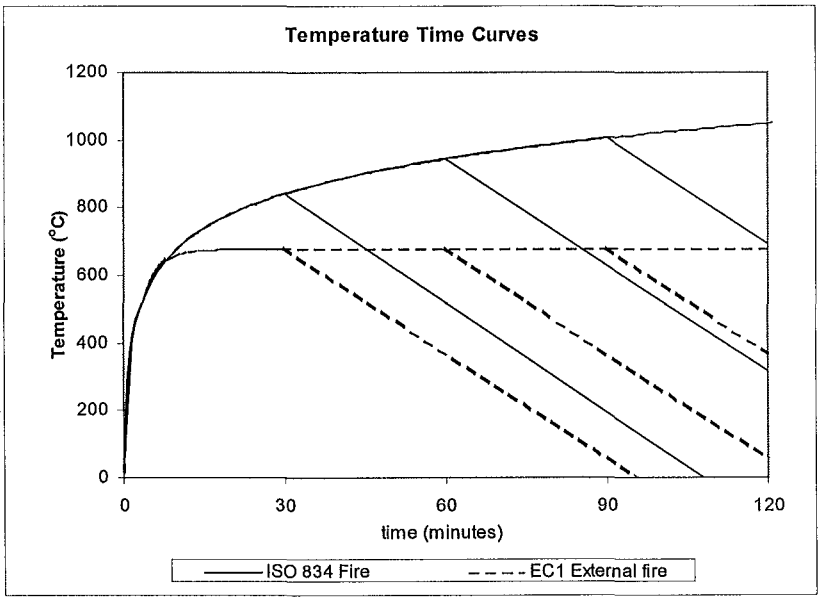

Figure 6-29: Time temperature curves.

The analysis cases that were investigated are shown in the table below. These fires are applied to walls with different heights, ranging from 6 meters to 12 meters with different temperature curves. Apart from the variation in the height of the wall, the geometric and material properties of the wall used in the analysis are of those used in the typical wall, stated in section 6.3. As with the ISO fire, the wall is assumed to be uniformly heated up its height.

Fire curve		EC1 External fire				ISO 834 fire			
Time (minutes)		ND	30	60	90	ND	30	60	90
Height	6m	Y	Y	Y	Y	Y	Y	Y	Y
	8m	Y	Y	Y	Y	Y	Y	Y	Y
	10m	Y	Y	X	X	Y	X	X	X
	12m	Y	X	X	X	Y	X	X	X

Table 6-8

Y - Temperature decay occurred before structural failure.

X - Structural failure occurred before temperature decay.

ND - No temperature decay.

- **EC1 external fire**

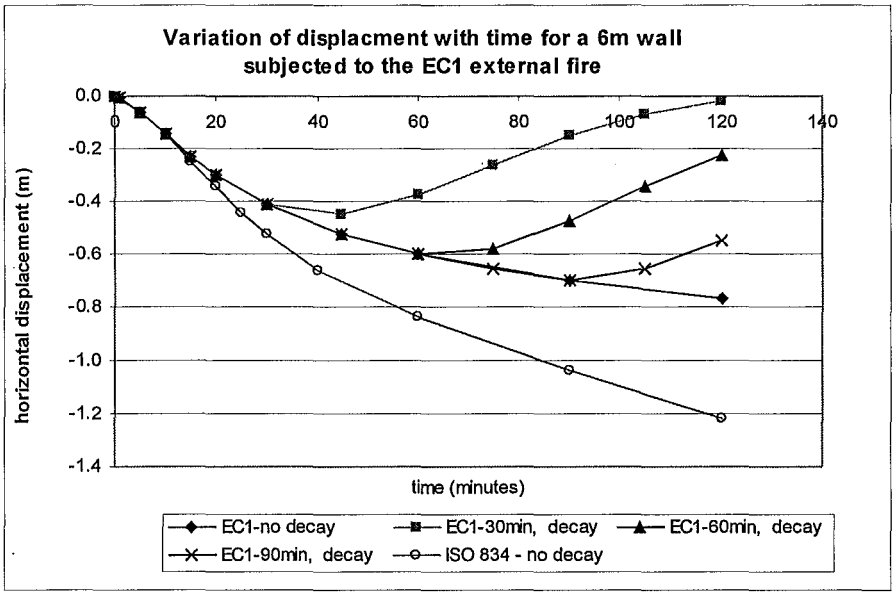

Figure 6.30: Variation of horizontal displacement with time for a 6m wall subjected to the EC1 external fire.

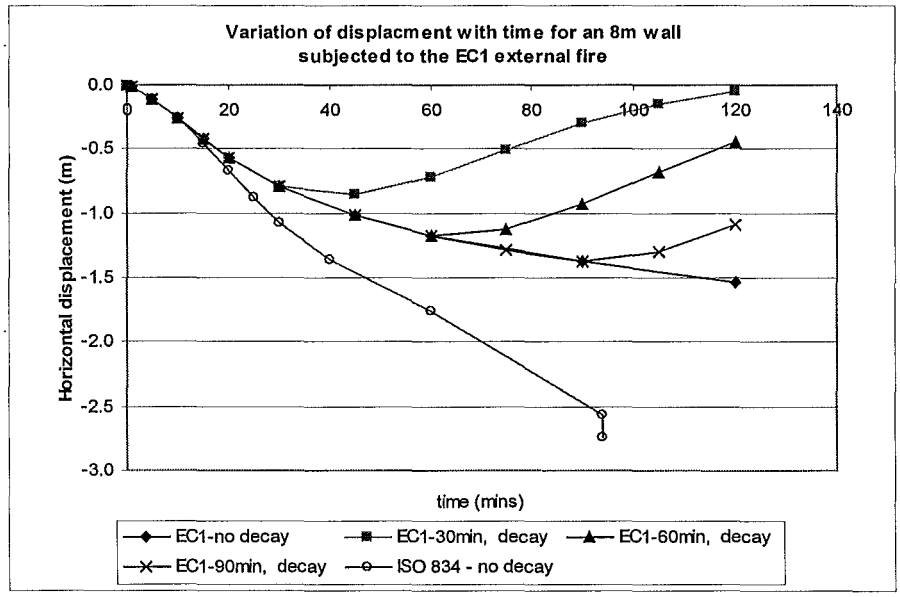

Figure 6.31: Variation of horizontal displacement with time for an 8m wall subjected to the EC1 external fire.

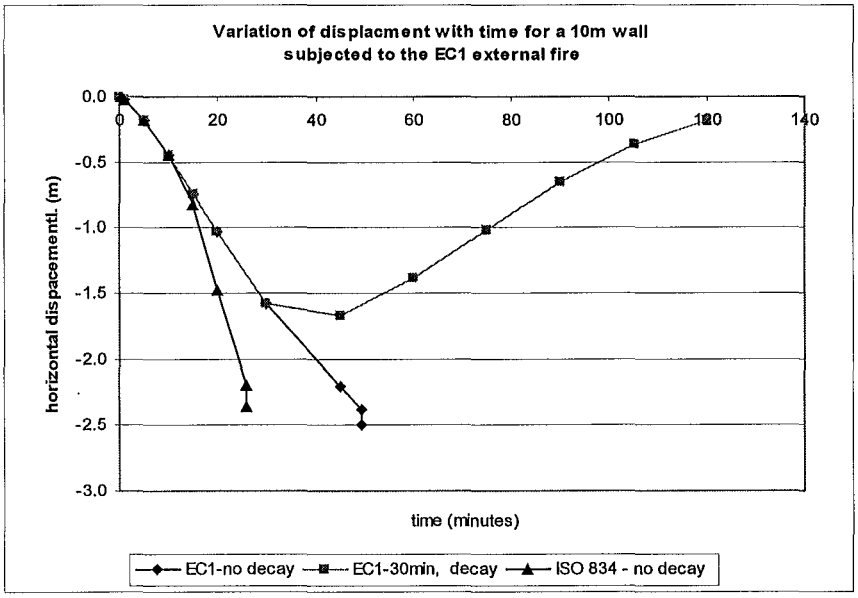

Figure 6.32: Variation of horizontal displacement with time for a 10m wall subjected to the EC1 external fire.

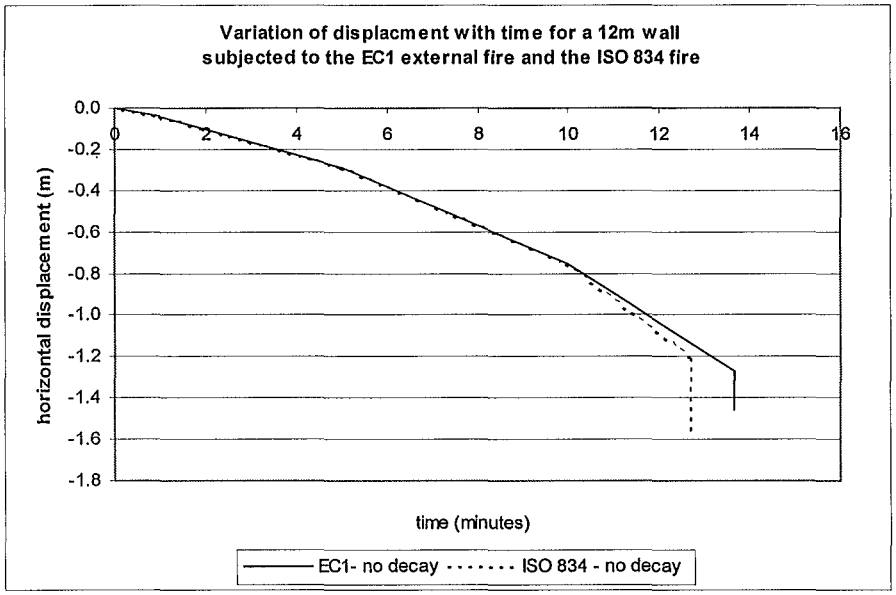

Figure 6.33: Variation of horizontal displacement with time for a 12m wall subjected to the EC1 external fire.

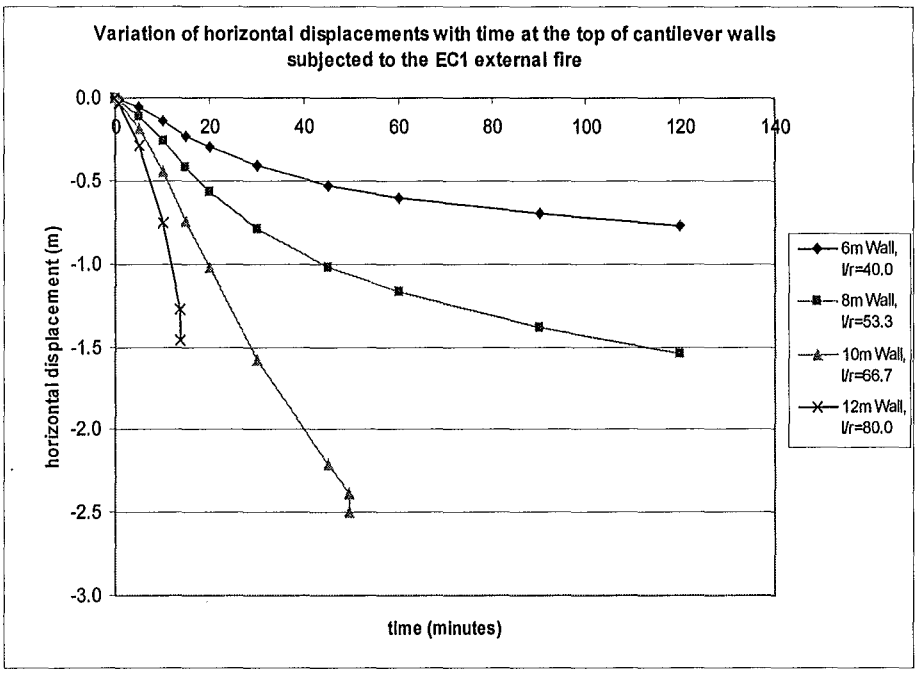

Figure 6.34: Variation of horizontal displacement with time for walls of different heights subjected to the EC1 external fire.

Figure 6.30 to Figure 6.34 show the deflections at the top of the walls subjected to the external fire with and without the decay phases included in the time temperature curve. The displacement trends of the respective walls due to the ISO fire are also included in the plots for comparison. The displacement trends for all the walls during the first 10 minutes are similar for both fire curves. By introducing a decay phase at any time to the external fire for the 6 meter and 8 meter walls, the displacements drop off slowly, deflecting back to its original shape. Unlike the ISO fire without decay, the external fire does not cause the 8 meter wall to fail.

Figure 6.32 shows that a 10 meter standard wall would fail if it was exposed to either the standard or external fires without the decay phase. When the decay phase is introduced to the external fire after 30 minutes, the wall deflects back to its undeformed shape. The 12 meter wall shows hardly any difference in the displacement trend when subjected to either the standard fire or the external fire.

- **ISO 834 fire**

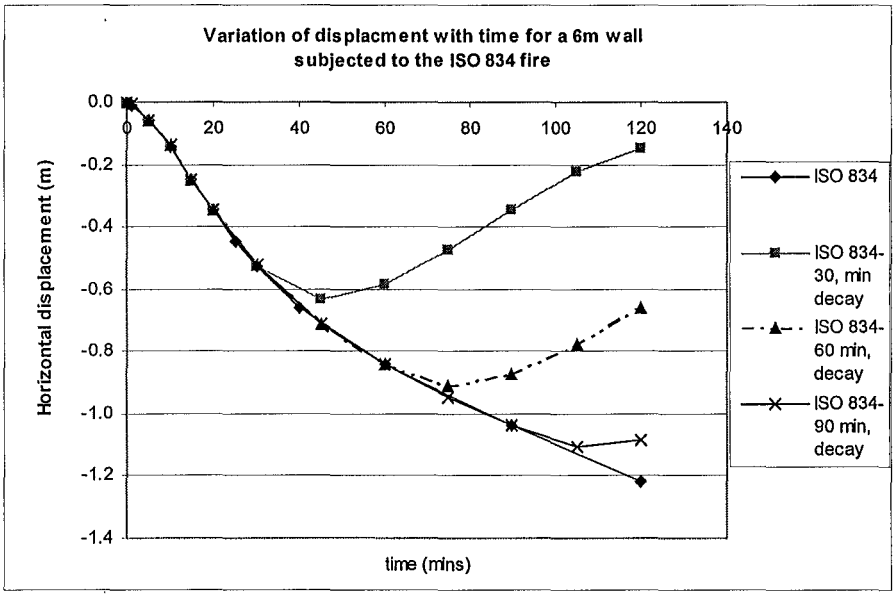

Figure 6.35: Variation of horizontal displacement with time for a 6m wall subjected to the ISO 834 standard fire.

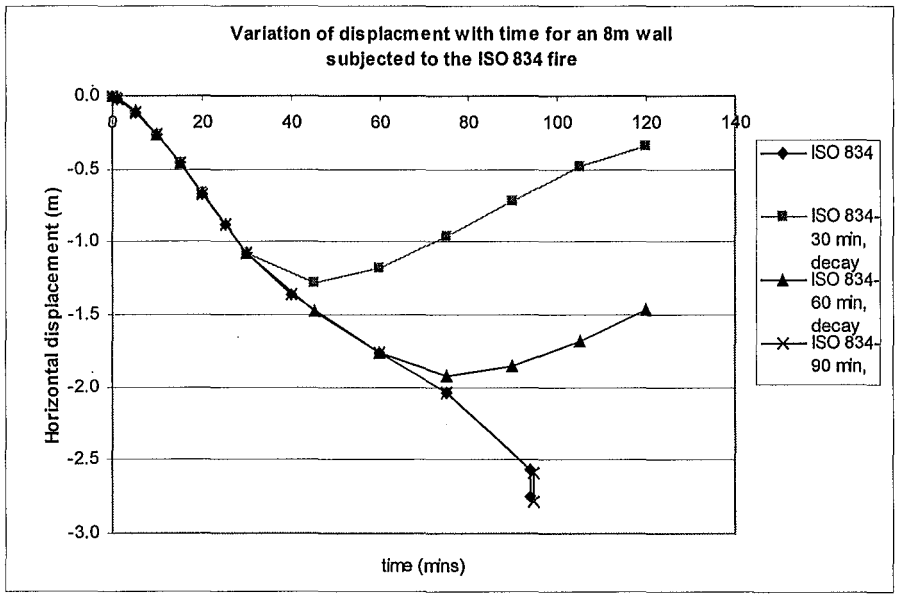

Figure 6.36: Variation of horizontal displacement with time for an 8m wall subjected to the ISO 834 standard fire

Figure 6.35 and Figure 6.36 show the displacements at the top of the 6 meter and 8 meter walls, respectively, when they are exposed to the ISO fire with and without decay phases. The decay phases were not applicable to the 10 meter and 12 meter wall as they failed before the decay phase of the fire occurred. Figure 6.35 shows that when the decay phase is introduced to the fire after any period of fire exposure, the 6 meter wall manages to deflect back to its original shape. The wall also manages to survive when subjected to the fire without a decay phase.

The 8 meter wall manages to survive the fire without a decay phase until 94 minutes. When the decay phase was introduced to the fire at 30 and 60 minutes, the wall tries to deflect back to its original form. However, when a decay phase is introduced to the fire curve at 90 minutes, the wall collapses five minutes after the decay phase has been introduced.

DISCUSSION

The displacement trends for all the walls during the first 10 minutes are similar for both fire curves. This is due to the same temperatures of the fire curves during that period, as shown in Figure 6.29.

The displacements of all the walls due to the external fire are smaller compared to the ISO standard fire. This is expected because the temperatures in the external fire are lower than the ISO standard fire. Therefore, the temperature difference across the wall section is smaller. The 12 meter wall failed at very similar times when exposed to either the ISO standard fire or the EC1 external fire. This is due to the similar fire temperatures during the initial stages, therefore inducing the same displacements in the walls. The mode of failure of the 12 meter wall exposed to both fires is by buckling.

The introduction of the decay phase to the fires decreases the deflections of the wall. The decreasing deflections reduce the bending moments at the base of the wall, thus preventing the wall from failing. The walls that managed to deflect back to their original form, sustain a permanent set at the end of the simulation. The permanent set is due to irrecoverable plastic deformation of the steel and concrete.

Although the external fire may not truly represent the actual temperatures that the wall is subjected to, it shows that lower fire temperatures would alleviate the large displacements the wall experiences. Therefore, in a real fire, the collapse of the roof and melting of the skylights would improve the performance of the wall in terms of deflections and structural stability.

The analysis has also shown that if an external fire can be extinguished during the first 30 minutes, all but the 12 meter wall will deflect back to its original shape and not collapse. However, if the fire severity is increased, only the 8 meter and 6 meter wall survive the fire long enough for a decay phase to occur. The 12 meter wall shows that in a fire of low or high severity, it will collapse during the initial stages of the fire.

Limitations of analysis

The analysis assumes that the walls can deflect back to its undeformed shape, provided the base connections of the walls remain intact and do not fail. The net deformation of the walls may also be larger due to irrecoverable deformation that may have occurred at the foundations.

CONCLUSIONS

The deflections of a wall in a well ventilated fire are smaller than in the ISO standard fire. The lower temperatures of the external fire allow the stockier walls to survive the fire for a longer duration. For the slender walls (λ= 66.7 and λ= 80), the lower temperatures of the external fire do not improve their performance as they also collapse at very early stages of the fire. The introduction of the decay phase at various stages of the fire allows the stockier walls to survive the fire.

6.5. Wind effects

This section investigates the effects of wind pressure imposed onto the cantilever walls during the event of a fire. The analysis so far has not taken account the effects of wind during a fire. The *Loadings Standard NZS 4203: 1992* (section 2.2.3) requires the cantilever walls to remain standing and be able to resist a uniformly distributed face load of 0.50 kPa after the fire. However, the standard does not state any requirements for the structure to resist wind loads during the fire. In reality, a structure on fire may be exposed to wind loads, which could be detrimental to the behaviour of the structure during the fire.

In this section, walls of different heights would be exposed to the ISO standard fire and to a uniformly distributed wind load. For the purpose of this investigation, the level of wind exposure is not taken as the highest, as the probability of a warehouse fire occurring while subjected to high wind forces is highly unlikely. A wind pressure of 0.25 kPa is applied to the fire-exposed side of the wall. This is half of the wind pressure that the structure is required to resist after a burnout of the compartment.

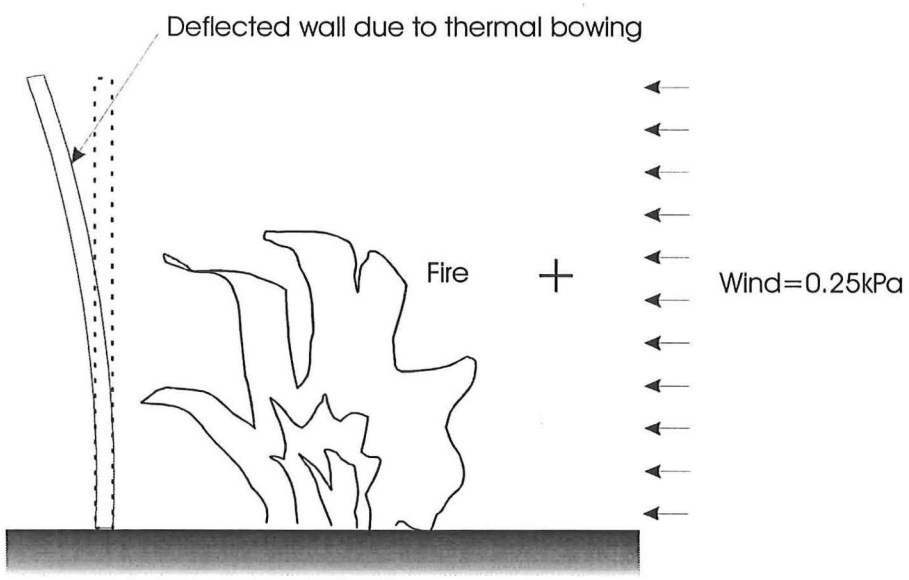

Figure 6.37: Wind pressures imposed on the wall during the fire.

The structural model of the wall used for the analysis is based on the standard wall, stated in section 6.3. The only variable that will be varied is the height of the walls. The thickness of the wall will be maintained at 150mm and the other variables will be kept constant.

Analysis case	Wall height	Slenderness ratio	Wind load
i)	6m	40	0.25 kPa
ii)	8m	53.3	0.25 kPa
iii)	10m	67.7	0.25 kPa
iv)	12m	80	0.25 kPa

Table 6-9: Analysis cases with different wall heights

RESULTS OF ANALYSES

- **Horizontal displacements at the top of the wall**

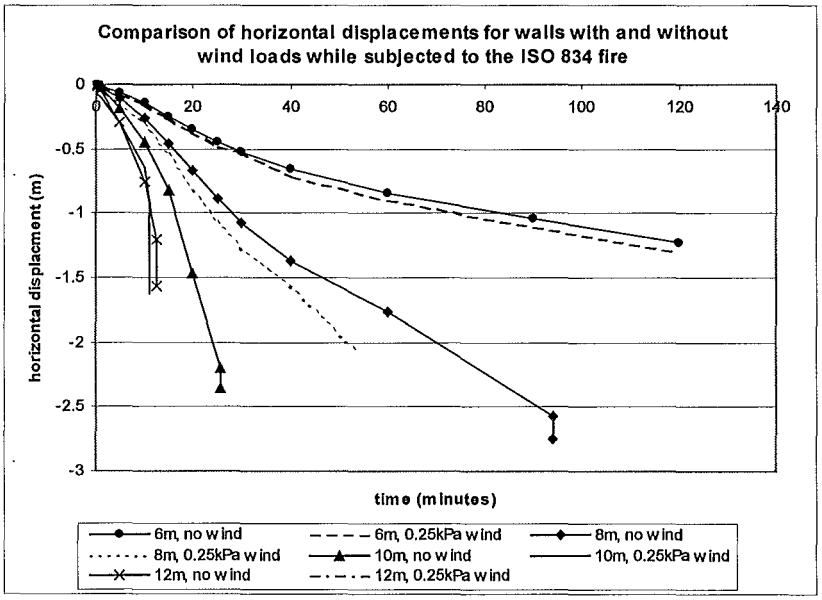

Figure 6.38: Comparison of horizontal displacements at the top of the walls with and without wind loads.

Figure 6.38 shows the comparison of the behaviour of walls simultaneously subjected to the ISO standard fire and wind loads. The graph shows that the wind loads decreased the time to collapse of each of the walls. The 6 meter wall exposed to wind loads did not collapse and

experienced deflections only marginally larger than the wall without wind loads. The 8 meter wall failed at a much earlier stage, 54 minutes compared to 94 minutes without the wind loads. The mode of failure of the 8 meter walls is by flexural yielding of the reinforcement, thus forming a plastic hinge at the base. The 10 meter wall subjected to the wind load failed at 11 minutes, compared to 25 minutes without the wind loads. The mode of failure of the 10 meter wall exposed to wind is by buckling, as cracking of the wall section at the base reduces the flexural rigidity, thus reducing the critical buckling load of the wall. Figure 6.38 shows that there is no displacement trend for the 12 meter wall subjected to the wind and fire. The 12 meter wall did not survive the wind loads during the heating phase as it collapsed due to instability at the initial stages of the analysis. Despite the wall having sufficient flexural strength to withstand the wind loads, cracking at the base of the wall caused it to buckle under its own weight.

CONCLUSIONS

This analysis shows that the presence of a wind during the fire is detrimental to the behaviour of walls with slenderness ratios in excess of 50. The wind load reduced the sustainable deflections of the walls and caused the walls to collapse earlier.

6.6. Approximate hand methods.

This section compares the results of the cantilever wall deflections obtained from SAFIR (refer to section 6.3.1) with the deflections predicted by using the equation proposed by Cooke (1987). This section also proposes a simple method for determining the out-of-plane deflections of a reinforced concrete wall subjected to the ISO standard fire.

6.6.1. Comparison of results

Cooke (1987) has proposed a hand method, in the form of a simple equation, for determining the thermal bowing deflections of a wall. The equation proposed is described below and in section 5.4. The lateral deflections of a cantilever wall, Δ, when it is exposed to a fire on one side is given as:

$$\Delta_c = \frac{\alpha \, H_{wu}^{\,2} (\Delta T)}{2 t_w} \qquad \textbf{Equation 6-2}$$

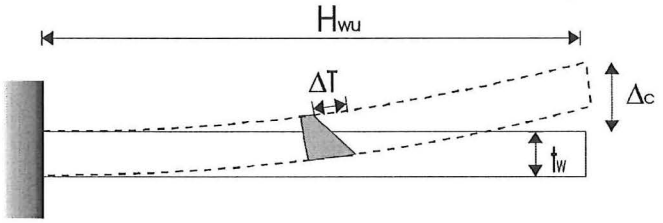

Figure 6-39: Thermal bowing deflections for a cantilever member (Cooke and Morgan, 1988).

Where: ΔT = Temperature difference between heated face and unheated face

α = Coefficient of linear thermal expansion

t_w = Thickness of wall

H_{wu} = Height of wall

The lateral displacements from Equation 6-2 are compared with the results obtained from SAFIR. The results that are obtained only consider the deflections due to free thermal expansion of the wall. The P-delta effects have been ignored for this comparison.

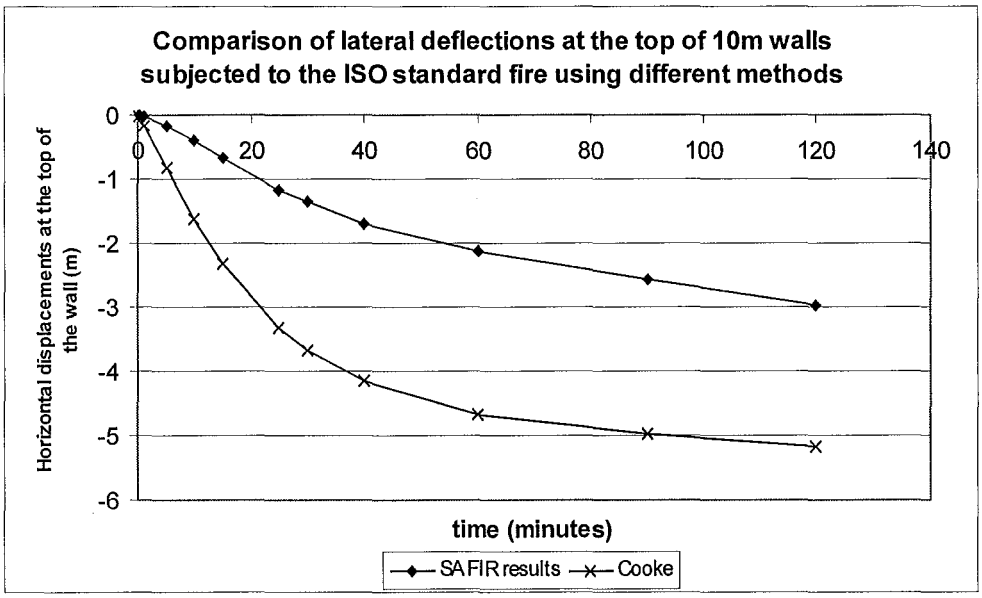

Figure 6.40: Comparison of horizontal deflections using different methods of analysis.

Figure 6.40 shows the comparison between the horizontal deflections obtained from SAFIR and the equation proposed by Cooke (1987). The deflections using the equation proposed by Cooke (1987) (Equation 6-2) are significantly larger than those obtained by SAFIR. The large difference in the results is because Equation 6-2 assumes a linear thermal distribution across the wall section. In reality, the thermal distribution across the wall section is curvilinear and its gradient is very steep at the heated face (refer to section 6.2.1). Therefore, Equation 6-2 is not accurate for determining the thermal bowing deflections of reinforced concrete walls.

6.6.2. Proposed equation for determining deflections

Based on this research project, the author has proposed an equation to determine the lateral deflections of reinforced concrete cantilever walls when exposed to a fire on one side. The proposed equation shown by Equation 6-3 below, is a modification of Equation 6-2 suggested by Cooke (1987). The derivation of this equation is based on the results obtained from the structural analysis conducted with SAFIR.

$$\Delta_c = \frac{\alpha \, H_{wu}{}^2 \left[\left(\psi (T_2)^2 + 20\right) - T_1\right]}{2t_{wu}} \quad \textbf{Equation 6-3}$$

Where: α = Coefficient of linear thermal expansion ($^oC^{-1}$)

t_{wu} = Thickness of wall (m)

H_{wu} = Height of wall (m)

T_2 = Temperature at the exposed face of the section (^oC)

$= fn\ (T_f)$

T_1 = Temperature at the unexposed face of the section (^oC)

$= fn\ (T_f)$

ψ =Temperature reduction factor accounting for the amount of reinforcing steel. (This coefficient takes into account the reduction of thermal expansion of the wall due to the reinforcement.)

T_f =Fire temperature (^oC)

Assumptions made for this equation

1. The deflection of the wall is only due to the free thermal expansion of the concrete wall. It does not consider the deflections due to the P-delta effects.
2. The equation applies only to a 150mm thick wall, reinforced with a central layer of steel in the middle of the section.
3. The equation is only valid for the ISO 834 standard fire.
4. The equation is applicable only for siliceous aggregate concrete, therefore $\alpha = 18 \times 10^{-6}$ /^oC.

Use of the proposed equation

The following section shows the steps for determining the horizontal deflections due to thermal bowing of a reinforced concrete wall. For a reinforced concrete wall with height, H_{wu}, made with siliceous aggregates and thickness, t_w, of 150mm:

1. Determine the duration of the fire, t (minutes)
2. Determine the ISO fire temperature, T_f (°C), based on the time of fire exposure, t:

$$T_f = 345\log_{10}(8t+1)+20$$

3. Given T_f, determine the fire at the exposed face, T_1 (°C), given by:

$$T_1 = 0.0012(T_f)^2 - 0.2685\ T_f + 20$$

4. Determine the fire at the unexposed face, T_2 (°C), given by:

$$T_2 = 20°C \qquad \text{if } T_f < 800°C$$

$$T_2 = 0.0020\ (T_f)^2 - 3.33\ T_f + 1411 \qquad \text{if } T_f \geq 800°C$$

5. Determine the temperature reduction factor, ψ, to account for the reinforcing steel:

$$\psi = 5.7 \times 10^{-4}(p)^{-0.1236} \qquad \text{where } p = \text{reinforcing steel ratio (\%)}$$

p is valid between 0.2% and 2.0%

6. Given the other variables (H_{wu}, α and t_w), substitute T_1, T_2 and ψ from steps 3, 4 and 5, respectively, into Equation 6-3 to determine the horizontal deflection of the wall, Δ_E.

Figure 6-41 and Figure 6-42 show some of the results obtained using the proposed equation. They show that for different quantities of reinforcing steel, the deflections due to the thermal expansion of the wall are very close to the results obtained from SAFIR. The author acknowledges that the proposed equation is far from perfect. The most severe shortcoming arises from the fact that the equation does not consider the deflections due to P-delta effects.

Comparison of results of SAFIR with the proposed method based on this research project.

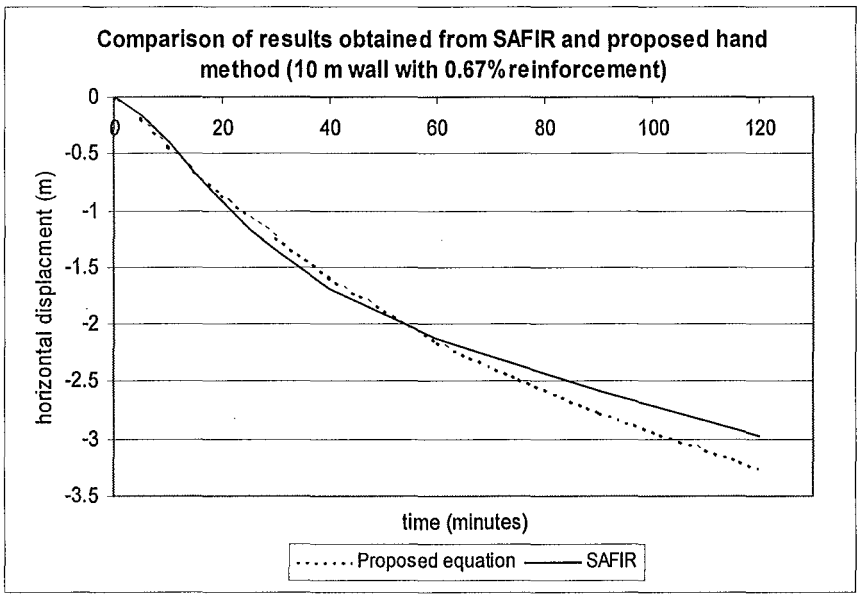

Figure 6.41: Comparison of results from SAFIR with the proposed hand method for a 10m cantilever wall with 0.67% reinforcing steel.

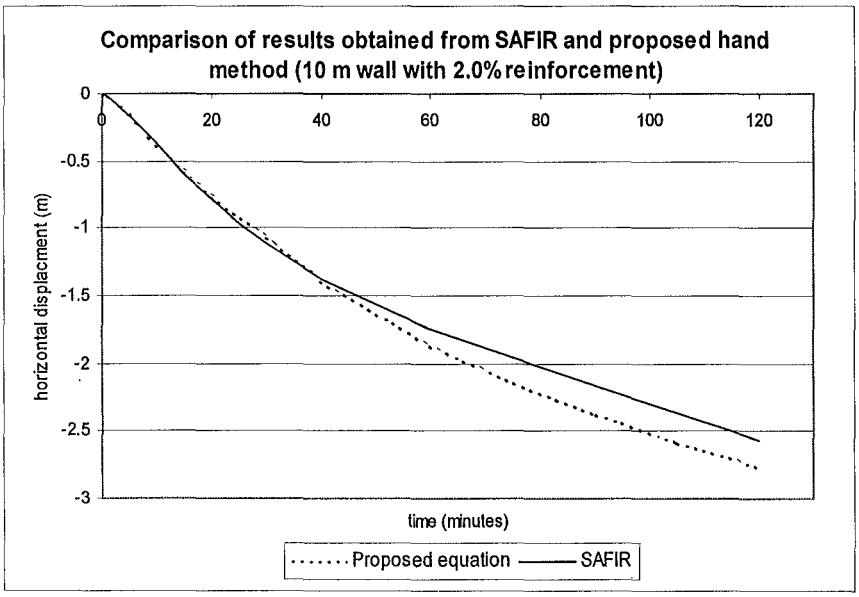

Figure 6.42: Comparison of results from SAFIR with the proposed hand method for a 10m cantilever wall with 2.0% reinforcing steel.

7. PROPPED CANTILEVER WALLS

7.1. Introduction

The behaviour of propped cantilever walls is analysed in this chapter. Propped cantilever walls represent a fire protected steel rafter attached to the top of cantilever walls. Walls of different heights and thicknesses will be analysed to investigate the behaviour of walls with varying slenderness ratios. The quantity of reinforcing and axial load level will also be varied. The behaviour of the walls subjected to different fire curves, with and without decay phases, will be analysed.

7.2. Behaviour of a typical propped cantilever wall

This section describes the behaviour of a typical propped cantilever wall when it is exposed to a fire on one side.

Structural model

Figure 7.1 shows the structural model used to analyse the propped cantilever wall in SAFIR. The section of the wall used in the analysis is shown in Figure 6.2. This figure shows the standard 10 meter wall with a typical amount of reinforcing (0.67%) in the middle of the section. The wall is formed with beam elements. The wall is fixed at the base and its displacements at the top are horizontally restrained, to simulate a fire protected rafter. The fire curve is applied on the right side of the wall. Unless stated otherwise, the ISO 834 standard fire is used to model the fire temperature

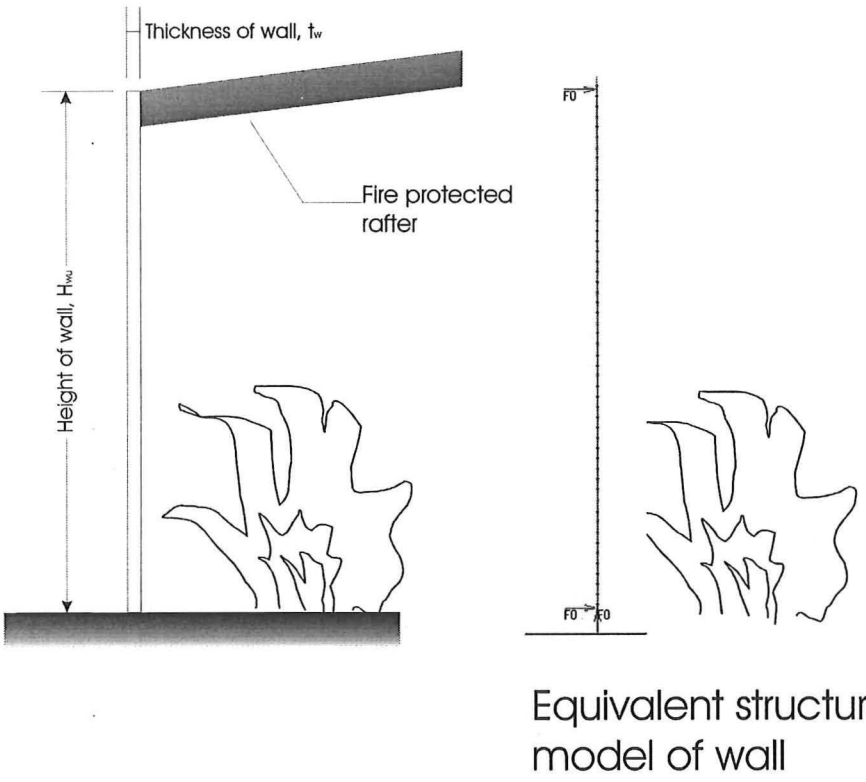

Figure 7.1: Structural model of propped cantilever wall.

The geometric and material properties of the wall used in the analysis are shown below. These properties are those of a typical wall that would be constructed in practice.

Height of wall, H_{wu}:	10.0m
Thickness of wall, t_w:	150mm
Slenderness ratio, λ:	66.7
Unit width of wall, L_w:	55mm
End conditions:	Fixed at the base, horizontally restrained at the top.
Concrete model:	Siliceous aggregate concrete according to the Eurocode, EC2 (1995)
Concrete compressive strength, f'_c:	30.0 MPa
Concrete tensile strength, f'_t:	0.0 MPa
Concrete Poisson's ratio, ν_c:	0.15
Concrete density, ρ_c:	24.0 kN/m^3
Concrete elastic modulus, E_c:	18.0 GPa (Default value in SAFIR)

Steel model:	Eurocode, EC2 (1995)
Reinforcing steel quantity:	1005mm^2/m, 0.67% in the middle of the section
Reinforcing steel elastic modulus, E_s:	210.0 GPa
Reinforcing steel yield strength, f_y:	430.0 MPa
Reinforcing steel Poisson's ratio, ν_s:	0.30
Steel density, ρ_s:	78.50 kN/m^3

The concrete tensile strength was ignored for this analysis as it was found that the iterations in SAFIR would stop prematurely when it was incorporated in the analysis. Therefore, the tensile resistance required in the flexural strength of the wall would be provided solely from the reinforcing steel.

Assumptions made in the analyses

- The wall is fully fixed at the base.
- The wall is uniformly heated throughout its entire height.
- Spalling of concrete does not occur.
- There is no slippage between the concrete and the reinforcing steel.
- Failure does not occur at the foundations.
- There are no initial eccentricities in the wall due to precambering.
- The steel of the fire protected rafter is not affected by temperature, i.e.: no loss of strength or thermal expansion occurs.
- The pinned connections between the rafter and the wall do not fail.

RESULTS OF ANALYSIS

This section describes the analysis results after the propped cantilever wall has been exposed to the ISO standard fire on one side.

▪ Deflections

Figure 7.2 shows the deflected shape of the wall when it has been exposed to the ISO fire on one side. It shows that the top of the wall is restrained from displacing horizontally but the rotation and vertical displacements are unrestrained. At the base, the displacements and rotations are fixed. Figure 7.3 shows the deflected shape of the wall after a plastic hinge has formed at the base. While the horizontal and vertical displacements are still fixed, the rotations at the base are unrestrained.

The horizontal displacements of the wall vary with time as shown in Figure 7.4. Node 51 represents the mid-height of the wall. The graph shows that during the initial stages, the displacements of the wall increase linearly with time until approximately 1550 seconds (26 minutes) when a plastic hinge forms at the base of the wall. Beyond this, the displacement rate increases while maintaining a linear trend. When the wall fails at 2100 seconds (35 minutes), the horizontal displacement trend becomes vertical.

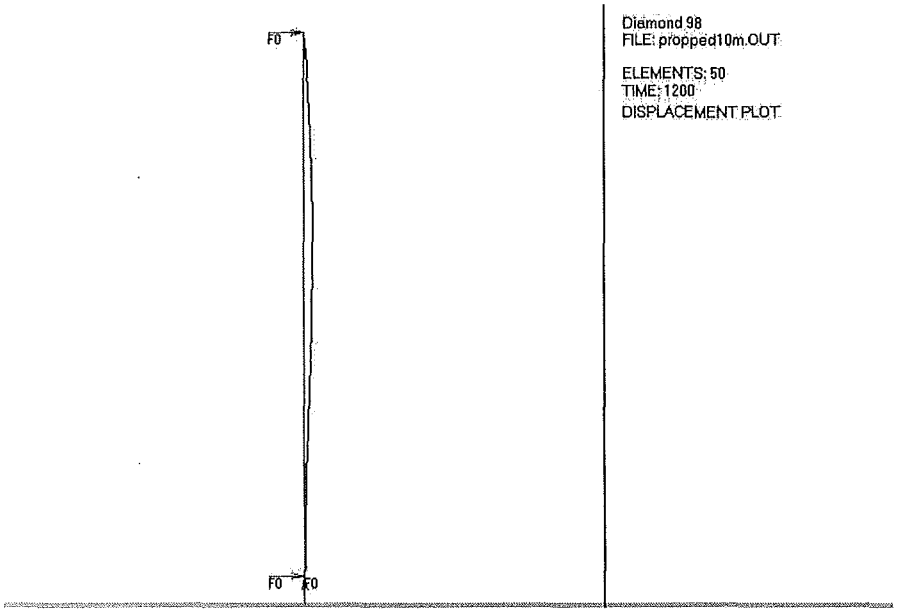

Figure 7.2: Deflected shape of the wall before a plastic hinge has formed at the base.

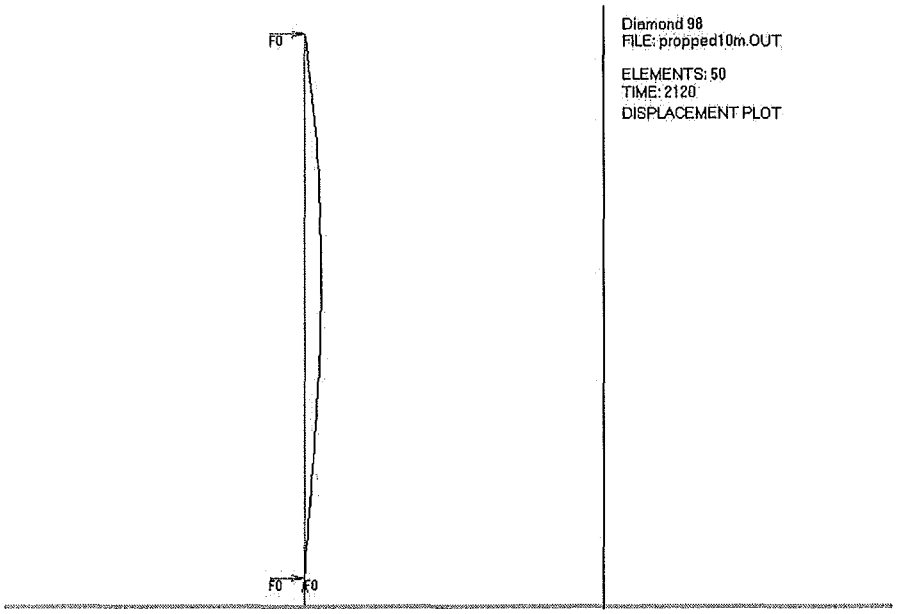

Figure 7.3: Deflected shape of the wall after a plastic hinge has formed at the base.

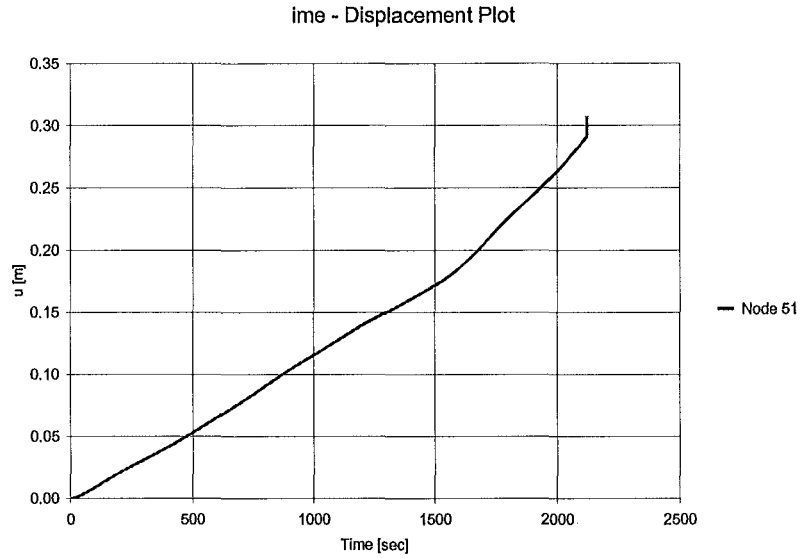

Figure 7.4: Variation of horizontal displacements with time at mid-height of the propped cantilever wall.

▪ Bending moments

The bending moment diagrams of the wall, before and after a plastic hinge has formed at the base, are shown in Figure 7.5 and Figure 7.6, respectively. The triangular shaped bending moment diagram shows that the largest bending moment occurs at the base.

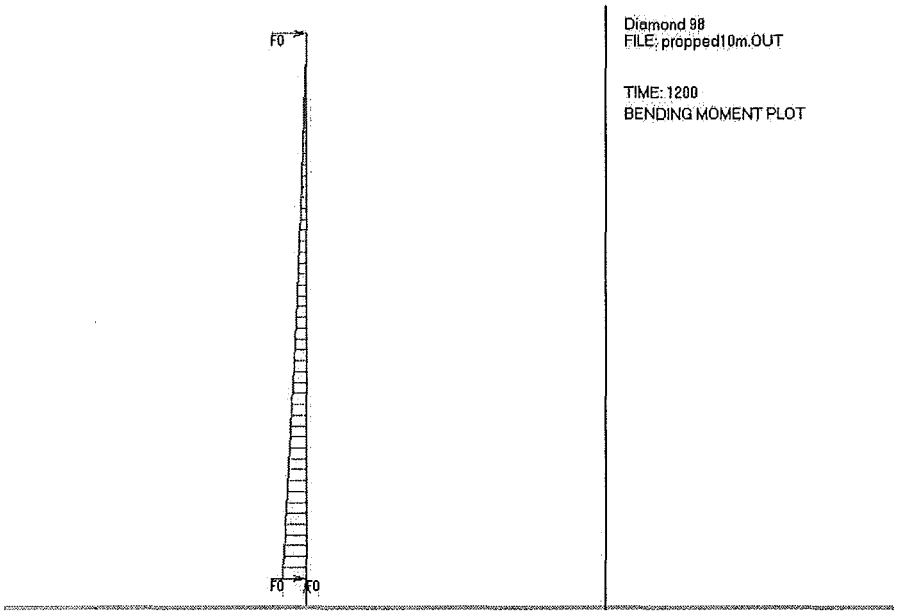

Figure 7.5: Bending moment diagram of the wall due to deflection before a plastic hinge has formed at the base.

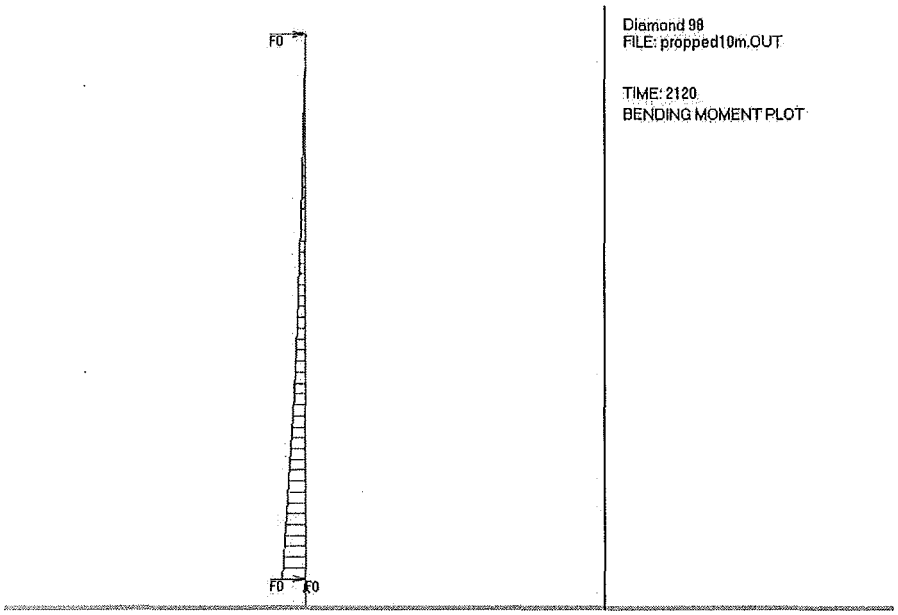

Figure 7.6: Bending moment diagram of the wall due to deflection after a plastic hinge has formed at the base.

The variation of bending moment at the base with time is shown in Figure 7.7. The graph shows that the bending moment increases in an almost linear trend during the initial stages of heating. The bending moment increment decreases after approximately 900 seconds (15 minutes) and plateaus after 1500 seconds (25 minutes). After reaching the plateau, the bending moment decreases slightly and the wall collapses at 2100 seconds (35 minutes).

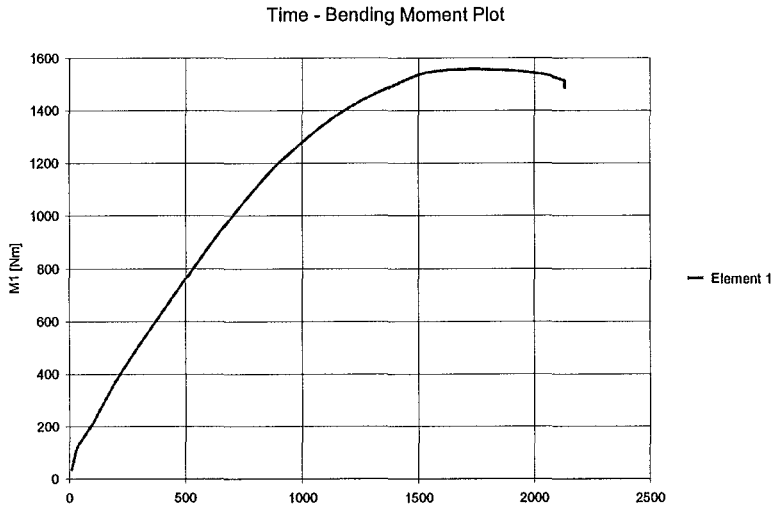

Figure 7.7: Variation of bending moment at the base of the wall.

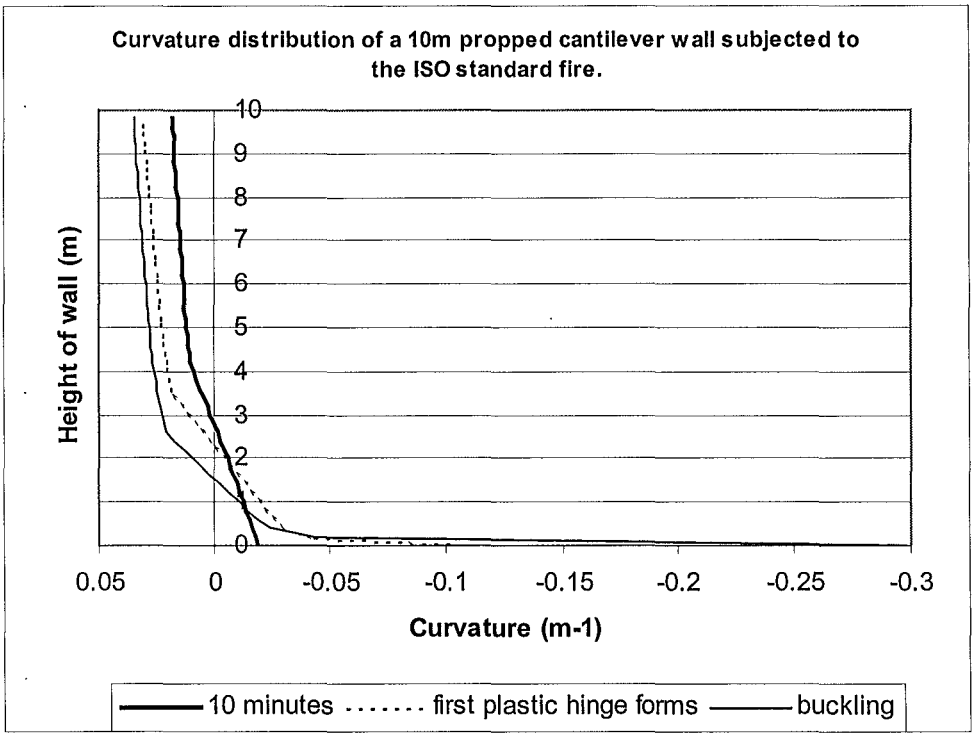

Figure 7.8: Curvature profile of a 10m wall at various stages of the ISO standard fire.

Figure 7.8 shows the curvatures of the 10 meter propped cantilever wall at various stages of the ISO standard fire. During the first 10 minutes of the fire, the curvatures of the wall are relatively small. The top 7 meters of the wall have positive curvature and the bottom 3 meters have negative curvature. The curvatures of the wall increase as the wall deflects further. At the same time, the point of inflection decreases, down the height of the wall.

When a plastic hinge forms at the base of the wall, the curvatures have become very large. After the plastic hinge has formed, the increase in curvature is localised at the base of the wall. The increasing curvatures at the base correspondingly decrease the stiffness of the wall. The stiffness degradation is due to cracking of the concrete and due to thermal effects on the concrete. At the point of buckling, the stiffness of the wall has decreased to a point where it is insufficient to support the wall. The curvatures at the base of the wall are very large at the point of collapse.

- **Variation of stresses at the base of the wall with time**

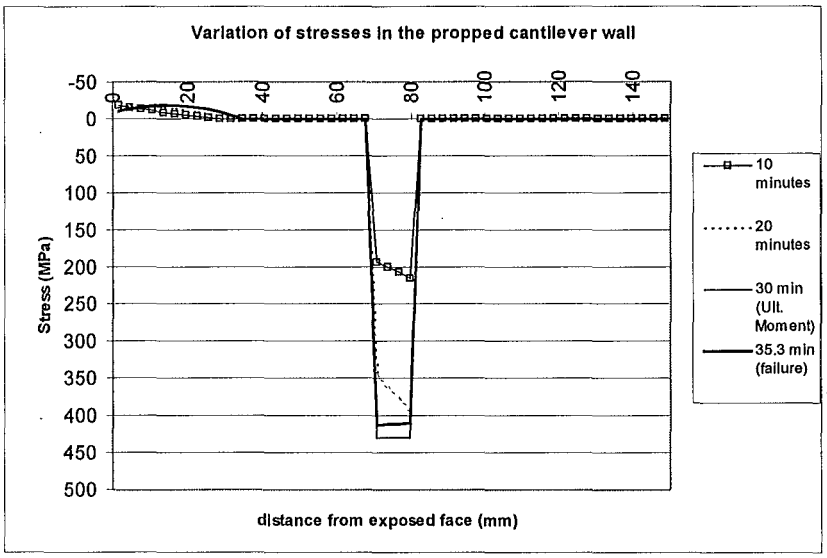

Figure 7.9: Stress profile at the base of a 10m propped cantilever wall.

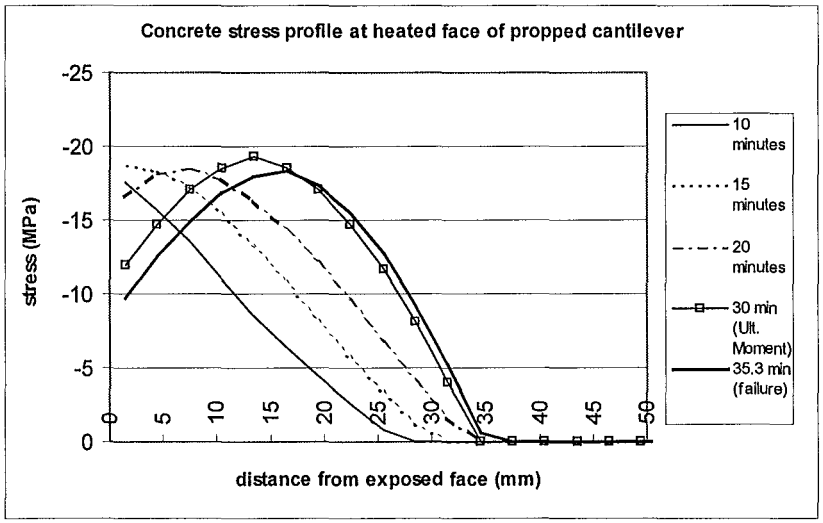

Figure 7.10: Concrete stress profile at the base of a 10 m propped cantilever wall.

The figures above illustrate the variation of the stresses in the section. The wall is heated on the left side of the graph. The tensile stresses in the reinforcing steel and the compressive stresses in the concrete increase as the wall is progressively heated (Figure 7.9). At approximately 900 seconds (15 minutes), the concrete in compression at the heated side had reached its compressive strength limit. The stress profile of the concrete in Figure 7.10 indicates that the concrete compressive strength has been reduced from 30MPa to approximately 19 MPa due to thermal effects.

The compressive stress distribution at the left side of the wall progressively shifts inwards from the heated face as time increases. This is due to the increasing curvatures from thermal bowing of the wall and due to temperature effects on the concrete compressive stress. During the advanced stage of the fire, the stresses at the extreme compressive fibre has reduced significantly and the strains are very high (Figure 7.10). The curvatures due to thermal bowing and the high temperatures increase the strains (refer to Figure 3.23) at the extreme compressive fibre of the wall. As the strains of the concrete increase, the corresponding stresses decrease, following the descending branch of the stress strain model.

DISCUSSION

The deflection of the propped cantilever wall is due to non-uniform thermal expansion across the section of the wall. The heated face of the wall expands more than the unheated side and induces a curvature which causes the wall to deflect. Since the top of the wall is restrained from deflecting horizontally, the wall bows into the direction of the fire. The deflected shape (Figure 7.2) shows that the compression side of the wall at the base is exposed to the fire. This causes the compressive strength of the concrete to progressively reduce due to high temperatures.

The moment due to the deflection of the wall causes the reinforcing steel to yield, thus forming a plastic hinge at 1550 seconds (26 minutes). The plastic hinge causes stiffness degradation of the wall and the rotation at the base to be unrestrained. The wall then behaves as a simply supported beam-column.

The decrease of the plastic moment prior to failure of the wall is due to the reduction of the yield strength of the steel due to thermal effects. At 2100 seconds (35 minutes), SAFIR detects instability in the wall when it buckles. The buckling is due to the reduction of the flexural rigidity of the wall due to thermal effects and significant cracking of the concrete. When the flexural rigidity of the wall had been reduced until it could not support the weight of the wall, the wall buckled.

Buckling load calculations

The buckling load calculation is done to verify that the wall has collapsed due to buckling and not due to a numerical failure.

The critical buckling load of the propped cantilever at the point of collapse can be determined as (Roark and Young, 1975):

$$(pa)' = K\frac{\pi^2(EI)_{eff}}{H_{wu}^{\ 2}} \quad \text{Equation 7-1}$$

Since a plastic hinge has formed at the base of the wall, the wall is assumed as a simply-supported beam column that is pinned at the base and its horizontal displacements are restrained at the top.

For a wall pinned at the base and horizontally restrained at the top:

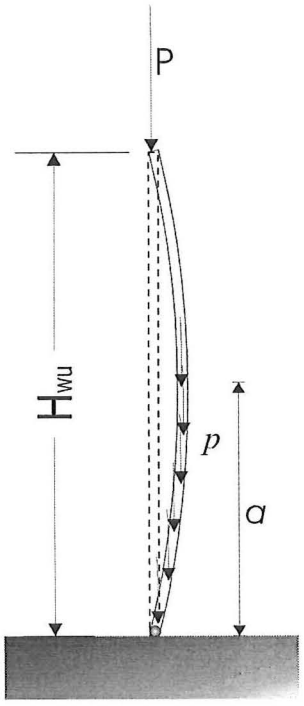

H_{wu}= unsupported length of the wall.

a = length of uniformly distributed load

p = uniformly distributed load

P = point load

For: $P/pa = 0.0$ $a/H_{wu} = 1.0$

Gives: K=1.88

The left part of Equation 7-1 represents the load of the wall:

$(pa)'$=3663N/m/m × 10m = 36630N/m (for a unit metre width of wall)

The right part of the equation is the buckling resistance of the wall:

$$K \times 3.142^2 \text{ x } (EI)_{eff} / (10000mm)^2$$

EI is obtained from the equation (Park and Paulay, 1975):

$$\phi = \frac{M}{EI}$$

A possible area of the wall where buckling could occur is in the midheight region of the wall. The curvature and corresponding bending moment at a point above the midheight of the wall (6.0 metres above the base) is chosen to determine the possibility of buckling. The respective curvature and bending moment at this point is approximately 0.030 m^{-1} and 5606 Nm/m. Therefore, *EI*, equals:

$$(EI)_{eff} = \frac{M_b}{\phi} = \frac{5606\,Nm/m}{0.030\,m^{-1}} = 188950\,Nm^2/m$$

Therefore, the critical buckling load of the wall equals:

$$\frac{K\pi^2(EI)_{eff}}{H_{wu}{}^2} = \frac{1.88 \times 9.87 \times 188950}{10^2} = 35060N/m$$

Since the load of the wall (36630 N/m) exceeds the critical buckling load of the wall (35060 N/m), the wall buckles and collapses.

7.3. Parameter study

This section investigates the effect of varying the parameters on the behaviour of a propped cantilever wall when it is subjected to a fire on one side. The parameters that will be varied are the influence of P-delta, the height of the wall, the thickness of the wall, the quantity of reinforcing and the vertical axial load. The bending moments at the base of the wall, the horizontal reaction, the horizontal and vertical displacements will be used to assess the effect of changing these parameters.

7.3.1. Influence of P-Delta

This part of the analysis serves to determine the effect of the self-weight on the behaviour of the propped cantilever wall. Two cases are analysed: one with its self-weight and the other without its self-weight (i.e.: no P-delta effects). All the other variables are kept constant as stated in section 7.2.

Case	Loads
i)	Self weight included
ii)	No self-weight

Table 7-1

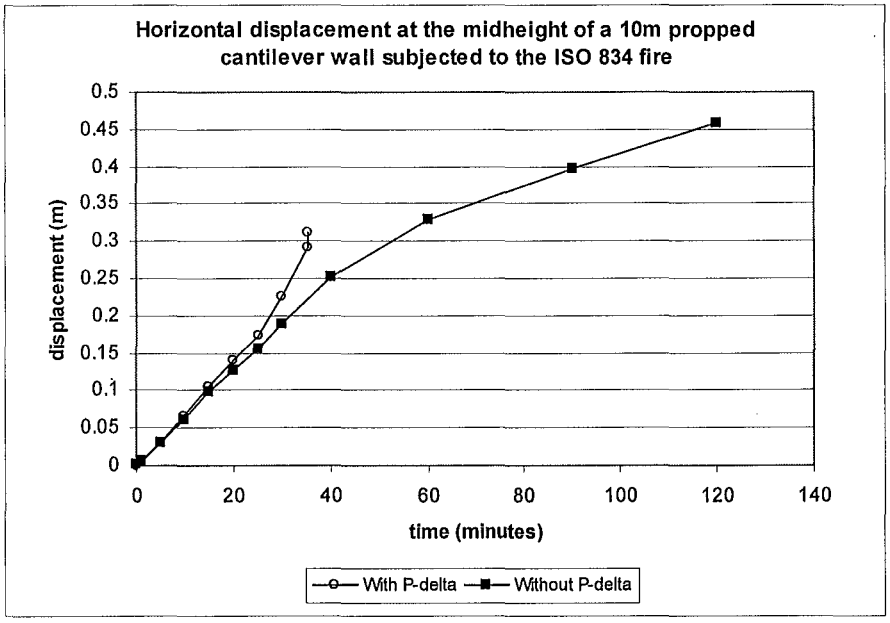

Figure 7.11:Variation of horizontal displacement at mid-height of propped cantilever walls analysed with and without the P-delta effect.

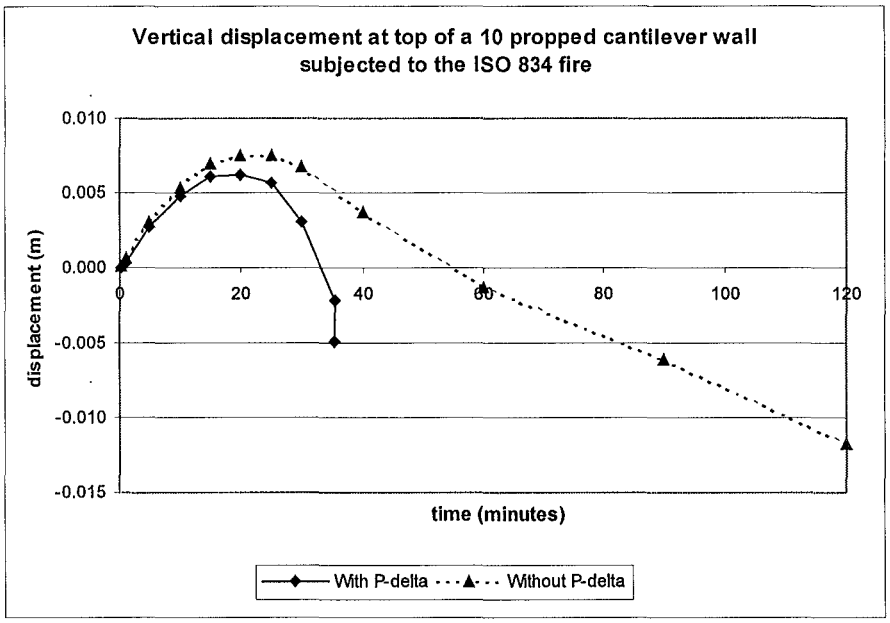

Figure 7.12: Variation of vertical displacement at the top of propped cantilever walls analysed with and without the P-delta effect

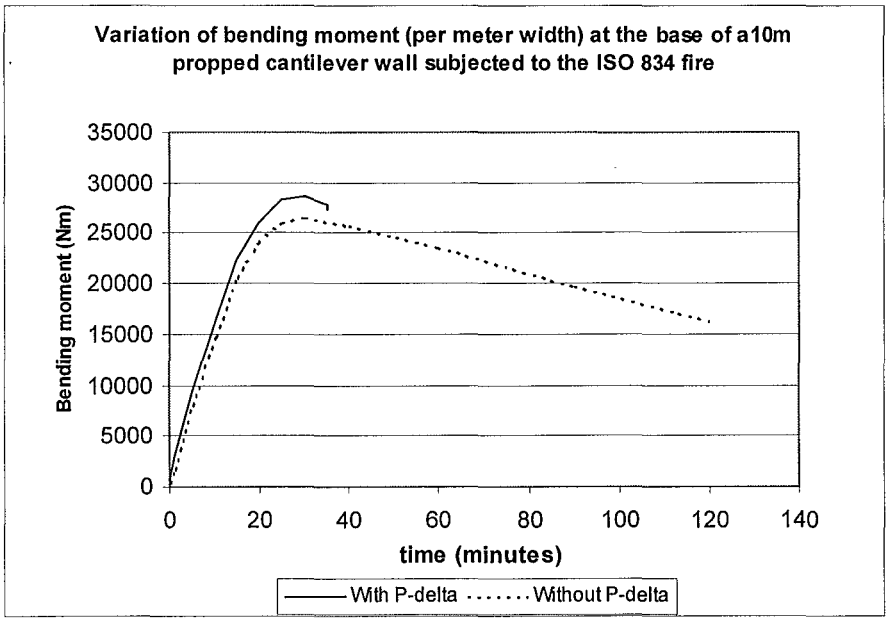

Figure 7.13: Variation of bending moment at the base of propped cantilever walls analysed with and without the P-delta effect

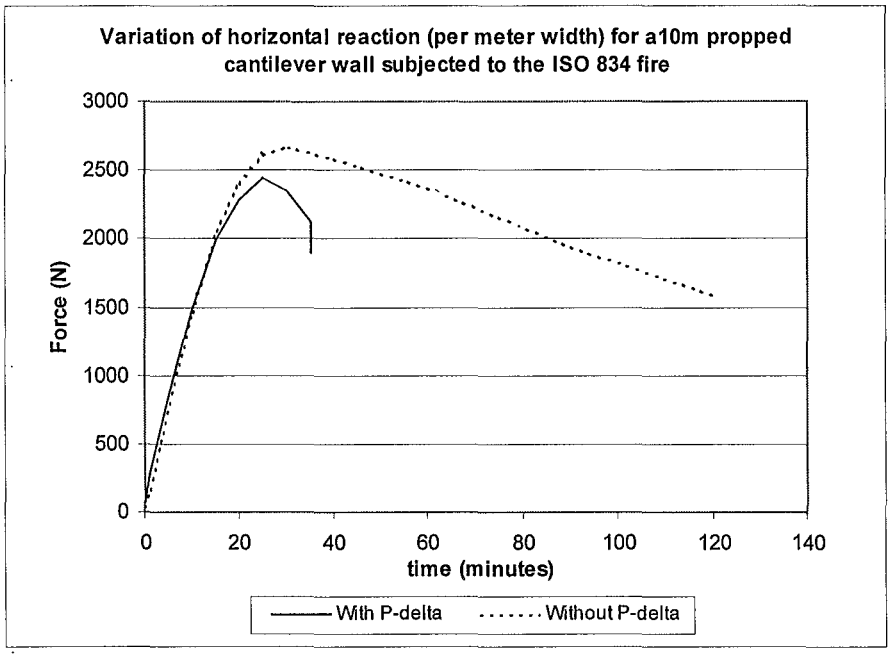

Figure 7.14:Variation of horizontal reaction at the top of propped cantilever walls analysed with and without the P-delta effect

- **Horizontal displacements at mid-height of the wall**

The horizontal displacements at mid-height of the wall for both walls initially increase linearly with time. The displacements in case i) increase more rapidly after approximately 25 minutes, showing the runaway displacement. Case ii) shows a gradual decrease in the displacement rate after the wall had reached its flexural capacity at 25 minutes.

- **Vertical displacements**

Figure 7.13 shows the variation of the vertical displacement at the top of the propped cantilever wall for walls analysed with and without the P-delta effect. During the first 15 minutes, the wall shows upward displacement. The vertical displacements plateau after 15minutes. After 25 minutes of fire exposure, the displacements start to decrease. The wall in case i) shows a rapid downward displacement and fails at approximately 35 minutes. In case ii), the wall does not show a runaway downward displacement but a gradual descending downward displacement.

- **Bending moments at the base of the wall**

Figure 7.13 shows the variation of bending moment at the base of the wall. For both cases, the bending moment increases linearly during the initial stages. The bending moment levels off after 15 minutes and reaches a plateau. The maximum moment reached in case i) is larger than case ii) (28.6kNm compared with 26.5kNm). For case i) the moment decreases slightly after the plateau has been reached and the wall collapses at approximately 35 minutes. However, for case ii) the bending moment decreases linearly after the moment plateau. Unlike the wall in case i), case ii) does not fail.

- **Horizontal reaction**

During the initial stage, the horizontal reaction increases linearly with time. After 15 minutes, the force increment decreases. For case i), the maximum force is reached at 25 minutes. After reaching its peak, the horizontal force declined rapidly.

For case ii), the horizontal reaction at the top of the wall increases linearly as in case i). However, the maximum force that it peaks is higher than in case i). The horizontal force decreases in a linear fashion in case ii) at the advanced stage of the fire.

DISCUSSION

• Horizontal displacements at mid-height of the wall

The wall deflects inwards due to the non-uniform thermal expansion of the wall. At approximately 30 minutes, a plastic hinge forms at the base, reducing the stiffness and rotational restrain at the base of the wall. This causes the displacement rate to increase. Apart from the temperature induced deflections, the P-delta effect takes place where the weight of the wall pulls itself downward, causing the wall to bow out further. Hence, the runaway displacement occurs.

The wall in case ii) does not exhibit a runaway displacement because there is no self-weight to amplify the displacements and to cause it to buckle. The horizontal displacement for this case is solely from thermal bowing.

• Vertical displacements

The initial upward displacement of the wall is due to thermal elongation. The downward displacement which follows after 25 minutes is due to the out-of-plane bowing of the walls, which causes the overall height of the wall to reduce. The reduction in the vertical displacement due to outward displacement is larger than the thermal elongation of the wall, thus producing a net downward displacement. The runaway downward displacement in case i) is due to the P-delta effects of the wall, dragging the wall downwards. The wall in case ii) does not show a runaway downward displacement but a gradual descending downward displacement as the P-delta effects are not present.

- **Bending moments at the base of the wall**

The difference in the plastic moments, M_p, of the two walls could be due to the concrete compressive stress in case i) being higher than in case ii). This is because the unstressed concrete compressive strength is lower than in stressed concrete (refer to section 4.2.9 and Figure 4.12). Therefore, the moment capacity of the wall with its self-weight is higher.

For case i) the wall fails at approximately 35 minutes due to buckling. At the point of buckling, the flexural rigidity at the base of the wall had been significantly reduced. The reduction of the flexural rigidity is due to cracking of the section and thermal effects on the elastic modulus of concrete. The wall in case ii) does not collapse as there is no self-weight to cause buckling of the wall. The linearly decreasing trend of the plastic moment is due to the reduction in the steel yield strength and the concrete compressive strength due to the thermal effects.

- **Horizontal reaction**

The horizontal reaction at the top of the wall is an important factor as it determines the amount of horizontal force that would be imposed on the steel beam attached to the wall. For case i), the maximum force occurs when the reinforcing steel has fully yielded and the nominal strength of the wall is reached. The horizontal force declined rapidly after the formation of the plastic hinge. The presence of the plastic hinge allows rotation to occur at the base and increases the amount of horizontal deflection. The deflection in turn absorbs and reduces the horizontal reaction at the top of the wall. The runaway reaction force at the time of failure is due to the collapse of the wall when it buckled.

The maximum force in case ii) is higher than case i). This is due to the presence of the self-weight of the wall in case i) which reduces the thrust due to thermal bowing. During the advanced stage of the fire, the horizontal force for case ii) decreases in a linear fashion due to the reduction of the plastic moment.

CONCLUSIONS

This analysis has shown that the P-delta effects of the wall have a very significant influence on the behaviour of the propped cantilever walls. The P-delta effects cause the propped cantilever wall to buckle when the critical buckling load of the wall is reached. Without P-delta effects, the wall does not collapse and continues to bow outwards.

7.3.2. Height of wall

The following analysis serves to investigate the behaviour of propped cantilever walls with varying heights. The heights of the wall will be varied and the other parameters will be kept constant as stated in section 7.2. The heights of the walls that were analysed are shown in Figure 7.2.

Analysis case	Wall height	Slenderness ratio
iii)	6m	40
iv)	8m	53.3
v)	10m	67.7
vi)	12m	80

Table 7-2: Analysis cases with different wall heights

RESULTS OF ANALYSES

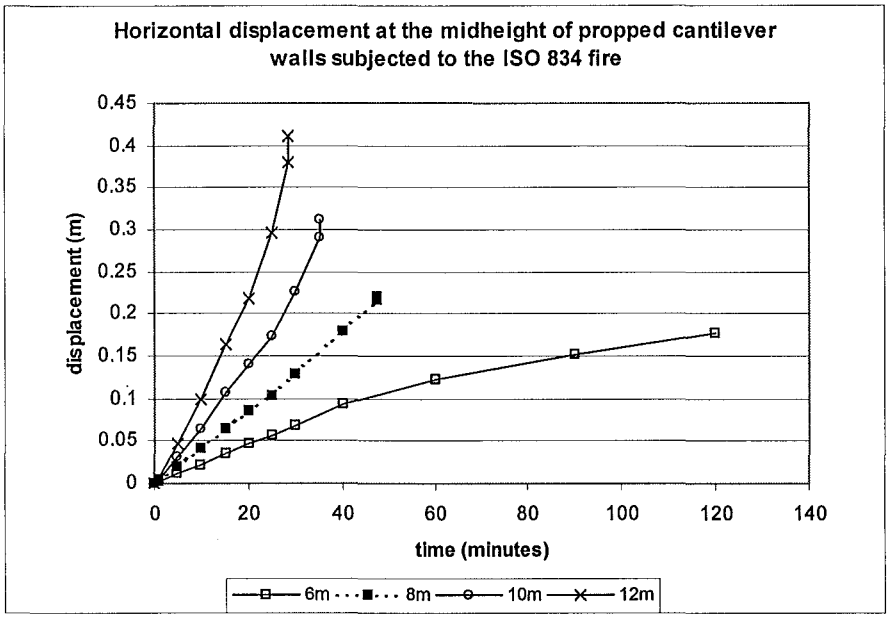

Figure 7.15: Variation of horizontal displacements at mid-height of propped cantilever walls of different heights.

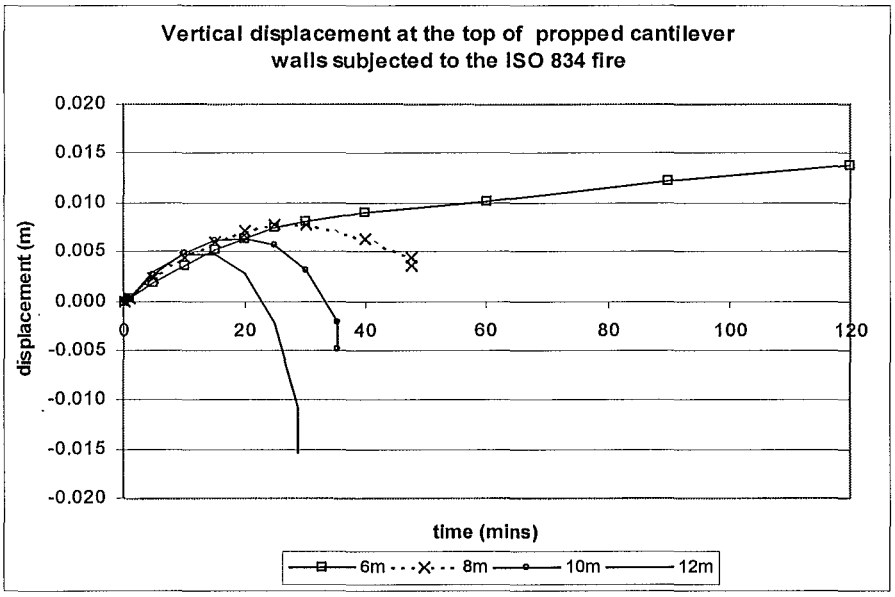

Figure 7.16: Variation of vertical displacement at the top of propped cantilever walls of different heights.

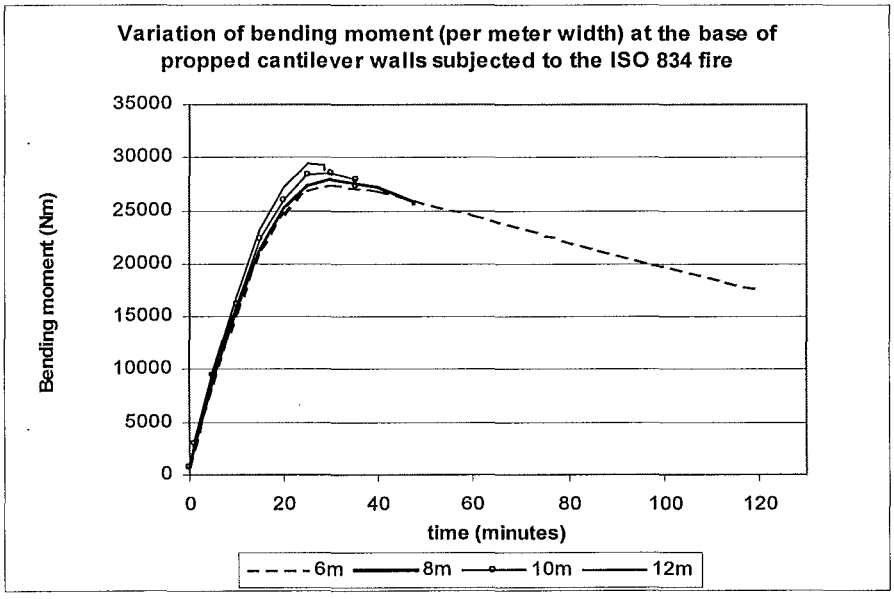

Figure 7.17: Variation of bending moment at the base of propped cantilever walls with different heights.

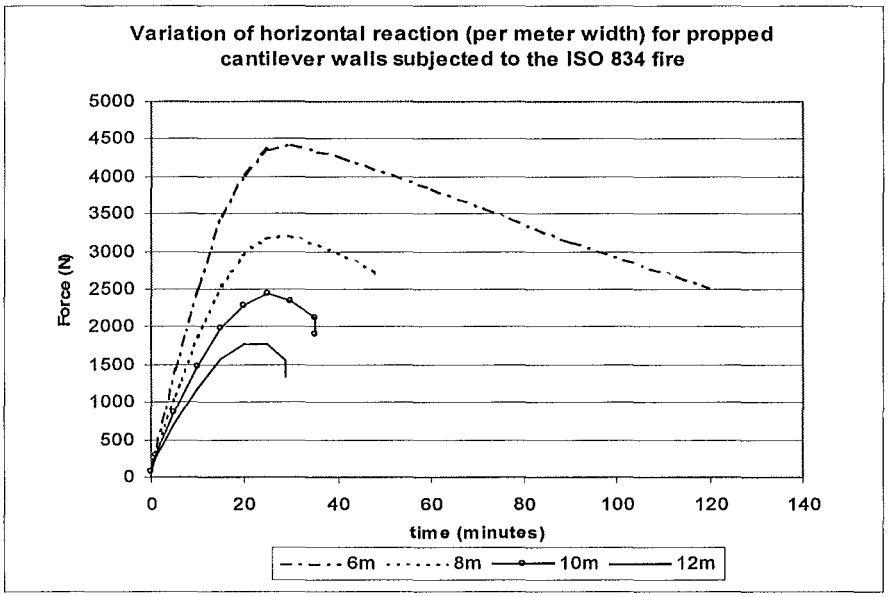

Figure 7.18: Variation of horizontal reaction at the top of walls with different heights.

- **Horizontal displacements at mid-height of the wall**

Figure 7.15 shows the variation of horizontal displacements at mid-height of propped cantilever walls of different heights. When the walls are heated, they deflect towards the fire. As the heights of the walls increase, the displacement rate increases.

The horizontal displacements of the 10 and 12 meter walls increase exponentially. They collapse at 35 minutes and 29 minutes, respectively. The 8 meter wall showed a linear displacement trend until approximately 48 minutes when the wall buckled. The 6 meter wall shows an almost linear increase in displacement initially. After approximately 45 minutes, the displacement rate decreases but still displays a linearly increasing trend.

The exponential trends of the heavier and taller walls are due to P-delta effects which pull the walls downwards, increasing the outward bow at the same time. When a plastic hinge forms, the rotational restraint at the base of the wall is lost. This allows the walls to deflect at a faster rate.

- **Vertical displacements**

Figure 7.16 shows the variation of the vertical displacements at the top of the propped cantilever walls with different heights. Despite the relatively small magnitudes, the vertical displacement trends are useful to determine the behaviour of the wall. Initially, all the walls experience an upward displacement. After the initial stages of the fire, all but the stockiest walls (6 meters) displace downwards, and eventually fail. Unlike the other walls, the displacements of the 6 meter wall increased linearly after the initial non-linear displacement trend.

The initial upward displacement of all the walls is due to the thermal expansion of the wall. The downward displacement of the walls is due to the outward deflection due to thermal bowing.

- **Bending moment at the base of the wall**

Figure 7.17 shows the variation of bending moments with time at the base of the wall. All the walls with different heights show similar trends. Initially, the bending moment increases linearly until approximately 15 minutes when the moment increment decreases and plateaus.

The moment plateau is due to a plastic hinge forming at the base of the wall. Although the walls have similar nominal moments, there are slight differences. As the height of the walls increase, the nominal moments of the wall increase. The level of stress from the self-weight of the wall increases as the heights of the walls increase. Therefore, the concrete compressive strength and nominal moments increase.

The bending moments for all the walls decrease in a similar trend, the only difference being the time which each of them fail. The taller walls fail earlier than the shorter walls. The bending moment at the base of the 6 meter wall decreases in a linear trend until the maximum time has been reached. Except for the 6 meter wall, all the other walls collapse. As the flexural rigidity is progressively decreased, due to cracking and thermal effects, the critical buckling load of the walls decrease. Since the shorter walls have lower buckling loads, they survive the fire longer.

- **Horizontal reaction**

The horizontal reaction at the top of walls with different heights is shown in Figure 7.18. The trends of the horizontal reaction are similar for the walls. They display a linear increase initially before levelling off and reaching a plateau. After that, the horizontal force drops off and failure occurs. The plateau of the horizontal force occurs when a plastic hinge has formed at the base. The presence of the plastic hinge reduces the stiffness of the structure, therefore reducing the thrust due to thermal expansion. The graph shows that the maximum horizontal reaction decreases with increasing height of the wall.

The horizontal reaction at the top of the wall decreases with increasing height. This is because the reaction at the top of the wall, H*, is approximately equal to:

$$H^* \approx \frac{M_b}{h_{wu}}$$

Where M_b =Moment at the base of the wall

h_{wu} = Unsupported height of the wall

Since the bending moment at the base of all the walls is almost constant at any time, the horizontal reaction is therefore, inversely proportional to the height of the wall. Compared to the shorter walls, the axial forces imposed on the connected rafters by the taller walls will be smaller. The shorter walls could pose as a significant factor in determining the behaviour of the overall structure as they would impose larger forces on the connected steel rafter.

DISCUSSION

The analyses have shown that the performance of the propped cantilever walls improves with decreasing wall height. The taller walls form plastic hinges at the base and buckle more rapidly compared to the shorter walls. The shorter walls on the other hand impose greater horizontal forces on the attached rafter compared to the taller walls. These large forces will be transferred to the connections at the base and between the wall panels and the rafter. Therefore, these connections have to be well designed and detailed to prevent outward collapse of the panels onto the neighbouring property.

CONCLUSIONS

Propping the cantilever walls with a fire protected rafter at the top prevents the cantilever walls from deflecting outwards. However, the mode of failure of the walls changes from flexural yielding of the reinforcement at the base, to buckling of the walls. The investigation has shown that the survival time of the walls decrease with increasing height. As the heights of the walls decrease, the horizontal axial force imposed onto the rafter due to thermal bowing, increase.

7.3.3. Thickness of wall

The effect of varying the thickness of the wall is investigated on the propped cantilevers. The standard wall as stated in section 7.2 is analysed for walls of different thicknesses. The height of the wall is kept constant at 10.0 meters. The thickness of the wall is varied from 150mm to other thicknesses in order to obtain the same slenderness ratio as analysed in 7.3.2. The thickness of the walls that are used in the investigation are shown in Table 7-3.

Analysis case	Wall thickness	Slenderness ratio
vii)	250mm	40
viii)	185mm	53.3
ix)	150mm	67.7
x)	125mm	80

Table 7-3: Analysis cases with different thicknesses.

RESULTS OF ANALYSES

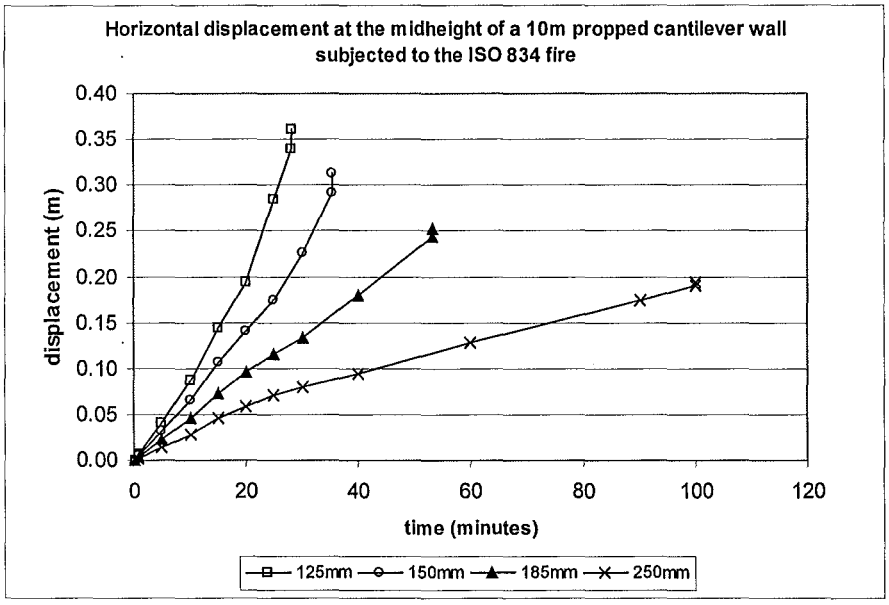

Figure 7.19: Variation of horizontal displacement at mid-height of propped cantilever walls with different thicknesses.

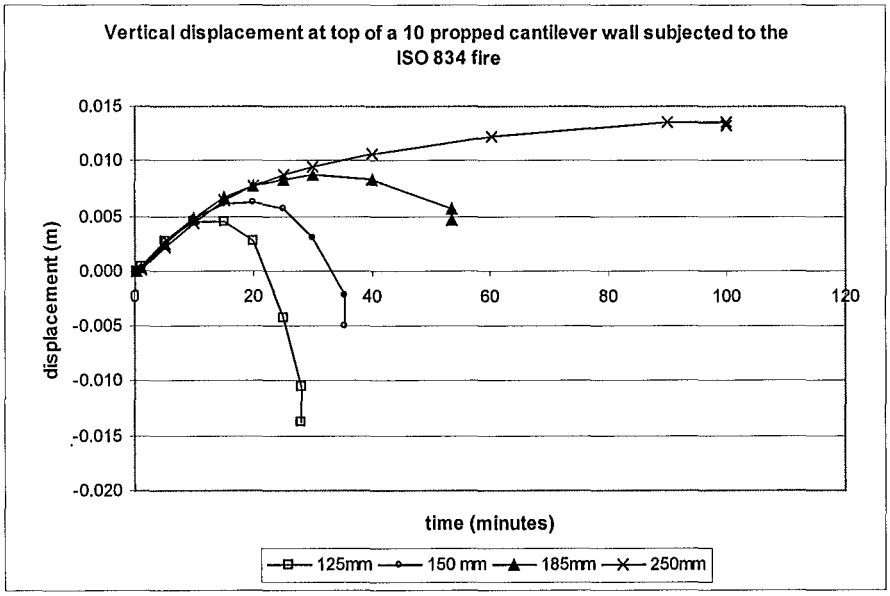

Figure 7.20: Variation of vertical displacement at the top of propped cantilever walls with different thicknesses.

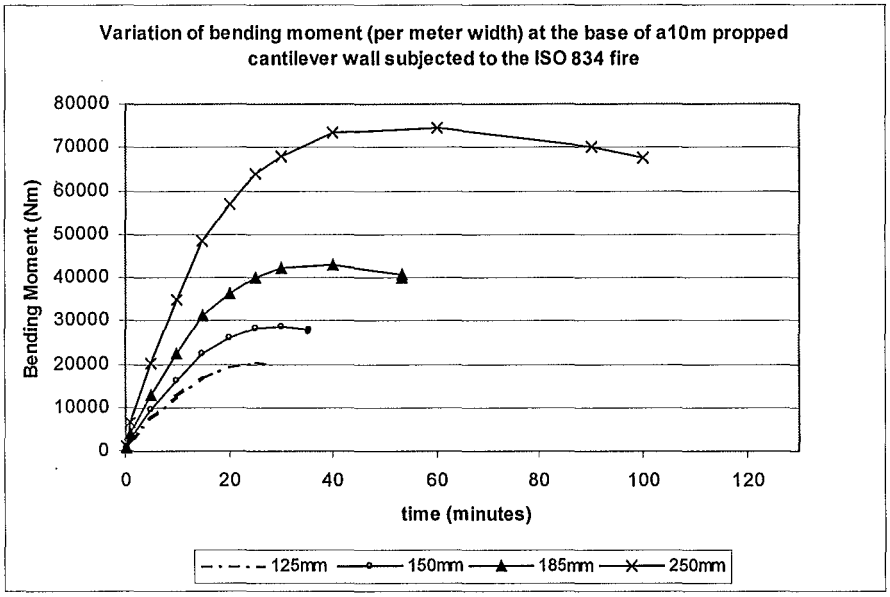

Figure 7.21: Variation of bending moment at the base of propped cantilever walls with different thicknesses.

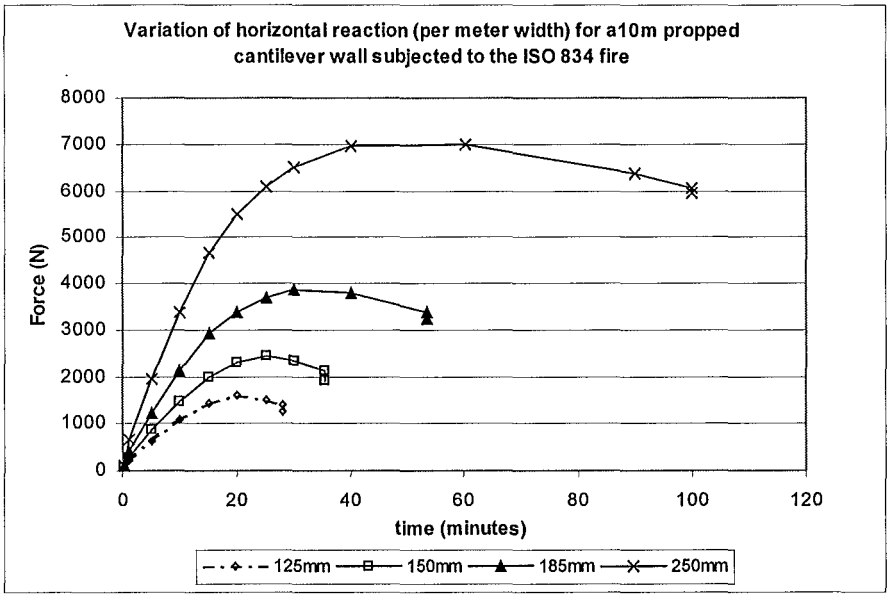

Figure 7.22: Variation of horizontal reaction at the top of propped cantilever walls with different thicknesses.

- ## Horizontal displacements at mid-height of the wall

Figure 7.19 shows the variation of the horizontal displacement at the mid-height of the propped cantilever for walls with different thicknesses. As the thicknesses of the walls decrease, the rate of deflection increases. The time to failure of the walls increase with increasing thickness. The trends of the displacements are very similar to those obtained in section 7.3.2 where the heights of the walls were varied. This close similarity is due to the same slenderness ratios obtained by varying the thicknesses for the 10 meter wall with the results obtained from 7.3.2.

- ## Vertical displacement

The variation of vertical displacements at the top of the walls with different thicknesses is similar to those in Figure 7.16, where the height of the walls were varied. This is again due to the same slenderness ratios in the walls which exhibit the same vertical displacement trends.

- **Bending moment at the base of the wall**

Figure 7.21 shows the variation of bending moments at the base of propped cantilever walls with different thicknesses. All the walls show similar trends in the bending moment trends where the moments show an initial steep rise, followed by a plateau. After the plateau has been reached, the bending moment decreases slightly before failure occurs. The graph shows that the nominal moments of the walls increase with increasing wall thickness.

- **Horizontal reaction at the top of the wall**

Figure 7.22 shows the variation of the horizontal reaction at the top of the walls with different thicknesses. The horizontal reaction at the top of the walls follows a similar trend as the bending moments at the base. As the thicknesses of the walls increase, the resulting reactions at the top of the walls increase. Therefore, the thicker walls would impose a larger axial force onto the connected rafter compared to the thinner walls.

DISCUSSION

Figure 7.21 shows that each wall has a different nominal moment due to the difference in thickness. The nominal moment of each wall section is proportional to the thickness of the wall since the moment capacity is a function of the internal lever arm.

$$M_n = A_s f_y jd$$

Where: M_n =Nominal moment of the wall

A_s =Area of reinforcing steel

f_y =Yield strength of reinforcing steel

jd =Internal lever arm

As the thickness of the wall increases, the survival time of the wall increases. The increase in the thickness of the wall allows for a larger neutral axis depth in the wall. Hence, the curvatures in a thicker wall will be smaller compared to a thinner wall at any given time.

$$\phi = \frac{\varepsilon_c}{c}$$

Where ϕ =curvature

ε_c =strain in extreme fibre in compression of concrete

c =neutral axis depth

A thicker section will take a longer time to reach its yield and ultimate curvatures. Thus, it will also take longer for the ultimate concrete strain to be achieved, and cause a plastic hinge to form at the base. Since the strains in a thicker section are lower than a thinner section at any given time, the corresponding stresses in the concrete will also be lower.

The thicker walls reduce the horizontal deflections of the walls and increase the survivability of the walls in a fire. However, the analyses have also shown that increasing the thicknesses of the walls will impose larger axial forces on the connected rafter. This requires good connections at the base and between the walls and rafter, or else the walls will collapse onto the neighbouring property.

CONCLUSIONS

This analysis has shown that by increasing the thickness of the walls, the deflections of the walls decrease. Apart from that, the time to failure of the wall increases. However, by increasing the thickness of the wall, the axial force imposed on the rafter increases.

7.3.4. Quantity of reinforcing

This part of the analysis serves to determine the effect of varying the quantity of reinforcing on the propped cantilever walls. The standard wall is analysed with various quantities of reinforcing steel to simulate the different sizes of reinforcement and spacings that would typically be constructed. These different quantities of reinforcement are modelled with an equivalent steel ratio in SAFIR. The thickness of the wall is 150mm. All the other variables are kept constant as stated in section 7.2.

The quantities of reinforcing modelled in the wall are summarised in Table 7-4.

Case	Reinforcing bar size	Bar spacing	Equivalent steel ratio
xi)	12 mm	200mm c/c	0.38%
xii)	16mm	200mm c/c	0.67%
xiii)	16mm	125mm c/c	1.07%
xiv)	16mm	100mm c/c	1.34%

Table 7-4: Cases analysed to investigate the effect of different amounts of reinforcing steel.

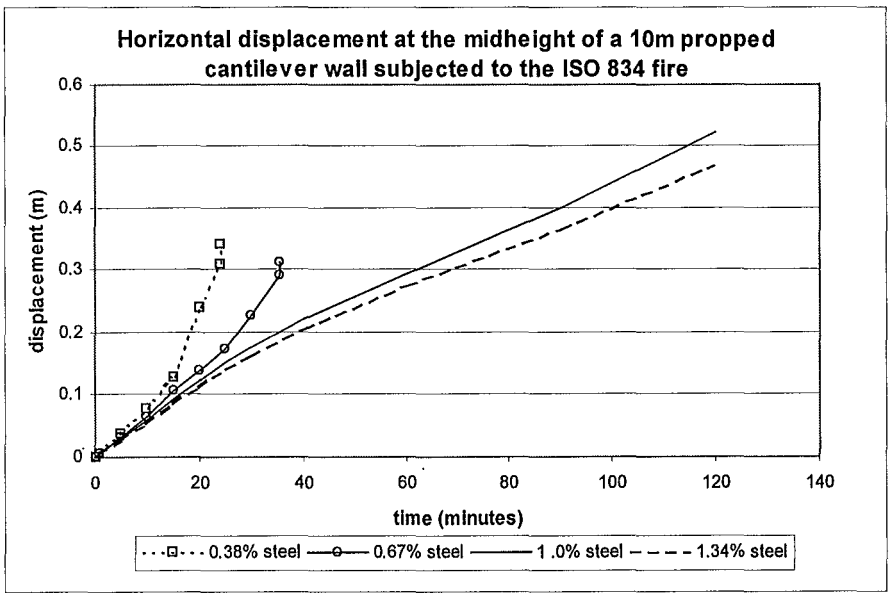

Figure 7.23 Variation of horizontal displacements at mid-height of a 10m propped cantilever wall with different quantities of reinforcing steel.

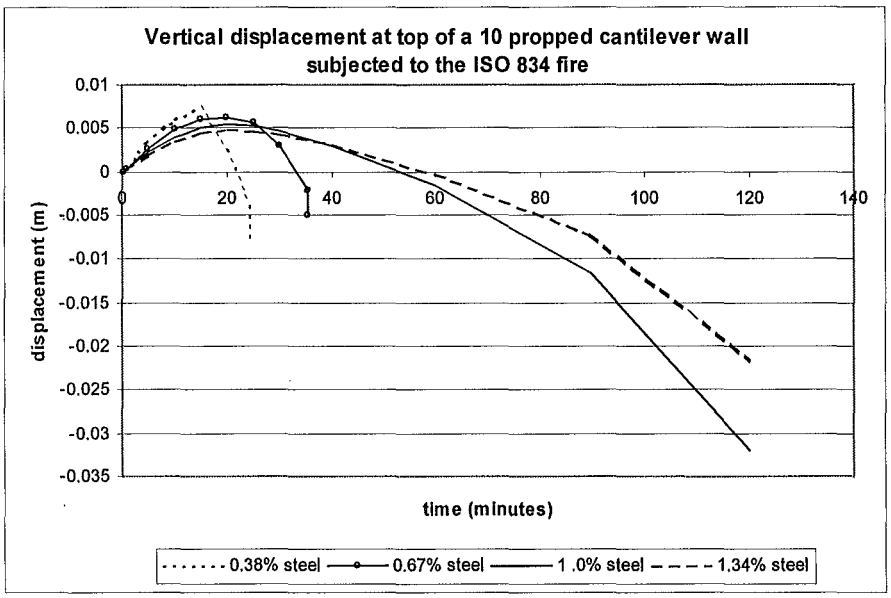

Figure 7.24: Variation of vertical displacements at the top of a 10m propped cantilever wall with different quantities of reinforcing steel.

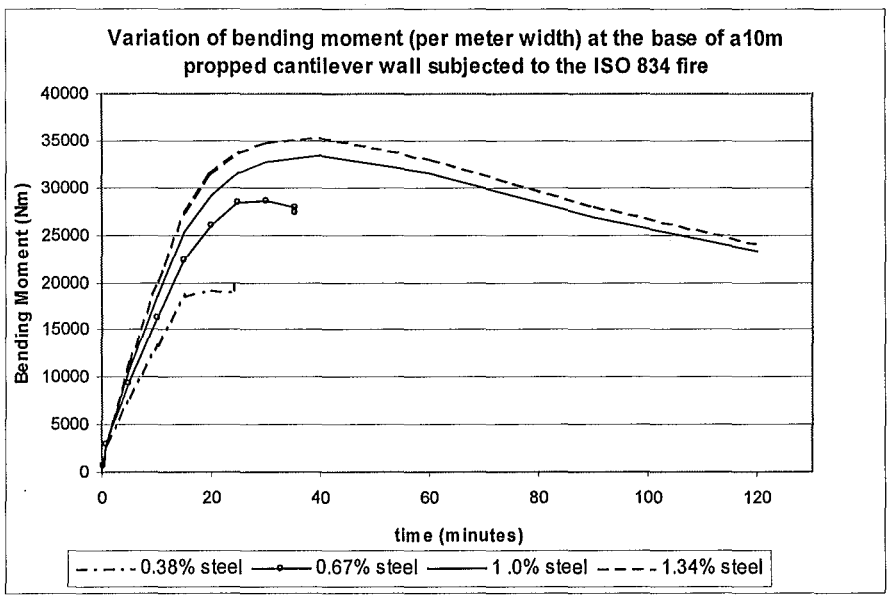

Figure 7.25: Variation of bending moment at the base of a 10m propped cantilever wall with different quantities of reinforcing steel.

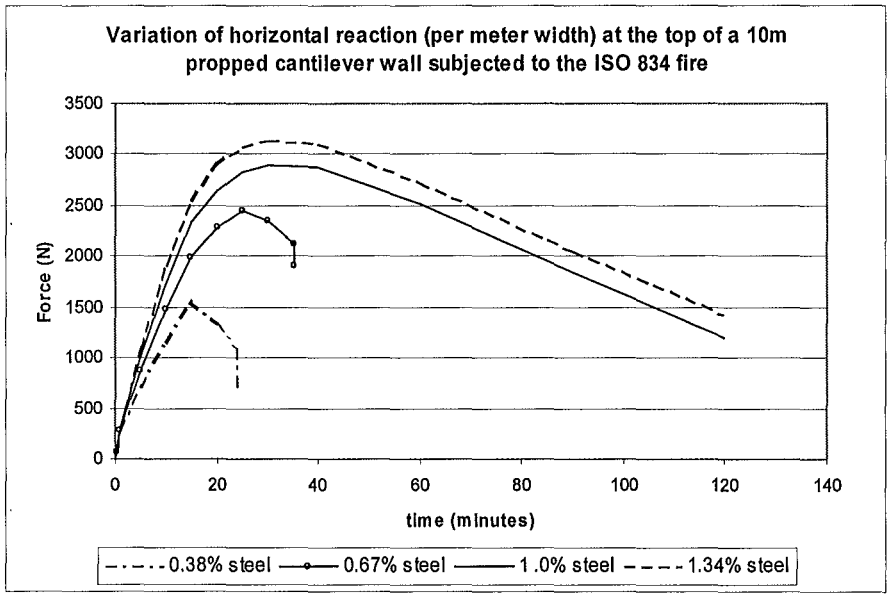

Figure 7.26: Variation of the horizontal reaction at the top of a 10m propped cantilever wall with different quantities of reinforcing steel.

- **Horizontal displacements at mid-height of the wall**

Figure 7.23 shows the variation of horizontal displacements with time at mid-height of the wall. During the initial stages, the displacements of all the walls increase linearly. The walls with 0.38 percent and 0.67 percent reinforcement show an increase in the displacement rate after 20 and 30 minutes, respectively. The rapid increase of the displacement of the walls with 0.38 percent and 0.67 percent reinforcement after 15 and 25 minutes, respectively, is due to plastic hinges that have formed at the base. The plastic hinges reduce the rotational restraint of the wall, thus allowing the walls to displace at a faster rate due to thermal expansion and P-delta effects. They eventually collapse at 24 minutes and 35 minutes, respectively. The walls with 1.07 percent and 1.34 percent reinforcement show an almost linear displacement trend throughout the entire simulation and do not collapse.

- **Vertical displacements**

The variation in vertical displacements for walls with different reinforcement quantities is shown Figure 7.24. The walls with low amounts of reinforcement (0.38 and 0.67 percent) show a parabolic displacement trend with the initial vertical rise due to thermal expansion. The walls with higher amounts of reinforcing (1.07 and 1.34 percent) show the same initial vertical rise as the other walls. However, their descent is more gradual at the later stages of the fire and there is no obvious runaway displacement.

- **Bending moment at the base of the wall**

Figure 7.25 shows the variation of bending moments at the base of a wall with different quantities of reinforcing. The nominal moment of the wall increases as the quantity of reinforcement is increased. All the cases analysed show very similar moment trends. The moment increases linearly during the initial stage before levelling off. The plateau is due to the plastic hinge forming. The nominal moments of the walls increase with increasing steel quantity.

Cases xi) and xii) fail at 24 and 35 minutes, respectively. Cases xiii) and xiv) survive the entire simulation without failing. Cases xi) and xii) with 0.38 and 0.67 percent reinforcing fail due to buckling, after the plastic hinges have formed at the base of the walls. The non-uniform

thermal expansion of the wall causes thermal bowing which in turn, causes cracking at the base of the wall. Coupled with high temperatures, the cracking reduces the flexural rigidity at the base of the wall. As the heating of the wall progresses, the buckling load of the wall is reduced to the point it cannot support the weight of the wall, therefore it collapses.

- **Horizontal reaction**

Figure 7.24 shows the variation of the horizontal reaction at the top of the wall with time. The walls with 0.38 percent and 0.67 percent reinforcement show a prominent drop in the reaction when the reaction reaches its maximum at 15 and 25 minutes, respectively. The drop in the horizontal force is due to the formation of the plastic hinge at the base which causes the wall to become more flexible. The plastic hinge allows more horizontal deflection to occur, thus absorbing and reducing the thrust produced by the wall due to thermal expansion. Apart from that, the self-weights of the walls decrease the horizontal thrust of the wall.

The reaction of the walls with 1.07 and 1.34 percent reinforcing decrease in a linear trend after the maximum horizontal force has been reached. The decrease of the reaction corresponds to the decreasing plastic moment at the base of the wall and increasing deflections which absorbs the thrust of the walls.

DISCUSSION

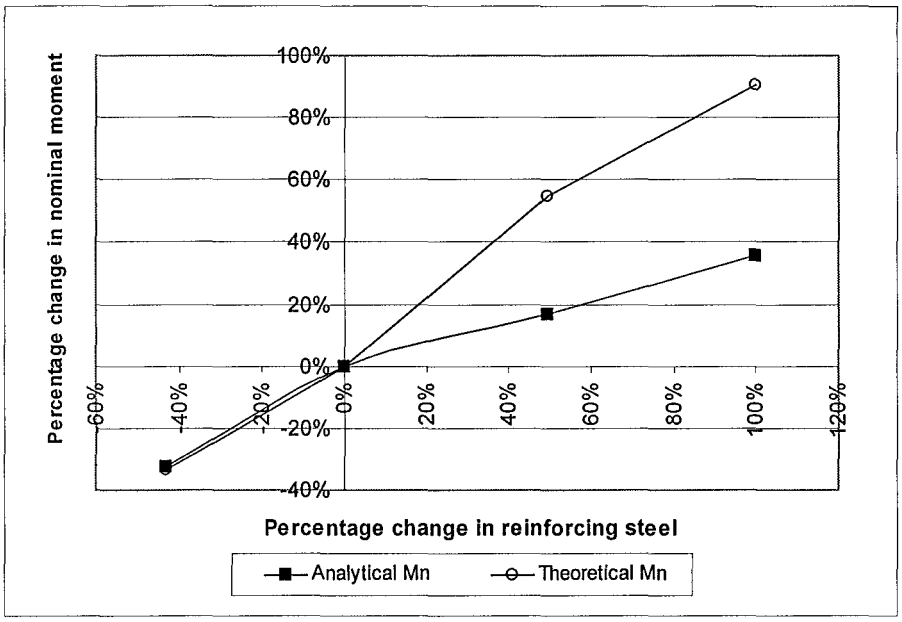

Figure 7.27: Variation of nominal moments and time to failure in walls with different reinforcement quantities, based on the standard wall with 0.67% steel.

Figure 7.27 shows the comparison of the theoretical and analytical nominal bending moments of the wall. The theoretical moment is the moment capacity of the wall at ambient temperatures. The analytical moment is the moment capacity of the wall obtained from the analyses, under elevated temperatures. The percentage changes in nominal moment are relative to the standard wall with 0.67 percent reinforcing.

There is a high amount of deviation between the theoretical and analytical moments for the sections with higher quantities of reinforcement (1.07 and 1.34 percent). The stresses in the wall with 1.34 percent steel are plotted in Figure 7.28 and Figure 7.29. Figure 7.28 shows that when the wall has reached its nominal moment at 40 minutes, the concrete had reached its ultimate compressive stress but the steel had not yielded. The steel and concrete stresses progressively decrease after the wall has reached its nominal moment. Figure 7.29 shows that the concrete compressive stress distribution and the neutral axis depth of the wall shifts inwards from the heated face of the wall as the wall is progressively heated. The ultimate stress of the concrete also decreases as the wall is progressively heated.

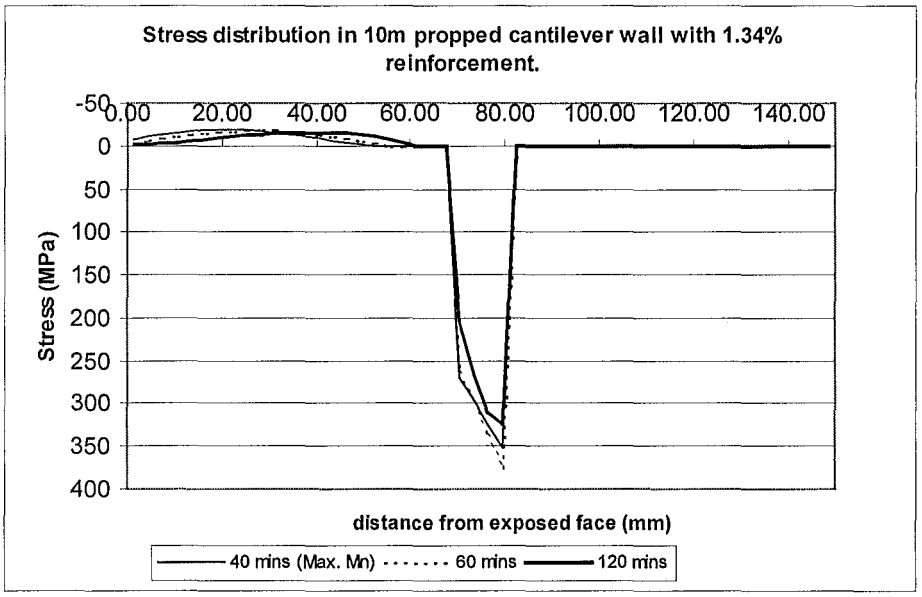

Figure 7.28: Stress distribution at the base of a10m propped cantilever wall with 1.34% reinforcement.

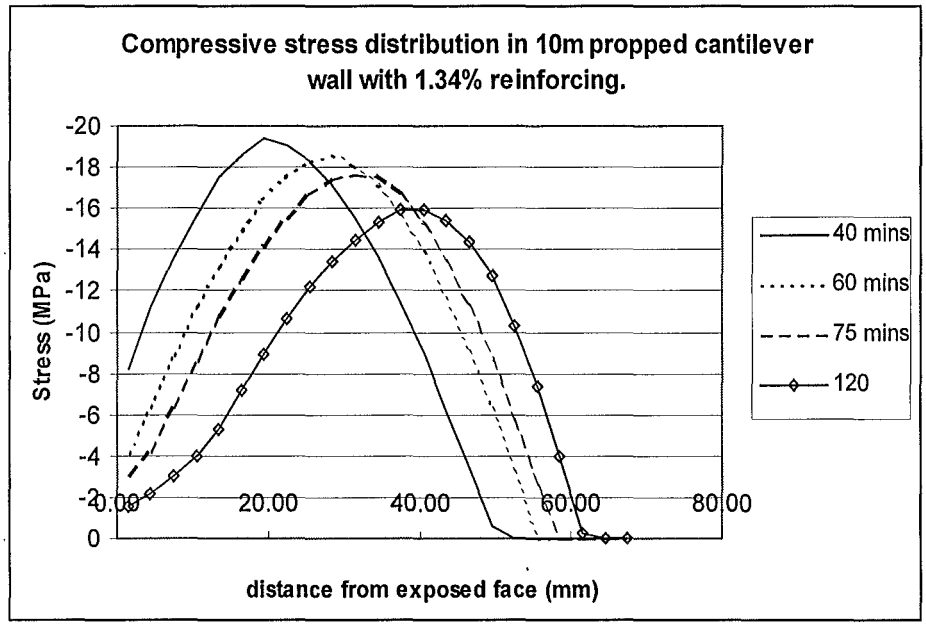

Figure 7.29: Compressive stress distribution at the base of a 10m propped cantilever wall with 1.34% reinforcement.

The analysis shows that by increasing the amount of reinforcing from 0.67 percent to 1.07 percent, the performance of the walls improve significantly. The walls are able to sustain much larger horizontal deflections and survive the fire throughout the entire simulation. The horizontal forces imposed onto the rafter are not significantly greater than the wall with 0.67 percent steel. Therefore, the strength of the connections of the wall at the base and to the rafter does not have to be enhanced significantly.

CONCLUSIONS

Propped cantilever walls with low amounts of reinforcing fail in a brittle manner almost immediately after the plastic hinges have formed. Increasing the reinforcement from the base value of 0.67 percent to 1.07 percent shows a marked improvement in the behaviour of the walls, allowing it to survive the fire for 120 minutes.

7.3.5. Axial load level

The effects of different levels of axial load on the behaviour of the wall when it is subjected to the ISO standard fire are investigated here. The axial loads imposed at the top of the wall represent the loads imposed by a rafter that is attached to the top of the wall. The axial load applied from the rafter is simulated in SAFIR by a single point load applied to the top of the wall. Table 7-5 shows the different analysis cases with different levels of axial load applied to the top of the wall. Case xv) represents the standard wall without any point loads applied to it.

Case	Axial load level ($N^*/A_g f'_c$)
xv)	0.0%
xvi)	1.0%
xvii)	5.0%
xviii)	10.0%

Table 7-5: Analysis cases for different axial load levels.

RESULTS OF ANALYSES

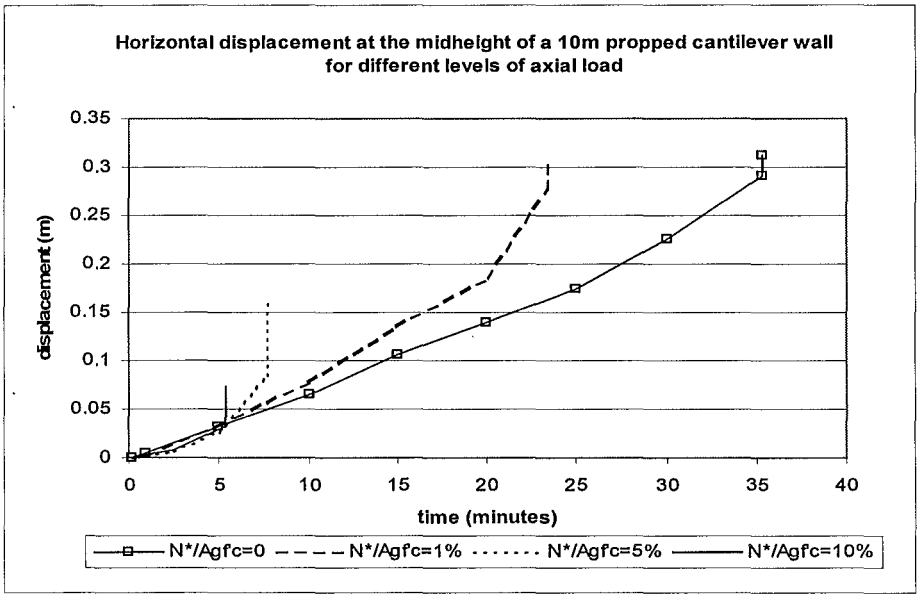

Figure 7.30: Variation of horizontal displacement at mid-height of a 10m propped cantilever wall with different levels of axial load.

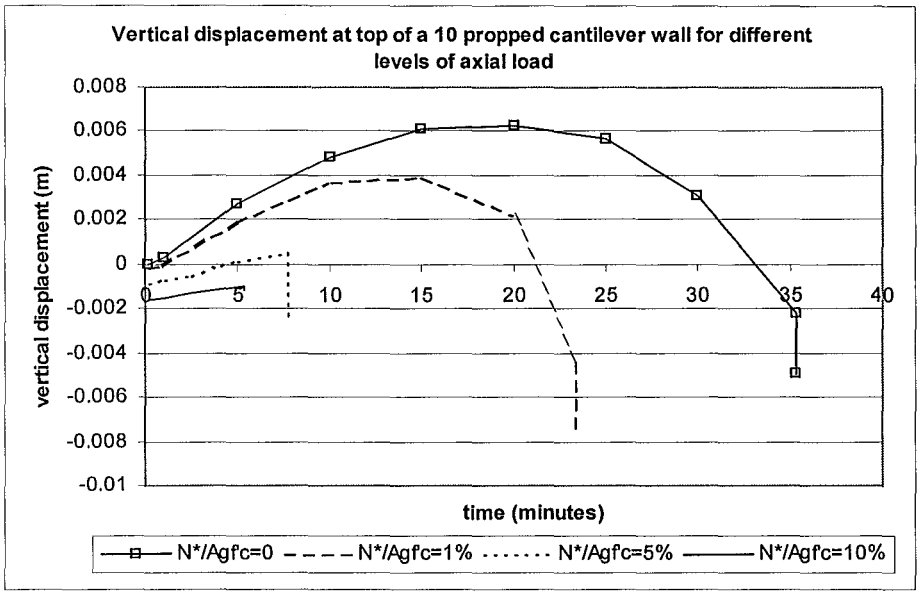

Figure 7.31: Variation of vertical displacement at the top of a 10m propped cantilever wall with different levels of axial load.

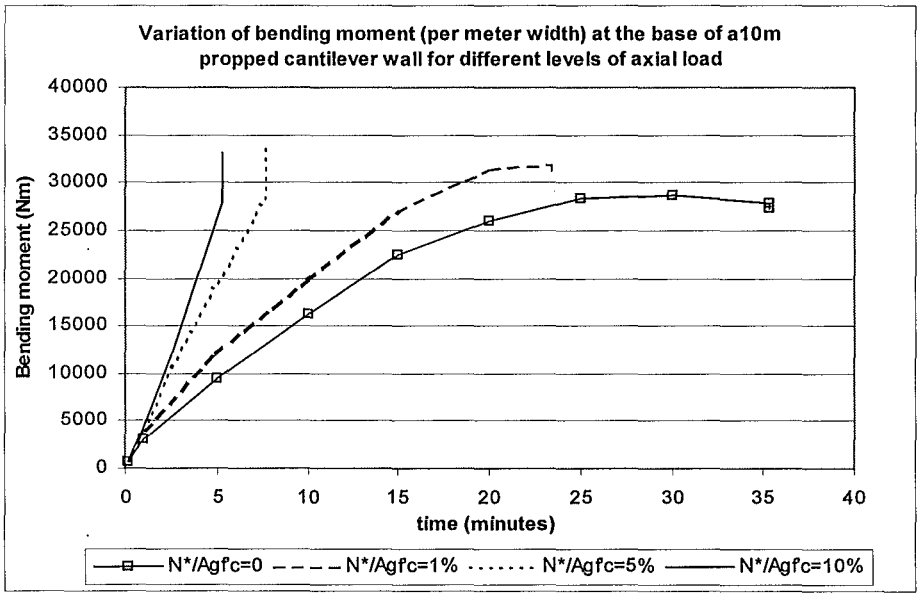

Figure 7.32: Variation of bending moment with time at the base of a 10m propped cantilever wall with different levels of axial load.

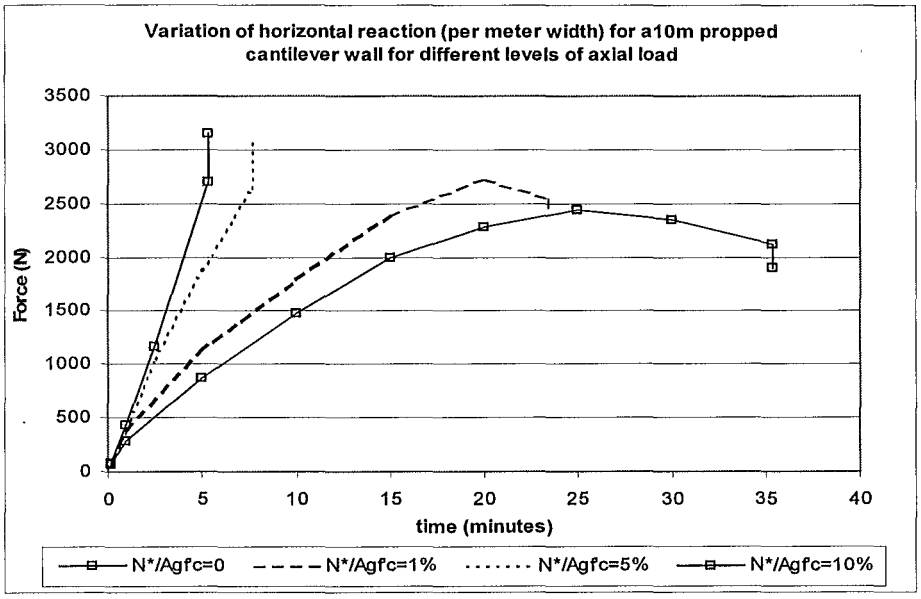

Figure 7.33: Variation of horizontal reaction for a 10m propped cantilever wall with different levels of axial load.

- **Horizontal displacements at mid-height of the wall**

Figure 7.30 shows the variation of horizontal displacements at mid-height of propped cantilever walls with different axial loads imposed. All the walls show a very similar initial trend, as they deflect outwards linearly with time. It shows that as the axial load level increases, the maximum sustainable displacement decreases. The time to failure of the wall also decreases as the axial load increases. The walls with high axial loads collapse at very small horizontal displacements. This is because the large axial force component causes very large P-delta effects. Apart from that, the wall with high axial loads reaches its critical buckling load very rapidly.

When a plastic hinge has formed at the base, the walls displace outwards very rapidly due to the lost of rotational restraint at the base. The wall without any axial load imposed, deflects 0.30 meters at mid-height and collapses after 35 minutes of fire exposure to the ISO fire. By increasing the axial load level to 10 percent, the time to failure drops to 5 minutes and the sustainable displacement is only 0.031 meters.

- **Vertical displacements**

The variation of vertical displacements at the top of the walls with different levels of axial loads is shown in Figure 7.31. The walls with low levels of axial load, cases xv) and xvi), display a parabolic displacement trend. The walls with high levels of axial loads, cases xvii) and xviii), have an initial net deformation due to the high level of axial load applied. Cases xvii) and xviii) exhibit some thermal elongation, although negligible, when they are heated.

- **Bending moment at the base of the wall**

The bending moment at the base of the walls with different levels of axial load vary with time as shown in Figure 7.32. The walls with high axial loads, cases xvii) and xviii), have a steep moment gradient during the initial stages. As the level of axial load increases, the survival time decreases and bending moment gradients increase. The walls with low axial loads show a more slower failure compared to those with high axial loads which show a very rapid failure as the plastic moments of the walls are reached in a very short time.

- **Horizontal reaction at the top of the wall**

The horizontal reaction at the top of the wall (Figure 7.33) varies with time in a similar manner as the bending moments.

DISCUSSION

The walls with low axial loads fail by buckling after yielding of the reinforcement. The mode of failure changes at high axial loads, to a rapid and brittle failure by buckling of the wall once a plastic hinge forms at the base. The walls with high axial loads, cases xvii) and xviii), have a steep bending moment rise during the initial stages. A very small horizontal eccentricity due to thermal bowing would induce large P-delta effects. This explains the rapid rise of the moments. When the plastic hinge has formed at the base, the wall buckles immediately and collapses.

CONCLUSIONS

Slender propped cantilever walls collapse when they are subjected to the ISO fire with or without any axial loads applied. The times to failure of the walls decrease with increasing level of axial load. High axial loads applied at the top of propped cantilever walls cause the walls to buckle very rapidly when the walls bow outwards.

7.4. Different fire curves

The behaviour of propped cantilever walls when subjected to different fire curves is investigated in this chapter. The fire curves used in the analyses of the wall are the EC1 external fire with and without the decay phase, and the ISO standard fire with the decay phase. The decay phase is applied to the standard fire and the external fire after a particular duration of fire exposure. The durations of the fire before decay occurs are 30, 60 and 90 minutes. The decay rate of the fire is taken as 625°C/hr (refer section 6.4).

The behaviour of the walls with heights of 6, 8 and 12 meters is compared with the standard 10 meter wall for the external fire curve. However, the decay phase for both the standard fire and the external fire is analysed only for the 10 meter wall. Table 7-6 shows a summary of the walls analysed.

Fire curve		EC1 External fire				ISO 834 standard fire			
Time (minutes)		ND	30	60	90	ND	30	60	90
Height	6m	Y	NA	NA	NA	NA	NA	NA	NA
	8m	Y	NA	NA	NA	NA	NA	NA	NA
	10m	Y	Y	Y	Y	Y	Y	X	X
	12m	Y	NA	NA	NA	NA	NA	NA	NA

Table 7-6

Y - Temperature decay occurred before structural failure.

X - Structural failure occurred before temperature decay.

ND - No temperature decay.

NA - Not analysed.

- **EC1 external fire without decay phase**

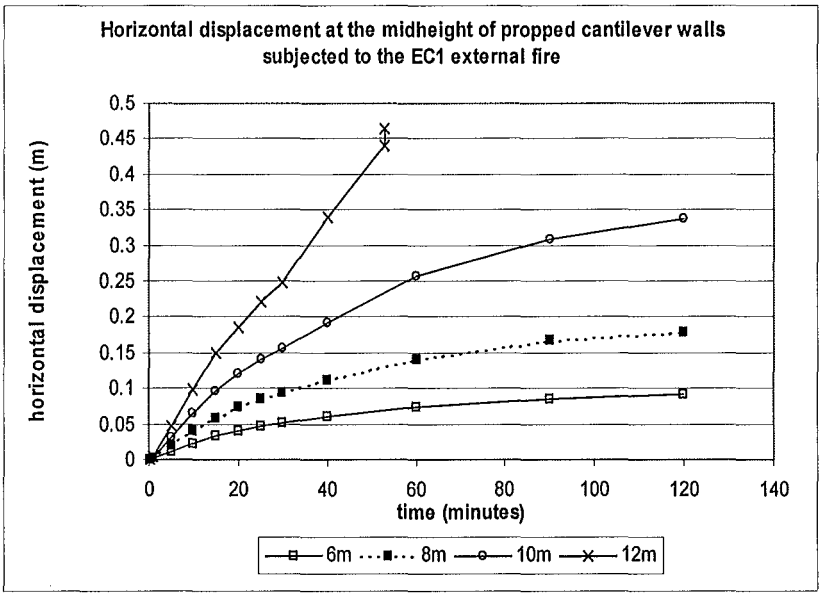

Figure 7.34: Variation of horizontal deflection at mid-height of propped cantilever walls with different heights subjected to the EC1 external fire.

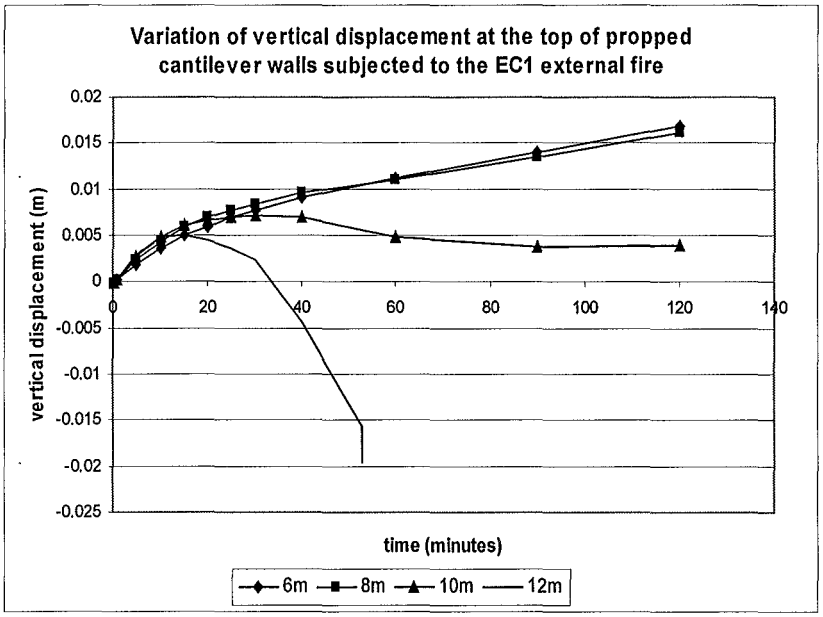

Figure 7.35: Variation of vertical deflection at the top of propped cantilever walls with different heights subjected to the EC1 external fire.

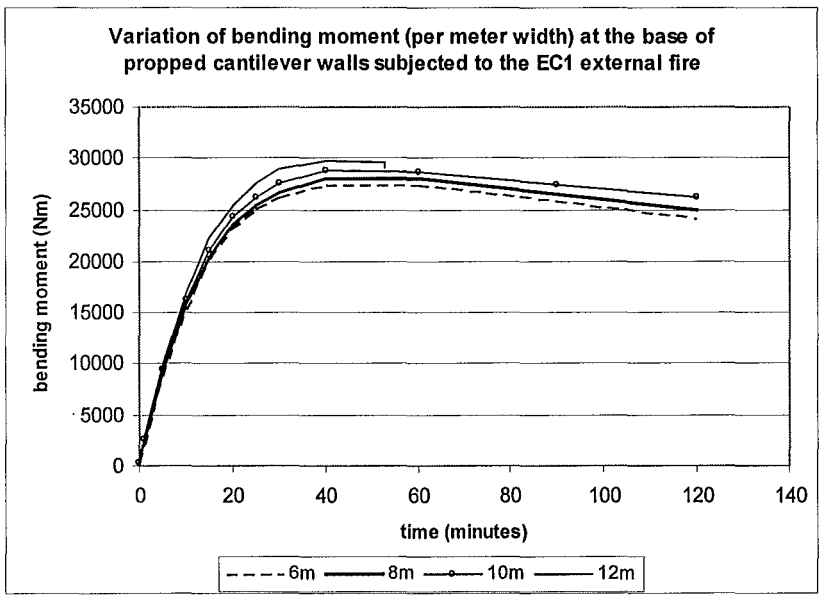

Figure 7.36: Variation of bending moment at the base of propped cantilever walls with different heights subjected to the EC1 external fire.

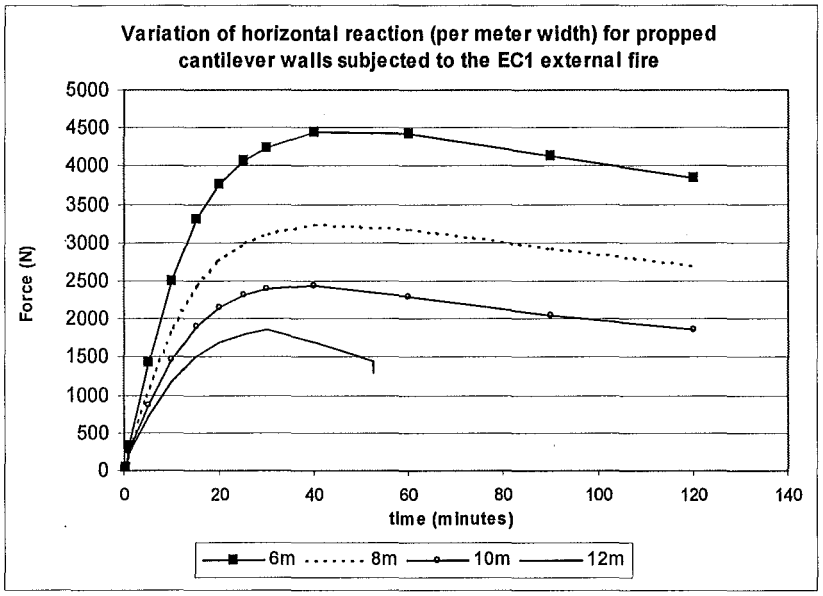

Figure 7.37: Variation of horizontal reaction at the top of propped cantilever walls with different heights subjected to the EC1 external fire.

- **Horizontal displacement at mid-height of the wall**

Figure 7.34 shows the variation of horizontal displacements at mid-height of the walls. The horizontal displacements of all but the 12 meter walls show an asymptotic trend, approaching a limiting displacement as heating occurs. The 12 meter wall managed to sustain a mid-height deflection of 0.44 meters (compared with 0.38 meters with the ISO fire exposure) before it collapsed at 53 minutes. All the walls were also able to sustain larger mid-height deflections than those subjected to the ISO fire.

- **Bending moment at the base of the wall**

Figure 7.36 shows the variation of bending moment at the base of the wall with time. All but the 12 meter wall survive the fire up to 120 minutes. The bending moments of the walls have similar trends, shown by a steep initial increase that slowly levels off and plateaus. All the walls have approximately the same ultimate moment of about 28kNm/m as the section properties of the walls are the same. The bending moment shows a linear decrease after the ultimate moment has been reached.

- **Horizontal reaction at the top of the wall**

Figure 7.37 shows the horizontal reaction at the top of the walls of different heights when they are subjected to the external fire curve. The trends of the graph are very similar to those in Figure 7.18. As the heights of the wall increase, the horizontal reaction at the top of the wall decreases.

DISCUSSION

The analysis shows that all but the 12 meter wall managed to survive the external fire without collapsing. All the walls managed to sustain larger mid-height deflections than the walls that were subjected to the ISO fire. The lower temperatures of the external fire do not reduce the strength and elastic modulus of the concrete as much as the ISO fire. Therefore, the walls exposed to the external fire retain more strength and stiffness and are able to sustain larger deflections without buckling.

- **EC1 external fire curve with the decay phase**

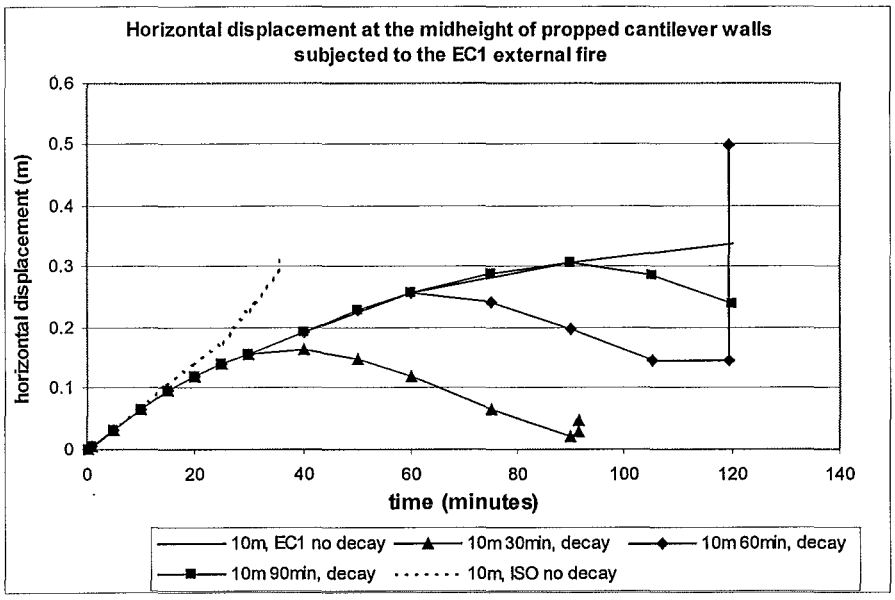

Figure 7.38: Variation of horizontal deflection at mid-height of a 10m propped cantilever wall subjected to different fire curves.

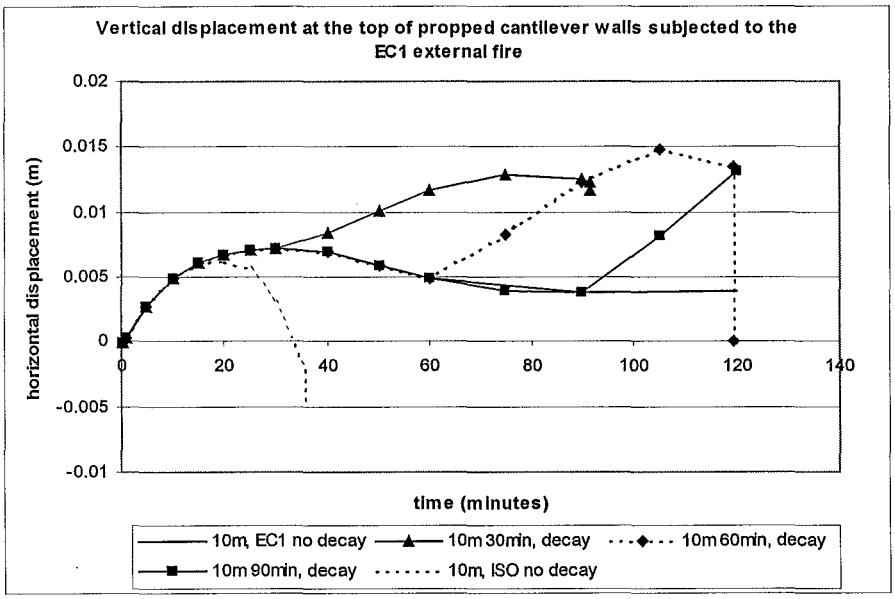

Figure 7.39: Variation of vertical deflection at the top of a propped 10m cantilever wall subjected to different fire curves.

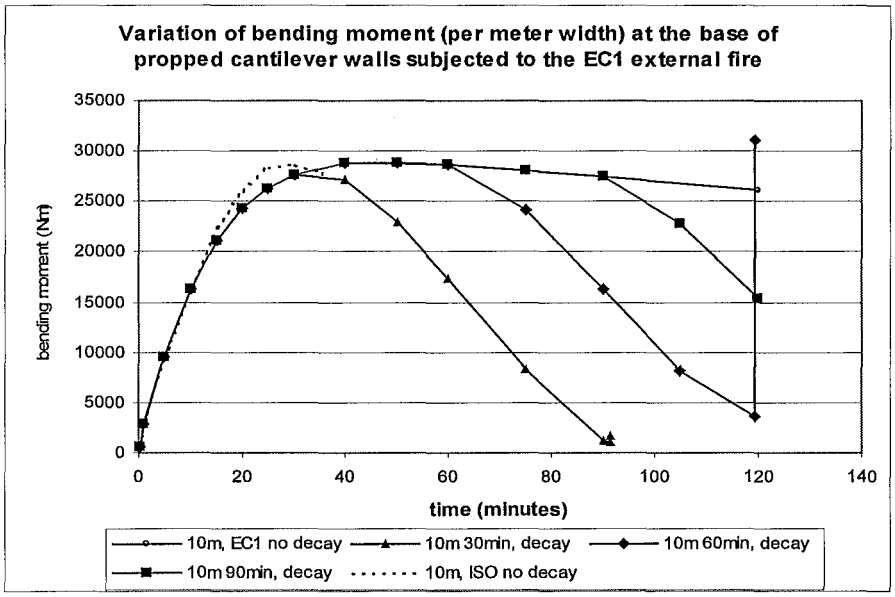

Figure 7.40: Variation of bending moment at the base of a 10m propped cantilever wall subjected to different fire curves.

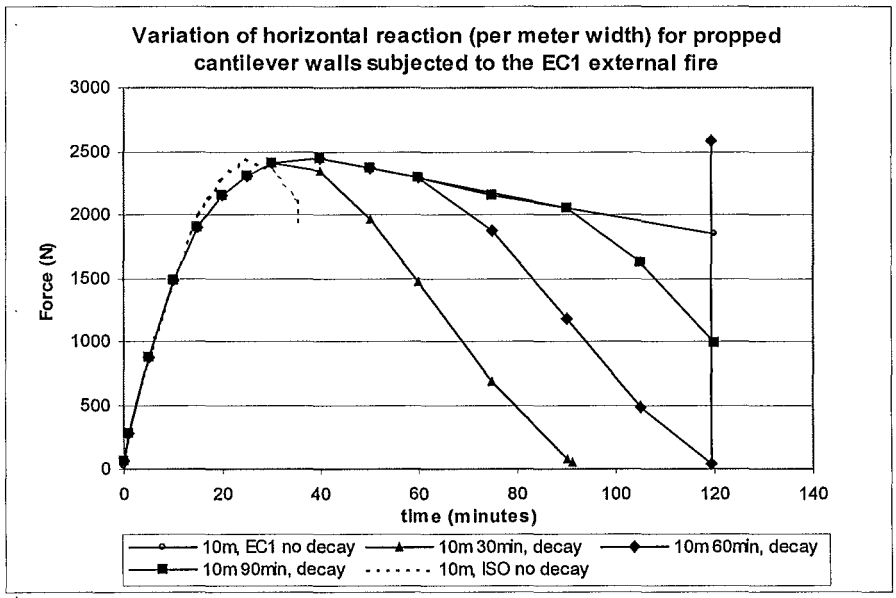

Figure 7.41: Variation of horizontal reaction at the top of a 10m propped cantilever wall subjected to different fire curves.

- **Horizontal displacement at mid-height of the wall**

Figure 7.38 shows the horizontal deflections at mid-height of a 10 meter propped cantilever wall subjected to the external fire curve with and without decay. The displacements of the wall exposed to the ISO fire without decay is included for comparison. The deflection of the wall increases linearly before a decay phase is introduced. When a decay phase is introduced after 30, 60 and 90 minutes of fire exposure, the wall deflects back to its initial shape. The deflection at the mid-height of the wall after a 30 minute fire reduces from its maximum deflection of 0.17 meters at 40 minutes, to 0.021 meters when the wall collapses. The collapse of the wall occurred at 91 minutes, approximately 60 minutes after the fire decay had occurred.

When a decay phase is introduced to the fire after 60 minutes, the displacement at mid-height of the wall drops off as the wall tries to deflect back to its undeformed shape. At approximately 105 minutes, the horizontal displacement reaches a sustained displacement of 0.145m. This sustained displacement is maintained until 119 minutes, when the wall collapses.

- **Vertical displacements**

Figure 7.39 shows the variation of vertical displacements at the top of the wall. During the initial stages, the wall displaces upwards and reaches a plateau at 25 minutes. Beyond this, the wall displaces downwards. When the decay phase is introduced to the fire at different times, the top of the wall displaces upwards as the wall deflects back to its undeformed shape. At the point of failure of the wall, the graph shows that there is a net displacement of the wall.

- **Bending moment at the base of the wall**

Figure 7.40 shows the variation of bending moment at the base of a propped cantilever wall when subjected to the external fire curve with and without decay phases. The bending moment trends for the walls with different fire curves are the same during the initial stages, showing a steep initial increase which levels off to a plateau. When a decay phase is introduced to the fire curve, the moments decrease as the wall deflects back to its initial shape. The walls with decay phases introduced after 30 and 60 minutes of fire exposure

The wall with the decay phase introduced after 90 minutes did not collapse by the end of the simulation because the programme had stopped iterating before collapse could occur.

- **Horizontal reaction at the top of the wall**

Figure 7.41 shows the variation of horizontal reaction at the top of the walls. The trends of the reaction force is very similar to those of the bending moments at the base of the wall.

DISCUSSION

- **Horizontal displacement at mid-height of the wall**

When a decay phase is introduced after 30, 60 and 90 minutes of fire exposure, the temperature difference across the section of the wall decreases. Therefore, the amount of thermal bowing reduces and the wall deflects back to its initial form.

However, the walls experienced a permanent horizontal displacement at the end of the simulation. This permanent deformation of the wall is due to the irrecoverable plastic deformation of the steel and concrete. When the decay phase introduced at 60 minutes, the permanent deformation sustained by the wall is 0.145 meters, compared with 0.021meters when the decay phase is introduced at 30 minutes. Coincidentally, the collapse of both walls occurred one hour after the decay phase started. The reason the walls collapsed at the end of the decay phase is unknown at the stage of writing this report.

- **Vertical displacements**

When decay phases are introduced to the fire, the tops of the walls displace upwards as the amount of bowing of the wall reduces and the wall deflects back to its undeformed shape. At the point of failure of the wall, the walls show a net upward displacement. The net displacement is due to the irrecoverable plastic deformation of the concrete and steel in the wall.

- **Bending moment at the base of the wall**

When a decay phase is introduced to the fire curve, the deflection of the wall back to its initial form reduces the P-delta effects. Consequently, the bending moments at the base of the wall decrease.

- **ISO fire with decay phase**

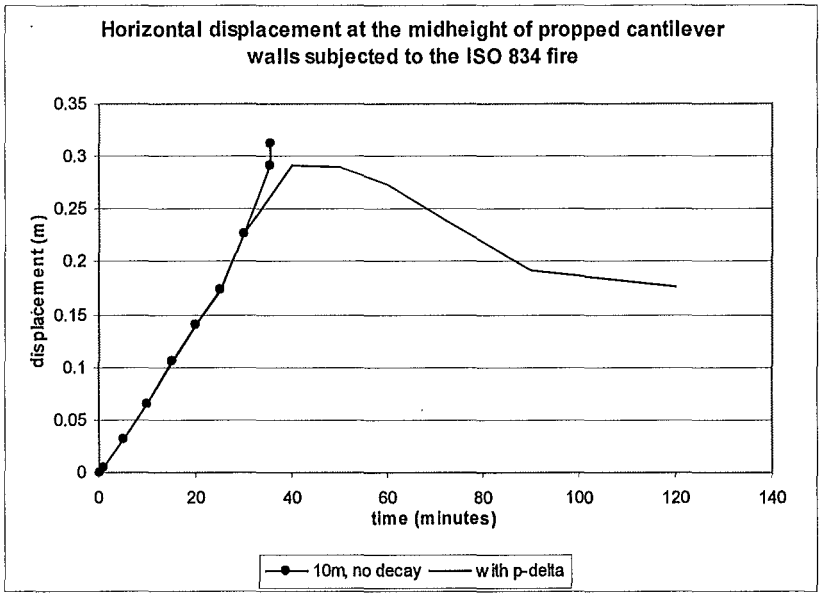

Figure 7.42: Variation of horizontal deflection at mid-height of 10 m propped cantilever wall subjected to the ISO standard fire with a decay phase.

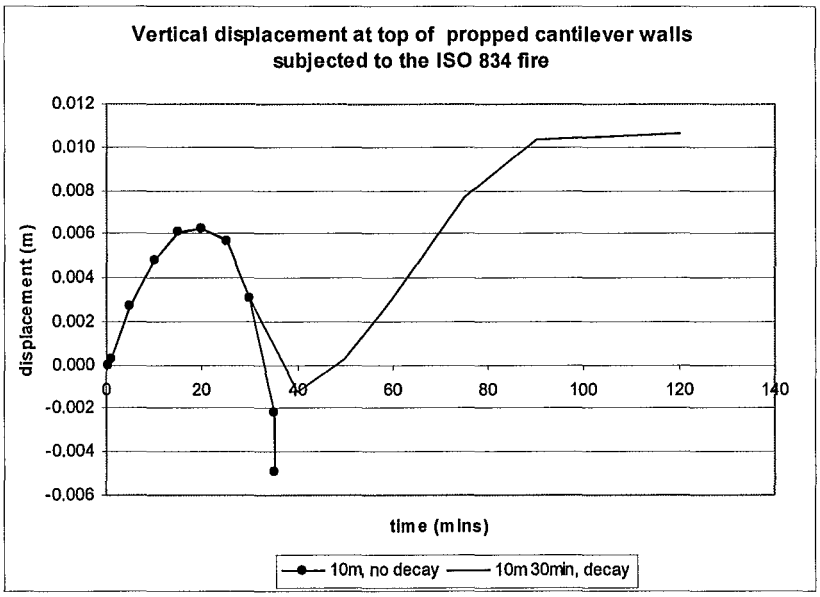

Figure 7.43: Variation of vertical deflection at the top of a 10m propped cantilever wall subjected to the ISO standard fire with a decay phase.

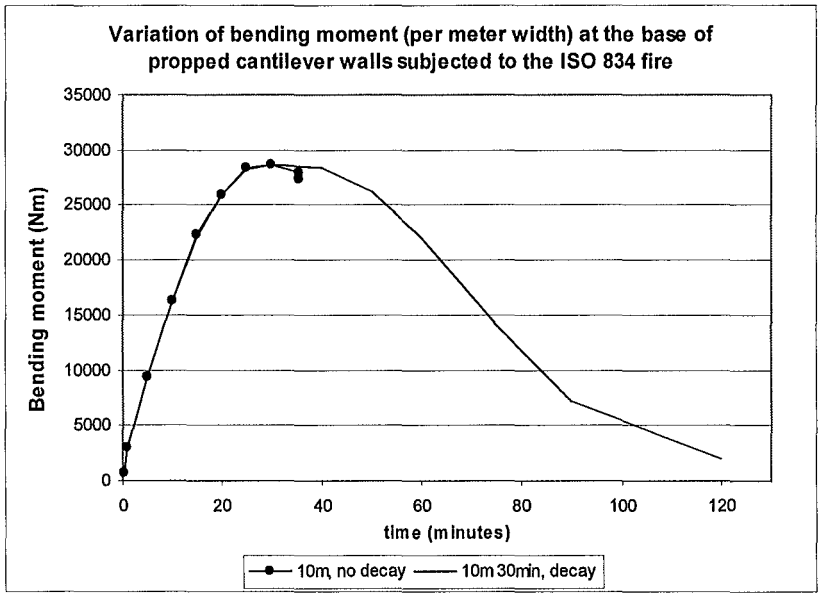

Figure 7.44: Variation of bending moment at the base of a 10m propped cantilever wall subjected to the ISO standard fire with a decay phase.

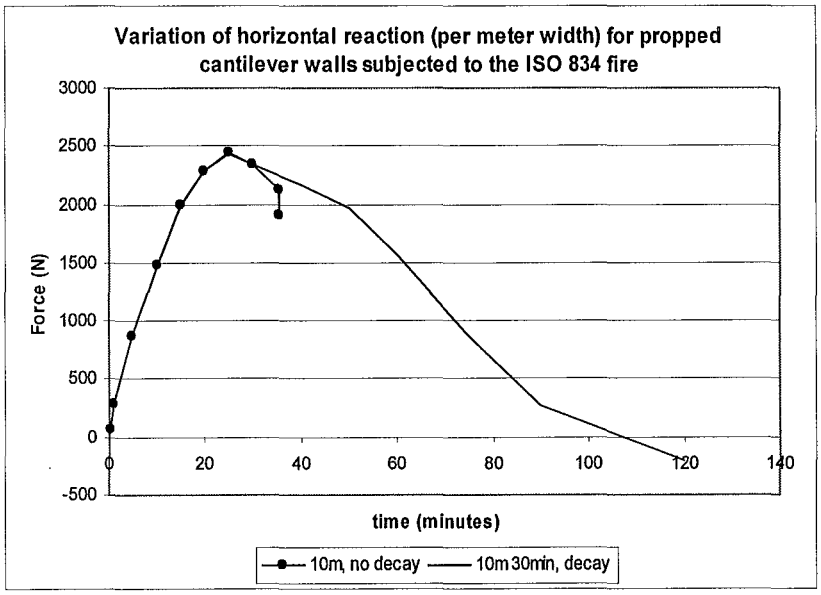

Figure 7.45: Variation of horizontal reaction at the top of a 10m propped cantilever wall subjected to the ISO standard fire with a decay phase.

Figure 7.44 to Figure 7.43 show the behaviour of the 10 meter wall when it is subjected to the ISO standard fire with a decay phase after a 30 minute fire. Introducing the decay phase at a later time was not feasible as the wall would have collapsed by then. The wall exposed to the standard fire without decay is included for comparison.

- **Horizontal displacements at mid-height of the wall**

Figure 7.42 shows that the horizontal displacements at mid-height of the wall increases linearly during the initial stages as the wall deflects towards the fire. The increment increases after 25 minutes due to the formation of the plastic hinge at the base of the wall. When the decay phase is introduced to the fire after 30 minutes, the horizontal deflection rate drops off and plateaus at approximately 0.29 meters. The deflection reduces in a bilinear fashion until the end of the simulation. At the end of the simulation, there is a net horizontal displacement of 0.18m at mid-height of the wall. Unlike the same wall exposed to the external fire and a decay after 30 minutes, this wall does not collapse.

This wall exposed to the standard fire has a much larger net displacement compared to the external fire exposure (0.18 meters compared with 0.021 meters). The larger displacement is due to the greater severity of the temperatures of the ISO fire. The reason why this wall does

not collapse, unlike the same wall exposed to the external fire, is unknown at the time of writing this report.

- **Vertical displacements**

The vertical displacements at the top of the wall shows a parabolic trend with time prior to the decay phase. For the fire curve that does not incorporate the decay phase, the wall collapses at approximately 35 minutes. When a decay phase is introduced at 30 minutes, the wall starts to displace upwards as the wall deflects back to its undeformed shape. The vertical displacements increase and level off at approximately 0.011 meters when the thermal expansion of the wall has ceased.

- **Bending moments at the base of the wall**

Figure 7.44 shows the variation of bending moment at the base of the wall with time. Before the decay of the fire, the bending moment trends for the fires with and without decay are similar. When a decay phase is introduced, the moments reduce in a non-linear fashion. After 90 minutes, the descent gradient reduces but the moment continues to decrease at a linear fashion.

- **Horizontal reaction at the top of the wall**

The horizontal reaction shows a very similar trend to the moment trend at the base of the wall. The reaction increases with increasing moment at the base of the wall. However, the reaction force decreases at different rates and becomes negative at the end of the simulation. The negative reaction at the end of the simulation means that the wall will be pulling the rafter into the building, rather than outwards, as in previous cases.

DISCUSSION

The walls of different heights performed better when exposed to a well ventilated fire compared with the ISO standard fire. All but the 12 meter propped cantilever walls in the analyses managed to survive the external fire for a two hour fire duration. All the walls managed to sustain much larger deflections at mid-height, compared to when they were exposed to the ISO standard fire.

The decay phases introduced to the fire after a certain period of fire duration allowed the propped cantilever walls to deflect back to its undeformed position. The walls exposed to the external fire for 30 and 60 minutes buckled one hour after the decay phase commenced. The reason of the collapse is unknown at the stage of writing the report.

When the decay phase was introduced to the ISO standard fire after 30 minutes of fire exposure, the horizontal deflections of the 10 meter wall decreased. Unlike the wall exposed to the external fire, the wall exposed to the ISO standard fire did not collapse after the decay phase had occurred.

8. INDUSTRIAL BUILDINGS WITH CONCRETE CANTILEVER WALLS AND STEEL ROOF FRAMES

8.1. Introduction

The preceding chapters have discussed the behaviour of individual structural elements of a building. This chapter investigates the behaviour of a two-dimensional three-bay frame, incorporating various structural components, when it is subjected to two types of fire. The purpose of incorporating the steel frame with the concrete cantilever walls is to investigate the overall structural behaviour when the building is exposed to different levels of fire intensity. The frame comprises a steel rafter supported by 10 metre high concrete wall panels and internal steel columns. The wall panels are 150mm thick. The analysis in this section assumes that a sway mode in the frame is prevented by the roof diaphragm and moment resisting joints between the beam and column.

The behaviour of the frames with walls of varying slenderness ratios will be discussed in Chapter 9, which considers the possibility of sway mode failures in the frames with different levels of bracing. Chapter 9 considers three-bay frames (Type A) and two-bay frames (Type B). The purpose of Chapter 9 is to determine the limiting slenderness ratio for the different levels of bracing in order to prevent outward collapse onto the neighbouring property. Only the ISO fire will be used in the analysis in Chapter 9.

Table 8-1 summarises the type of frame analysed in this chapter and the corresponding sections where the results are described.

Section	Heading	Page Number	Bracing	Frame configuration	Beam-column connection	Fire
8.3	Analytical model	216	Braced	A	Fixed	-
8.4	ISO standard fire	226	Braced	A	Fixed	ISO
8.5	EC1 external fire	234	Braced	A	Fixed	EC1
8.6	Conclusion	242	-	-	-	-

Table 8-1: Configurations of frames analysed in chapter 8.

8.2. Comparison of two fire exposures on braced 3-bay frames

In this section, the behaviour of the frame is investigated when it is subjected to two types of fire. The frame that will be used in this investigation is shown in Figure 8-1. It features a steel frame with a rafter spanning across three bays, supported by internal steel columns and concrete cantilever walls at the perimeter. The steel members of the frame are not protected against fire. The frame will be subjected to the ISO 834 fire and the EC1 external fire. The ISO fire represents an upper bound and more intense fire while the external fire curve represents a lower bound and less severe fire. The level of intensity of a real fire may lie between these bounds or even exceed the upper limit. The time temperature graphs of the ISO and EC1 external fire curves are shown in section 6.4.

8.3. Analytical model of two dimensional frame (Type A)

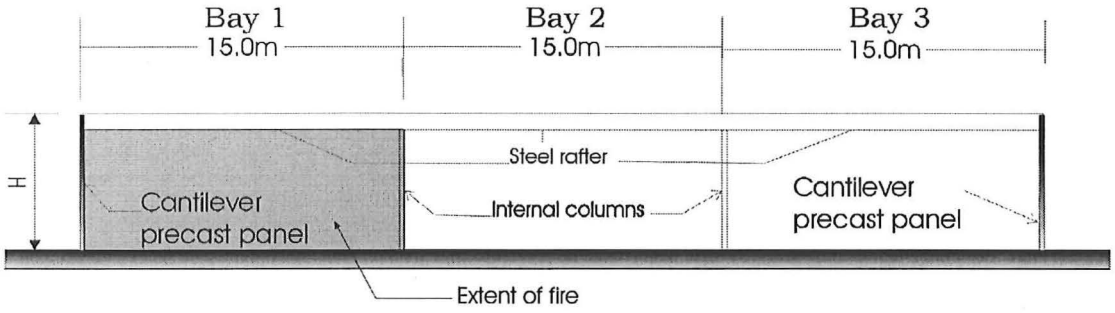

Figure 8-1: Frame of industrial building used for computer modelling (Frame A)

In the analysis of the two-dimensional frame, a migrating fire is assumed to occur inside the building. For this analysis, *Bay One* (Figure 8-1) is assumed to be involved in a fully developed fire. The other bays of the frame are assumed to be affected by the fire but not sufficient to degrade the structural performance. Therefore, the unheated section of the frame is assumed capable of providing lateral restraint to the frame involved in the fire, in the form of the unheated purlins and diaphragm action which transfer the lateral forces to the side walls. The other rafters that lie parallel to the heated rafter are also assumed to be unaffected by the fire. This is a simplistic assumption about fire behaviour but is considered sufficient for the purposes of this study.

The frame shown in Figure 8-1 is modelled and is divided into two halves at the axis of symmetry (Figure 8-3). Figure 8-4 illustrates the structural model of the frame which features a concrete cantilever wall and a steel column supporting a steel rafter. At the axis of symmetry, the horizontal displacements and rotations are restrained, but the vertical

displacements are free. The restraint at the axis of symmetry prevents a sway mode from developing, simulating the lateral restraint provided by the other half of the frame and by diaphragm action from the unheated roof.

The column is pinned at the base, where the horizontal and vertical displacements are restrained but the rotations are unrestrained. The top of the column has a moment resisting connection to the beam. The cantilever wall is fully fixed at the base. The actual dimensions of a typical concrete panel, measuring 2.80m wide by 150mm thick, are modelled in the analysis. The thicknesses of the walls are not varied and held constant at 150mm. The full sized wall is modelled in this case as its behaviour as a load-bearing element in the frame is important. Therefore, its size cannot be scaled down, as reducing the size of the wall would misrepresent the ability of the wall to support the frame. The rafter is connected to the wall by a pin connection.

Dimensions of structure:

Number of spans:	3
Span of rafters between columns:	15.0m
Height of walls:	10.0m
Height of columns:	10.0m
Spacing of rafters:	8.40m centres

8.3.1. Loads

The loads applied on the structure are the self-weights of the structural elements and the weights from the roof, services and purlins. The model takes account of the rafter loaded on every third panel by summing the loads of the tributary width. Figure 8-2 shows the tributary width of the roof that will be loaded onto each steel frame.

Cold calculations:

In order to analyse the frame under elevated temperatures, the types of elements of the frame must first be determined. The design of the frame elements is based on the dimensions shown in the preceding page. The loads for determining the sizes of the beam and column in the steel frame are as follows:

Total dead load (services, purlins, rafter and steel sheeting), G:	0.5kPa
Live load, Q:	0.25kPa
Design load, 1.2G + 1.6Q:	1.0kPa
Tributary width of roof:	3 panels x 2.80m = 8.40m
Tributary load on rafter:	8.40m x 1.0kPa= 8.4 kN/m

The sizes of the steel elements for the frame are determined from hand calculations and are shown in Figure 8-8 and Figure 8-9. The load-bearing wall panel that will be used to support the frame is a full sized wall, measuring 2.80 metres long by 150 mm thick. The plan view of the wall is shown in Figure 8-6.

Fire calculations:

The analysis assumes that the dead load from the roof, services and purlins remain connected to the rafter throughout the fire. Even when the rafter has deformed significantly, the loads from the purlins, roof and services are assumed to be applied to the rafter. For analysing the structure under elevated temperatures, the loads that will be imposed on the structure are as follows:

Total dead load, G:	0.5kPa
Design load, 1.0G:	0.5kPa
Tributary width of roof:	3 panels x 2.80m = 8.40m
Tributary load on rafter:	8.40m x 0.5kPa= 4.2 kN/m

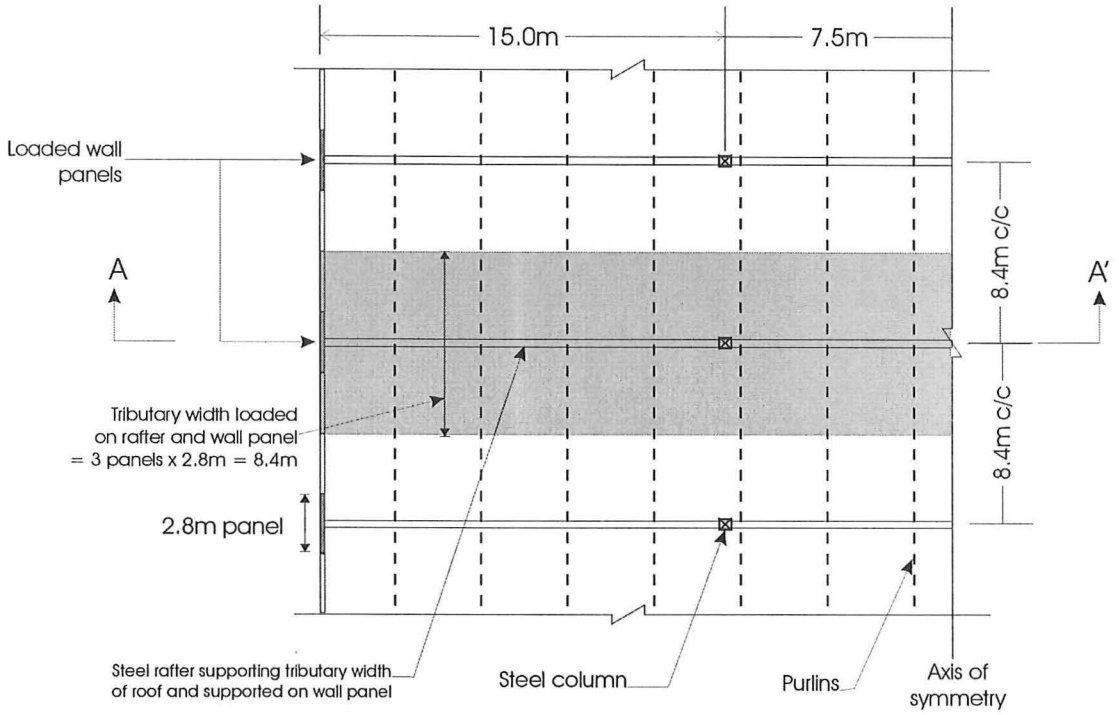

Plan view of industrial building

Figure 8-2: Plan view of industrial building showing the tributary area of the rafter.

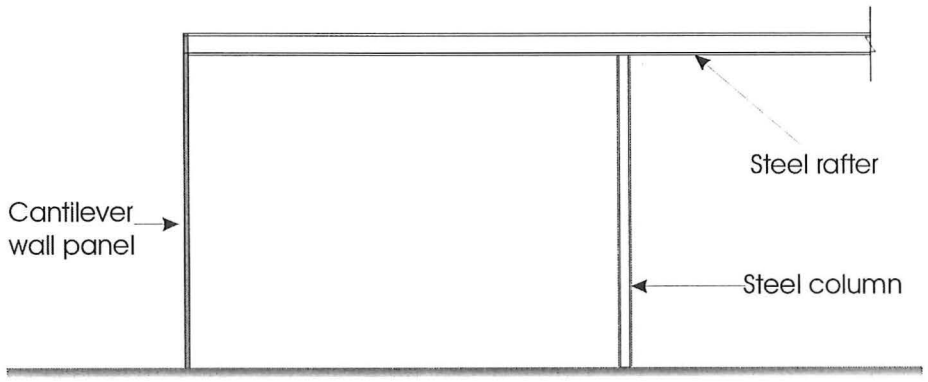

Section A-A'
(Steel frame with concrete cantilever walls)

Figure 8-3

8.3.2. Structural model (Frame A)

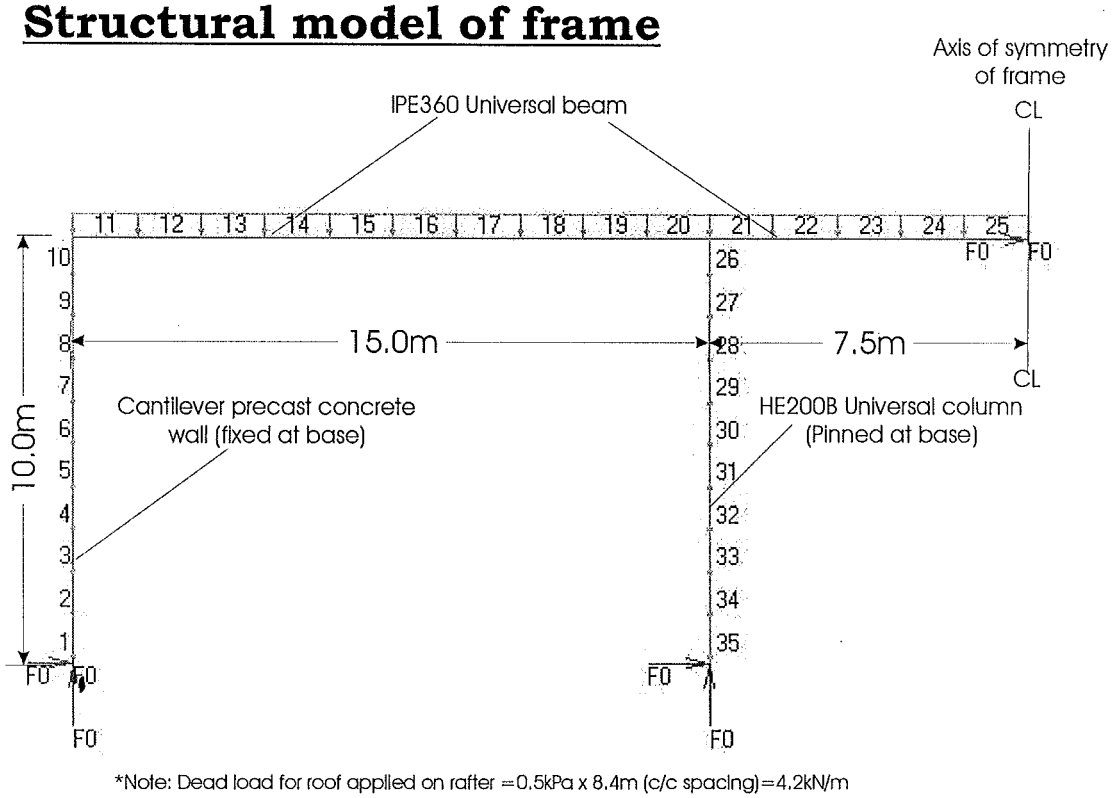

Figure 8-4: Structural model of frame in SAFIR showing the element numbers.

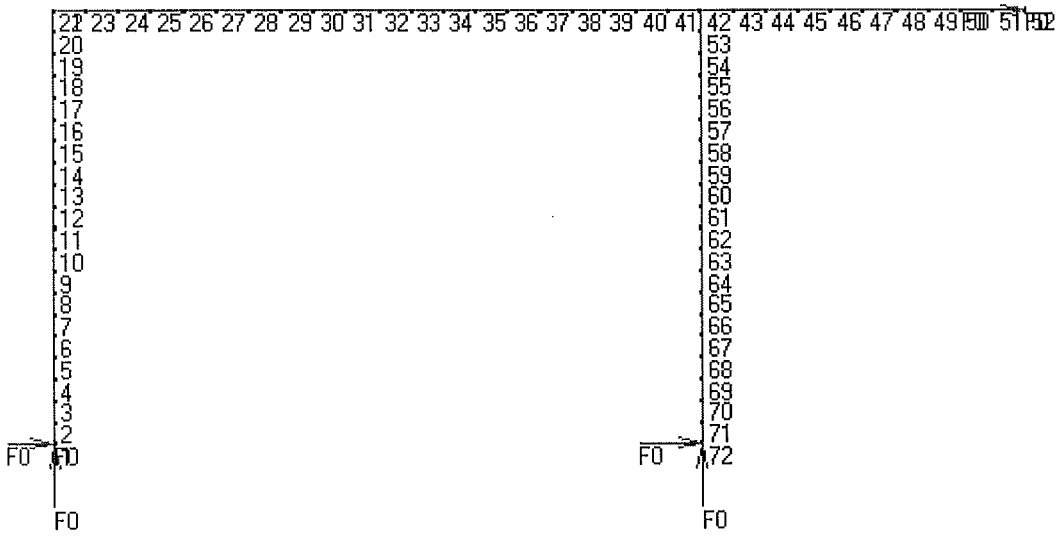

Figure 8-5: Structural model of frame showing node numbers.

*Note: The element numbers and the node numbers of the structure (Figure 8-4 and Figure 8-5, respectively) will be referred in the following pages.

8.3.3. Time temperature curves

The temperature curves that will be applied to the frame are the ISO standard fire curve and the EC1 external fire curve. The ISO standard fire represents a severe fire condition and the external fire represents a less severe and well-ventilated fire. A migrating fire is assumed to have occurred and affects only one half of the frame. The fire curve is applied to one side (inside face) of the wall, while the beam and column are exposed at three and four faces, respectively.

8.3.4. Assumptions made in the analyses

- The wall is assumed fully fixed at the base.
- The elements are uniformly heated throughout their entire length.
- Spalling of concrete does not occur.
- There is no slippage between the concrete and the reinforcing steel.
- Failure does not occur at the foundations.
- There are no initial eccentricities in the wall due to precambering.
- Horizontal restraint provided by the cold parts of the frame to the unheated frame is in the form of diaphragm action from the cooler roofs, steel purlins and rafters.
- Lateral buckling of the rafter does not occur in the analysis.
- The pin connections between the rafter and the wall do not fail.

8.3.5. Properties of frame elements

Wall:

Height of wall, H_w:	10.0m
Thickness of wall, t_w:	150mm
Slenderness ratio, λ:	66.7
Width of wall, L_w:	2800mm
End conditions:	Fixed at the base
Concrete model:	Siliceous aggregate concrete according to the Eurocode, EC2 (1995)
Concrete compressive strength, f'_c:	30.0 MPa
Concrete tensile strength, f'_t:	0.0 MPa
Concrete Poisson's ratio, ν_c:	0.15
Concrete density, ρ_c:	24.0 kN/m^3
Concrete elastic modulus, E_c:	18.0 GPa
Steel model:	Eurocode, EC2 (1995)
Reinforcing steel quantity:	1005mm^2/m, 0.67% in the middle of the section
Reinforcing steel elastic modulus, E_s:	210.0 GPa
Reinforcing steel yield strength, f_y:	430.0 MPa
Reinforcing steel Poisson's ratio, ν_s:	0.30
Steel density, ρ_s:	78.50 kN/m^3

Figure 8-6 shows the plan view of part of the wall used in the frame analysis. It constitutes of quadrilateral finite elements with concrete and steel material properties from the Eurocode (EC2, 1995). Elements with steel properties are placed in the middle of the section at 200mm centres to represent the 16mm diameter reinforcing steel. The ISO standard fire is applied to one face of the wall and the thermal distribution across the wall section after one hour of exposure to the fire is shown in Figure 8-7. In the frame analysis, the concrete tensile strength was omitted, as including it would cause SAFIR to stop iterating prematurely.

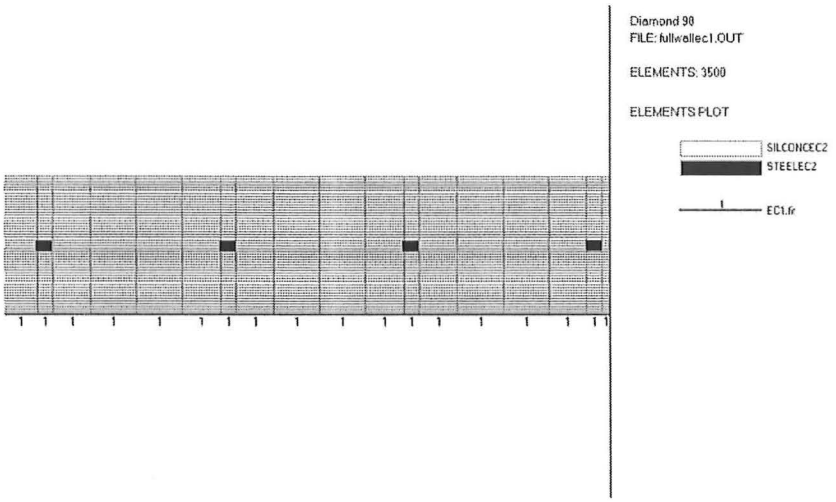

Figure 8-6: Plan view of part of the wall used in the frame analysis.

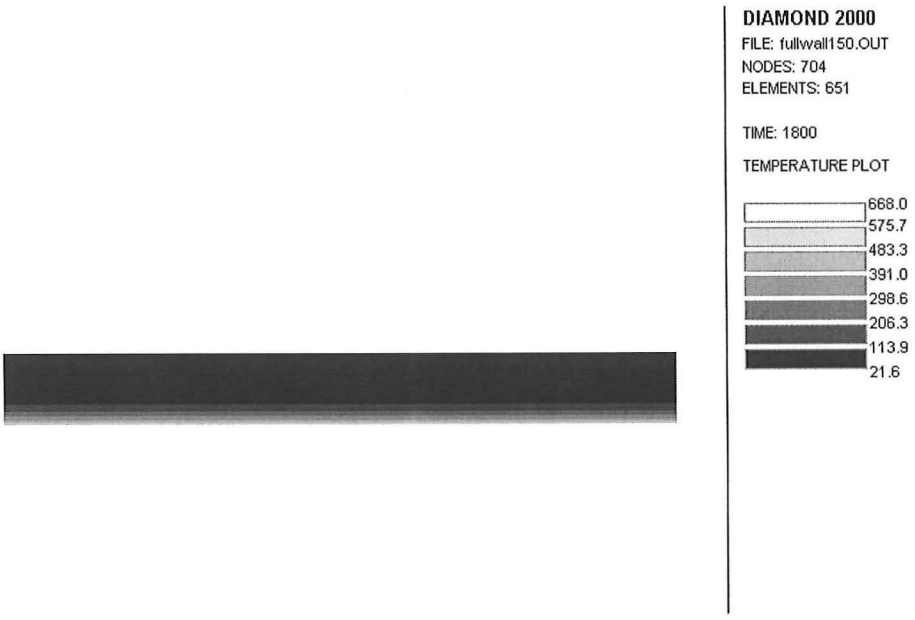

Figure 8-7: Thermal distribution across the section of the entire wall subjected to the ISO standard fire.

Columns

Type:	HE200B ≅ 200UC59.5
Depth of section:	200mm
Flange width:	200mm
Flange thickness:	15mm
Web thickness:	9mm
Weight:	61.3kg/m
Yield strength, f_y:	430MPa
Elastic modulus, E_s:	210.0 GPa
Steel Poisson's ratio, ν_s:	0.30
Steel density, ρ_s:	78.50 kN/m^3
End conditions:	pinned at base

Figure 8-8 shows the cross section of the column that will be used in the frame analysis. The extent of the fire in Bay 1 is such that the column is heated on four sides. The figure below shows a typical thermal distribution of the column when it is subjected to the ISO fire on four sides.

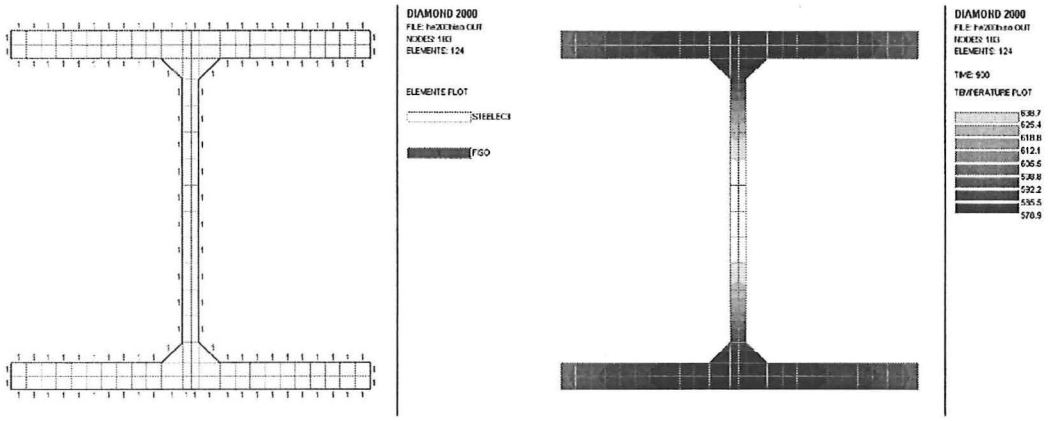

Figure 8-8: Thermal distribution of column after 15 minutes of four-sided exposure to the ISO fire.

Beam

Type:	IPE360 ≅ 360UB50.7
Depth of section:	360mm
Flange width:	170mm
Flange thickness:	12.7mm
Web thickness:	8mm
Weight:	57.1kg/m
Yield strength, f_y:	430MPa
Elastic modulus, E_s:	210.0 GPa
Steel Poisson's ratio, ν_s:	0.30
Steel density, ρ_s:	78.50 kN/m^3

Figure 8-9 shows the cross section of the I-beam that will be used in the frame analysis. The beam is subjected to a three-sided fire exposure. The figure shows a typical thermal distribution of the beam when it is subjected to the ISO fire on three sides of the section.

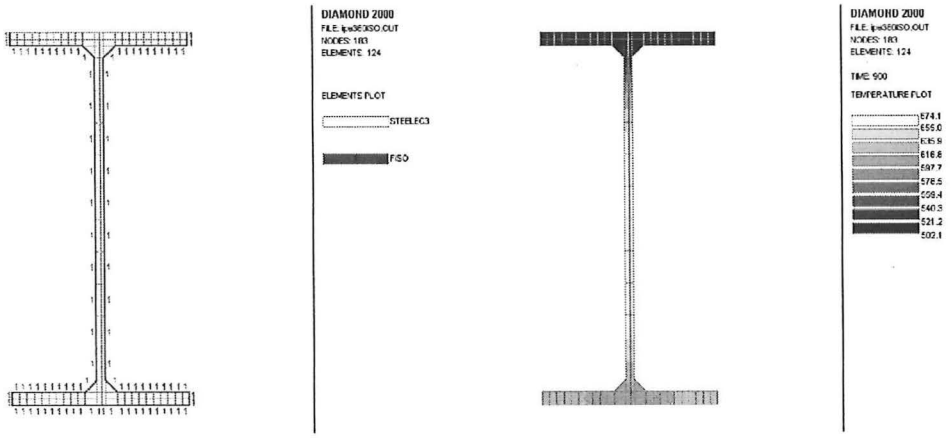

Figure 8-9: Thermal distribution of the I-beam after 15 minutes of three-sided exposure to the ISO fire.

8.4. ISO standard fire

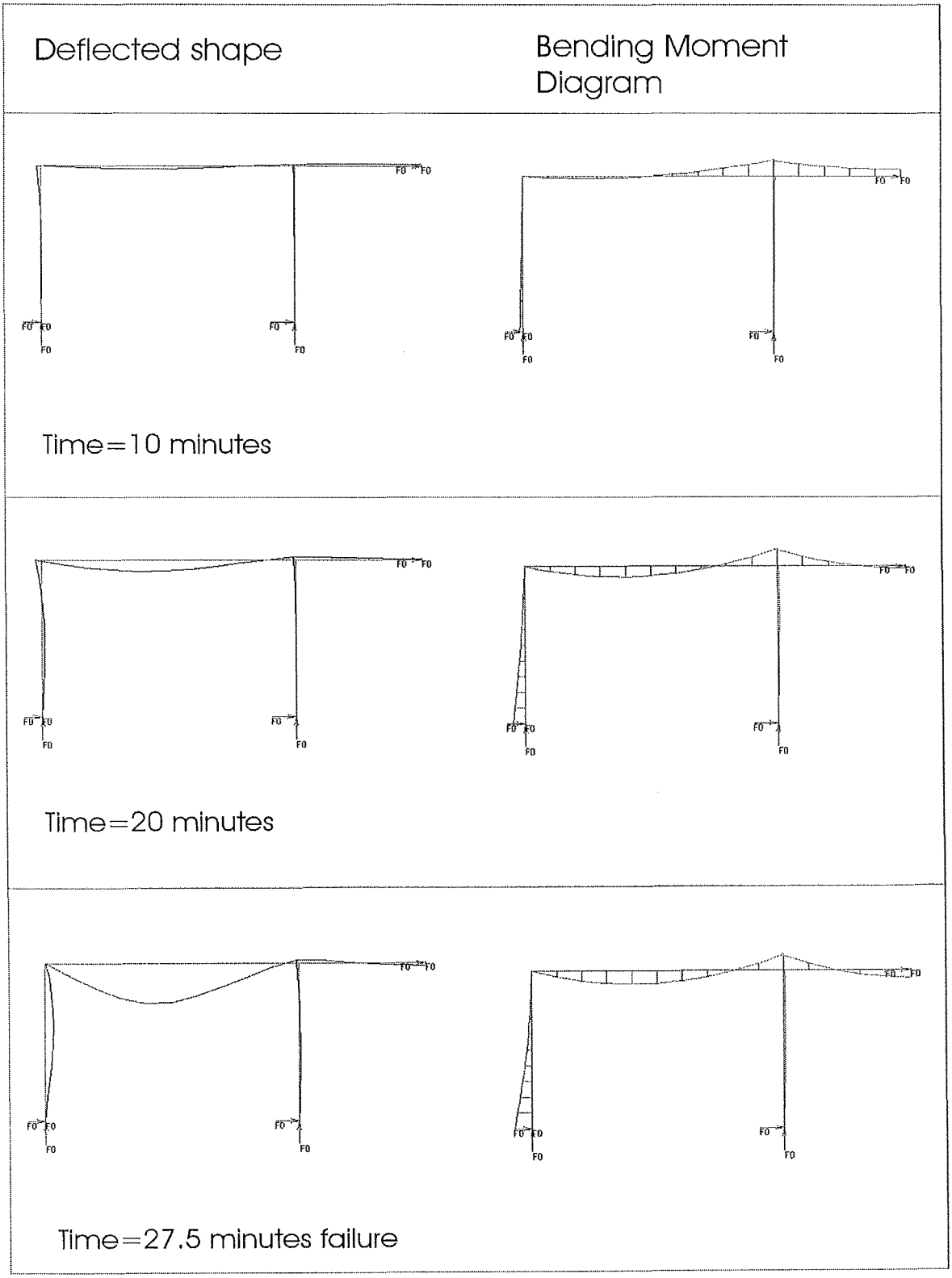

Figure 8-10: Deflected shape and bending moment diagram of frame subjected to the ISO standard fire.

(*Note: deflections magnified by 2)

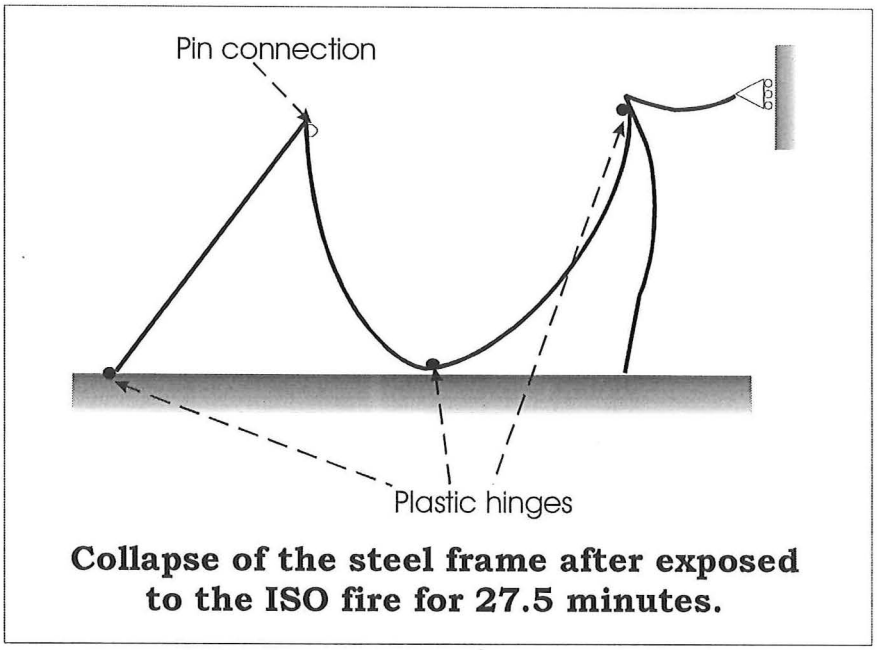

Figure 8-11: Collapse of the steel frame after exposed to the ISO fire.

Behaviour of frame subjected to the ISO standard fire

Figure 8-10 shows a summary of the deflected shape and bending moment of the frame when it is subjected to the ISO standard fire. As the frame is heated, the rafter displaces downwards due to the thermal effects on the unprotected steel and the loads on the rafter (Figure 8-12). The increasing deflection at midspan of the rafter is primarily due to the reduction of the elastic modulus of steel as the temperature increases. This consequently decreases the flexural rigidity of the rafter and increases the deflections. Another cause of the deflection is due to the creep strain of the steel which is very sensitive to high temperatures.

While the rafter deflects downwards, the top portion of the wall deflects outwards due to thermal bowing, pulling the rafter along. At the same time, the lower part of the wall deflects inwards. The deflection and behaviour of the wall is similar to a propped cantilever wall.

At the point of failure (27.5 minutes), the rafter has sagged enough to drag the wall downwards into the building. Two plastic hinges have formed in the rafter. The sagging rafter induces a horizontal axial force at the top of the wall, which generates a bending moment at the base of the wall. When the axial force has generated sufficient moment, a plastic hinge forms at the base of the wall. This third plastic hinge causes the structure to behave as a mechanism, therefore, collapse occurs.

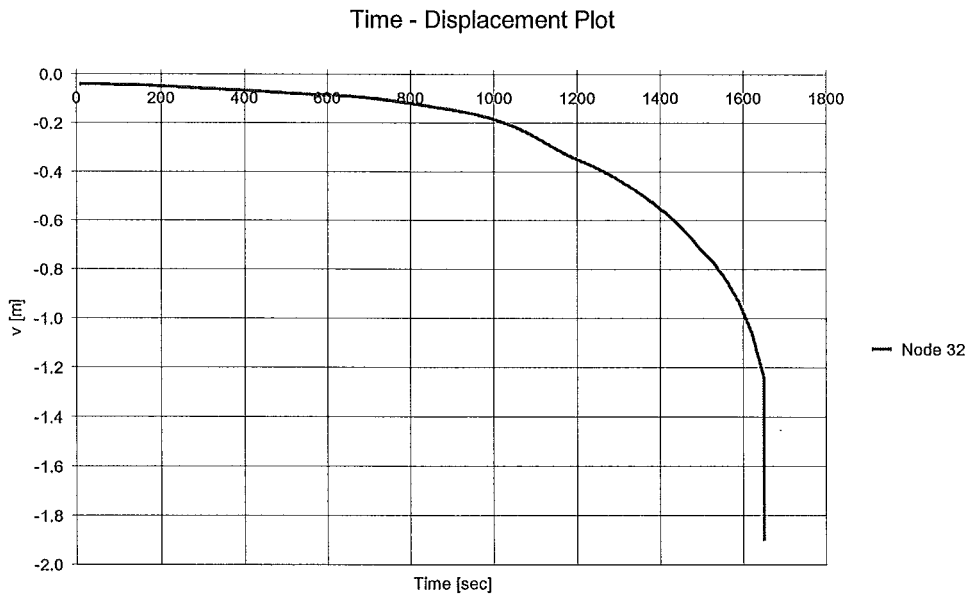

Figure 8-12: Variation of vertical displacement at midspan of rafter.

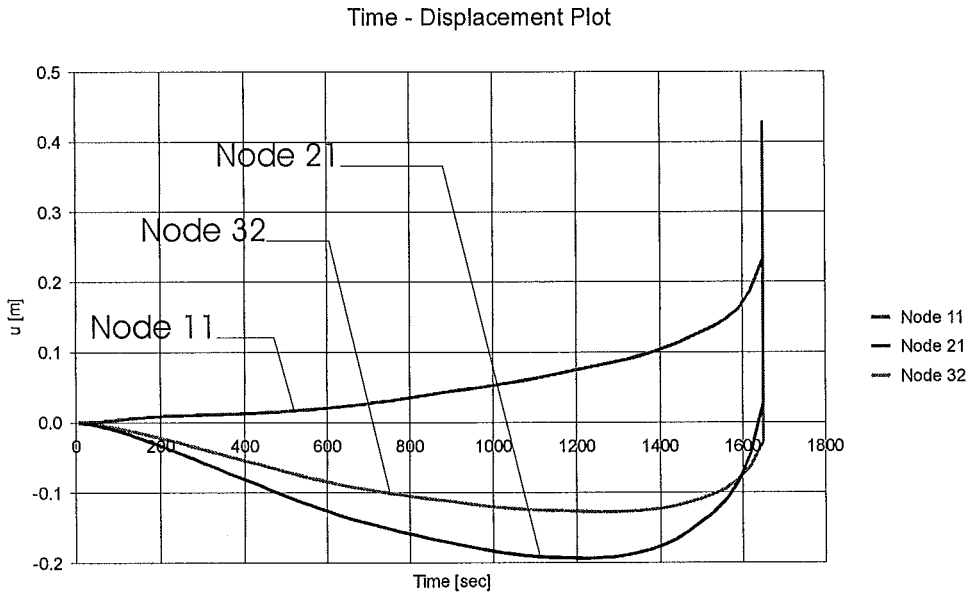

Figure 8-13: Variation of horizontal displacement at mid-height (Node 11) and the top (Node 21) of the wall and at midspan of the rafter (Node 32).

Deflections of structural elements

Figure 8-12 shows the variation of vertical displacements at midspan of the rafter. The rafter displaces downwards very gradually until approximately 1000 seconds (17 minutes) where the displacement trend changes and increases exponentially. At 1650 seconds (27.5 minutes), the rafter shows the runaway displacement where it collapses, dragging the wall down with it.

Figure 8-13 shows the variation of horizontal displacement at various parts of the structure. Nodes 11 and 21 refer to positions at mid-height and the top of the wall, respectively. Node 32 represents the position at midspan of the rafter. The positive displacement in the graph represents inward deflection of the wall and negative displacement represents outward deflection of the wall, away from the frame.

When the wall is heated on the inside, the non-uniform thermal expansion across the section of the wall causes the lower part of the wall to bow inwards. The rafter attached to the top of the wall restrains the wall from bowing outwards. However, some outward deflection occurs at the top of the wall due to thermal elongation of the rafter. After the initial outward bow, the top of the wall is pulled back to its original position after 1560 seconds (26 minutes) as the horizontal force from the collapsing rafter exceeds the thrust due to thermal bowing. The pull back of the wall occurs very rapidly as the runaway failure of the rafter occurs. At 1650 seconds, a plastic hinge forms at the base of the wall (in addition to two that have formed in the rafter) causing the wall to collapse inwards. This third plastic hinge forms a mechanism in the structure, causing the entire frame to collapse.

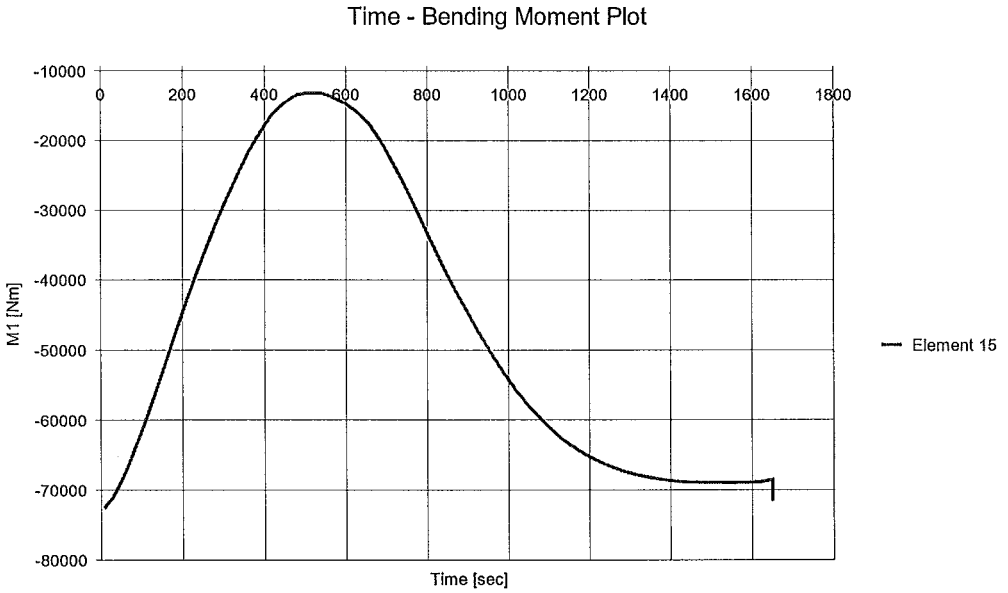

Figure 8-14: Variation of bending moment at midspan of the rafter.

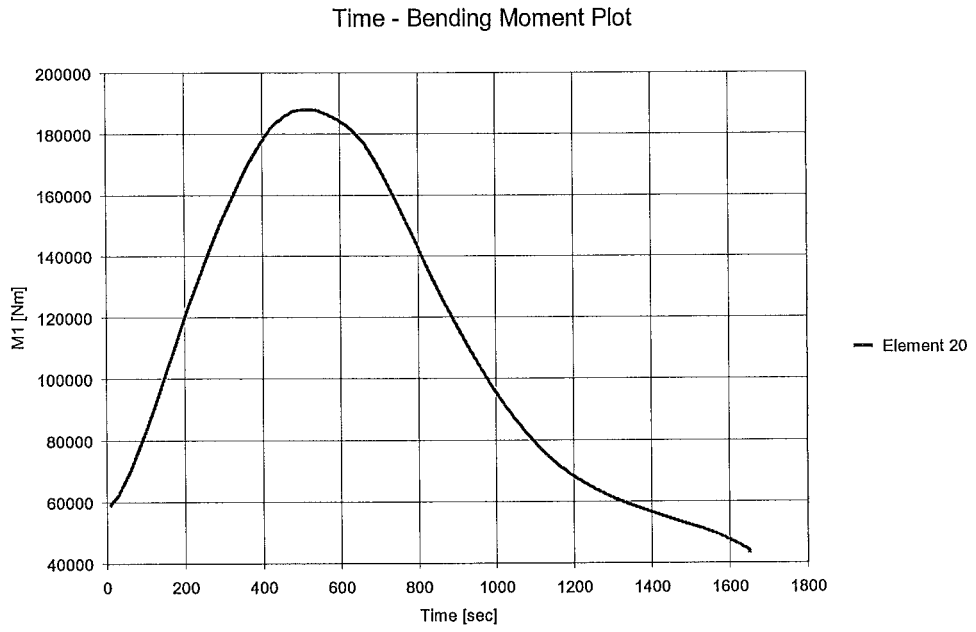

Figure 8-15: Variation of bending moment of the rafter at the column intersection.

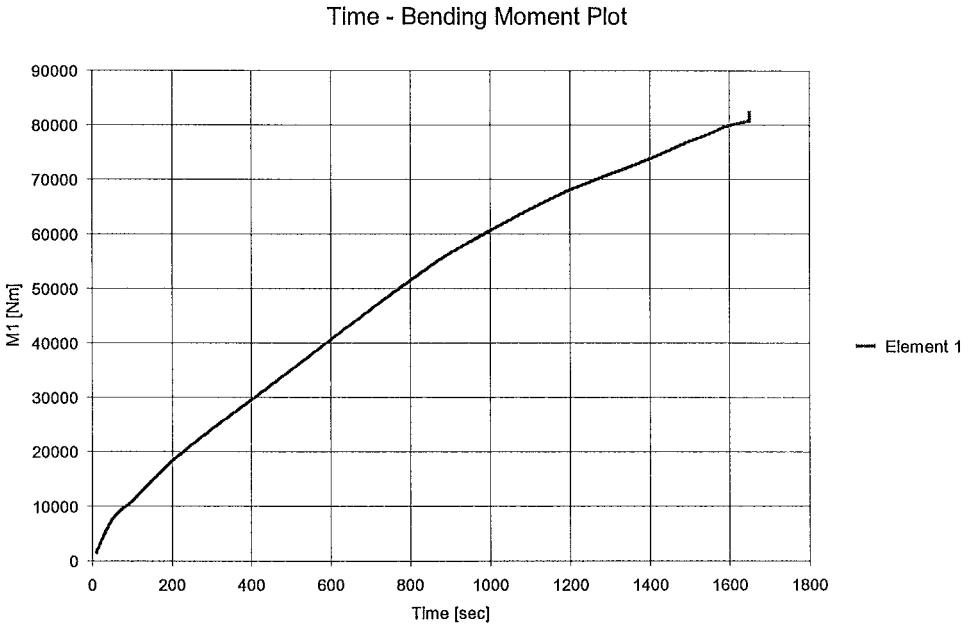

Figure 8-16: Variation of bending moment at the base of the wall.

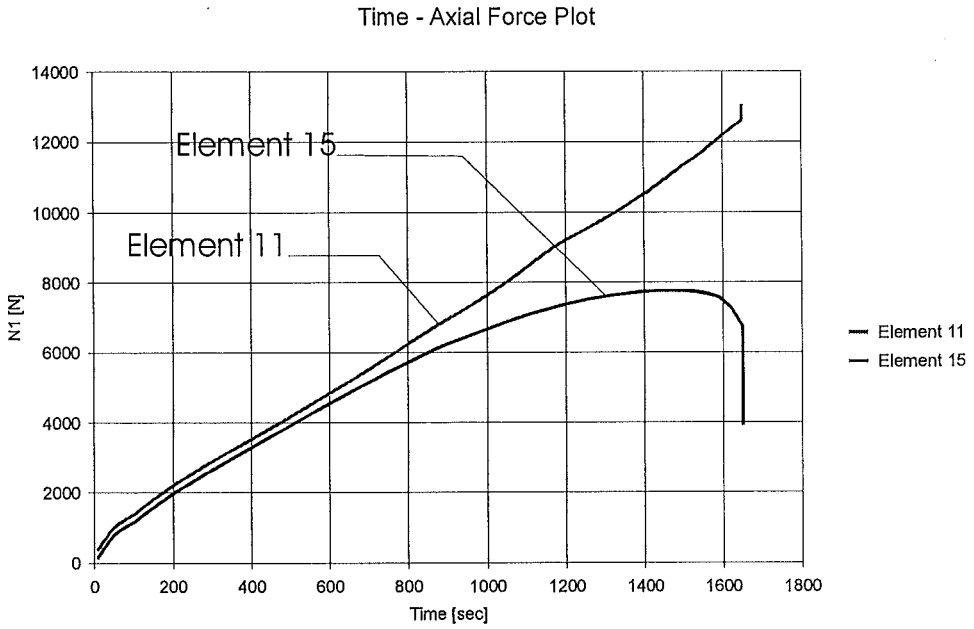

Figure 8-17: Variation of horizontal axial force at the left side (closest to the wall, element 11) and midspan (Element 15) of rafter.

Bending moments in the walls and the beam elements

Figure 8-14 and Figure 8-15 show the variation of bending moment of the rafter at midspan and adjacent to the column support. When the rafter is unheated, the bending moment is approximately -72kNm at midspan and 60kNm at the support. The negative sign represents positive bending.

During the initial stages of the fire, the bending moments in the rafter increase linearly. This is due to the redistribution of the bending moments from midspan to the supports. However, the moment increment at both elements reduces and peaks at 500 seconds (42 minutes). After the bending moment at midspan (Element 15) has peaked, it decreases linearly before levelling off. The bending moment at element 20 decreases in a similar fashion but does not level off. Instead, it continues to decrease at a lesser rate. The reduction of moment is due to the reduction of the yield strength which decreases with increasing steel temperature. At approximately 1600 seconds, two plastic hinges form at midspan and at the support of the rafter.

Figure 8-16 shows the variation of bending moment at the base of the wall with time. The bending moment increases in an almost linear trend until 1650 seconds (27.5 minutes) when a plastic hinge forms at the base. The nominal moment of the wall is approximately 80kNm. When a plastic hinge forms at the base of the wall, the wall loses its rotational restraint. Therefore, a mechanism forms in the structure and it collapses.

Axial force in beam elements

Figure 8-17 shows the variation of horizontal axial force at various positions of the rafter. Element 11 labelled in the graph represents the position of the rafter immediately adjacent to the wall panel. Element 15 represents the position at the midspan of the rafter. The axial force in element 11 increases linearly until 1650 seconds when a mechanism forms and the frame collapses. The axial force in this element is due the thrust of the wall as it bows outwards, coupled with the downward force from the sagging rafter.

The axial force in element 15 increases linearly in a similar trend to element 11. The force increment decreases after 800 seconds (13.3 minutes) and plateaus at 1500 seconds (25 minutes). It drops off very rapidly at 1650 seconds (27.5 minutes). The plateau of the axial force is due to the runaway displacement at that position of the rafter. The drop in the axial force after the plateau is due to the compressive force from the rest of the rafter collapsing, thus reducing the net tension in the rafter.

8.5. EC1 external fire

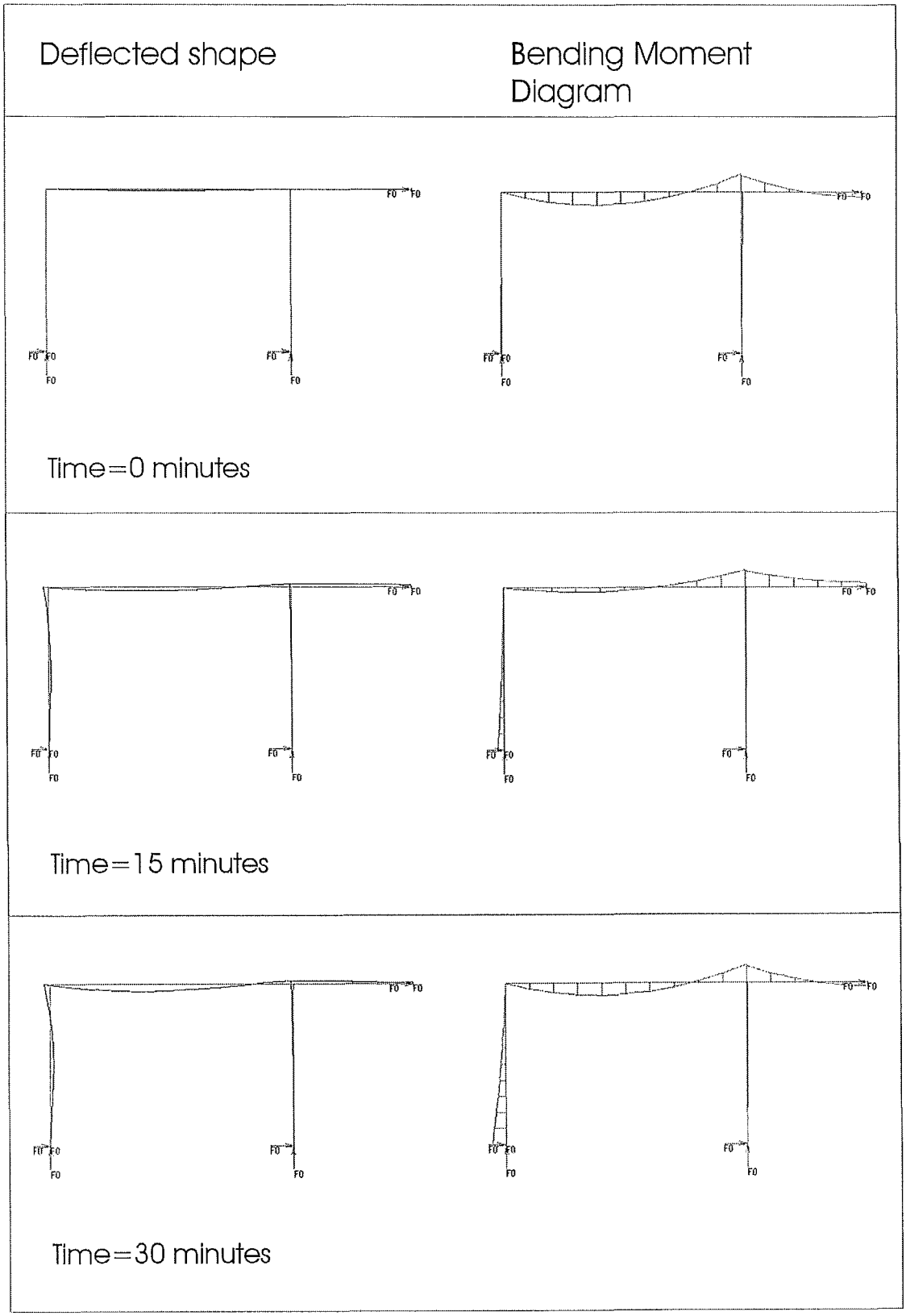

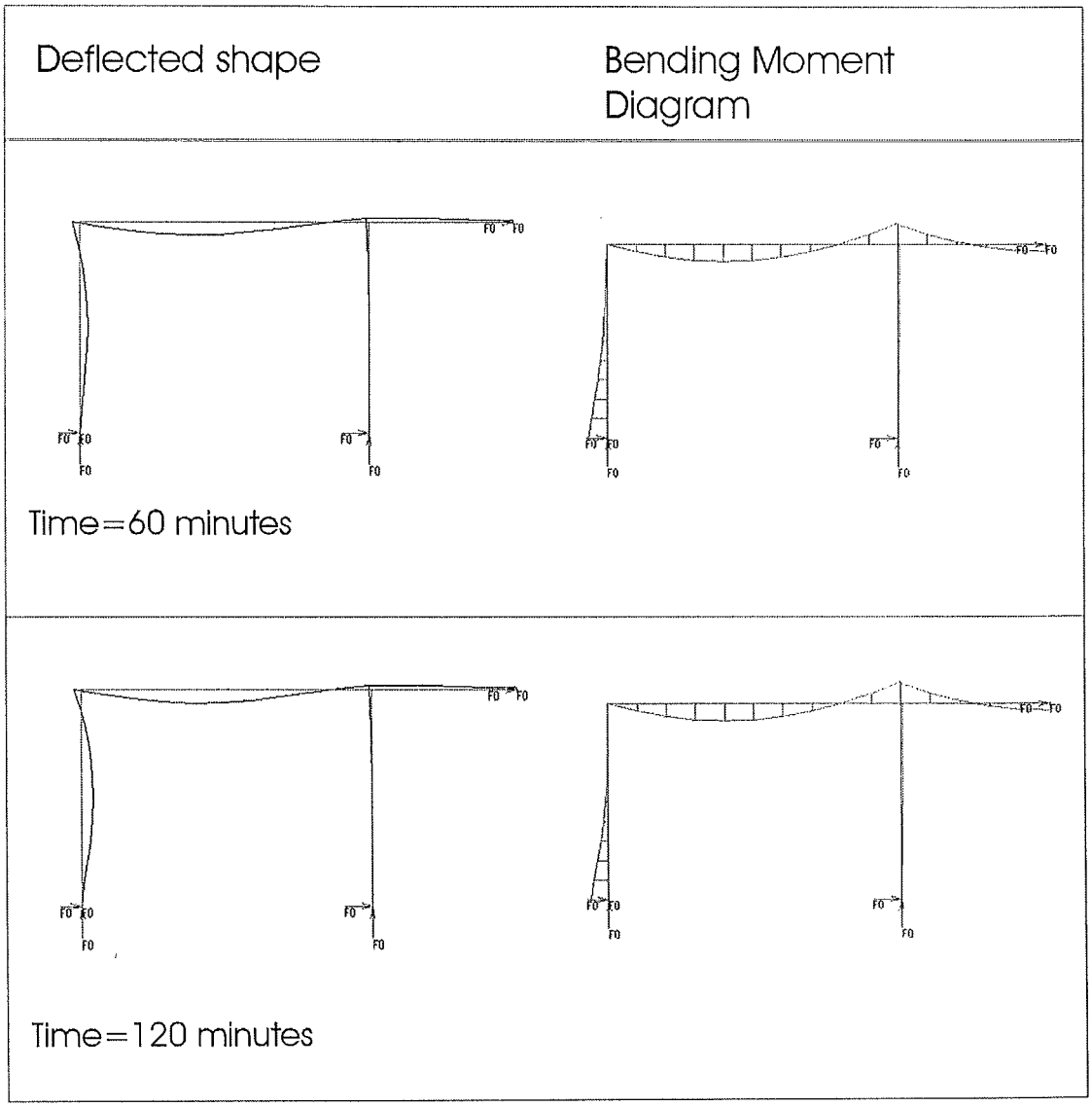

Figure 8-18: Deflected shape and bending moment diagram of frame subjected to the EC1 external fire. (*Note: deflections magnified by 2)

Behaviour of a frame subjected to the EC1 external fire

Figure 8-18 shows the deflected shape and corresponding bending moment diagram of the frame when it is subjected to the EC1 external fire. During the initial stages of the fire, moment redistribution in the rafter occurs as the rafter deflects downwards due to the reduction of the elastic modulus of the steel. As the fire progresses, thermal bowing causes the lower part of the wall to bow into the building. Lateral displacement at the top of the wall occurs when the lateral restraint from the rafter is relaxed due to thermal elongation of the steel. Despite the rafter being unprotected, it has sufficient stiffness to act as a prop to prevent excessive deflection of the wall due to thermal bowing. As the wall continues to bow, the curvature of the wall increases, thus increasing the bending moment at the base of the wall. At approximately 3000 seconds (50 minutes), a plastic hinge forms at the base of the wall.

The frame manages to survive the fire until 120 minutes without collapse. The reason why the frame does not collapse is due to the steel rafter not forming any plastic hinges, which would consequently form a mechanism in the structure. Unlike the ISO fire, the temperature of the external fire is not hot enough to reduce the yield strength of the steel and cause plastic hinges to form.

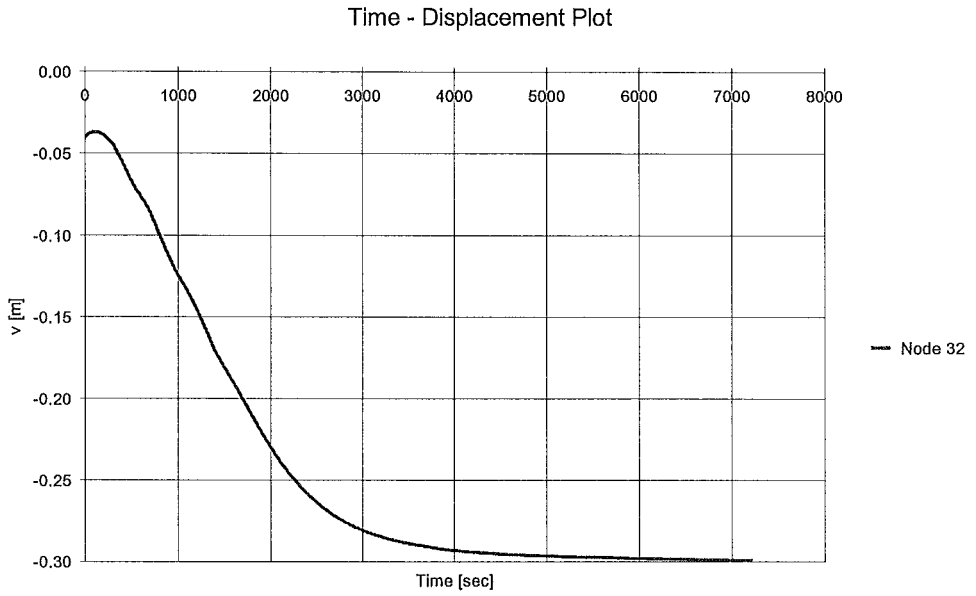

Figure 8-19: Variation of vertical displacement at midspan of rafter.

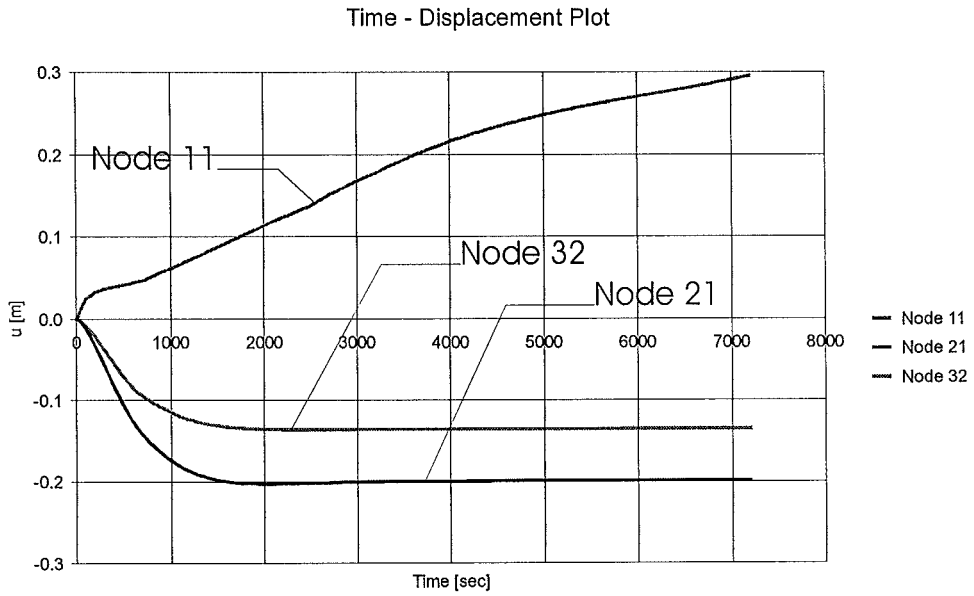

Figure 8-20: Variation of horizontal displacement at mid-height and the top of the wall.

Deflections of structural elements

Figure 8-19 shows the variation of vertical displacement at midspan of the steel rafter. The negative displacement on the graph represents downward deflection of the wall, while positive displacement represents upward deflection of the wall. The deflection trend shows a slight kink upwards during the initial stages before dropping in an almost linear trend during the first 2100 seconds (35 minutes) of the fire. Beyond this time, the rate of change of deflection reduces and the deflection plateaus throughout the rest of the fire duration at –0.30 metres. Unlike the ISO fire, the deflection of the rafter in this case does not show a runaway trend.

Figure 8-20 shows the variation of horizontal displacements at various positions of the wall and beam. Node 11 and node 21 represent the mid-height and top of the wall, while node 32 represents the midspan of the rafter (refer to Figure 8-5). The negative displacement represents outward deflection of the wall while positive displacement represents inward deflection of the wall. During the initial stages of the fire, the deflections at node 21 and 32 displace outwards rapidly. The deflection is due to the horizontal thrust exerted by thermal bowing of the wall. Although the rafter provides lateral restraint against outward deflection, thermal expansion of the steel and creep cause the rafter to elongate, allowing some lateral displacement at the top to occur. At the same time, the lower part of the wall deflects inwards.

At approximately 1500 seconds (25 minutes), the horizontal deflections at the top of the wall and midspan of the rafter level off and reach a steady state displacement of –0.20 metres and –0.135 metres, respectively. The steady state outward deflection is reached due to the limit of thermal expansion and creep of the steel when the temperatures in the rafter reach a steady state in the external fire. The deflection at mid-height of the wall however, still takes place in an almost bilinear fashion from 900 seconds (15 minutes) till the end of the simulation. The deflecting lower portion of the wall increases the curvature of the wall and the moment at the base. This causes a plastic hinge to form at the base of the wall at 3000 seconds (50minutes).

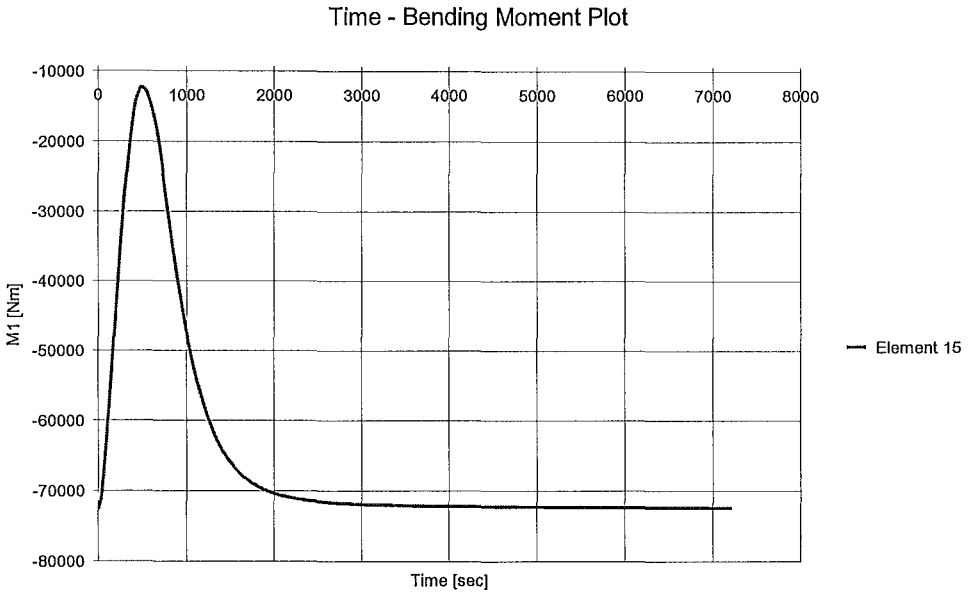

Figure 8-21: Variation of bending moment at midspan of the rafter.

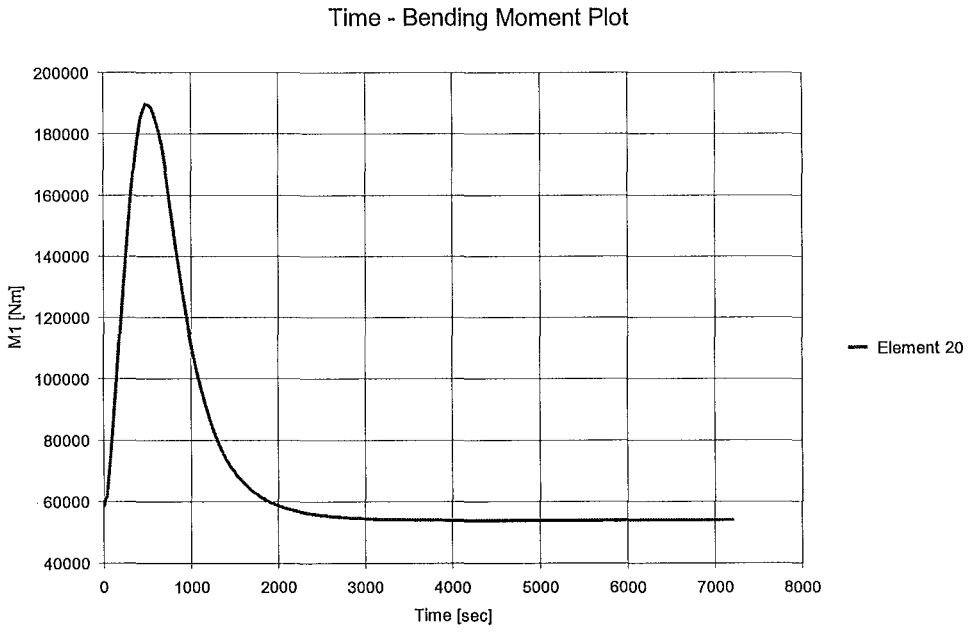

Figure 8-22: Variation of bending moment of the rafter at the column intersection.

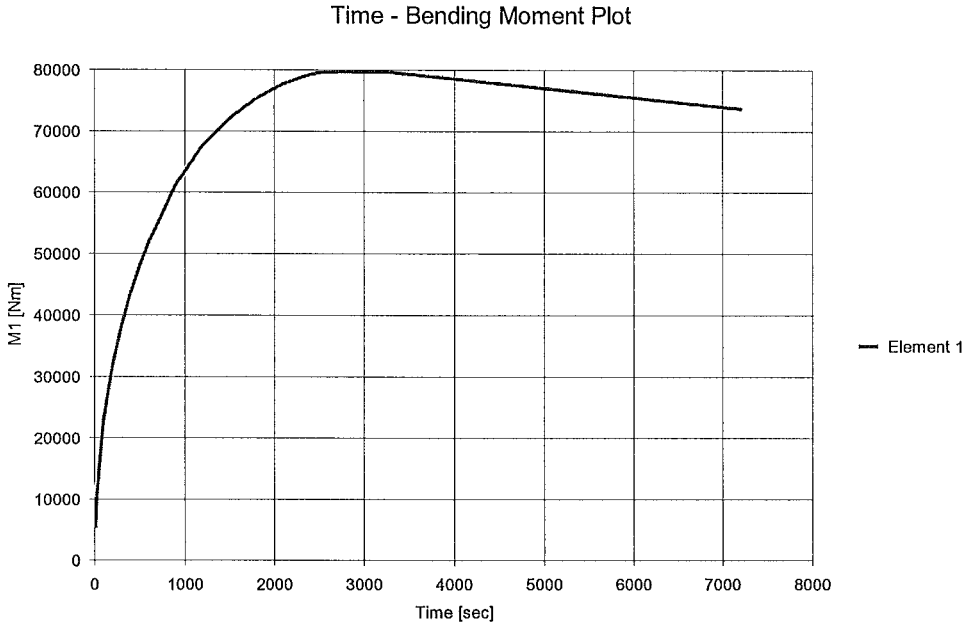

Figure 8-23: Variation of bending moment at the base of the wall.

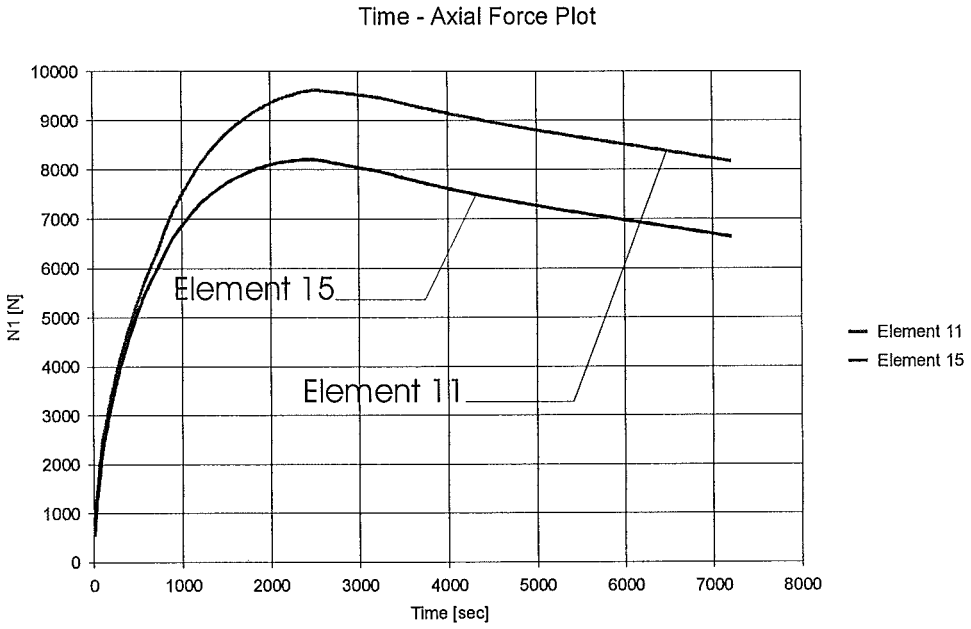

Figure 8-24: Variation of horizontal axial force at the left side (closest to the wall) and midspan of rafter.

Bending moments in the walls and the beam elements

Figure 8-21 and Figure 8-22 show the variation of bending moments at midspan of the rafter and at the column support, respectively. During the first 500 seconds, the bending moment at midspan of the rafter redistributes to the supports. When the moment redistribution reaches its peach at 500 seconds, it drops off again and reaches a steady state after 3000 seconds (50 minutes). The drop in the bending moment after the peak is due to the reduction of the yield strength of the steel at both the midspan of the rafter and adjacent to the column support. This causes the bending moment to redistribute again until equilibrium is obtained. Once the yield strength of the steel has stopped reducing, the bending moments at midspan and the support reach equilibrium. The moment at steady state is similar to the moment during the initial stages, before the fire occurred.

Figure 8-23 shows the variation of bending moments at the base of the wall. The bending moment rises very steeply initially and levels off slowly when the reinforcing steel at the base yields. At 2500 seconds (42 minutes), a plastic hinge forms at the base of the wall. The plastic moment gradually decreases as the yield strength of the reinforcing steel in the wall decreases. Unlike the case with the ISO fire, the single plastic hinge at the base of the wall was insufficient to form a collapse mechanism in the structure.

Axial force in beam elements

Figure 8-24 shows the horizontal force in the beam elements with time. The positive sign in the graph represents axial tension. The axial force in the beam elements immediately adjacent to the wall (element 11) and at midspan of the rafter (element 15), exhibit very similar trends to the bending moment trend at the base of the wall. This is due to the linear relation between the horizontal axial force in the beam and the moment at the base of the wall. The horizontal axial force in the beam, H^* is approximated as:

$$H^* \propto \frac{M_b}{H_{wu}}$$

Where: M_b = moment at the base of the wall (Nm)

H_{wu} = height of the wall (m)

Figure 8-24 shows that the beam is constantly in tension. It increases very rapidly initially and slowly reaches a peak before slowly decreasing. The peak occurs when a plastic hinge at the base of the wall forms. The reduction of the axial force at the advanced stages corresponds to the reduction of the plastic moment of the wall. The peak of the axial force in element 11 is higher than in element 15, due to the downward force from the loads acting on the rafter.

8.6. Conclusion

The analyses have shown that the frame behaved differently when subjected to different fire conditions. The frame subjected to the more severe fire, the ISO fire, collapsed after 27.5 minutes when plastic hinges formed in the rafter and the base of the wall. The high temperatures in the ISO fire caused the yield strength of the steel rafter to drop significantly, reducing its load bearing capacity. This led to plastic hinges forming in the rafter and subsequent collapse of the frame, with the wall falling inward.

The frame subjected to the well-ventilated fire, the EC1 external fire, survived the fire up to 2 hours when the simulation stopped. The lower maximum temperatures of the external fire were not sufficient to cause formation of plastic hinges in the rafter, so it did not sag and collapse.

9. THE BEHAVIOUR OF FRAMES WITH VARYING WALL SLENDERNESS RATIOS

9.1. Introduction

In this chapter, the behaviour of two types of frames with varying wall slenderness ratios is analysed. The purpose of the analyses is to investigate the different modes of failure when the frames are subjected to migrating fires. Various levels of bracing, in the form of diaphragm action from the roof and frame action, will be provided to the frames and the possibility of sway mode failures in the frames will be considered. The analyses also serve to determine the limiting wall slenderness ratio in the frames that would allow the frames to deform and collapse in an acceptable manner. Only the ISO 834 standard fire will be used in the analysis in this chapter. The following table summarises the different types of frames analysed in this chapter and the corresponding sections where they are described.

Section	Heading	Page Number	Bracing	Frame configuration	Beam-column connection	Fire
9.2	Analytical models	244	Braced/ unbraced/ Partially	A & B	Pinned/fixed	ISO
9.3	Unbraced frames	251	Unbraced	A & B	Pinned	ISO
9.4	Non-sway mode					
9.4.1	Frame A	261	Braced	A	Fixed	ISO
9.4.2	Frame B	270	Braced	B	Fixed	ISO
9.5	Partial restraint					
9.5.1	Frame A	278	Partially	A	Fixed	ISO
9.5.2	Frame B	293	Partially	B	Fixed	ISO
9.6	Wall to rafter connections	308	-	-	-	-
9.7	General discussion	311	-	-	-	-
9.8	Conclusions	314	-	-	-	-

Table 9-1: Configurations of frames analysed in chapter 9.

9.2. Analytical model

To determine the behaviour of the frame with different wall slenderness ratios, two types of frames were analysed. *Frame A* (Figure 9-1) is identical to the frame analysed in section 8.3 which features a steel rafter spanning across three bays, supported by two internal steel columns and concrete cantilever walls at the perimeter. *Frame B* is another type of frame configuration (Figure 9-2) that is popular in parts of New Zealand (Clifton, G.C., Personal Communication). *Frame B* features a steel rafter spanning across two bays, supported by one internal steel column and concrete cantilever walls at the perimeter. The analysis of the frame was conducted only for plane-frame analysis. The analysis was not extended to three-dimensions, as its two-dimensional behaviour has not been fully understood.

9.2.1. Extent of fire in the frame

For this investigation, a migrating fire is assumed in the building. The entire frame is unlikely to be exposed to a fully developed fire in a large industrial building. Full involvement is possible, for example: the plastics factory in Christchurch, page 71. In order to model the behaviour of the frames in a fire, half of the structure is assumed to be affected by a migrating fire while the other half is assumed unaffected (Figure 9-1 and Figure 9-2). The migrating fire is also assumed to affect only one frame of the entire building, leaving the other parts of the structure unaffected. The migrating fire in the plane frame analysis does not consider the interaction of the heated frame with the rest of the building. These assumptions are simplistic but are sufficient for the purposes of this study. The heated structural elements are exposed to a fire with temperatures equivalent to the ISO standard fire. This fire is conservative compared to an external fire but is not unlikely, given the fact that industrial buildings may have very high fuel loads. In *Frame B*, the internal steel column is unexposed to the fire and its strength is unaffected.

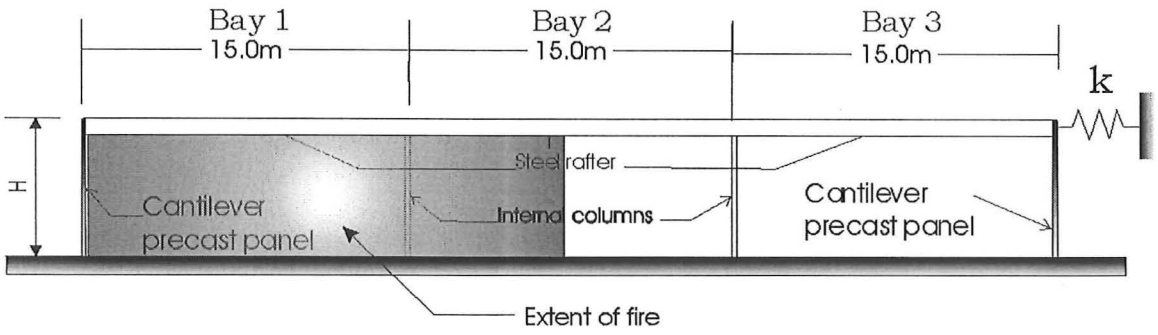

Figure 9-1: Structural configuration of Frame A and the extent of the migrating fire.

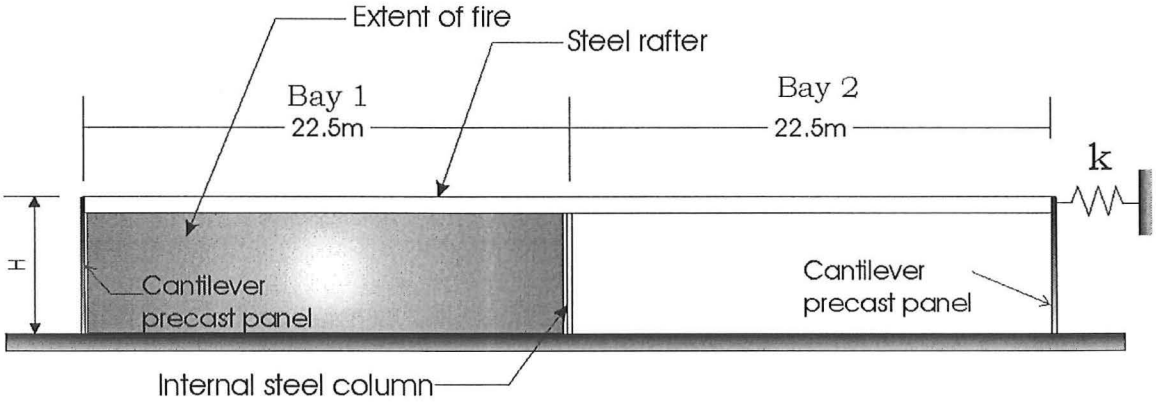

Figure 9-2: Structural configuration of Frame B and the extent of the migrating fire.

9.2.2. Boundary conditions of the frame

Figure 9-3 and Figure 9-4 show the elements and boundary conditions of the two different frames used in the finite element model. The concrete wall panels are fully fixed at the base, where the rotations and displacements are restrained. The steel rafter is connected to the top of the wall panels by pin connections, where the rotations are unrestrained. The internal steel columns are also pinned at the base. The connections between the rafter to the steel column are varied between fully rigid connections (moment resisting connections) to pinned connections. The spring represents the horizontal restraint provided by the roof diaphragm at the top right corner of the steel frame.

9.2.3. Assumptions made in the analyses

The assumptions made in the following analyses for both frames are identical to those made in section 8.3.

FRAME A

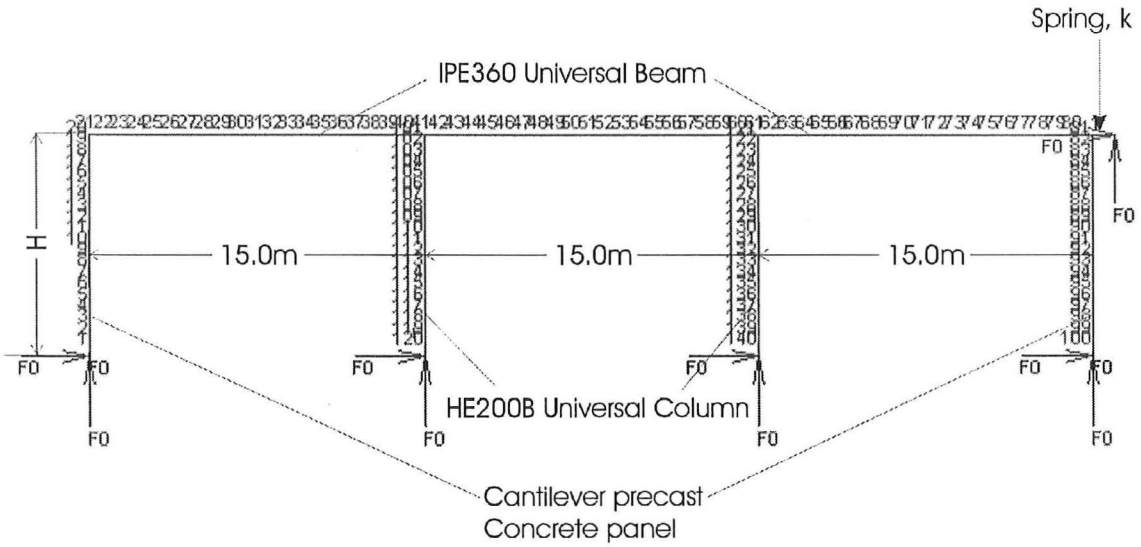

Figure 9-3: Structural model of *Frame A* in SAFIR.

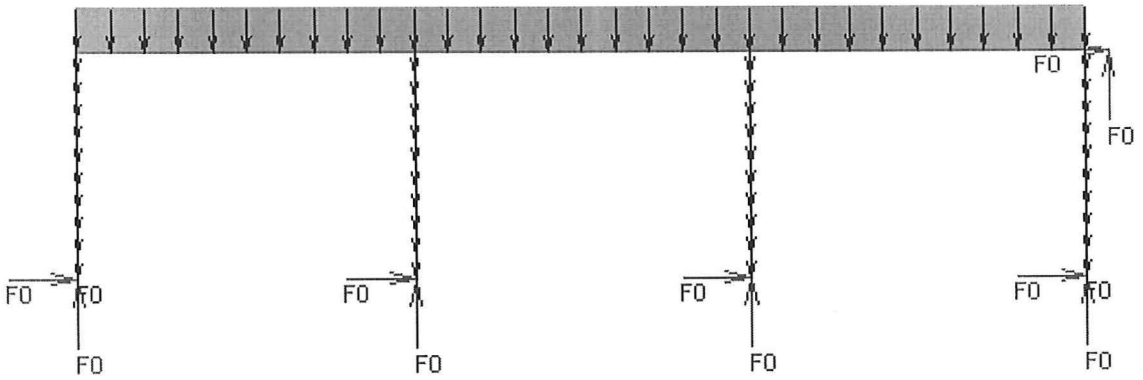

Figure 9-4: Applied loads on *Frame A*.

FRAME B

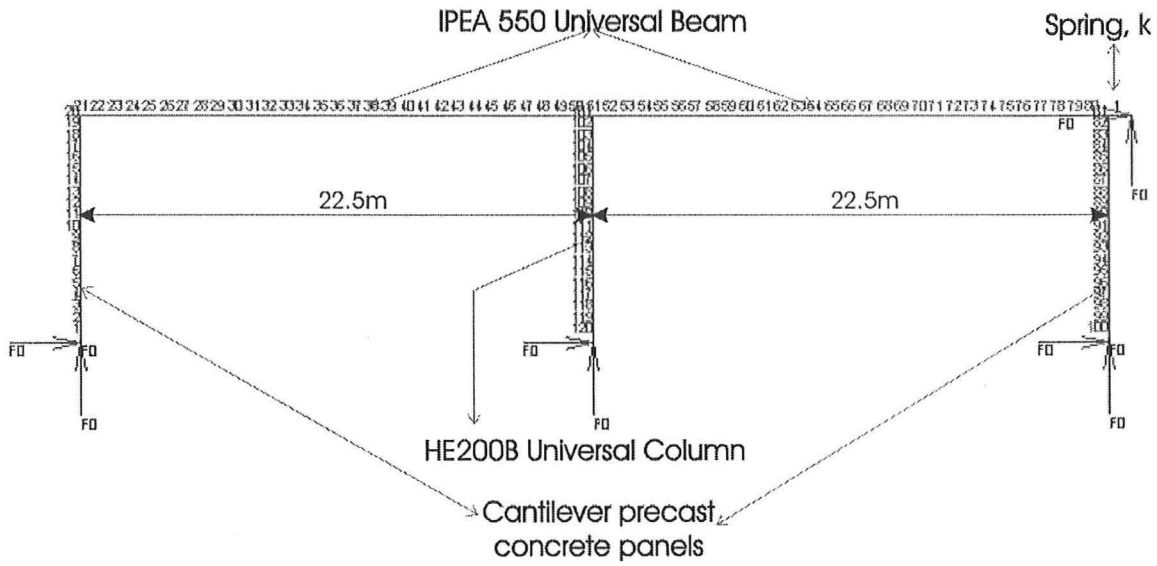

Figure 9-5: Structural model of *Frame B* in SAFIR.

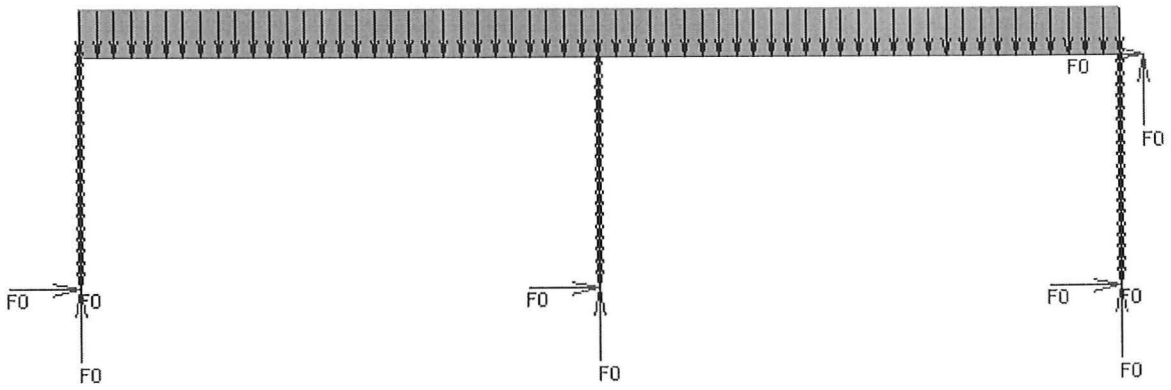

Figure 9-6: Applied loads on *Frame B*.

9.2.4. Properties of frame elements

In order to determine the limiting slenderness ratio of the walls in the frames, the heights and thicknesses of the walls are varied to model the different types of walls that would be constructed in practice. The heights and thicknesses of the walls that will be used in the analyses will be described in the following sections. The mechanical and thermal properties of the walls and other structural elements are unchanged (refer to pages 223 - 225), unless stated otherwise. For *Frame B*, the rafter size was increased to compensate for the larger span between supports. The size of the beam was changed from the IPE 360 universal beam to an IPEA 550 universal beam. The properties of the larger beam are shown below:

Beam (for *Frame B*)

Type:	IPEA550 ≅ 530UB92
Depth of section:	547mm
Flange width:	210mm
Flange thickness:	15.0mm
Web thickness:	9.0mm
Weight:	92.1kg/m
Yield strength, f_y:	430MPa
Elastic modulus, E_s:	210.0 GPa
Steel Poisson's ratio, ν_s:	0.30
Steel density, ρ_s:	78.50 kN/m^3

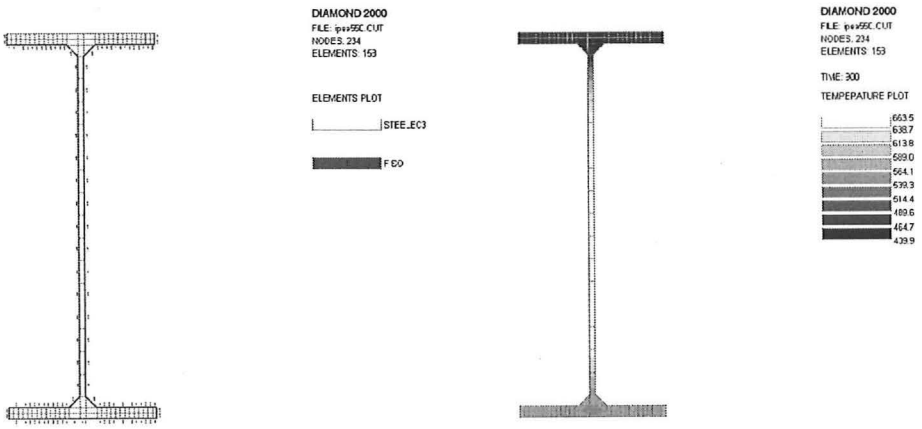

Figure 9-7: Thermal distribution of the I-beam used in Frame B after 15 minutes of three-sided exposure to the ISO fire.

9.2.5. Modelling of horizontal restraint

Three different levels of horizontal restraint in the frame are analysed to determine the behaviour of the structure at elevated temperatures. These restraint conditions apply to both types of frames but are illustrated only for *Frame* A.

i. NO HORIZONTAL RESTRAINT (SWAY MODE)

This case assumes that there is no horizontal restraint provided by diaphragm action. The spring attached at the top of the frame has zero stiffness, hence it will not be modelled in the analysis. Therefore, the amount of horizontal restraint in the frame is minimal, provided only by the moment resistance of the cantilever walls. There is also no moment resistance provided by frame action, so the connections between the beam and the columns are modelled with moment releases.

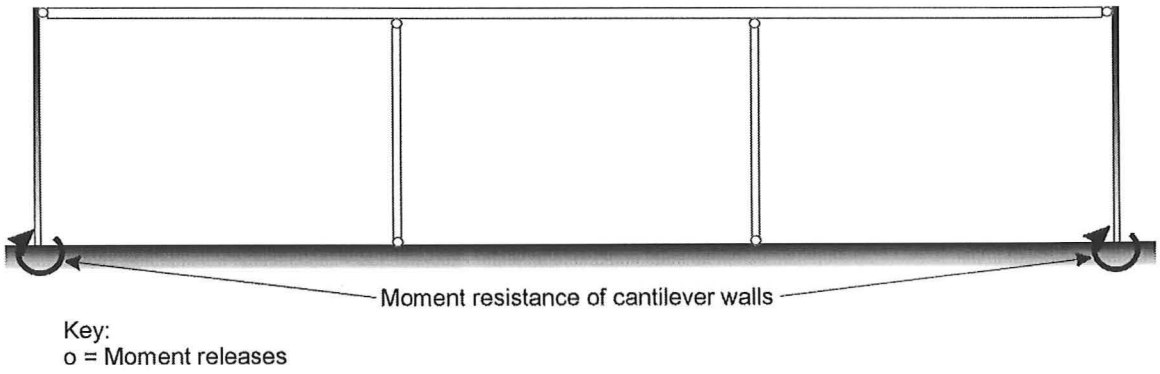

Figure 9-8: Typical unrestrained frame.

ii. FULL HORIZONTAL RESTRAINT (NON-SWAY MODE)

This case assumes that there is infinite horizontal restraint provided by diaphragm action and from rigid moment resisting beam column joints. The spring attached at the top of frame is assumed infinitely stiff. In this case, the spring can be modelled by a pinned support at the top right corner of the frame. This support condition restrains the horizontal and vertical displacements but permits rotations. This condition is similar to the frame modelled in section 8.3.

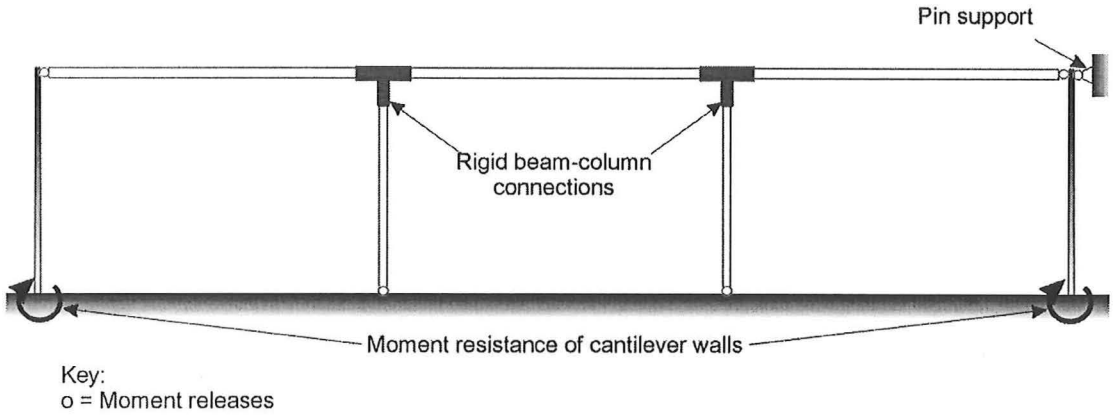

Figure 9-9: Fully restrained frame

iii. PARTIAL RESTRAINT

This case assumes that there is partial horizontal restraint provided by diaphragm action, modelled by a moment resisting frame. This is modelled by incorporating rigid connections at the beam-column joints. The moment resistance of the frame depends on the flexural strength of the beams and columns.

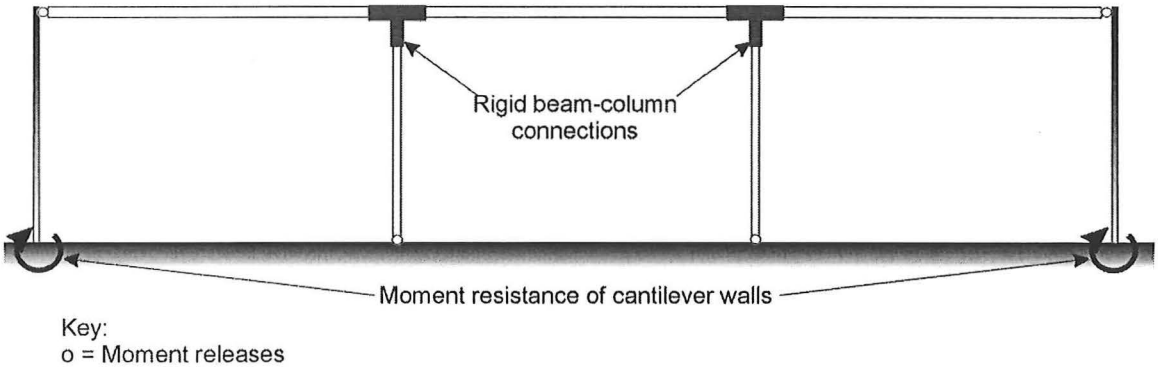

Figure 9-10: Partially restrained frame

The amount of diaphragm action present in the event of a fire is uncertain. In the worst case scenario, the entire roof, along with the purlins and eaves ties may have collapsed or lost all its strength and stiffness due to thermal effects. Therefore, there would be no diaphragm action present in this situation. This is depicted by condition (i) stated above. Condition (ii) represents the most favourable scenario where the roof diaphragm is undamaged and provides full horizontal restraint to the structure. In reality, the degree of horizontal restraint provided to the frame in the event of a fire lies between the two conditions stated above. Condition (iii) is a situation where some horizontal restraint exists and the degree of restraint lies between the extremes of conditions (i) and (ii).

9.3. Unbraced frame

This section describes the results of the analysis of the unrestrained frame. The analysis of unrestrained frames was performed only for a very limited number of frame configurations. This is due to the high instability of the frames with slender walls as they proved to be numerically very difficult to model in SAFIR. Only *Frame A* was analysed as *Frame B* proved to be very unstable and numerically difficult to model without instability occurring in the programme. The different wall heights that were analysed with *Frame A* are shown in Table 9-2.

Case number	Wall height (m)	Wall thickness (mm)	Slenderness ratio
1)	6	150	40.0
2)	8	150	53.3
3)	10	150	66.7
4)	12	150	80.0

Table 9-2: Wall slenderness ratios used in modelling the unrestrained frame

Results of analyses

The results of the analyses for the unbraced frames with the wall slenderness ratios are shown in the following table:

Case number	Wall height (m)	Slenderness ratio	Mode of failure	Time to failure (minutes)
1)	6	40.0	Outward collapse	22.2
2)	8	53.3	Outward collapse	1.30 *
3)	10	66.7	Outward collapse	0.83 *
4)	12	80.0	Outward collapse	0.50 *

Table 9-3: Results of analyses of the unbraced frame

*Note: These short failure times are believed to be due to numerical problems and not the actual times that the structure collapses.

The numerical problems encountered were due to SAFIR being unable to converge to a solution although measures were taken to try to obtain a converged solution. The only frame configuration that did not fail due to numerical failure was case 1), which will be described in further detail in the following discussion. Due to the very short failure times of the walls with slenderness ratios in excess of 50, further analysis with different wall thicknesses was not conducted, as it was believed that they would also produce similar numerical problems at higher slenderness ratios. *Frame B* was not analysed, as it also produced numerical problems, even for the walls with very low slenderness ratios. For the purposes of analysing the behaviour of a typical unbraced frame, the analysis results of case 1) will be described.

6 m unbraced frame: Outward collapse

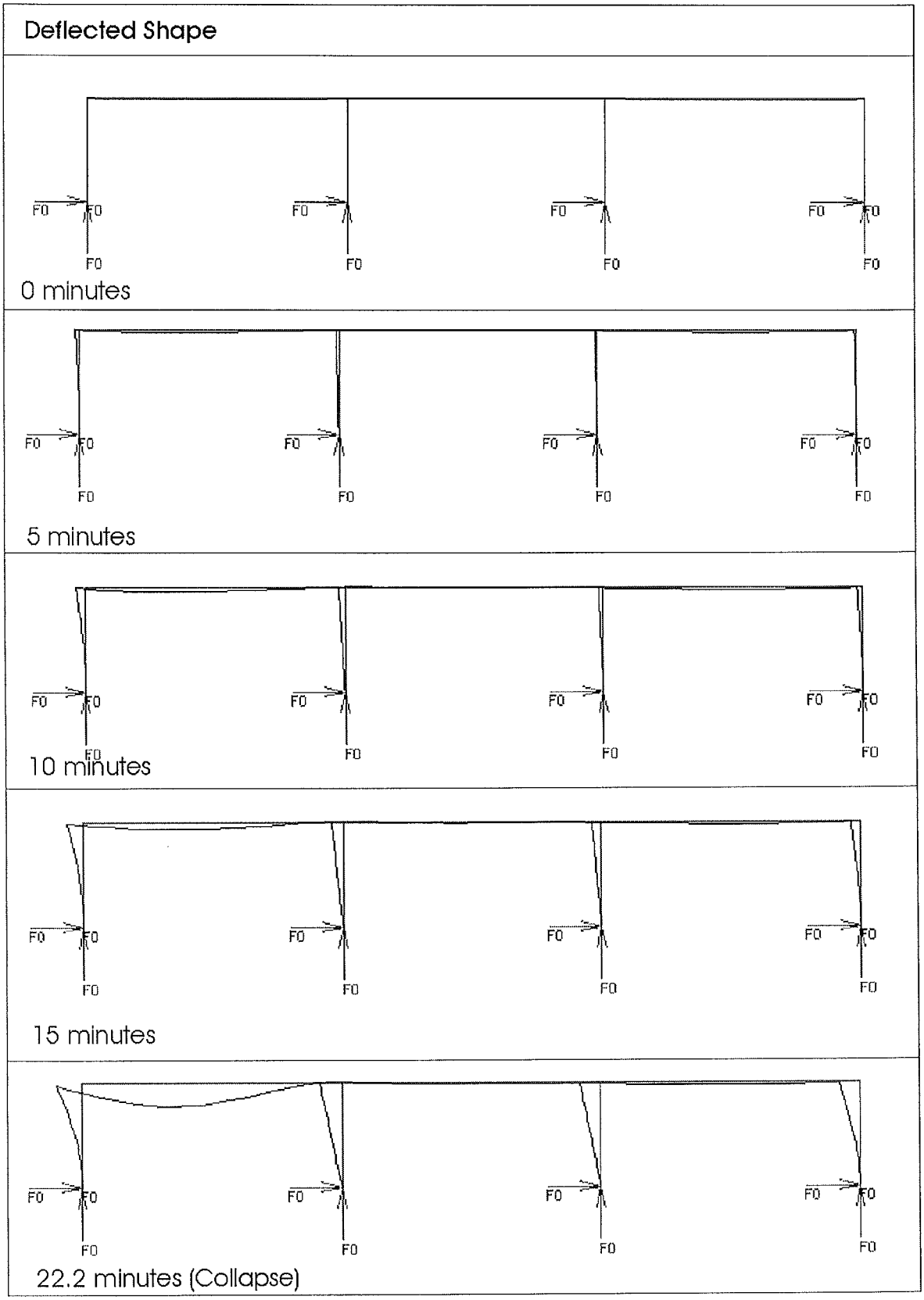

Figure 9-11: Sequence of deformation of the unbraced frame with a 6m wall. *Note: Deflections are magnified by 2.

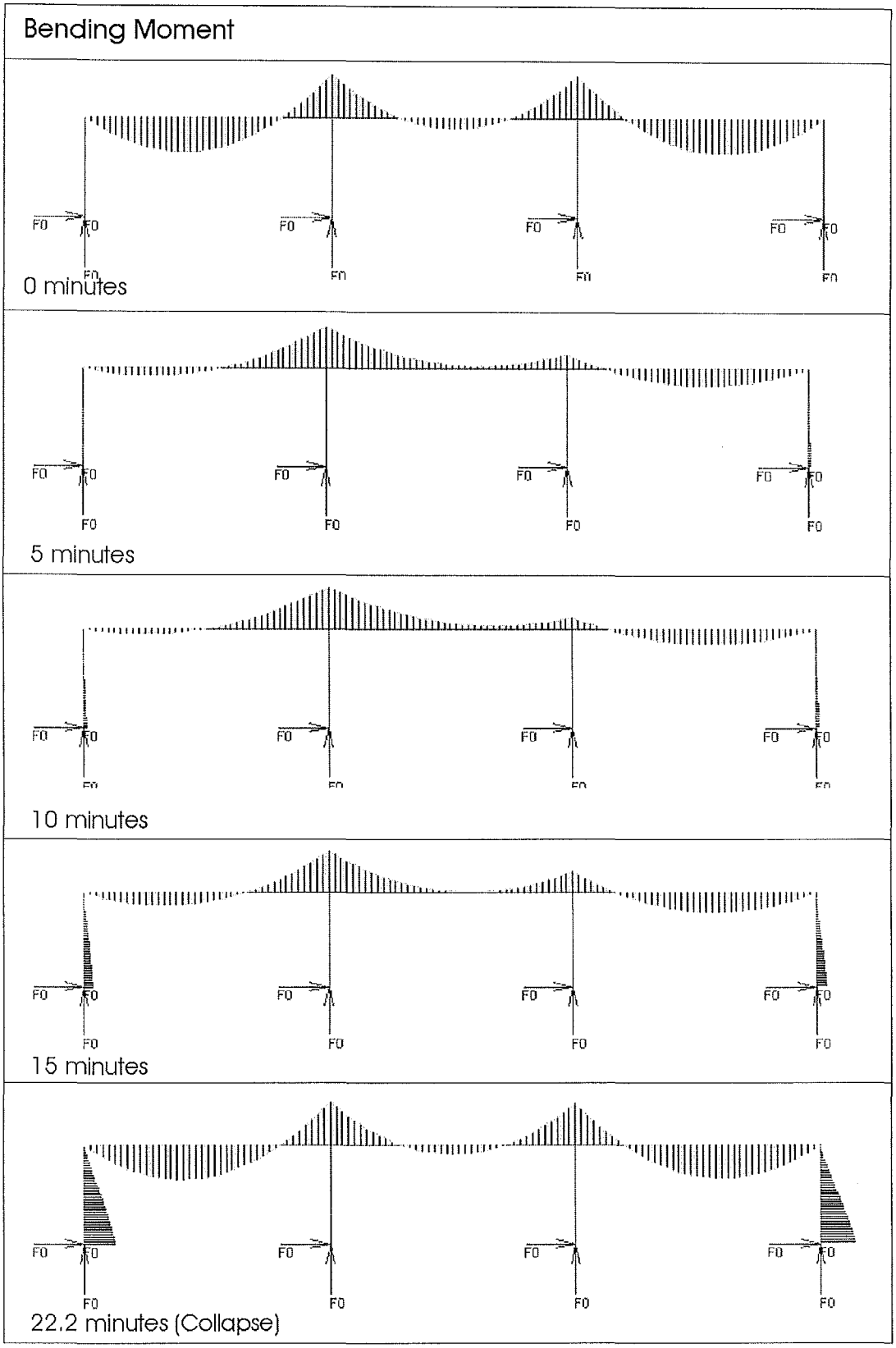

Figure 9-12: Bending moment diagrams corresponding to the deformation of the unbraced 6m frame.

Behaviour of the unbraced 6m frame

When a fully developed fire occurs in the building, non-uniform temperatures form across the thickness of the wall panels, causing differential thermal expansion and thermal bowing (Figure 9-13). The attached steel frame is pulled outwards, causing sway in the frame. The sway is resisted only by the flexural strength at the base of the wall panels as there is no horizontal resistance from diaphragm action. While the frame sways outwards, the steel rafters in bays 1 and 2 deflect downward due to thermal effects on the elastic modulus of the rafter (Figure 9-14).

During the first 10 minutes of the fire, the moments redistribute from the midspan region of the beams to the support (Figure 9-12 and Figure 9-15). This is graphically shown by the rapid increase of the bending moments at the supports. The redistribution of the moments from the midspan region to the supports during the initial stages is because the beam has higher negative flexural strength compared with its positive flexural strength. During the initial stages, the top flange of the beam is cooler compared to the lower flange and the web of the beam. This causes the positive bending moments from the midspan region to redistribute to the supports, allowing the negative flexural strength of the beam at the supports to resist the moments.

The rate of moment redistribution decreases after approximately 7 minutes of fire exposure. The reduction of the rate of redistribution is due to the increasing temperatures in the top flange of the beam by conduction from the heated sides. This causes the negative flexural strength of the rafter to be depleted, thus reducing the negative moment capacity of the beam. The moment redistribution reaches its peak at approximately 8 minutes followed by a decrease in the moments at both the supports and the midspan region. This is due to the thermal effects on the yield strength of the steel, which reduces the negative and positive flexural strength of the rafter. The time when the plastic hinges form in the beam is not known exactly but is expected to occur during the phase when the moments at the supports and midspans decrease. The collapse of the frame can be approximated by modelling a propped cantilever beam with the same loading and support conditions, which will be discussed in further detail in the following section.

Moment resistance of the wall panels

The horizontal deflections of the frame increase with time, not only due to thermal bowing of the heated wall, but also due to P-delta effects. As the frame progressively deflects outwards, the bending moments at the base of the walls increase to resist the overturning moments. This is shown by the increasing moments of the walls with increasing time (Figure 9-16). (The different signs of the bending moments are due to the sign conventions in the programme.) There is slightly more moment resistance provided by the unheated wall as it has a higher stiffness compared with the heated wall. Therefore, it attracts more force. When the bending moment in the unheated wall reaches its plastic moment, the frame loses its moment resistance and collapses outwards. Figure 9-12 shows large moments at the base of the heated and unheated wall, indicating that the plastic hinge is about to form.

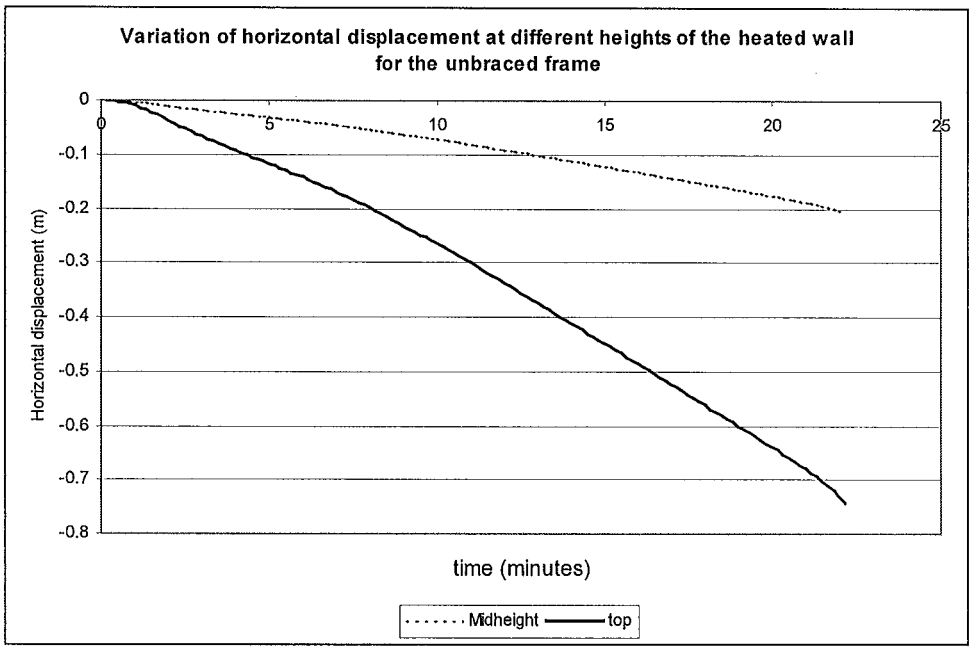

Figure 9-13: Variation of horizontal displacements of the heated wall panel.

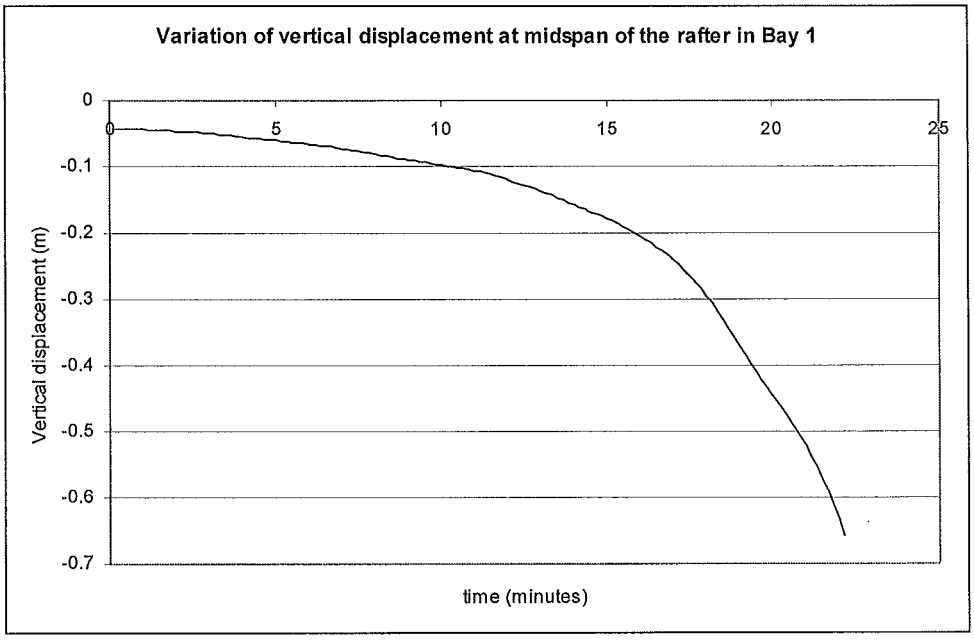

Figure 9-14: Variation of vertical displacement at midspan of the heated rafter.

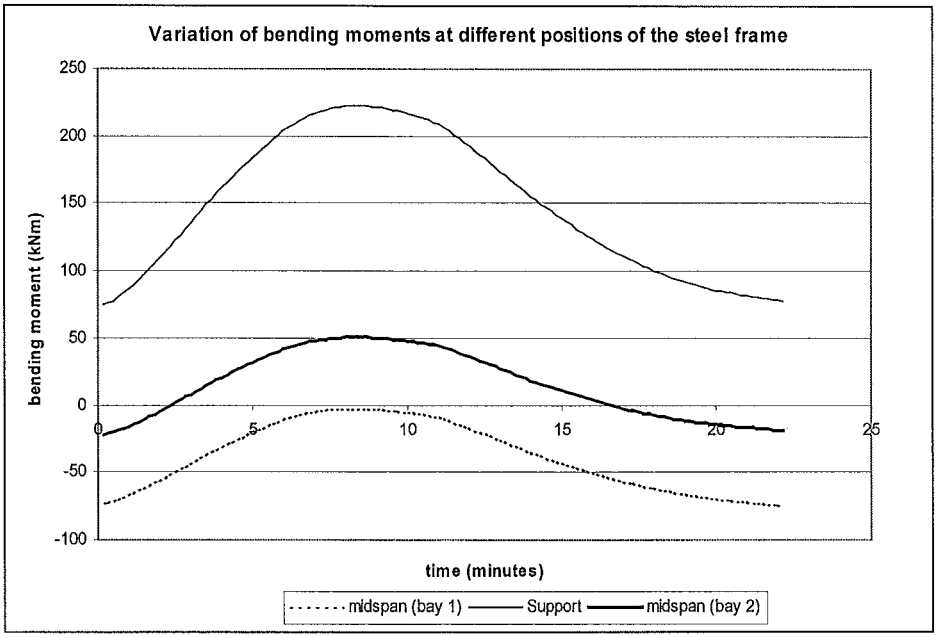

Figure 9-15: Variation of bending moments at different positions of the steel rafter.

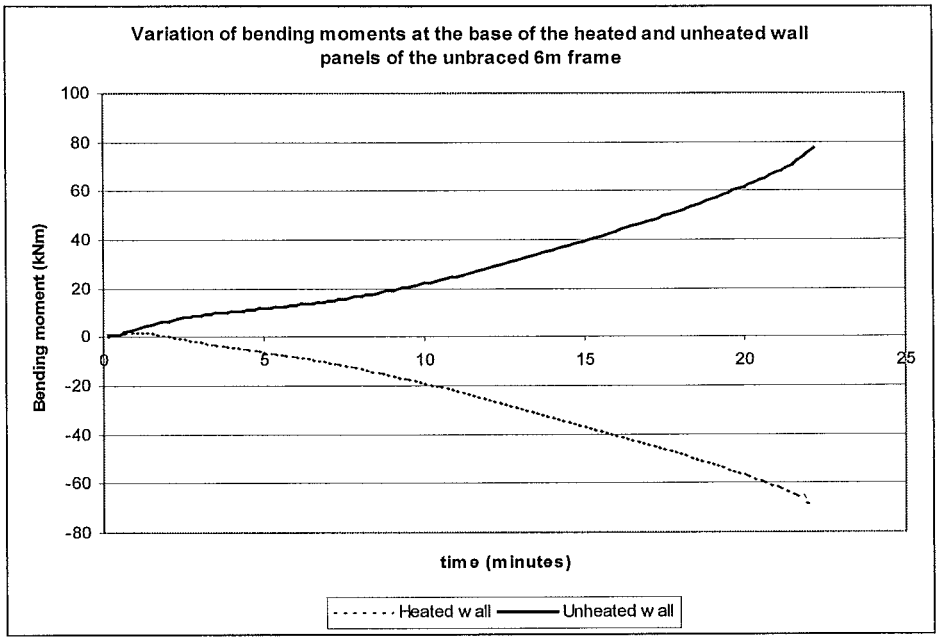

Figure 9-16: Variation of bending moments at the unheated and heated wall panels.

Discussion

Unbraced frames are very dangerous, as they are very likely to collapse outwards onto the neighbouring property. This could cause serious damage to the adjacent property or threaten the safety of fire-fighters who happen to be standing close to these walls while attending to a fire in the building. The analysis has shown that even with squat walls, the frames are very susceptible to outward collapse. Therefore, sufficient bracing by diaphragm action of the roof sheeting or any other means must be provided to prevent such a collapse mode.

9.4. Non-sway mode

In this section, the behaviour of *Frames A* and *B* with different wall slenderness ratios is investigated when full horizontal restraint is provided. Full horizontal restraint to the frame is provided by the roof diaphragm and is modelled as a pinned support, shown in Figure 9-9. The analysis is carried out for walls with different thicknesses and heights as shown in Table 9-4. The purpose of providing full restraint to the frame is to investigate the different modes of failure, particularly buckling of the wall panels.

Height of wall (m)	Thickness (mm)		
	125mm	150mm	175mm
6m	48.0	40.0	34.3
8m	64.0	53.3	45.7
10m	80.0	66.7	57.1
12m	96.0	80.0	68.6

Table 9-4: Slenderness ratios of walls with varying heights and thicknesses.

The thicknesses and heights of the walls are varied to determine the limiting slenderness ratio to prevent outward collapse. The heights of the walls are varied from 6.0 metres to 12.0 metres while the thicknesses of the walls range from 125mm to 175mm. These are typical dimensions that would be constructed in practice.

For each of the slenderness ratios shown in Table 9-4, the structural analysis for *Frames A* and *B,* based on the models shown in Figure 9-3 and Figure 9-5 are carried out in SAFIR. The other structural members and loads on the frame were unchanged in the analysis. The self-weights of the walls were adjusted accordingly for the different wall thicknesses.

9.4.1. Non-sway mode (Frame A)

Results of analyses

Wall dimensions				Collapse times (minutes)
				Mode of failure
Case no	Thickness (mm)	Height (m)	Slenderness ratio	Inward collapse
1)	125	6	48.0	28.5
2)		8	64.0	28.0
3)		10	80.0	28.0
4)		12	96.0	25.5
5)	150	6	40.0	29.5
6)		8	53.3	29.0
7)		10	66.7	28.5
8)		12	80.0	27.5
9)	175	6	34.3	31.5
10)		8	45.7	29.5
11)		10	57.1	29.0
12)		12	68.6	28.0

Table 9-5: Times and modes of collapse of frames with walls of different heights (Frame A).

Table 9-5 shows that for the wall slenderness ratios analysed, the frame will collapse inwards if full horizontal restraint is provided. The times to collapse of the frames are very similar for all the slenderness ratios shown above, decreasing slightly with increasing slenderness. The similarity in the collapse times is because they are governed by the times when plastic hinges form in the steel rafter, which in turn are dependent on the temperature of the rafter. Therefore, when the steel in the rafter reaches a limiting temperature for an applied load ratio, a plastic hinge will form at that position.

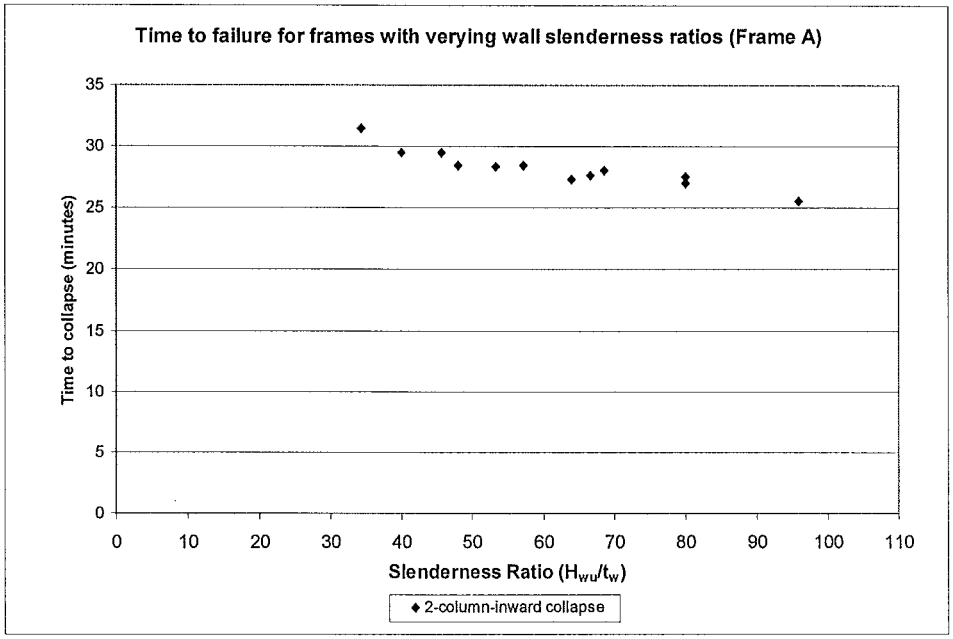

Figure 9-17: Times and modes of failure for different slenderness ratios in a fully braced frame (Frame A)

The following diagrams illustrate the deformation sequence and its corresponding bending moment diagram of a typical braced frame that has collapsed inwards. Although all the frames collapsed inwards, there are slight differences in the way they collapsed. Some of the frames formed plastic hinges at the base of the walls before the other plastic hinges formed in the steel rafter. This situation applied to cases 3), 4) and 8) (Table 9-5). The other frames formed plastic hinges in the rafter, which pulled the wall panels inwards, causing a plastic hinge to form at the base. The following discussion will compare this difference in order to justify the modes of collapse.

i) Plastic hinging in rafters before wall

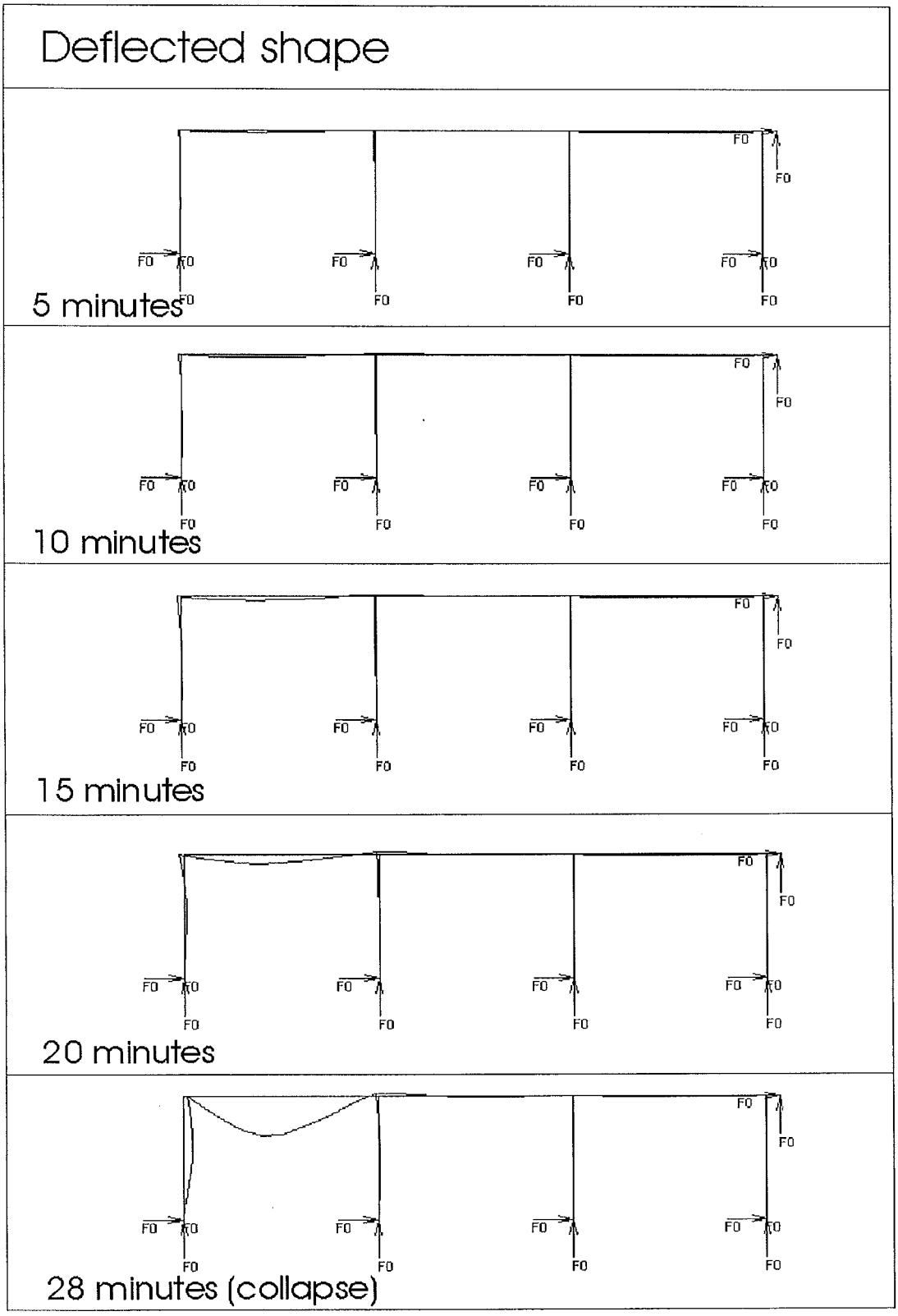

Figure 9-18: Sequence of deformation of a horizontally braced frame (Frame A) with 10m high and 150mm thick walls. *Note: Deflections are magnified by 2.

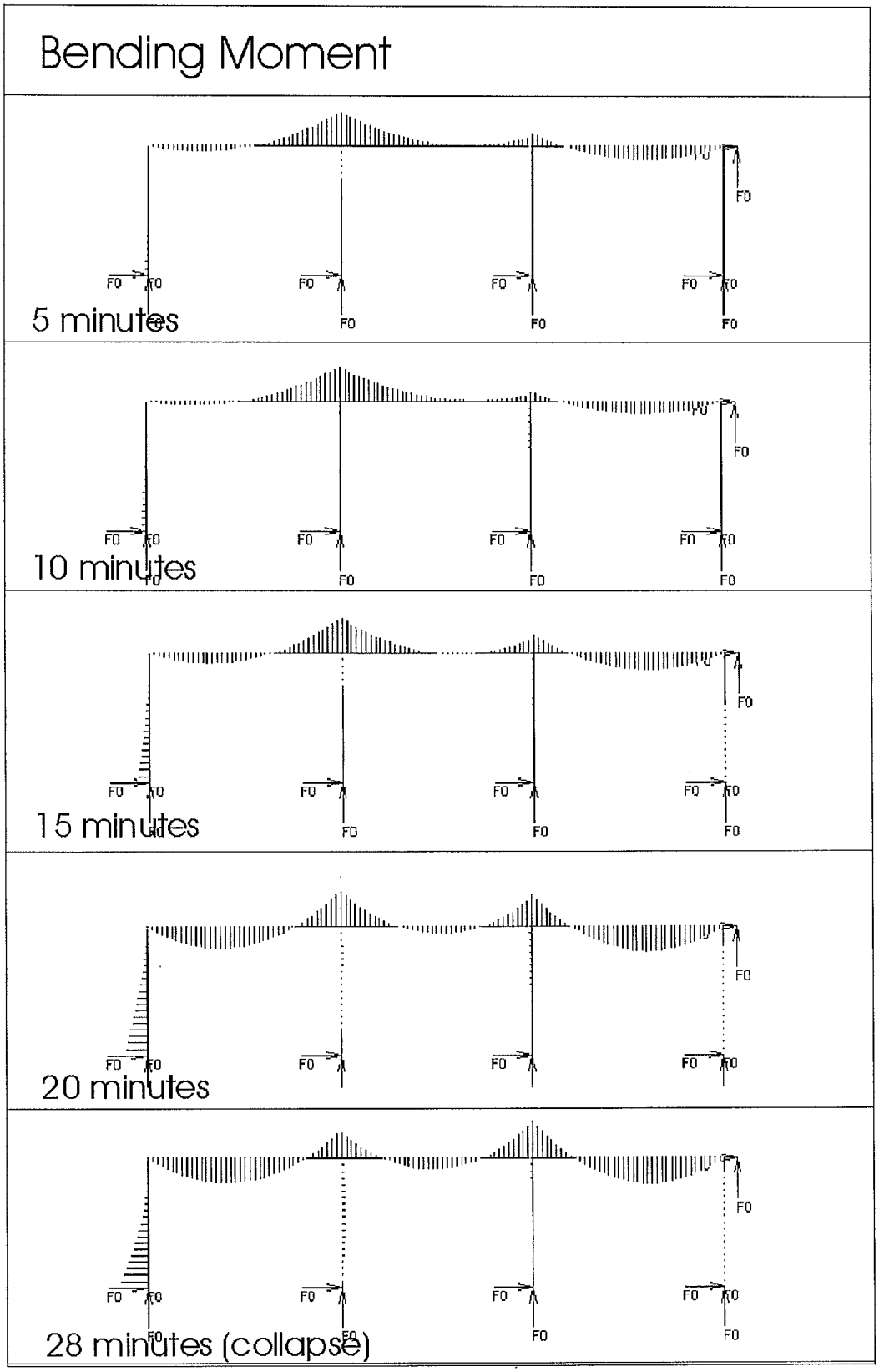

Figure 9-19: Variation of bending moments corresponding to the deformation of the 10m braced frame.

Deformation of the fully braced frame (*Frame A)*

Figure 9-18 shows the deformation of a typical frame that has formed plastic hinges in the rafter before forming at the base of the wall. The frame does not sway due to the horizontal restraint provided by the roof diaphragm. However, there is some horizontal displacement at the top of the heated wall due to thermal expansion of the steel rafter. While the heated wall deflects, the heated rafter progressively sags as the elastic modulus of steel decreases with increasing temperature (Figure 9-21). The deflection at the top of the wall reaches a plateau at approximately 18.5 minutes. This is due to the heated rafter which is about to undergo runaway failure. The runaway failure is due to the loss of strength and stiffness of the rafter, causing plastic hinges to form at the supports and the clear spans. When two plastic hinges have formed in the rafter, it collapses downwards, pulling the wall panel inwards (Figure 9-20). Consequently, a plastic hinge forms at the base of the wall when it has reached its plastic moment.

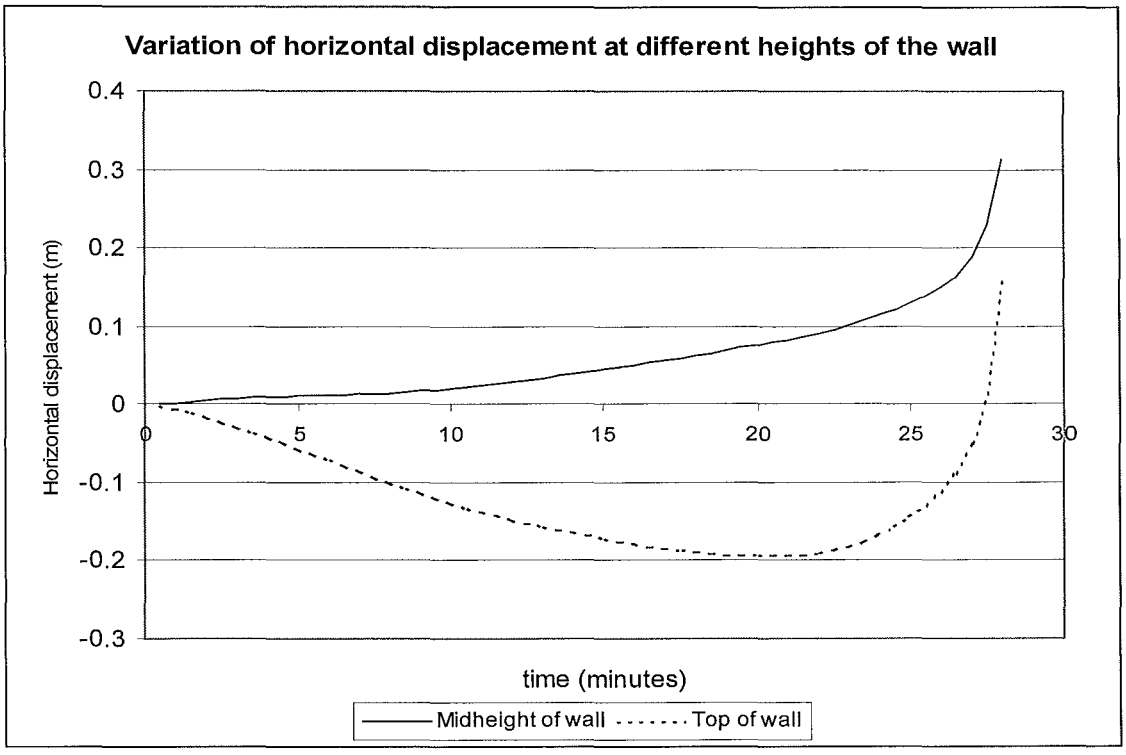

Figure 9-20: Variation of horizontal displacement at different positions of the heated wall

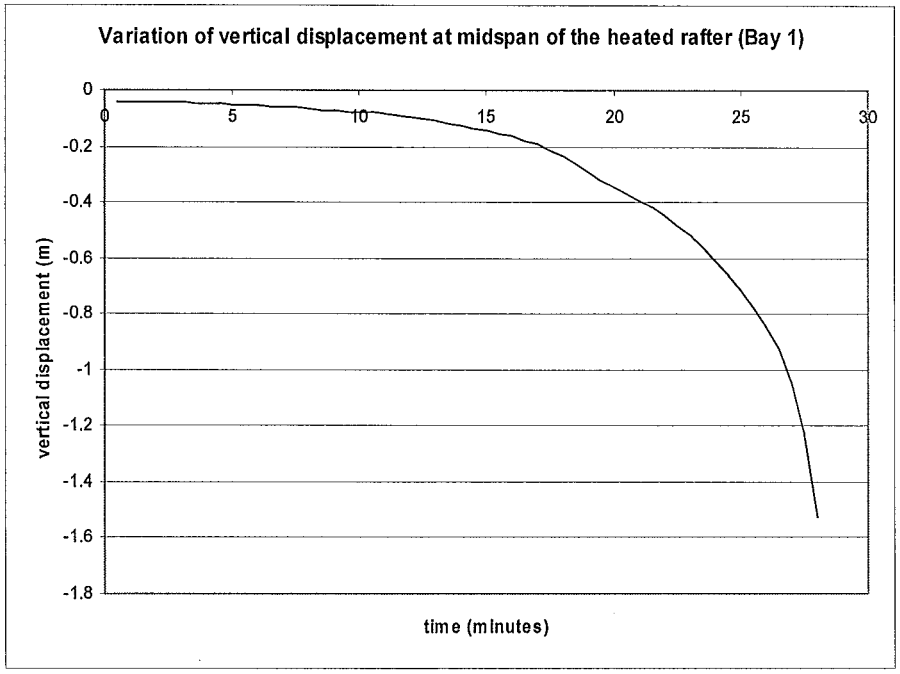

Figure 9-21: Variation of vertical displacement at midspan of the heated rafter

Bending Moments

Figure 9-19 shows the bending moments in the braced frame when it is subjected to a migrating fire. As with the other frames discussed so far, the bending moments from the clear spans of the rafter redistribute to the supports when the rafter deforms due to reduction of the elastic modulus. The rate of redistribution reduces and peaks at 8 minutes (Figure 9-22). Beyond this, the bending moments at the supports redistribute back to the midspans due to the reduction of the steel strength. As the bending moments redistribute again, the rafter experiences runaway failure, indicating that plastic hinges have formed at the support and midspans of the rafter. The runaway failure of the rafter pulls the wall panels inward, which resists the collapse by cantilever action. When the reinforcing steel at the base of the wall yields, a plastic hinge forms, resulting in a mechanism and subsequent collapse of the structure.

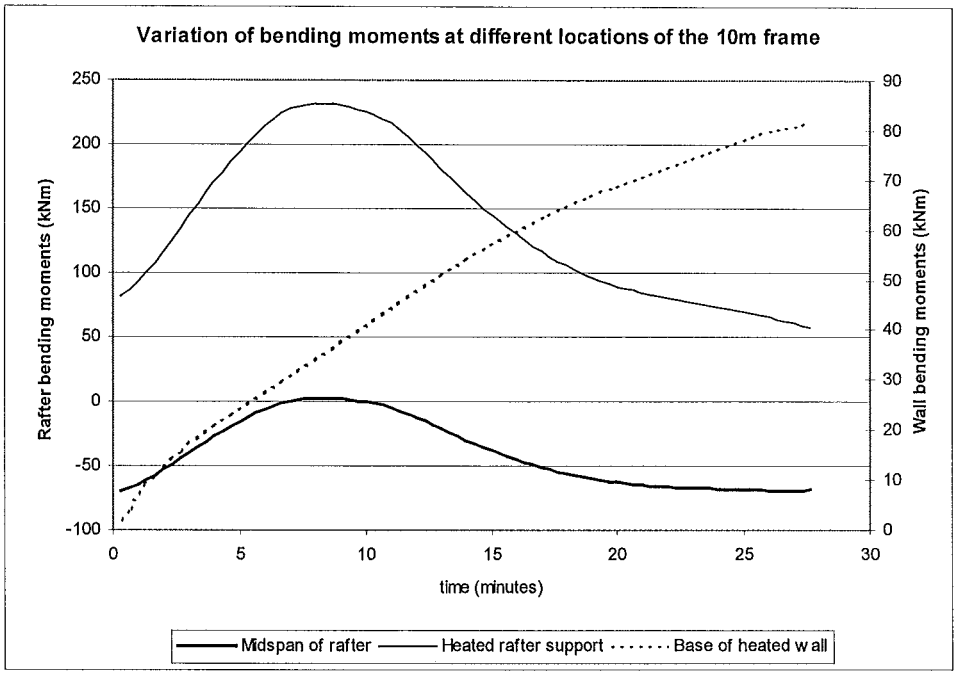

Figure 9-22: Variation of bending moments at the rafter and the heated wall of the 10m frame.

ii) Plastic hinging at base of the wall before rafter

In the analysis cases 3), 4) and 8), a plastic hinge formed at the base of the wall before the other plastic hinges formed at the rafter. In this case, the thermal bowing of the wall panels caused sufficient curvature and moment to yield the reinforcing steel at the base of the wall, resulting in a plastic hinge.

The graphs on the following pages refer to a frame with wall panels that are 12 metres high and 150mm thick (case 8). When the wall panel is subjected to a fire on one side, differential thermal expansion causes the walls to bow. The thermal bowing of the heated wall, coupled with the P-delta moments generate a bending moment large enough to yield the reinforcing steel at the base. This caused the formation of a plastic hinge at the base of the wall at 24.5 minutes (Figure 9-23). The bending moments at the base of the wall plateaus when the reinforcing steel reaches its yield plateau.

When the plastic hinge formed at the base of the wall, the midspan deflection of the rafter had reached only –0.70 metres, indicating that there is not much rotation at the heated support. However, the vertical deflection of the rafter doubles during the last 2.5 minutes as it approaches the steep phase of the runaway displacement. At this stage, the rafter has rotated significantly at the support and at midspan as plastic hinges have formed there.

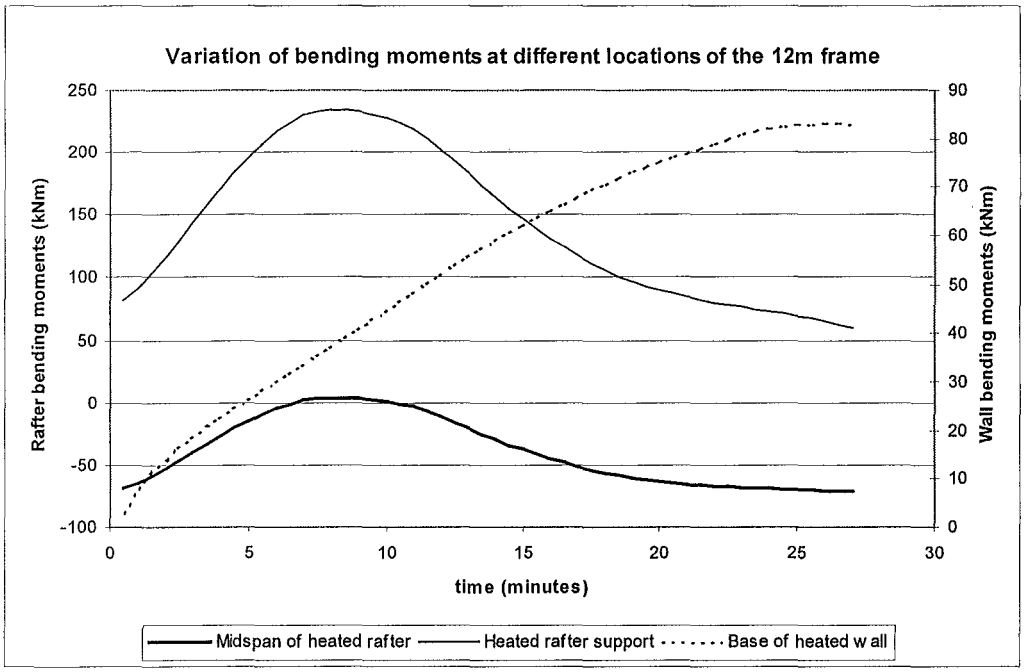

Figure 9-23: Variation of bending moments at the rafter and the heated wall of the 12m frame.

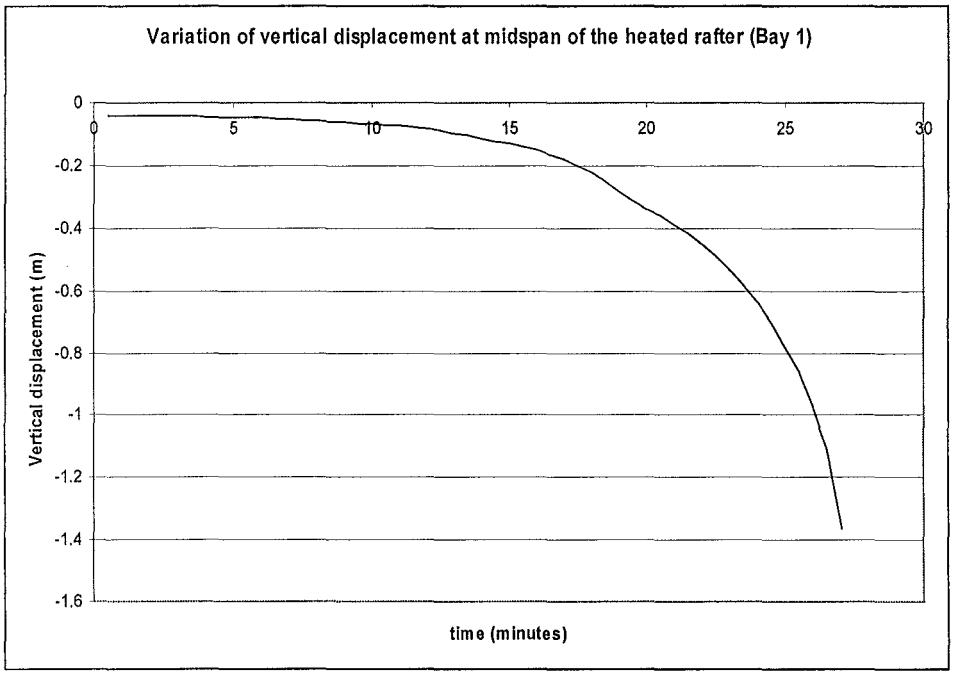

Figure 9-24: Variation of vertical displacement at midspan of the heated rafter in the 12m frame.

Discussion

The analyses of the braced frames with two internal columns have shown that for any of the wall slenderness ratios analysed, the heated wall panels collapsed into the burning building as they are pulled inwards by the collapsing rafter. Buckling of the wall panels was not observed even for very high slenderness ratios as it was prevented by the inward collapse of the wall panels. The wall panels built into a frame with two internal columns can have its slenderness ratio (H_w/t_w) as high as 96, provided sufficient bracing from the roof diaphragm is available during a fire to prevent a sway failure. The steel rafters play a crucial role in producing an acceptable mode of failure because they fail to pull the walls in before buckling failure can occur. Therefore, they should not be fire protected, to ensure that they deflect and collapse into the building, pulling the walls inwards.

9.4.2. Non-sway mode (Frame B)

The analysis conducted for *Frame A* in section 9.4.1 is repeated for *Frame B*, with the same wall slenderness ratios. The loads and boundary applied onto the frame are identical to *Frame A*. The only differences between *Frame A* and *Frame B* are the size of the steel rafter and the number of internal columns supporting the frame.

Results of analyses

Wall dimensions				Collapse times (minutes)
				Mode of collapse
Case no	Thickness (mm)	Height (m)	Slenderness ratio	Inward collapse
13)	125	6	48.0	28.5
14)		8	64.0	28.0
15)		10	80.0	27.5
16)		12	96.0	22.5
17)	150	6	40.0	29.0
18)		8	53.3	28.5
19)		10	66.7	28.0
20)		12	80.0	28.0
21)	175	6	34.3	29.5
22)		8	45.7	29.0
23)		10	57.1	28.5
24)		12	68.6	28.0

Table 9-6:Times and modes of collapse of frames with walls of different heights (Frame B).

The results of the analyses for *Frame B* indicate all the frames collapsed inwards and none of the walls in the frames failed by buckling, despite the higher axial load from the larger beam spans. The vertical axial load imposed at the top of each cantilever wall from the weight of the rafter in *Frame B* is approximately 47 percent higher than *Frame A*. The analyses showed that the failure of the frames occurred at very similar times (Figure 9-25). Likewise for *Frame A,* some of the frames formed plastic hinges at the base of the walls before collapse occurred (cases 14, 15, 16, 19 and 20). The other frames collapsed as a result of runaway vertical displacement when plastic hinges formed in the rafter. The runaway displacement of the rafter

pulled the wall panel inwards very rapidly, yielding the reinforcing steel at the base of the wall. When the reinforcing steel at the base of the wall yielded, the wall lost its rotational restraint at the base and collapsed inwards.

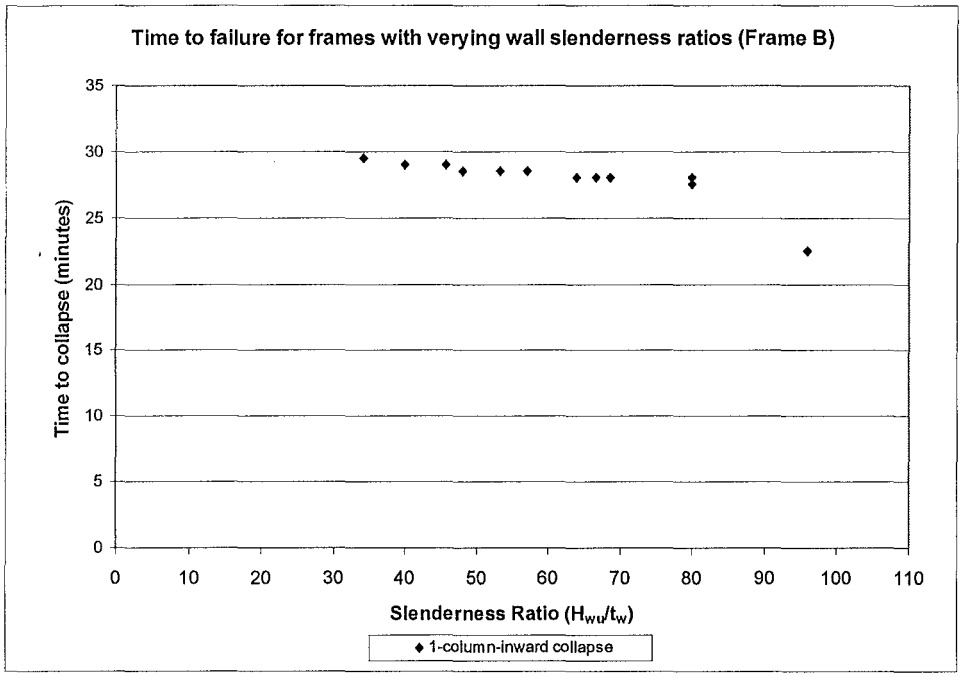

Figure 9-25: Times to failure for different slenderness ratios in the fully braced frame (Frame B)

The diagram on the following page depicts the sequence of inward collapse of a braced *Frame B* configuration when one bay of the frame is subjected to the ISO fire. The frame has concrete cantilever wall panels that are 10 metres high and 150mm thick (case 19).

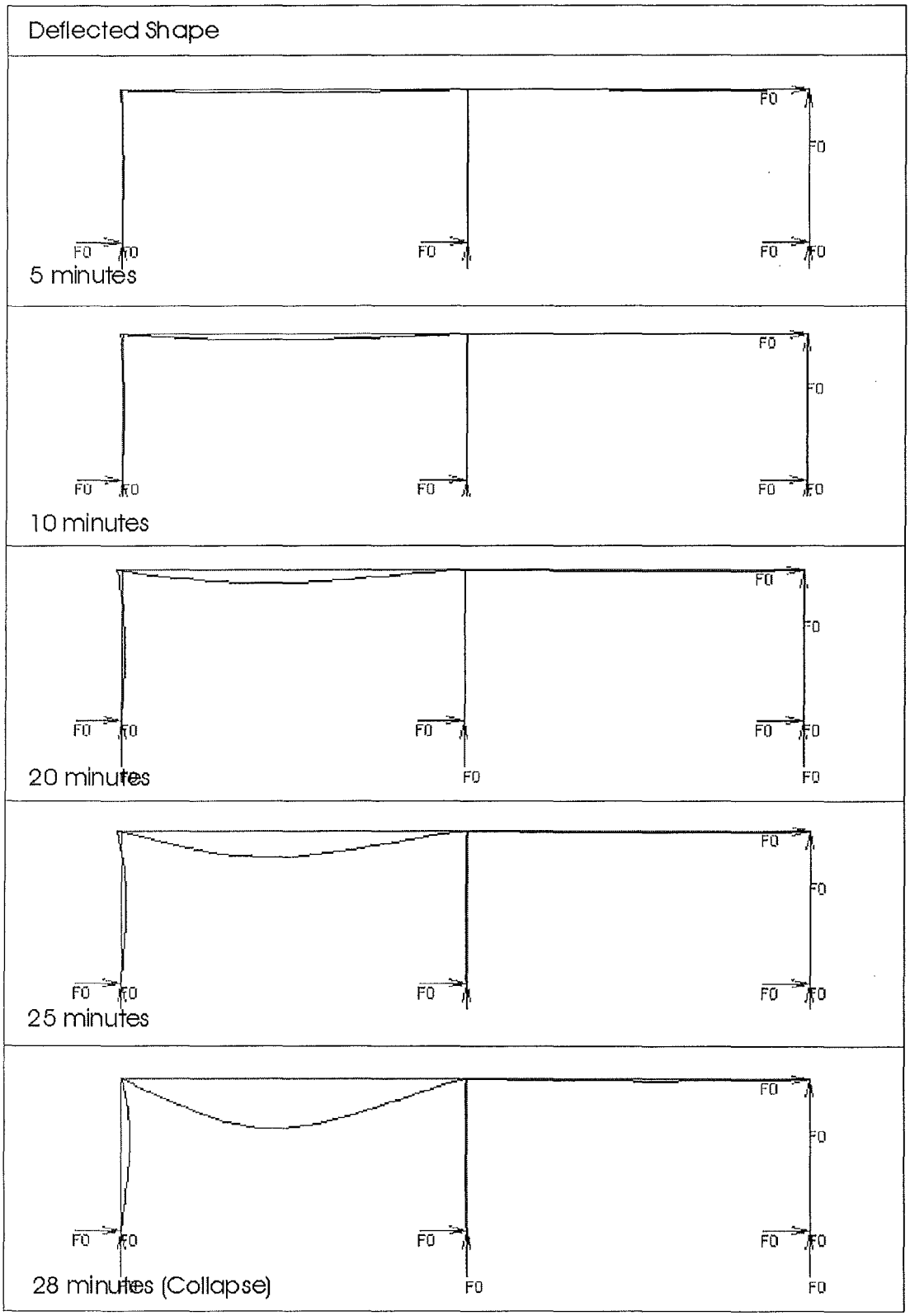

Figure 9-26: Sequence of deformation of a horizontally braced frame (Frame B) with 10m high and 150mm thick walls. *Note: Deflections are magnified by 2.

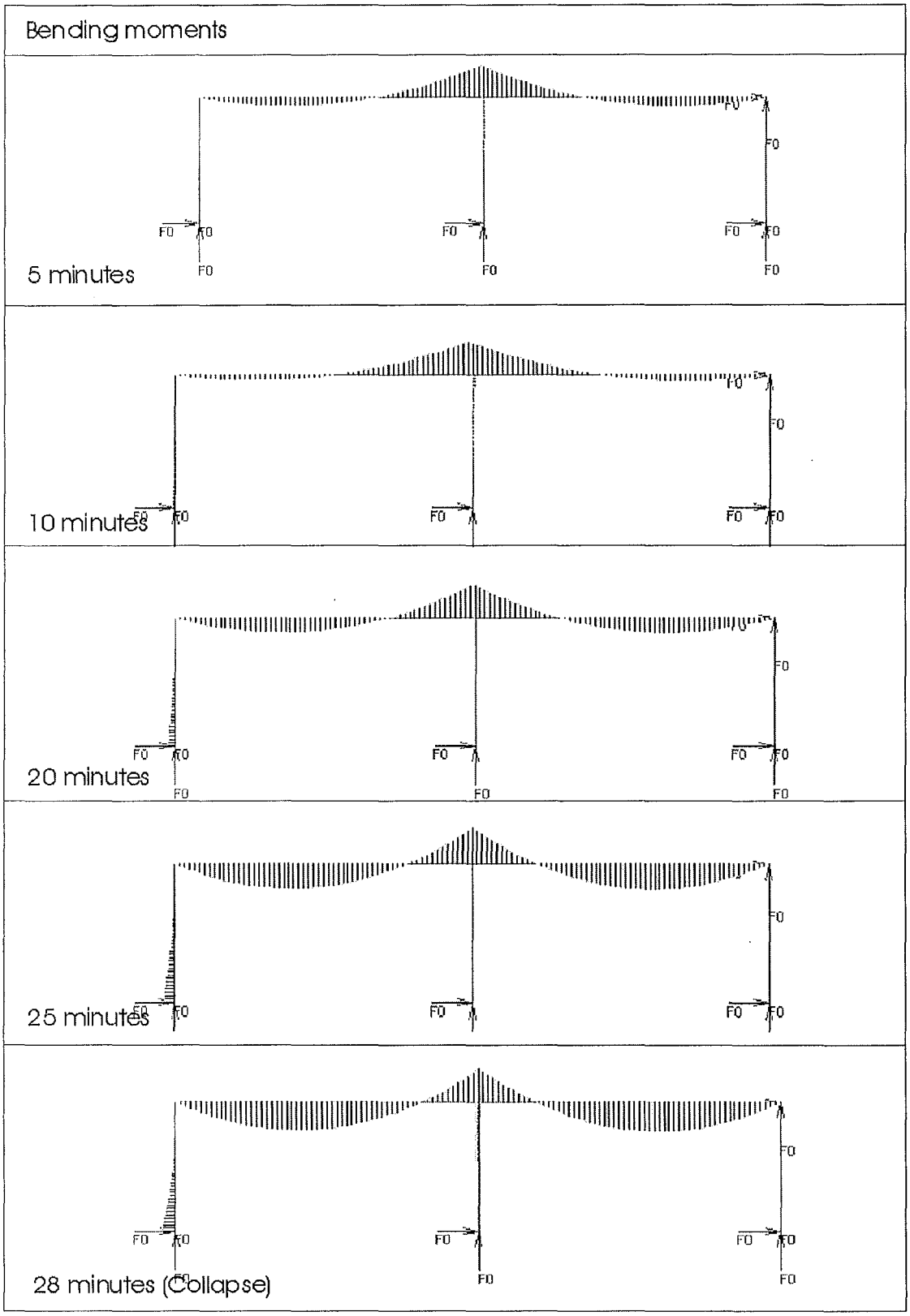

Figure 9-27: Variation of bending moments corresponding to the deformation of the 10m braced frame

Behaviour of the fully braced frame (*Frame B)*

Figure 9-27 shows the deformation of a typical braced frame. Sway of the frame is prevented by the roof diaphragm, simulated by a pinned support at the top right corner of the frame. Some horizontal displacement occurs at the top of the heated wall due to thermal expansion of the steel rafter. While the heated wall deflects outwards, the heated rafter progressively sags as the elastic modulus of steel decreases with increasing temperature. During the initial stages of the fire, the rafter loses its positive flexural strength more than its negative flexural strength; hence, the moments in the rafter are redistributed and resisted by the negative flexural strength at the supports. The bending moments redistribute back to the midspan from the supports during the advanced stages of the fire when the negative flexural strength is also depleted.

In this particular case (case 19), a plastic hinge formed at the base of the wall before forming at the rafters. The thermal bowing of the heated wall and P-delta effects generate bending moments at the base of the wall that are large enough to yield the reinforcing steel at the base. This plastic hinge at the base of the wall does not cause the frame to collapse because there are insufficient plastic hinges to form a mechanism in the structure. The loss of strength in the rafter caused plastic hinges to form at the supports and midspan, leading to runaway failure. The two plastic hinges in the rafter produce a mechanism in the structure, causing downward collapse, pulling the wall panel inwards.

Discussion

The analyses of the braced frames with single internal columns have shown that they behave very similarly to the frames with two internal columns. Despite the higher vertical axial loads imposed on the top of the cantilever walls, the wall panels did not buckle even for very high slenderness ratios. Buckling failure was prevented by the collapse of the steel rafter, which dragged the walls inwards. Therefore, if the steel roof sheeting is able to provide sufficient diaphragm action to prevent sway during a fire, the frame will not collapse outwards and the wall panels will not buckle.

9.4.3. Discussion (Braced frames)

From the results of *Frame A* and *Frame B*, the inward collapses of the frames are very dependent on the strength and stiffness of the rafter. Regardless whether a plastic hinge has formed at the base of the wall, the frames will only collapse when the rafter has lost sufficient strength to form plastic hinges and cause runaway displacement.

- If a plastic hinge forms at the base of the wall panel before forming in the rafter, the frame will not collapse until sufficient plastic hinges have formed in rafter, producing a mechanism in the structure.
- If two plastic hinges have formed in the steel rafter (before a hinge forms at the base of the wall), runaway deflection of the rafter will pull the wall panel inwards. This will eventually yield the reinforcement at the base of the wall panel and form the third plastic hinge necessary for a mechanism in the structure.
- For the wall slenderness ratios analysed, buckling of the wall panels was not observed. Some of these walls may have been close to a buckling failure, but the steel rafter collapsed and pulled the walls inwards before a buckling failure could occur.

The results for *Frame A* and *B* in the non-sway mode showed that for any of the wall slenderness ratios shown above, the frame will collapse inwards. However, wall slenderness ratios should not be constructed higher than the maximum slenderness that was analysed (H_{wu}/t_w=96), as it would increase the likelihood of buckling of the wall panels. Higher axial loads would also increase the probability of buckling.

9.4.4. Collapse mechanism of frame

The inward collapse of the steel frame is analogous to a propped cantilever beam shown in Figure 9-28. The beam cantilevers from the fixed support on the right and is vertically and horizontally restrained on the left support. The fixed support on the right of the beam is equivalent to the beam supported on the column. The rotational restraint provided at the base of the wall is analogous to a horizontal spring as it restricts the amount of horizontal movement at the beam support.

When the beam is subjected to a fire from below, the beam will progressively lose its strength and stiffness. As the beam deflects downwards, it imposes a horizontal force which progressively extends the spring. When the strength of the beam is sufficiently depleted, two plastic hinges will form at the locations shown in Figure 9-28 (2). This causes a mechanism to form in the beam. The beam does not collapse immediately as it is restrained by the spring. However, it will sag very rapidly, imposing a large force very rapidly onto the spring. This causes the spring to eventually yield (equivalent to a plastic hinge forming at the base of the cantilever wall), causing the lost of horizontal restraint and downward collapse.

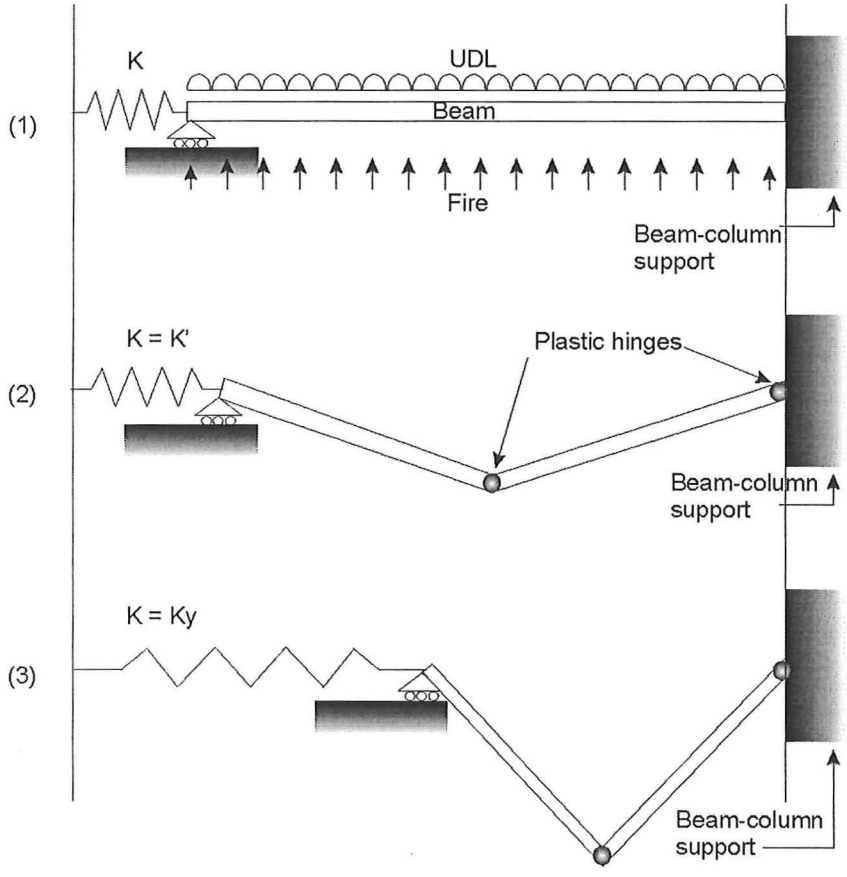

Figure 9-28: Inward collapse of the frame.

9.4.5. Prediction of wall buckling with the Euler buckling formula

From the analyses of *Frames A* and *Frames B*, the Euler buckling equation could not be appropriately applied to determine the buckling loads of the cantilever walls as it produced results inconsistent to those obtained from SAFIR.

The critical buckling load of a column can be determined from (Roark and Young, 1975):

$$(pa)' = K\frac{\pi^2(EI)_{eff}}{H_{wu}^{\ 2}}$$

Where: K accounts for the different end conditions and levels of axial load relative to its self-weight.

	both ends pinned
P/*pa*	**K**
0	1.88
0.25	1.3
0.5	0.89
1	0.66

Where: P = Axial load at the top of the wall

pa = self-weight of the wall

Table 9-7: K coefficients for different axial load levels for pinned-ended columns (Roark and Young, 1975)

The Euler buckling equation was difficult to use for frame analysis as it would under-predict the critical buckling load of the wall, concluding that the wall had buckled, when it actually collapsed inwards. Possible reasons for this inconsistency are:

- The K coefficient is applicable for elements that are pinned at both ends and assumes no horizontal movement at the either end. In the frame, the top of the wall is not fully restrained in the horizontal direction and some movement occurs, depending on the stiffness of the frame and thermal expansion of the rafter.
- The plastic hinge formed at the base of the wall is assumed equivalent to a pinned support.
- In order to account for different axial load levels (P/*pa*), K is interpolated linearly, which may cause slight differences in the results.

9.5. Partial restraint

This section describes the behaviour of partially braced *Frames A* and *B* when they are subjected to a fire. The steel roof sheeting is assumed capable of providing only partial horizontal restraint to the frame, modelled by moment resisting beam-column connections. The sway of the frame is resisted by frame action and is limited by the moment resistance of the frame members. The slenderness ratios of the walls that are analysed are shown in Table 9-4.

9.5.1. Partial restraint (*Frame A*)

Results of analyses

Wall dimensions			Collapse times (minutes)	
			Mode of collapse	
Thickness (mm)	Height (m)	Slenderness ratio	Inward collapse	Outward collapse
125	6	48.0	29.0	
	8	64.0	28.2	
	10	80.0		19.5
	12	96.0		11.5
150	6	40.0	30.0	
	8	53.3	29.0	
	10	66.7		25.0
	12	80.0		14.5
175	6	34.3	32.5	
	8	45.7	30.5	
	10	57.1		29.2
	12	68.6		12.5

Table 9-8: Times and modes of collapse of frames with different slenderness ratios.

Table 9-8 summarises the times and modes of collapse of the frames with different wall slenderness ratios. The walls with heights in excess of 8 metres collapsed outwards, irrespective of their thicknesses. There was no buckling of the wall panels and numerical instabilities did not occur.

Behaviour of walls less than 9 metres high

The results show that when the heights of the walls are less than or equal to 8 metres, in partially braced frames, the wall collapsed inwards. The thermal bowing deflections of the shorter walls were insufficient to produce an overturning moment large enough to cause the

frame to collapse outwards. As a result, a different collapse mechanism was produced when sufficient plastic hinges formed in the frame, resulting in inward collapse of the wall panels. This mode of failure is similar to those discussed in 9.4.1 and 9.4.2. The times to collapse are very similar, increasing marginally with increasing wall thickness. The close similarity is because the collapse times are governed by the time the strength of the rafter is depleted to form sufficient plastic hinges, which leads to its runaway deflection. The runaway deflection will lead to a plastic hinge forming at the base of the wall, resulting in a mechanism and collapse of the structure.

Behaviour of walls greater than 9 metres high

The partially braced frames with wall heights of 10 metres and 12 metres collapse outwards, irrespective of their thicknesses. When the walls thickness was increased for the 10 metre walls, it increased the time to failure of the frame because the higher thickness reduces the thermal bowing deflections and overturning moments imposed onto the frame; which resulted in a longer time to collapse. However, the extra thickness became a weight penalty for the 12 metre high wall as it increased the P-delta effects markedly, which shortened the times to collapse.

Compared to the shorter walls, the taller walls experienced larger horizontal deflections at the top, due to thermal bowing effects and larger P-delta effects. The larger deflections would also cause a larger portion of weight from the roof to be carried by the walls, worsening the P-delta effects. The large outward deflections of the walls would prevent the steel rafter from pulling the walls back inwards, making the outward collapse mode inevitable.

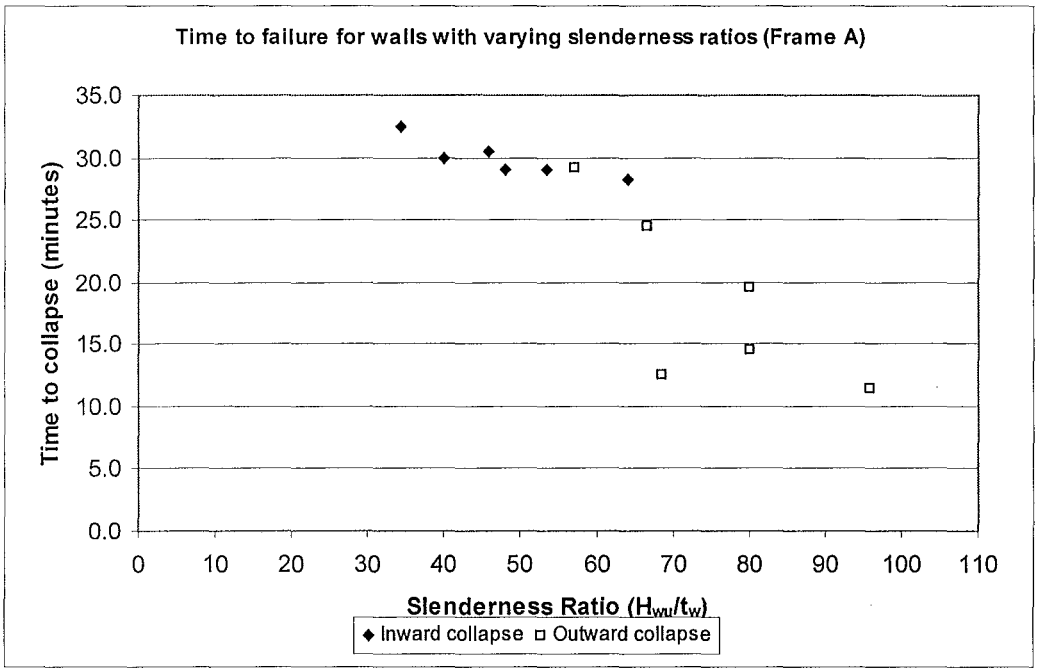

Figure 9-29: Times and modes of collapse of frames with walls of different slenderness ratios.

Figure 9-29 shows the times and modes of collapse of frames with different wall slenderness ratios. The walls with slenderness ratios above 65 collapse outwards with an exception of one case where the slenderness ratio was 57. This was for the case of a 10 metre wall and 175mm thickness. When the slenderness ratios of the walls increase in excess of 65, the times to collapse of the frames reduce. Based on this graph, the times to outward collapse of this type of frame are not only dependent on the slenderness ratio, but on the thicknesses of the walls.

The following pages discuss the two modes of failure in detail. A steel frame with 10 metre concrete cantilever walls will be used to illustrate a typical outward collapse. The inward collapse mode, which features the walls collapsing back into the building, will be illustrated using a steel frame with 6 metre concrete cantilever walls. The thicknesses of the walls in both cases are 150mm, giving slenderness ratios of 66.7 and 40. These two different wall heights illustrate the different possible deformation modes for walls of different slenderness ratios. Therefore, their behaviour will be discussed separately.

i) 10m partially braced frame: Outward collapse

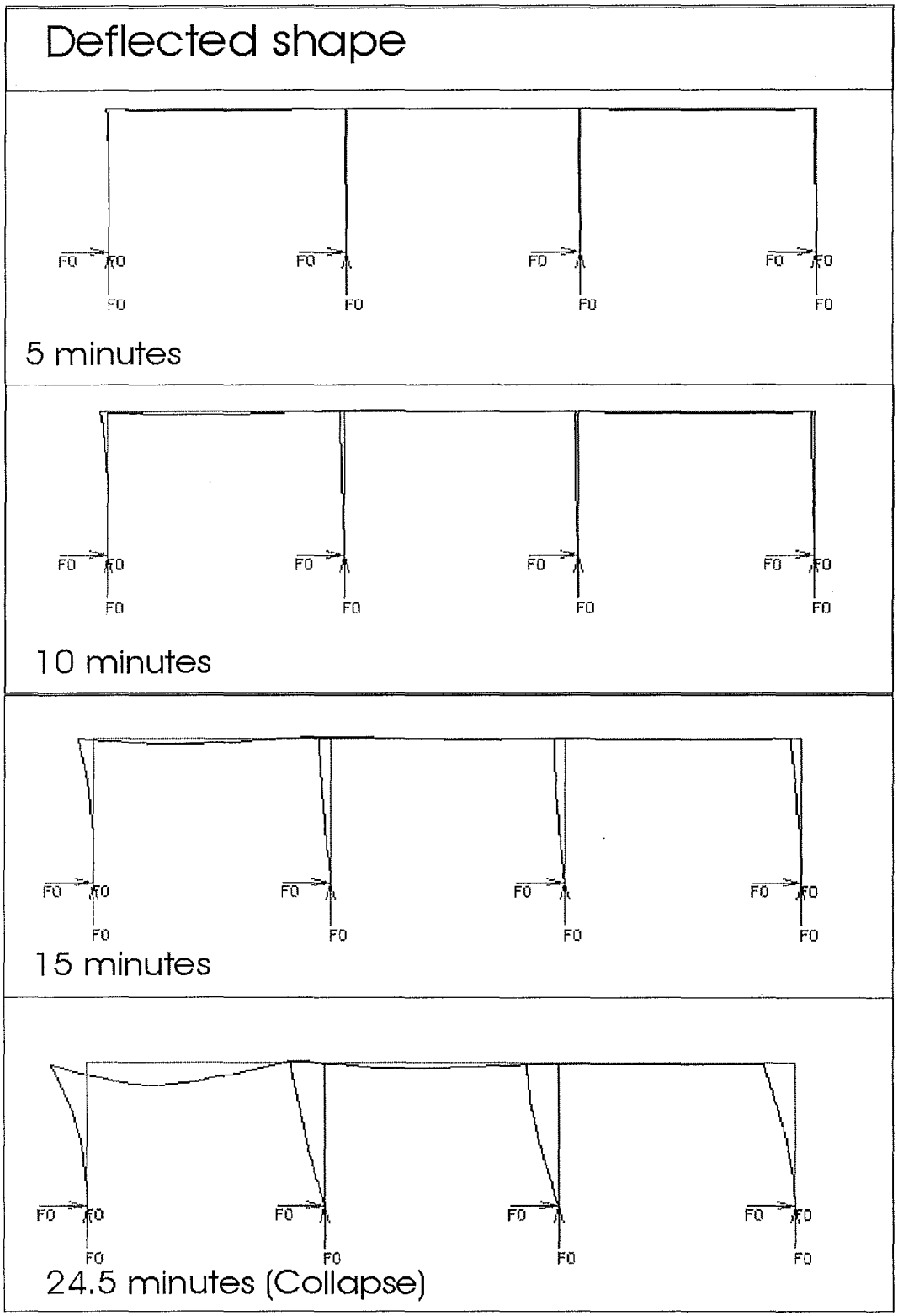

Figure 9-30: Sequence of deformation of partially braced frame with 10m wall. *Note: Deflections are magnified by 2.

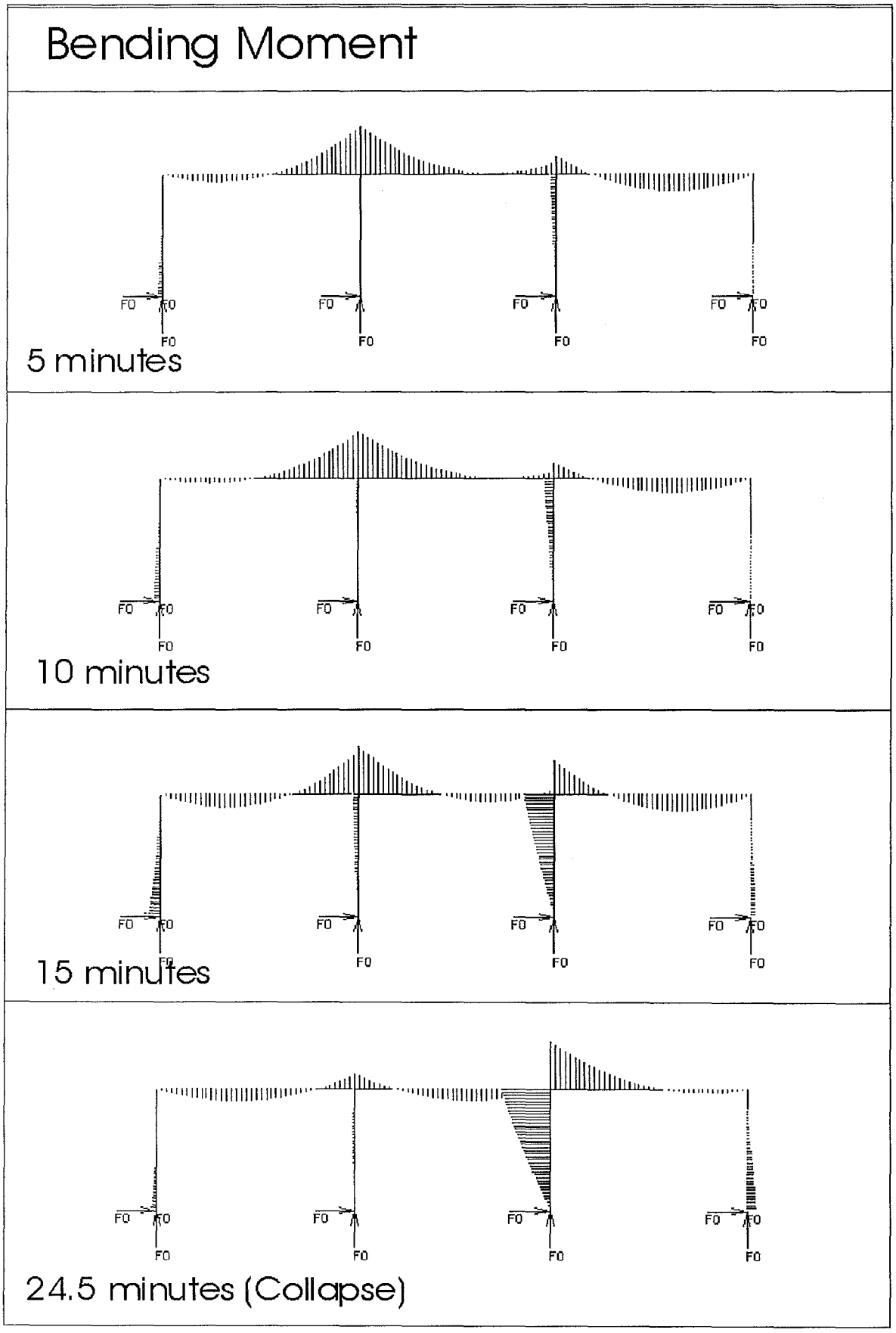

Figure 9-31: Bending moment diagrams corresponding to the deformation of the 10m frame.

Deformation of the partially braced 10m frame (*Frame A*)

Figure 9-30 shows the deformation sequence of a frame with 10 metre walls exposed to the ISO standard fire. As the left side of the frame is exposed to the fire, the wall deflects outwards due to thermal bowing. As the heated wall bows outwards, it pulls the internal columns and the unheated wall which are attached by the steel rafter. The sway of the frame is resisted by frame action and by moment resistance of the wall panels. While the heated wall deflects horizontally due to thermal bowing, the heated rafter in the first and second bay elongates and sags due to the reduction of the elastic modulus of steel and due to the creep strain of steel. The frame sways progressively due to the P-delta effects from the thermal bowing of the heated wall. It collapses at 24.5 minutes when the overturning moment had exceeded the moment resistance of the frame.

Bending Moments

Figure 9-31 shows the variation of bending moments in the frame as the frame deforms. As the steel frame is heated during the initial stages, bending moments at the clear spans redistribute to the supports. The redistribution of the sagging moments from midspan of the rafters to the supports causes the hogging moments at the supports to increase. (In SAFIR, the sign conventions show that sagging moments are represented by negative values, and vice versa for the hogging moments). The redistribution of moments to the support allow the negative bending strength of the rafter to be utilised to resist the bending moments in the rafter. However, the yield strength of the steel is depleted during the advanced stages of the fire, thus reducing the flexural strength of the beam at the support. This causes the moments to redistribute back to the midspan, resulting in the bending moments being resisted by positive bending.

As the frame deforms outwards, the moments in the unheated internal column increases due to the increasing horizontal reaction at the base of the column as the frame tries to resist the sway due to thermal bowing. The moments in the heated column are much smaller than the unheated column because the flexural strength had been depleted due to the high temperatures. Most of the sway resistance is provided by frame action from the unheated column (Figure 9-31).

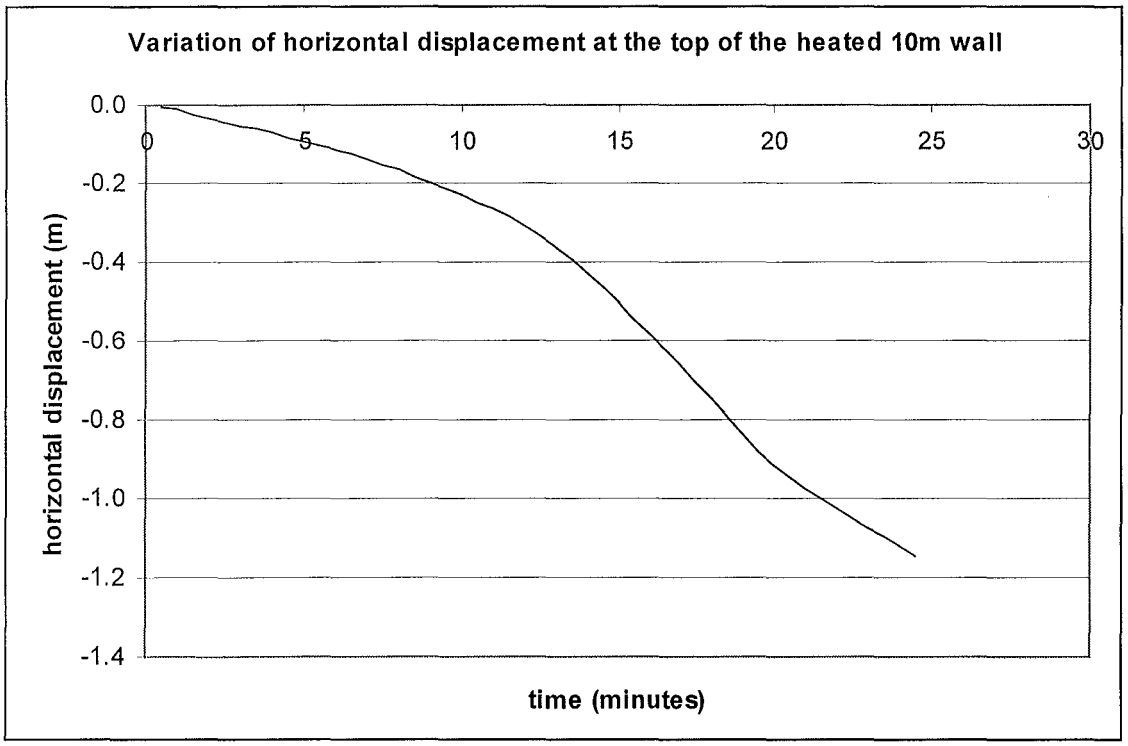

Figure 9-32: Variation of horizontal displacement at the top of the heated wall.

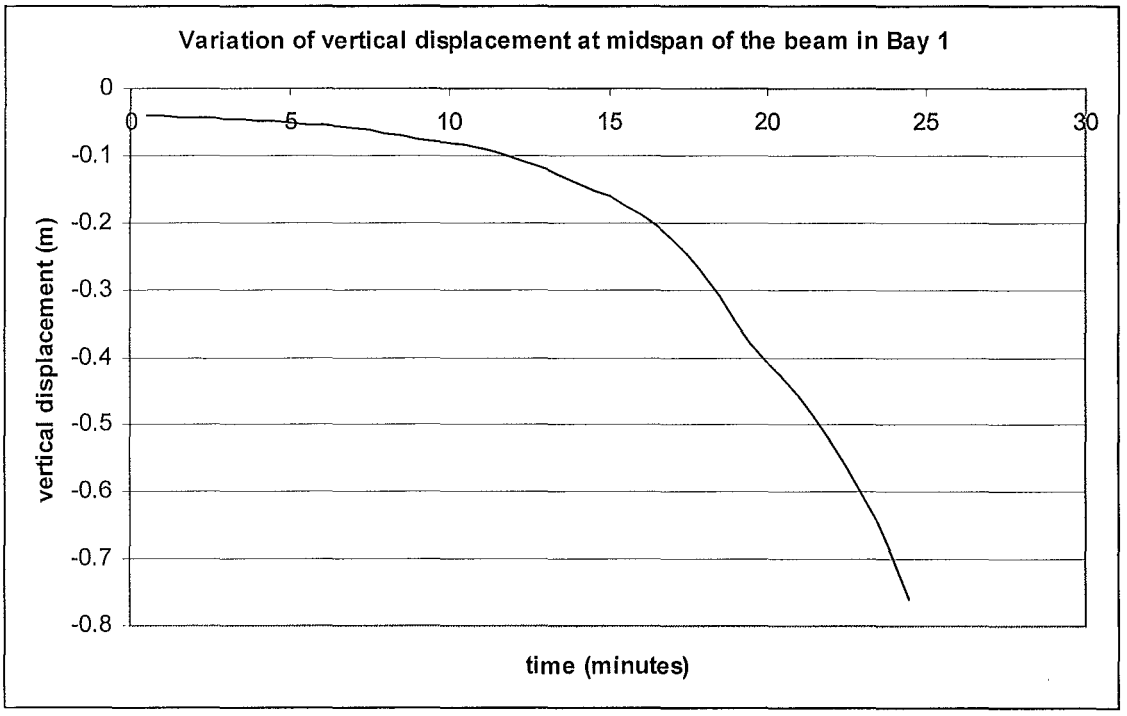

Figure 9-33: Vertical displacement at midspan of the steel rafter in Bay 1.

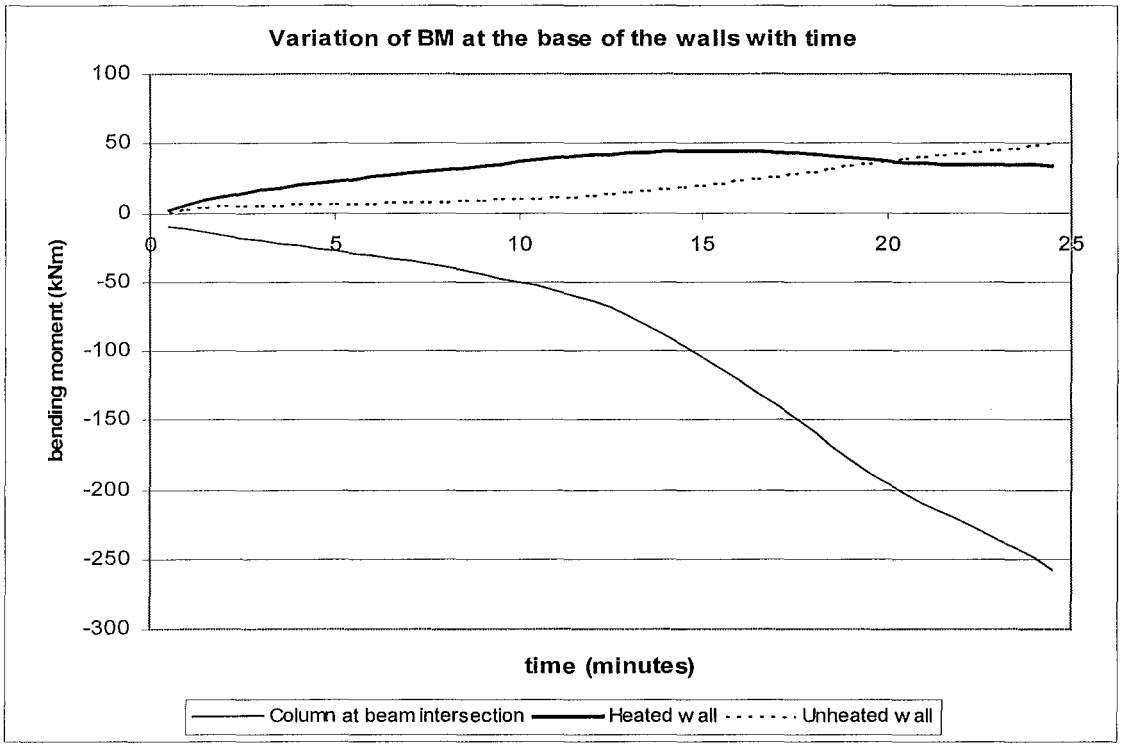

Figure 9-34: Variation of bending moments at the beam-column joint and the base of the cantilever walls.

Figure 9-32 shows the variation of horizontal displacement at the top of the heated wall as it is progressively heated. The graph shows a bilinear trend displacement trend where the rate of displacement of the wall increases after approximately 12.5 minutes. At the last five minutes, between 20 minutes to 24.5 minutes, the displacement rate decreases slightly, possibly due to the increasing deformation of the sagging rafter which reduces the rate of outward collapse.

Figure 9-33 shows the variation of vertical displacement at midspan of the steel rafter as it is subjected to the ISO fire. The rafter deflects downwards in an exponential fashion due to the reduction of the stiffness of the steel rafter and also due to the runaway creep strain of steel at high temperatures.

Figure 9-34 shows the variation of bending moments at the base of the walls and at the beam-column joint. The beam-column joint is a rigid moment resisting connection at the top of the column member where it meets the rafter. The rigid beam-column joint enables the sway of the frame to be resisted by frame action. The bending moments at the base of the heated wall progressively increase when the wall bows outwards and plateaus at 44kNm (Note: the plastic moment of the 150mm thick wall is approximately 80kNm). As the bending moment plateaus at the base of the heated wall, the moments in unheated wall and the unheated column-rafter connection increase at a higher rate. This is possibly due to the moment resistance being

transferred to the cooler elements which have higher stiffness. Figure 9-31 and Figure 9-34 show that most of the moment resistance is provided by the cooler steel frame as there is a large moment in the cooler beam-column joint. When the column reaches its plastic moment, a plastic hinge forms at the top of the column and the frame loses its moment resistance. This causes the mode of moment resistance to be transferred to the cooler wall which is unable to withstand such a large moment, resulting in a outward collapse of the entire frame.

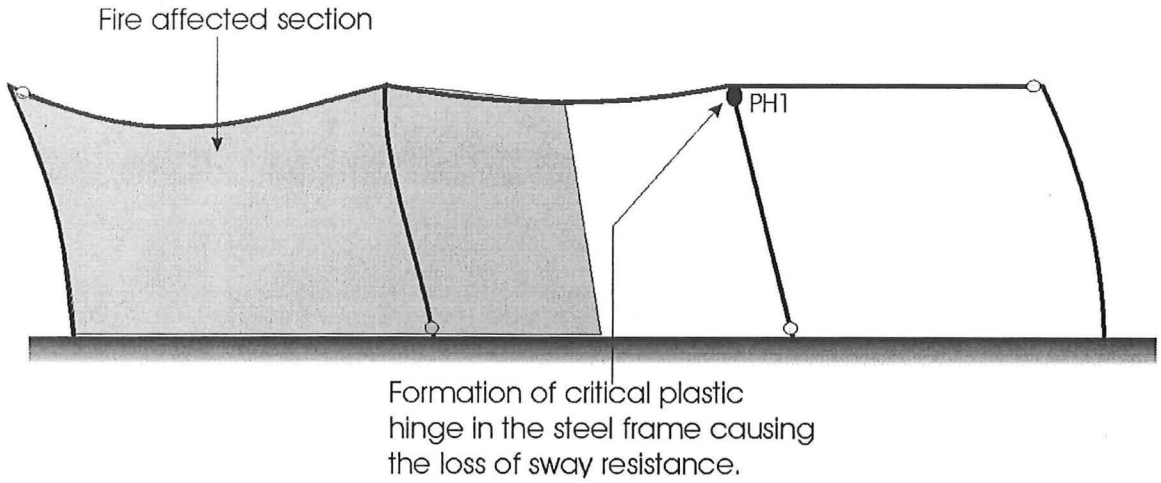

Figure 9-35: Collapse of frame due to formation of plastic hinge in the steel column.

ii) 6m partially braced frame: Inward collapse

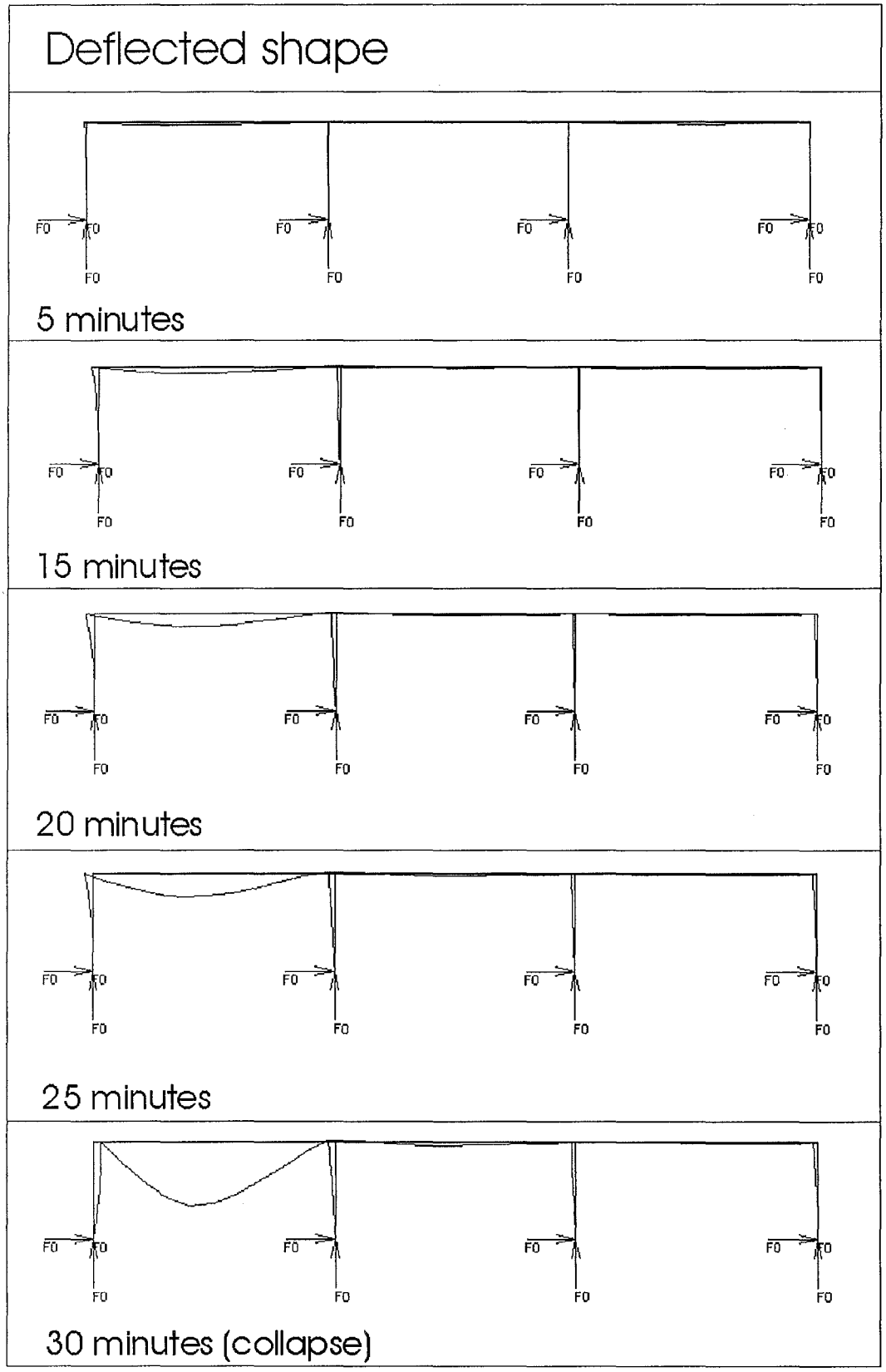

Figure 9-36: Sequence of deformation of partially braced frame with 6m wall. *Note: Deflections are magnified by 2.

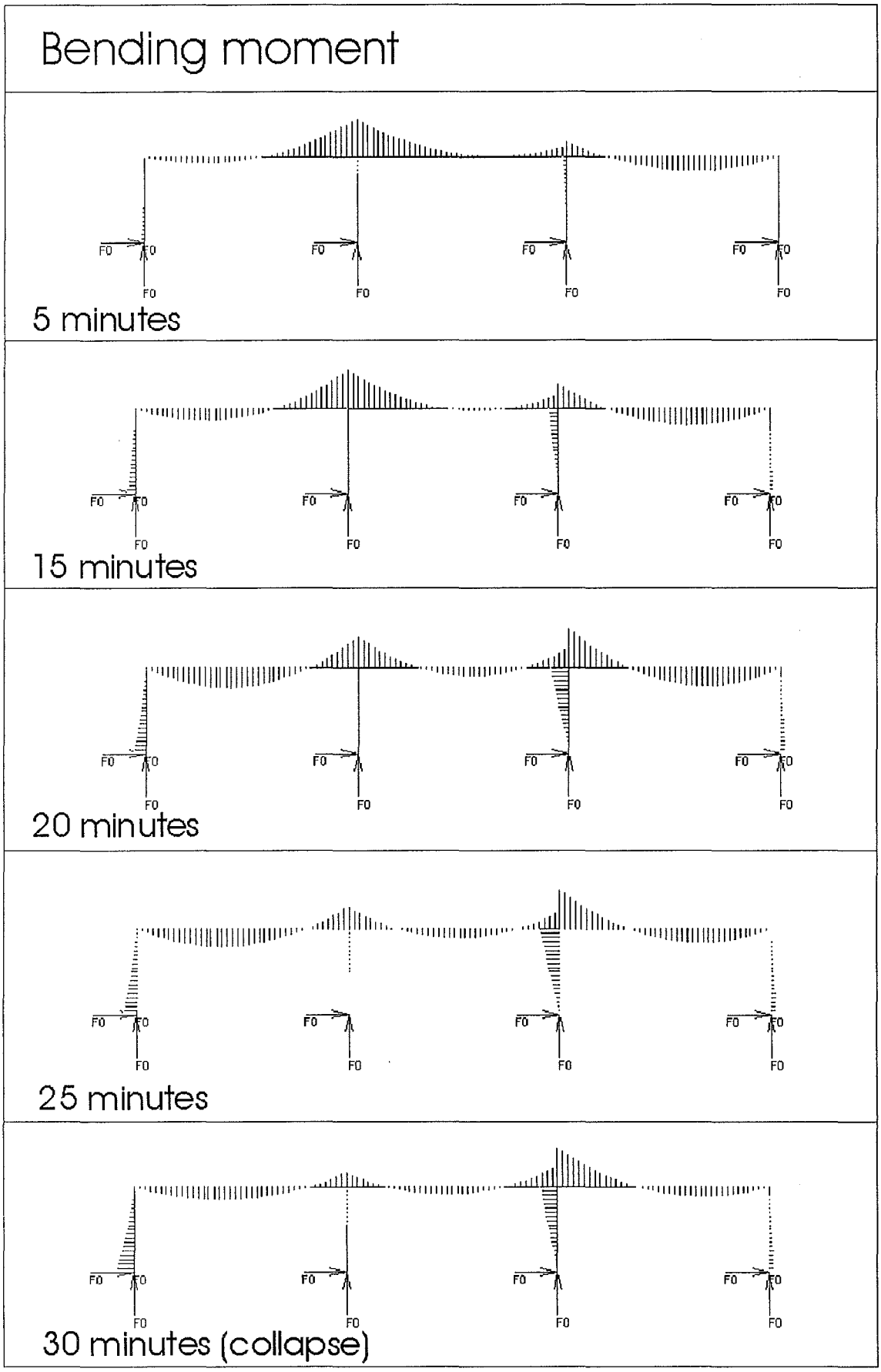

Figure 9-37: Bending moments corresponding to the deformation of the 6m frame.

Behaviour of the partially braced 6m frame

Figure 9-36 shows a typical inward collapse of a frame. When the frame is exposed to the fire, the wall bows outwards progressively due to thermal bowing pulling the rest of the frame along. At the same time, the steel rafter sags due to the thermal effects on the stiffness of the rafter. The positive bending moments at midspan of the rafter are redistributed to the support allowing the negative flexural strength of the beam at the support to be utilised. This is shown clearly in the first frame of Figure 9-37 and in Figure 9-38. When the yield strength of the steel rafter starts to decrease due to thermal effects, the negative bending moments at the heated support decrease as the negative flexural strength decreases, causing the moments from the support to redistribute back to the clear spans of the rafter.

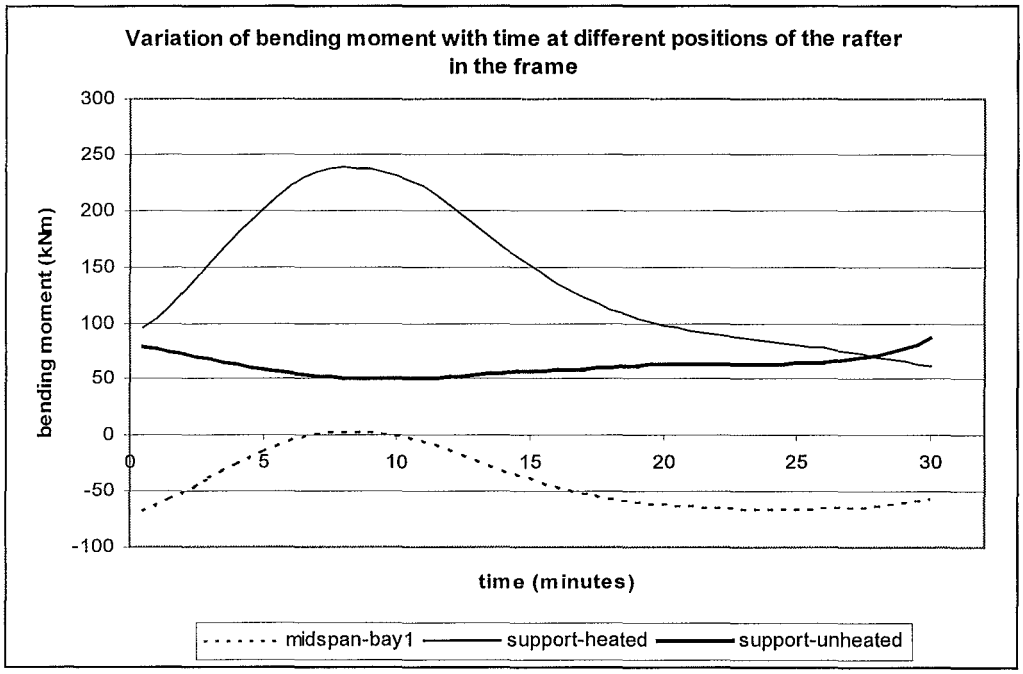

Figure 9-38: Variation of bending moments at different positions on the steel rafter.

When sufficient plastic hinges have formed in the rafter, it collapses inwards, pulling the wall panels inwards. This imposes a very rapid moment increment at the base of the wall, causing the steel to yield rapidly and forming a plastic hinge (Figure 9-41). When a plastic hinge forms at the base of the heated wall, the rotational restraint is lost and a mechanism forms in the structure. The collapse of the steel rafter prevents the outward collapse onto the adjacent property and increases the fire separating distance.

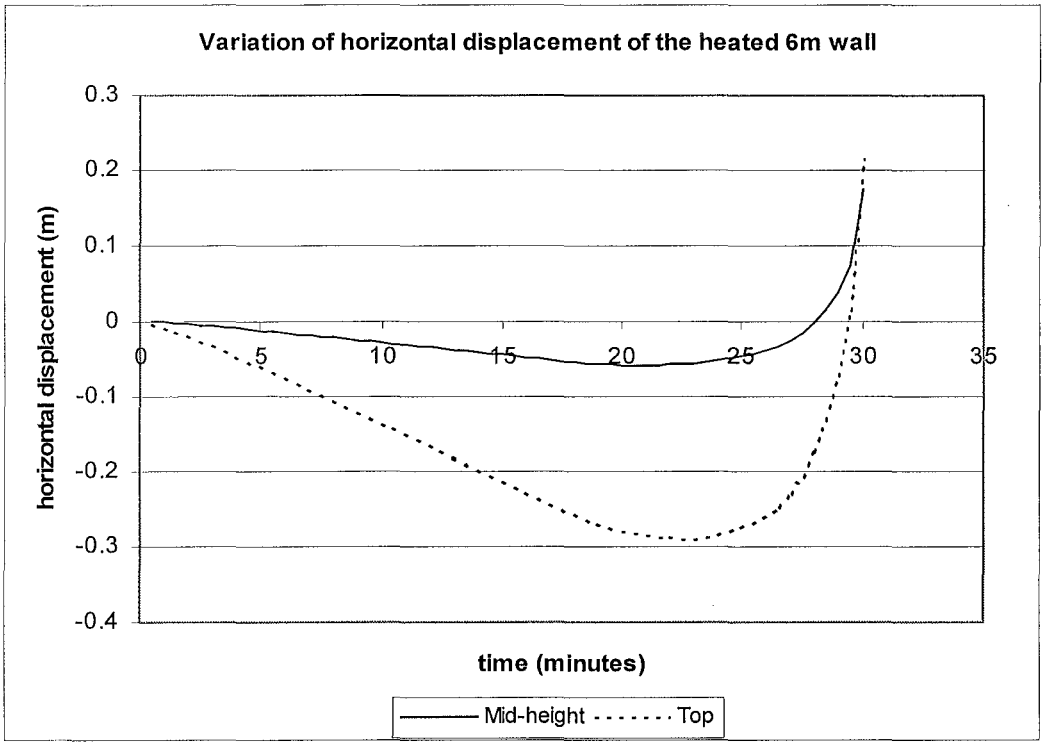

Figure 9-39: Variation of horizontal displacement at the top of the heated wall and the heated column for the 6m frame.

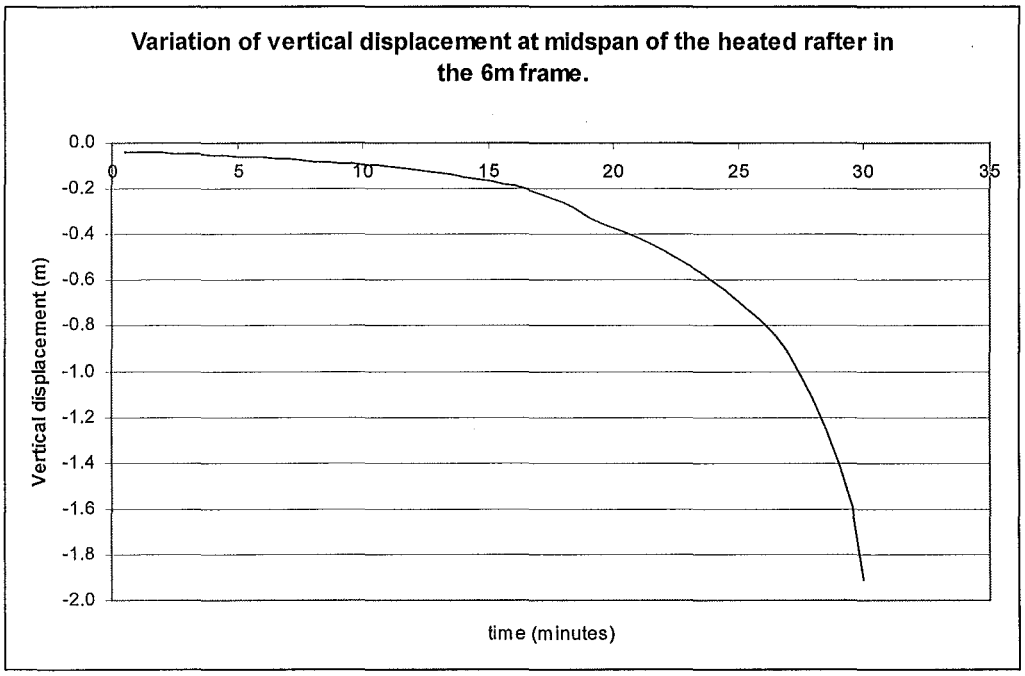

Figure 9-40: Variation of vertical displacement at midspan of the heated rafter in the 6m frame.

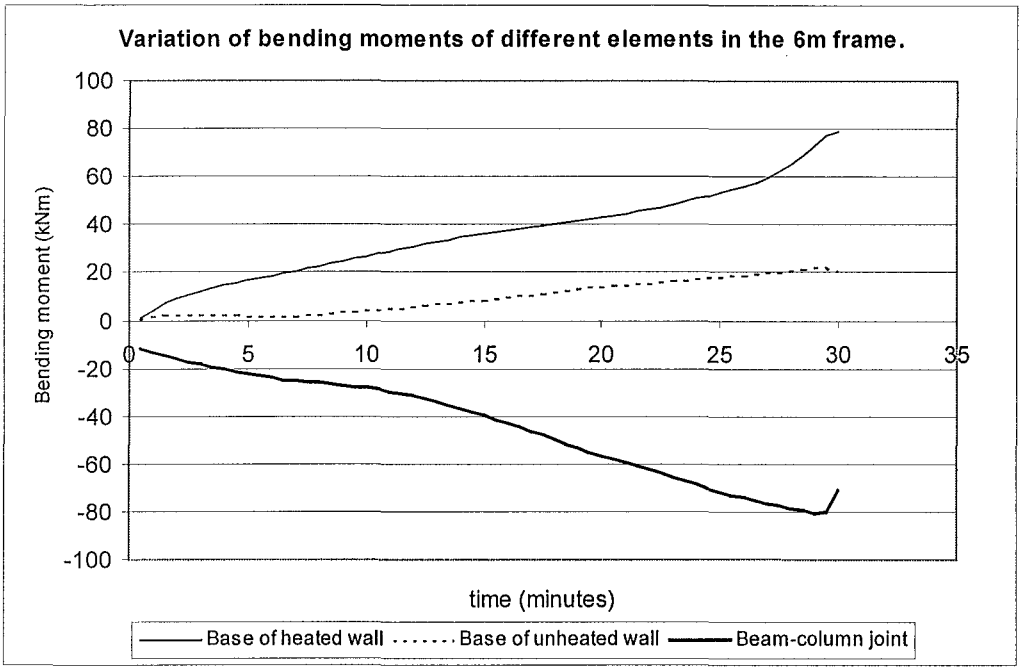

Figure 9-41: Variation of bending moments for different elements in the 6m frame.

Figure 9-39 shows the evolution of horizontal displacement at mid-height and the top of the heated wall. As the wall is progressively heated, it deflects outwards in a linear trend until approximately 20 minutes when it levels off. Between 25 minutes and 30 minutes, the wall shows a drastic change in the deflection trend when it deflects inwards. This is a result of the rapid collapse of the steel rafter which pulls the wall panel inwards. The vertical deflection at midspan of the heated rafter is significantly larger for inward collapse (Figure 9-40) compared with the outward collapse mode (Figure 9-33).

Variation of rafter depth

Further analysis was conducted by increasing the size of the steel rafter *Frame A* from an IPE360 to an IPE450 section. The purpose of this was to investigate the effect of having a stronger rafter on the collapse time of the frame. This was only conducted for walls with 150mm thicknesses with heights ranging from 6 metres to 12 metres.

	IPE360	**IPE450**
Depth (mm)	360	450
Plastic modulus(mm^3)	1.019×10^6	1.702×10^6
Second moment of area (mm^4)	162×10^6	337.4×10^6

Table 9-9: Comparison of section properties of beams used in the analysis.

Wall dimensions Thickness = 150mm		Collapse times (minutes) Mode of collapse	
Height (m)	Slenderness ratio	Inward collapse	Outward collapse
6	40.0	41.5	
8	53.3		32.5
10	66.7		25.0
12	80.0		15.5

Table 9-10: Times and modes of collapse of frames with 150mm thick walls and IPE450 beam.

The results show that when the size of the rafter is increased, the time to collapse of the 6 metre frame increased from 30.0 minutes to 41.5 minutes. The 8 metre wall (slenderness ratio of 53.3) managed to survive the fire marginally longer with the IPE450 beam but it collapsed outwards. In this case, the larger rafter had a lower section factor (Heated perimeter to cross sectional area) and suffered less vertical deflections as it is significantly stiffer. Consequently, the beam retained its load capacity for a longer time, allowing the frame to collapse outward as a result of the sway induced by thermal bowing of the wall. The frames with 10 and 12 metre walls collapsed outwards and did not show any significant difference in the times to collapse.

From Table 9-10, the times to inward collapse of the frame depend on the strength and stiffness of the rafter. If the rafter possesses sufficient strength and stiffness, a sway mode would occur, as the rafters would not have enough time to sag sufficiently to pull the heated walls inwards.

Discussion

The analyses of the partially braced frames in the *Frame* A configuration have shown that the walls with heights in excess of 9 metres cause the frames to collapse outwards. The outward collapses of these walls are irrespective of the wall thicknesses analysed. The analyses conducted have assumed that the stiffness of the steel roof sheeting in a fire is equivalent to the stiffness provided by frame action in the model. The yielding at the top of the steel column is equivalent to losing the diaphragm action in a real frame.

9.5.2. Partial restraint (*Frame B*)

The analysis conducted for *Frame A* in section 9.5.1 is repeated for *Frame B* which features the steel frame support on only one internal column. The internal column is not exposed to the fire, therefore its strength and stiffness do not decrease with increasing time. The single beam column joint is the primary moment resisting component of the frame. The frames are analysed for walls with thicknesses and heights shown in Table 9-4. The structural analysis of the frame is based on the model shown in Figure 9-5.

Results of analyses

Wall dimensions			Collapse times (minutes)	
			Mode of collapse	
Thickness (mm)	Height (m)	Slenderness ratio	Inward collapse	Outward collapse
125	6	48.0	29.0	
	8	64.0	28.5	
	10	80.0		15.0
	12	96.0		1*
150	6	40.0	29.5	
	8	53.3	29.5	
	10	66.7		25.0
	12	80.0		1*
175	6	34.3	30.0	
	8	45.7	29.5	
	10	57.1	29.5	
	12	68.6		3*

Table 9-11: Times and modes of collapse of frames with different slenderness ratios.

*Note: These short times to failure are believed to be due to numerical problems and not the actual times that the structure collapses.

Table 9-11 shows the times and modes of failure of the frames with walls of different heights and slenderness ratios. The walls with heights in excess of 8 metres collapsed outwards while inward collapse occurred for walls with heights equal to or shorter than 8 metres. These different modes of failure occurred irrespective of the wall thicknesses used in the analyses shown above.

The walls with heights of 12 metres failed at very early stages of the fire. This is believed not to be the true structural failure but of a numerical nature. The numerical failure is due to the

highly unstable structure which results when small horizontal deflections form in the structure. Therefore, convergence to a solution is difficult, as numerically instabilities occur very rapidly. Even though measures were taken to try to obtain a solution, the programme was unable to converge to a solution when small amounts of sway occurred in the structure. Apart from the 12 metre high frames, the results of the other frames are very similar to those in *Frame A*. The outward collapse of the frames occurred due to plastic hinges forming at the top of the column, causing the loss of sway resistance by frame action. The inward collapses of the shorter frames were due to the formation of plastic hinges in the rafter, followed by hinges at the base of the wall panels. This causes the formation of a mechanism in the structure and eventual collapse. Buckling failure of the wall panels was not observed in the analyses despite the higher axial loads on the wall panels.

The times to outward collapse of the 10 metre frames increase proportionately with the thicknesses of the walls. This is due to the higher stiffness of the thicker walls which reduces the thermal bowing deflections and the overturning moments due to P-delta effects. While increasing the wall thicknesses can reduce the deflections, the height of the wall has a significant contribution to the behaviour of the wall as shown in section 9.4.

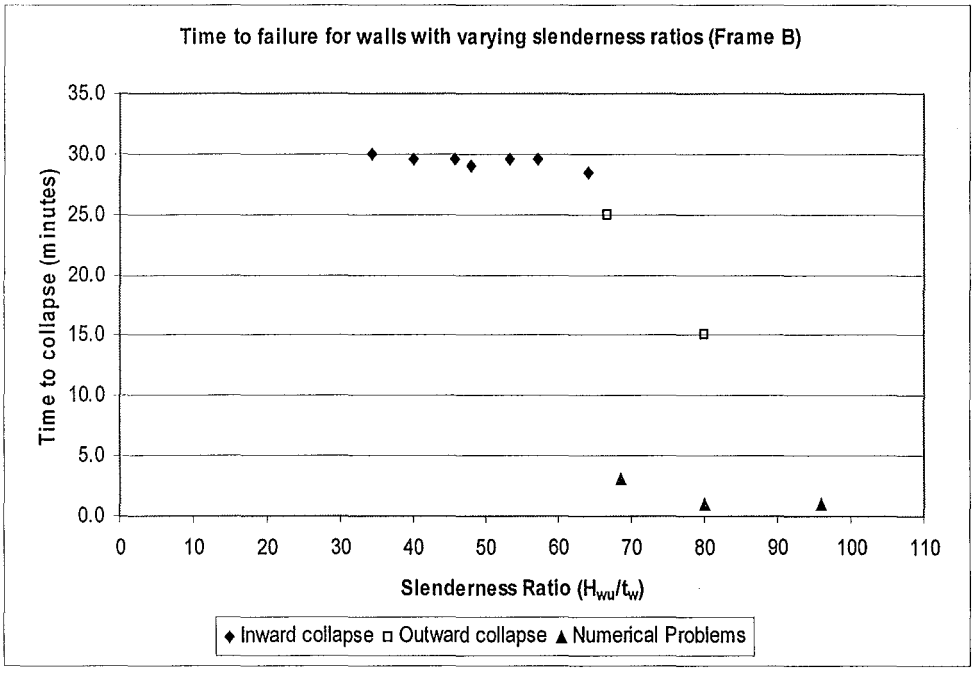

Figure 9-42: Times and modes of failure of frames with different wall slenderness ratios.

Figure 9-42 shows that frames with wall slenderness ratios in excess of 65 collapsed outwards. Beyond this slenderness ratio, the times to collapse of the frame decrease with increasing slenderness. Frames with wall slenderness ratios below 65 collapse inwards at a time that is dependent on the formation of sufficient plastic hinges to form a mechanism in the structure. These results obtained for *Frame B* are similar to the results obtained for *Frame A.*

The following section describes in detail, the two modes of failure for *Frame B.* The outward collapse will be described using a 10 metre high frame while the inward collapse will be described with a 6 metre high frame. The thicknesses of the walls in the frames in this discussion are 150mm.

i) 10m partially braced frame: Outward collapse

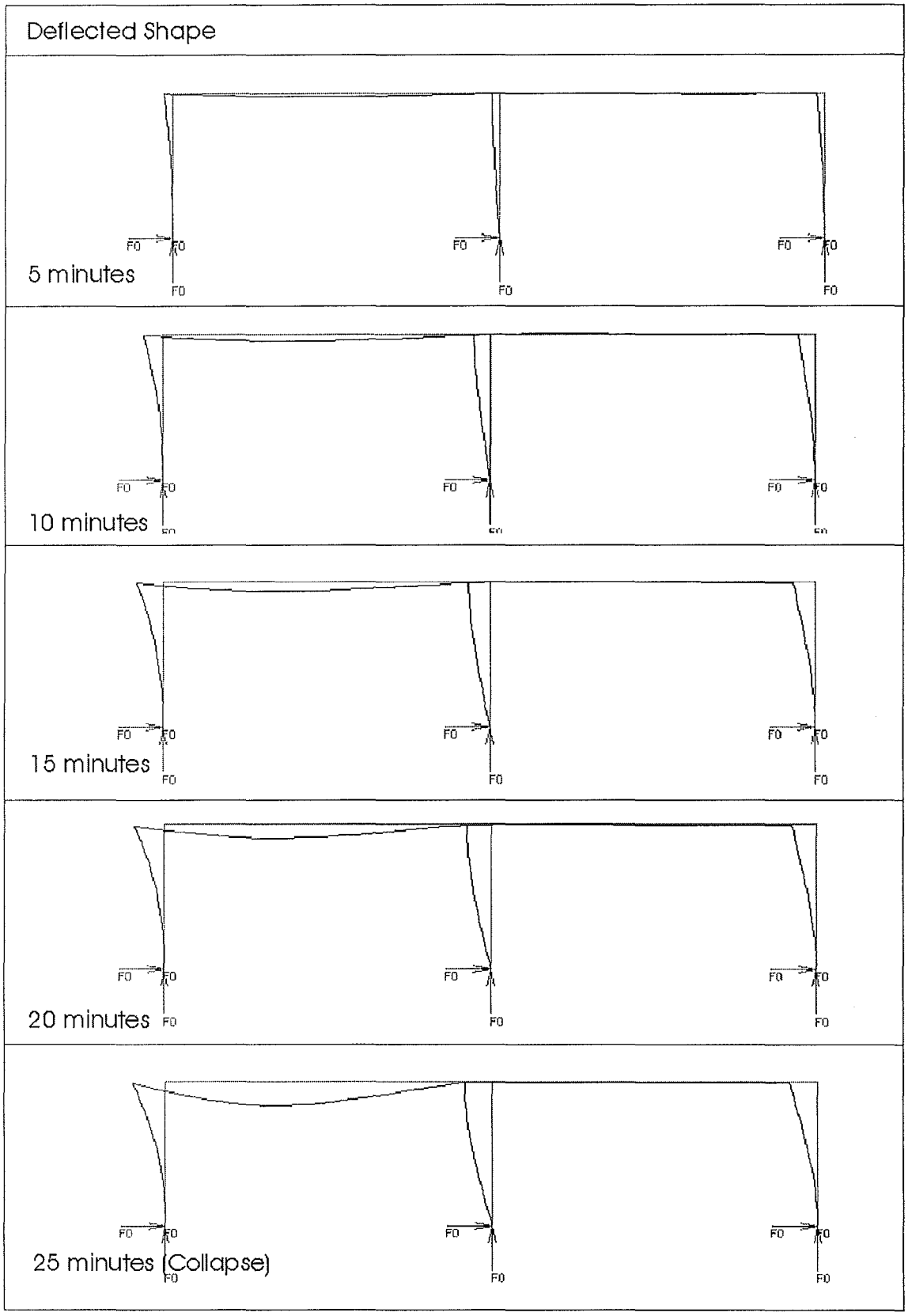

Figure 9-43: Sequence of deformation of partially braced frame with 10m wall. *Note: Deflections are magnified by 2.

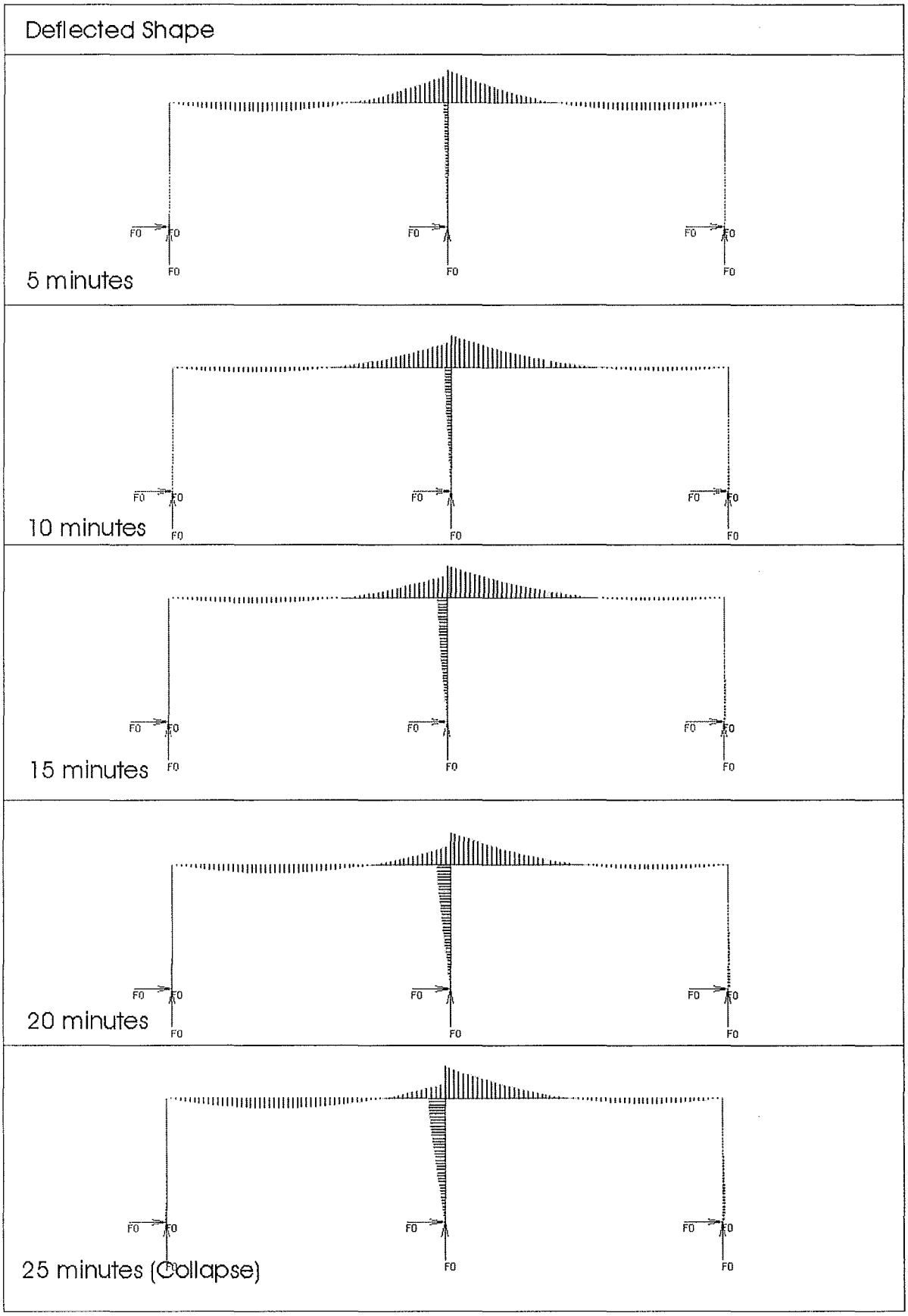

Figure 9-44: Bending moments corresponding to the deformation of the 10m frame.

Behaviour of the partially braced 10m frame (*Frame B*)

Figure 9-43 shows the sequence of deformation of the partially braced 10m frame. The deformation of *Frame B* is similar to *Frame A* where the heated wall bows when the left side of the frame is exposed to the fire. The wall deflects outwards very rapidly during the first 12 minutes but reduces and deflects slower after the initial phase, producing a bilinear displacement trend (Figure 9-45). When the top of the wall has displaced to approximately -1.12 metres, the programme ceases to iterate as the frame collapses outwards.

As the frame progressively sways outwards, the heated rafter deforms downwards due to the reduction of its stiffness. The heated rafter also deforms in a bilinear trend where it initially deflects downwards in a linear trend (Figure 9-46). After approximately 19 minutes, the rafter deforms at a faster rate. The sudden increase in the displacement rate is not enough to pull the wall panels to form an inward collapse.

Figure 9-44 shows the bending moments corresponding to the deformation of the frame. During the initial stages of the fire, the bending moments in the heated span of the rafter redistributes to the supports, causing the negative bending moments to increase. However, due to the reduction of strength in the rafter due to thermal effects, the negative flexural strength of the rafter reduces and redistributes back to the spans of the rafter. At the same time, the bending moments in the beam-column joint increases progressively to resist the overturning moments imposed onto the frame by the P-delta effects. Figure 9-47 shows that the cantilever walls provide some moment resistance, although most of the sway resistance is provided by frame action. When the beam-column reaches its plastic moment (270kNm), a plastic hinge forms at the beam-column intersection and the frame loses its sway resistance. Consequently, the frame collapses outwards. At this stage, the cantilever walls have not reached their plastic moments yet (M_p=80kNm).

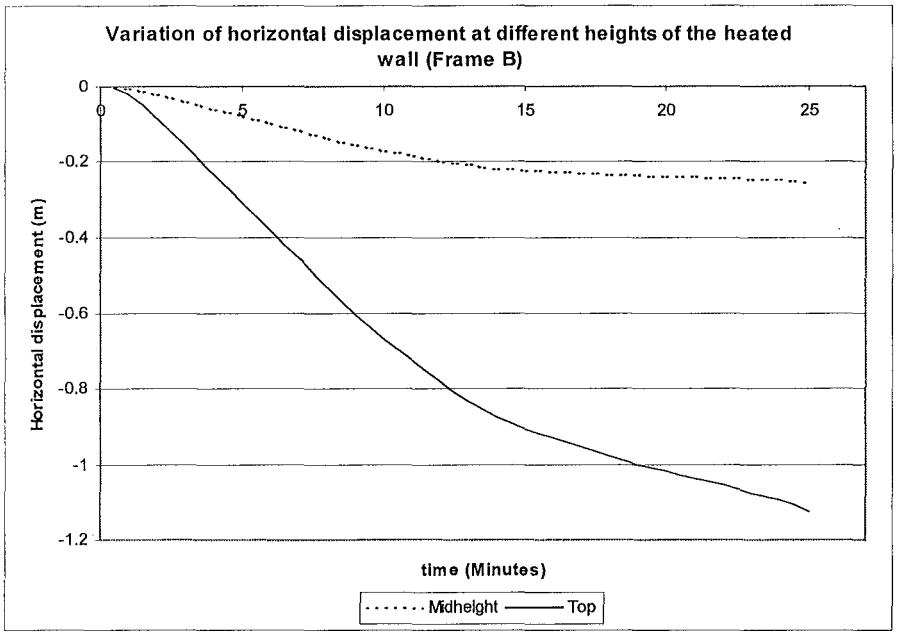

Figure 9-45: Variation of horizontal displacement at different heights of the heated wall.

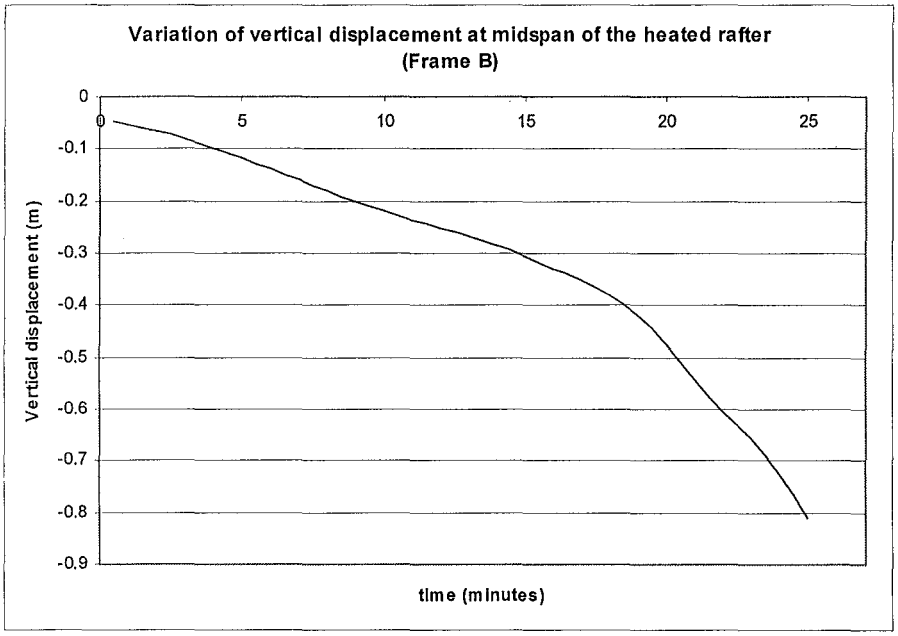

Figure 9-46: Variation of vertical displacement at midspan of the heated rafter.

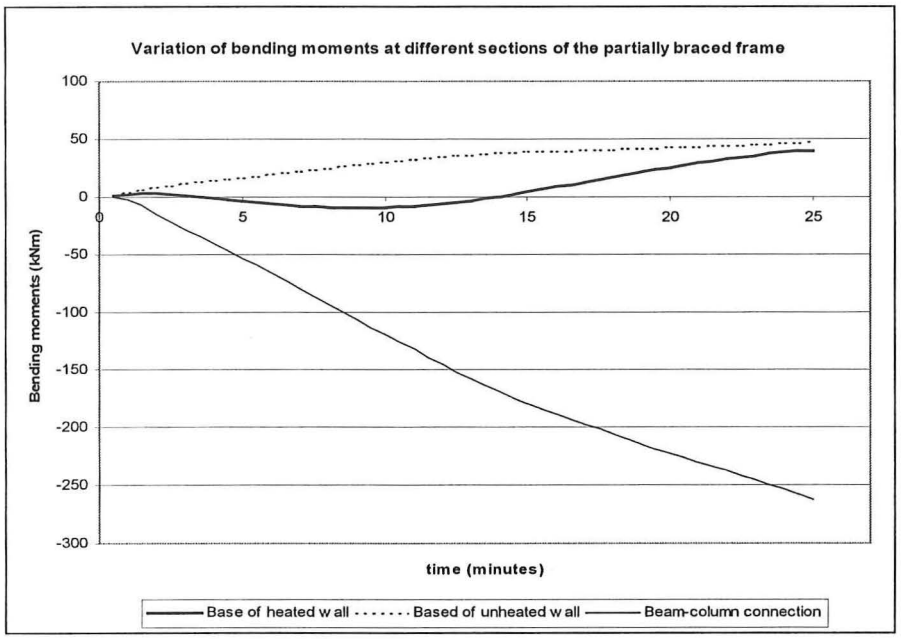

Figure 9-47: Variation of bending moments at the beam-column joint and the base of the cantilever walls.

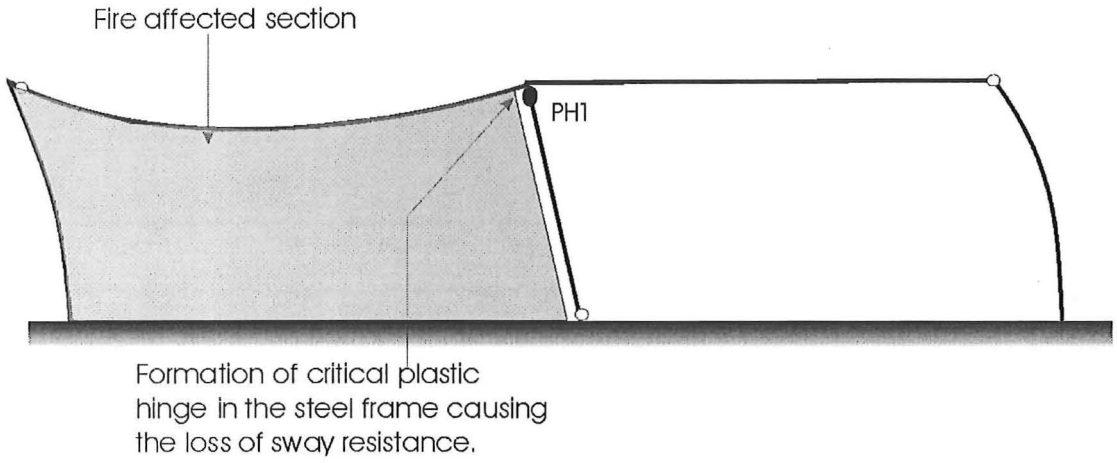

Figure 9-48: Outward collapse of frame due to formation of plastic hinge in the steel column.

ii) 6m partially braced frame: Inward collapse

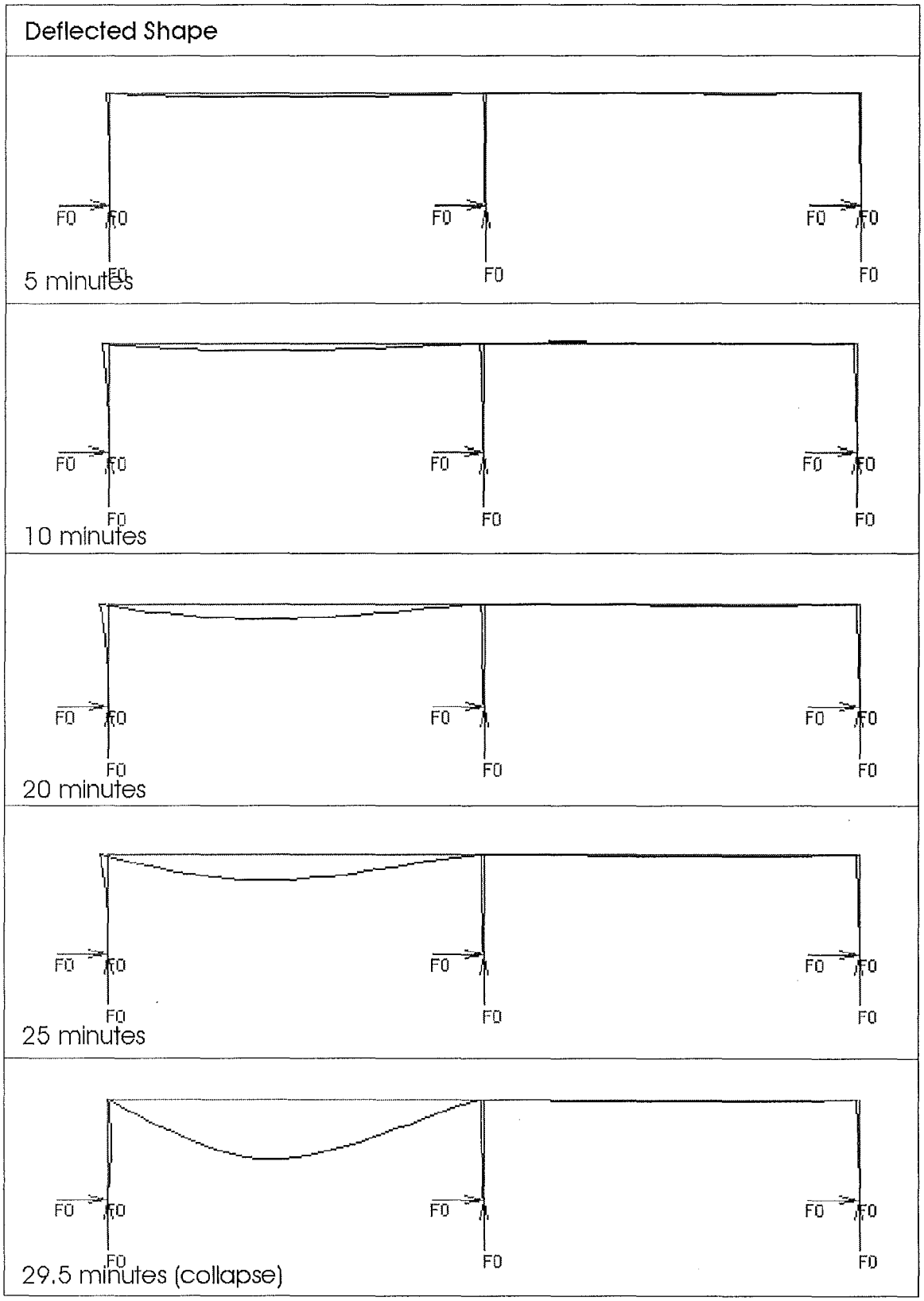

Figure 9-49: Sequence of deformation of partially braced frame with 6m wall. *Note: Deflections are magnified by 2.

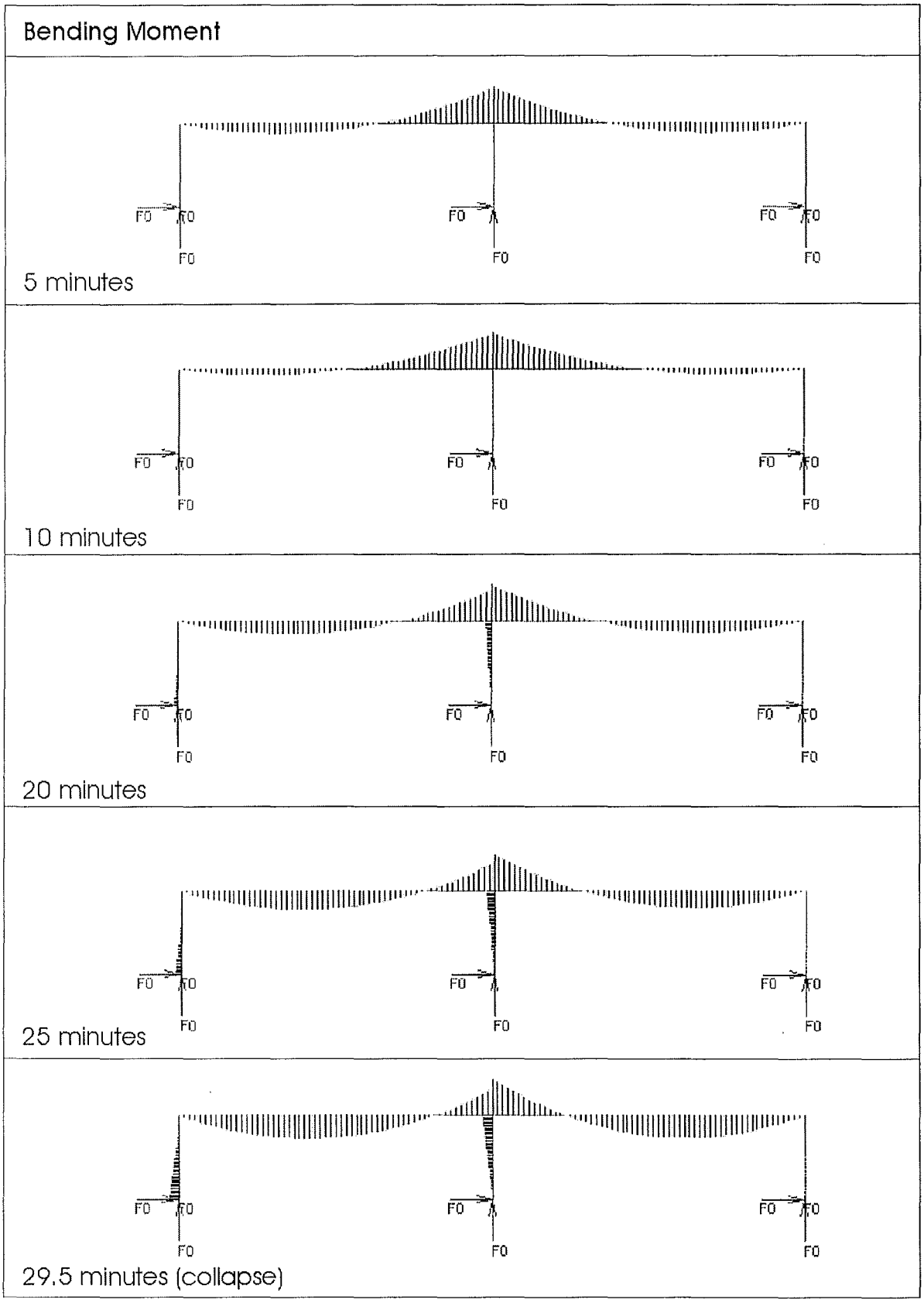

Figure 9-50: Variation of bending moments corresponding to the deformation of the 6m frame.

Behaviour of the partially braced 6m frame (*Frame B*)

When a partially braced frame with a stocky wall is exposed to a migrating fire it will collapse inwards. Figure 9-49 shows the sequence of the frame deformation when it is subjected to the migrating fire. The heated wall bows outwards progressively due to differential thermal expansion and pulls the rest of the structure outwards. At the same time, the rafter deflects downwards as the stiffness of the beam decreases due to thermal effects. Figure 9-51 shows that the top of the heated wall deflects outwards very rapidly during the first 10 minutes of the fire. The deflection rate then reduces and remains at a constant deflection of approximately 0.275 metres between 15 minutes and 24 minutes during the fire. Within this time frame, the deflection at midspan of the rafter starts to increase very rapidly, from 0.25 metres to 0.66 metres (Figure 9-52). Beyond this point, the rafter experiences runaway deflection, due to sufficient plastic hinges that have formed in the rafter to form a mechanism. The runaway vertical deflection of the rafter pulls the heated wall panel inwards, resulting in the inward collapse of the frame.

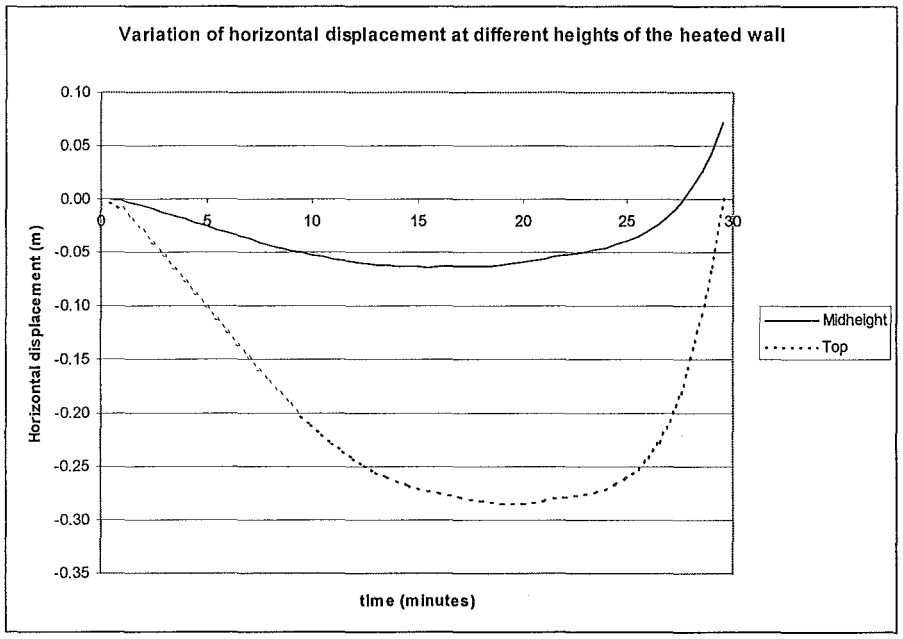

Figure 9-51: Variation of horizontal displacement at different heights of the heated wall.

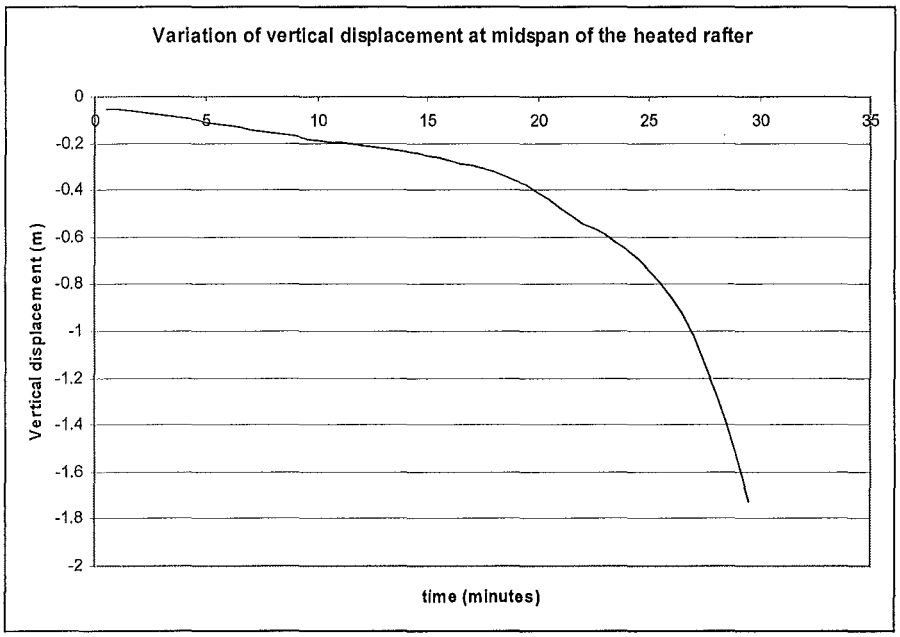

Figure 9-52: Variation of vertical displacement at midspan of the heated rafter

Figure 9-50 shows the variation of bending moments corresponding to the deformation of the frame. As with the other scenarios, moment redistribution occurs in the early stages of the fire from the spans to the supports, causing the moments to increase. The rate of moment redistribution reduces and plateaus at approximately 11 minutes and follows a decreasing trend as the yield strength of the steel in the rafter decreases due to thermal effects (Figure 9-53). The runaway deflection at midspan of the rafter pulls the heated wall panel inwards, shown by the steady rise in bending moments at the base of the heated wall after approximately 10 minutes. Prior to this, the bending moments at the base showed only small fluctuations between +5kNm to –5kNm (Figure 9-54). When a plastic hinge forms at the base of the wall panel (M_p=80kNm), it loses its rotational restraint and collapses inwards. Note that the bending moment in the beam-column joint is still low and has not yet approached its plastic moment.

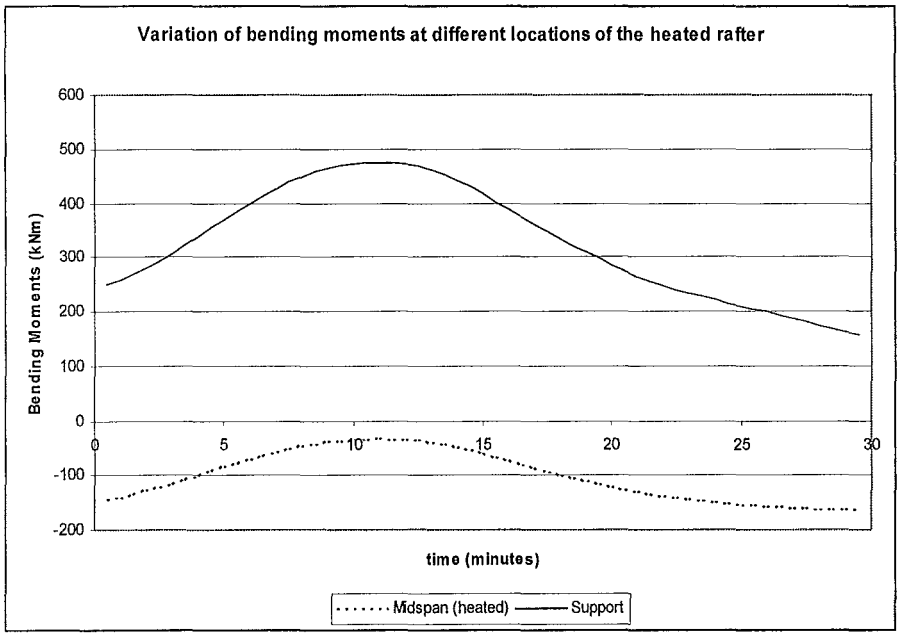

Figure 9-53: Variation of bending moments in the heated rafter.

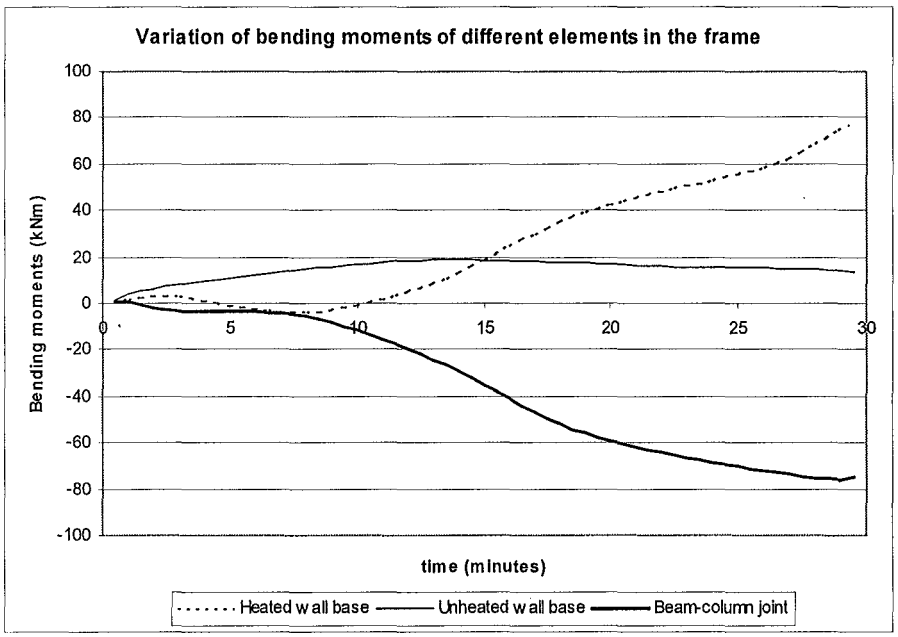

Figure 9-54: Variation of bending moments at the wall panels and the beam-column joint.

Discussion

The analyses of the partially braced frames in the *Frame B* configuration have shown that the walls with heights in excess of 9 metres or with slenderness ratios in excess of 65 cause the frames to collapse outwards. Walls with geometries in excess of these limits are very dangerous, as they are very likely to cause the frames to collapse outwards onto the neighbouring property during a fire. Buckling of the wall panels did not occur for any of the slenderness ratios analysed. Frames with 12 metre high walls were numerically difficult to analyse due their high instability. Likewise, for *Frame* A, the stiffness of the steel roof sheeting in a fire is assumed to be equivalent to the stiffness provided by frame action in the model. The yielding at the top of the steel column is equivalent to losing the diaphragm action in a real frame.

9.5.3. Discussion (Partially braced frames)

The analyses have shown that *Frames A* and *B* behaved very similarly. The behaviour of the frames is highly dependent on the strength and stiffness of the steel rafter. A frame with stocky walls will collapse inwards when sufficient plastic hinges have formed in the rafter. This will cause it to collapse downwards, pulling the wall panels inwards. Outward collapse occurs for frames with slender walls. For the partially braced frames modelled in this section, if a plastic hinge forms at the top of the column, the frame would lose its horizontal restraint and collapse outwards. In reality, this would be equivalent to losing the diaphragm action in the steel roof. If a hinge does not form at the top of the column, the frame will retain its overturning moment resistance and not collapse outwards.

The partially braced steel frames will collapse inwards if the height of the wall panel is below 9 metres and the slenderness ratio is less than 65. If either one of these limits is exceeded, the frame would collapse outwards.

There was only one exception to these limits, where the wall panel was 10 metres high and 175mm thick. In a 2-column frame, it collapsed outwards after 29 minutes of fire exposure but in the 1-column frame, it collapsed inwards. The reason for this is due to the larger load applied on the rafter in *Frame B* which enabled the rafter to collapse inwards. In *Frame A*, the applied load on the rafter is smaller (due to the smaller span), hence it was not able to pull the wall panel inwards.

9.6. Horizontal force at rafter-wall connection

Another variable in the frame analysis that requires attention is the amount of horizontal axial force imposed at the connection between the rafter and the wall. The horizontal axial force is a result of bending of the wall due to thermal bowing and from the catenary force from the sagging steel rafter. The level of horizontal force is useful for designing the wall to rafter connections and the eaves tie. If the connections pull out from the wall panel, the walls would be free to cantilever and may collapse onto the neighbouring property.

Figure 9-55 and Figure 9-56 show the variation of horizontal axial force at the connection between the wall panel and the rafter for braced and unbraced frames, respectively. *Frame B* is investigated in this case as the larger span would result in larger horizontal forces at the connections. The horizontal axial force in the beam at the top of the wall, H^* is approximated as:

$$H^* \propto \frac{M_b}{H_{wu}}$$

Where: M_b = moment at the base of the wall (kNm)

H_{wu} = height of the wall (m)

The 175mm wall was chosen as it has the highest flexural strength (compared to the 125mm and 150mm walls) and would produce the largest horizontal force (H^*) at the connection to the rafter. Apart from the horizontal force imposed from the moments at the base of the wall, additional horizontal forces are imposed on the rafter-wall connections from the catenary forces as the rafter sags. The positive sign represents axial tension in the beam member. The graphs show that the highest axial force is imposed from the shortest wall, consistent with the equation above.

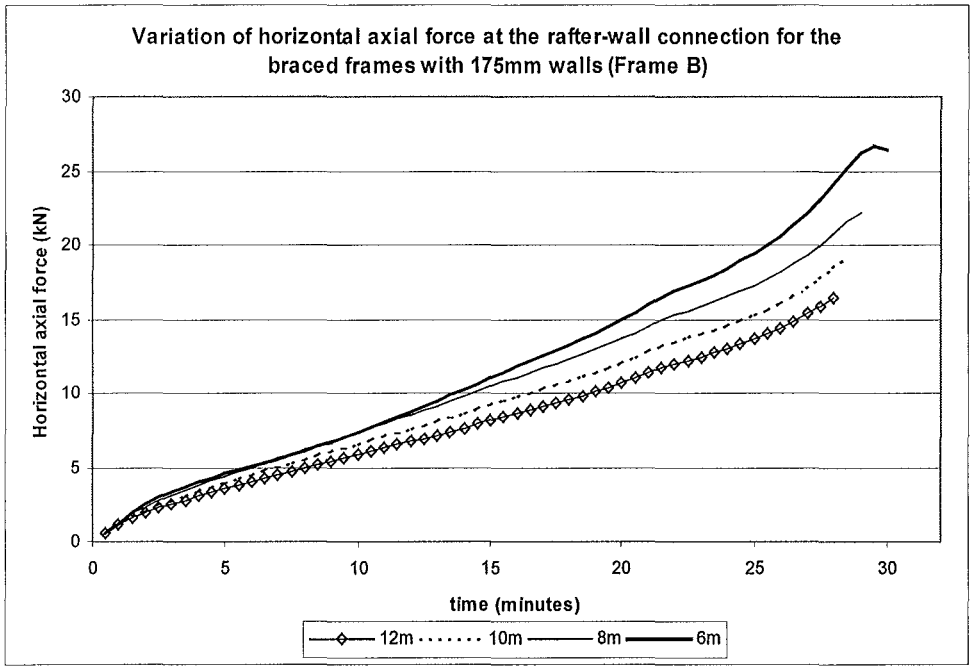

Figure 9-55: Variation of horizontal axial force at the rafter-wall connection for the horizontally braced frames with 175mm walls.

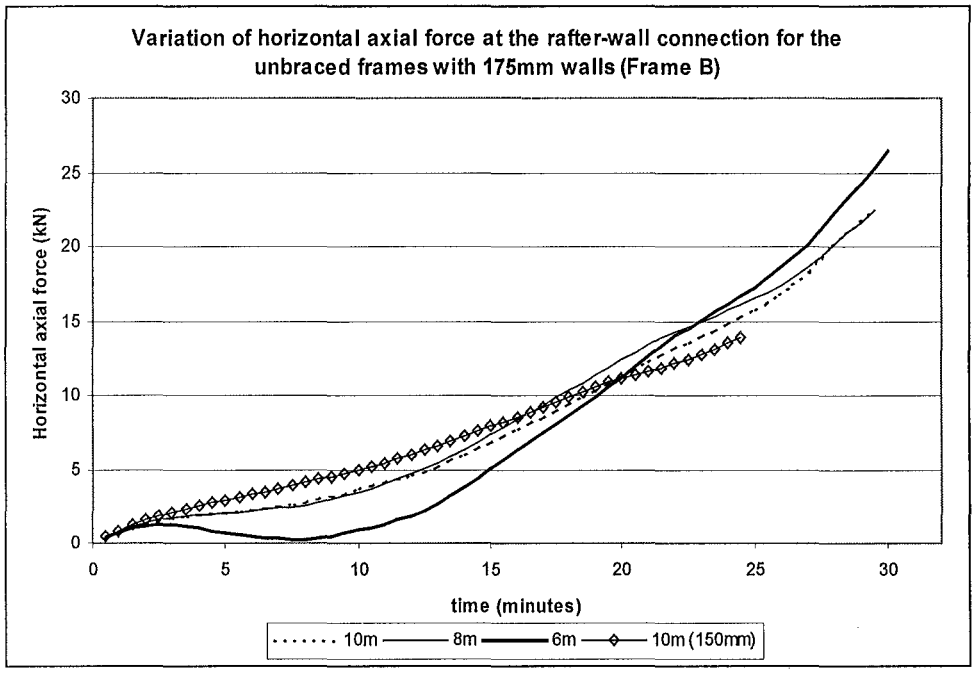

Figure 9-56: Variation of horizontal axial force at the rafter-wall connection for the unbraced frames with 175mm walls.

The horizontal forces in the rafter increase with slightly different trends for the unbraced and braced frames. The horizontal forces in the braced frames rise at a steady rate throughout the fire (Figure 9-55). The unbraced frames show smaller horizontal forces during the first 15 minutes of the fire compared to the braced frames, but it rises more rapidly during the advanced stages (Figure 9-56). A 10 metre high by 150mm thick wall (which collapsed outwards) was compared with the 175mm walls to compare the forces in the inward and outward collapse modes. In the outward collapse of the frame, the trend of the horizontal force does not differ from the inward collapse mode. Its maximum force is also lower compared with the inward collapse modes.

Frame B	**Maximum horizontal force in rafter-wall connection (kN)**	
Wall height (m)	**Unbraced**	**Braced**
6	26.5	26.5
8	22.5	22.1
10	22.5	19.1
12	NA	16.4

Table 9-12 : Maximum axial forces at rafter-wall connections

Table 9-12 shows that the maximum axial forces present in the connections increase with decreasing wall height. These are the forces at the connections at the point of collapse of the frame. The maximum forces in the shorter walls are higher than in the taller walls as it requires a smaller force to reach the plastic moment in the taller walls compared to the taller walls. The forces for the unbraced 12 metre frame was not included as the frame collapsed due to numerical instability. The design of the connections should incorporate safety factors to account for thermal effects on the strength and stiffness on the connecting elements and on the strength of concrete.

As mentioned in section 2.2.4, the Building Code of Australia 1996 (BCA) provides some recommendations on the levels of horizontal forces in the design of the connections in the event of fire. These recommendations should also be applied in the design of the connections for these slender tilt-up panels. The effects of concrete spalling should also be considered in the design of the connection elements. These axial forces must be maintained throughout the fire exposure. Epoxy grouted connections must not be used because they would fail very easily in a fire.

9.7. General discussion on steel frames

9.7.1. Wall panels

When a concrete panel is exposed to a fire, it will bow and produce a horizontal force on the attached rafter or the eaves ties. The thrust of the wall due to thermal bowing is significant and it resists the catenary forces of the sagging rafter. Provided there is sufficient horizontal restraint from the rest of the frame and diaphragm action from the roof, the wall will not fall out onto the neighbouring property. While decreasing the height of the wall reduces the likelihood of outward collapse, it increases the horizontal force which has to be designed for, at the top of the wall.

For frames that are susceptible to outward collapse, increasing the thickness of the walls has some advantages and some disadvantages in resisting the overturning moments of the frame. In the case of the 10 metre walls of the partially braced frames, increased thickness of the walls decreased the thermal bowing deflections. However, for the 12 metre walls, the increased thickness does not improve its performance because the P-delta effects become more significant and would cause the frame to collapse outward.

9.7.2. Rafter

The rafter, and any loads imposed on it, governs the overall behaviour of the structure. In order to prevent outward collapse, the frame must possess sufficient horizontal restraint in the form of diaphragm action or the steel rafter must collapse as soon as possible in a fire. In a very severe fire, the unprotected rafter will sag, pulling the wall inwards. This will lead to a satisfactory failure mode. If the roof and skylights collapse, allowing venting of the hot gases, the conditions imposed on the steel frame may not be as severe. If the steel frame is braced and has sufficient inherent fire resistance characteristics or is fire protected, it may not sag severely, thus preventing structural collapse.

An important assumption made in all the analyses is that the loads remain on the rafter. If the loads from the purlins and ceiling services detach from the rafter and collapse on the floor, the load left on the rafter would be minimal. This would reduce the horizontal force that would be available to pull the walls inwards, thus increasing the possibility of outward collapse of the frame.

9.7.3. Wall to rafter connections

The connections between the wall and the rafter must be able to withstand the effects of high temperatures to allow the rafter to remain connected to the wall. This connection is crucial to produce an acceptable mode of structural failure, by allowing the wall to be pulled inwards by the collapsing rafter. If the connection fails, the steel rafter would collapse, leaving the walls free to bow and collapse outwards onto the neighbouring property. Epoxy grouted connections must not be used because they are extremely unsafe and would fail very easily in a fire.

9.7.4. Horizontal restraint

Diaphragm action of the steel roof sheeting must be maintained during the fire as it plays a crucial role in the sway resistance of the frame. In a real fire, the effectiveness of the lateral restraint from either diaphragm action, purlins and eaves tie is questionable. It is also assumed in this analysis that the roof consists of steel sheeting, screw fixed to cold-rolled steel purlins, bolted to purlin cleats on the steel rafter. If the purlins are of timber, they will burn away early in the fully developed fire, leading to collapse of the roof and loss of diaphragm action.

Another scenario that may lead to significant loss of diaphragm action is the utilisation of large amounts of plastic skylights or aluminium roofing. Plastic skylights in the roof will melt in the event of a fire. If a large portion of the roof is skylights, their loss in a fire will cause large openings in the roof, preventing horizontal force transfer to the rest of the horizontal load resisting components in the system. The performance of aluminium roofing is very poor compared to steel roof sheeting as its melting point is approximately 580°C to 660°C. In the event of a fire, an aluminium roof would melt through very rapidly, causing loss of continuity in the sheeting and diaphragm action.

9.7.5. Extent of fire in the building

The analyses conducted in this report have assumed that only part of the building is involved in the fire and that the loss of the roof diaphragm would be localised. The cooler parts of the roof diaphragm will be able to provide horizontal restraint to the heated rafter. However, in a large scale fire where full room involvement occurs, a large portion of the steel roof may be affected by the fire, causing a significant loss of diaphragm action in the structure. This would

present a very dangerous condition, as the amount of horizontal restraint would be minimal, only in the form of the purlins and the eaves ties, probably resulting in the wall panels collapsing outward.

Another assumption in the analysis is that the temperatures of the fire are equivalent to the ISO standard fire. The temperatures of the ISO fire are considered on the upper bound, but are possible in buildings that contain high rack storage and flammable material.

9.7.6. Connection of wall panels

The wall panels of the building should be securely tied together with eaves ties to minimise the likelihood of outward collapse of individual panels during a fire. If the wall panels are tied together, outward collapse due to thermal bowing of the heated panels can be resisted by the adjacent cooler panels. The overturning moments of the heated panels, transferred through the eaves tie, can be resisted by the flexural strength of the adjacent panels. Connecting the wall panels together will also prevent outward collapse of other panels when inward collapse of the steel rafter drags the heated wall panel in. The inward collapse of a steel rafter will also constrain the rest of the connected panels in the building to collapse inwards.

9.8. Conclusions

As noted in separate sections of this chapter, the following conclusions may be drawn:

- Unbraced frames will perform very poorly because they collapse outwards, even for wall heights as low as 6 metres.
- If the frames are fully braced, the walls will collapse inward without buckling of the wall panels, even with slenderness ratios as high as 96.
- For partially braced frames, outward collapse can be prevented if the walls are no greater than 9 metres high or the slenderness ratio is no greater than 65.
- The connections between the walls panels to the steel rafter and the eaves ties should be designed and detailed carefully. The Building Code of Australia 1996 (BCA) provides guidance on the levels of axial force for design purposes and should be used as a design guide.
- The Euler buckling equation cannot be used as a hand method to accurately predict buckling of the wall panels in the frames. The buckling equation is difficult to use as the effective flexural rigidity during a fire is difficult to evaluate, even with finite element software.

10. CONCLUSIONS AND RECOMMENDATIONS

10.1.Introduction

This research project was conducted to analyse the behaviour of slender cantilever concrete wall panels in industrial buildings. The industrial buildings comprise steel rafters supported on internal steel columns and load-bearing precast panels at the perimeter of the building. The steel frame is not fire protected. The precast concrete panels are cantilevered at the base and do not have columns attached.

The analysis of this project was conducted using SAFIR, a non-linear finite element programme. The scope of the analysis covered the behaviour of free-standing cantilever walls, propped cantilever walls and cantilever walls attached to the steel frame.

10.2.Concrete walls

10.2.1. Free standing cantilever walls

The behaviour of the concrete walls is very sensitive to the slenderness ratio of the walls. Walls with high slenderness ratios experience very large deflections when exposed to a fire on one side. The deflections, due to thermal bowing and P-delta effects, will lead to outward collapse if the walls do not have sufficient flexural strength at the base, or if the foundations do not have sufficient resistance to the overturning moment.

If the wall panels cannot be effectively connected to the steel frame, then measures have to be taken to control the thermal bowing deflections including the following:

- Provide intermediate concrete columns fixed to the wall panels.
- Increase the thickness of the wall panels.
- Increase the quantity of reinforcement in the wall panels.

10.2.2. Propped cantilever walls

Propped cantilever walls do not experience large out-of-plane deflections when subjected to a fire on one side. They bow inwards towards the fire and form a plastic hinge at the base. After a plastic hinge has formed at the base of the walls, accompanied by significant cracking, the walls

may then buckle under their own weight. Slender walls exhibit larger out-of plane deflections and shorter survival times compared to stockier walls. Stockier walls, however, impose larger horizontal forces on the supported rafter compared to the more slender walls.

10.3.Frames

10.3.1. Unbraced frames

Unbraced frames perform very poorly because they collapse outwards, even for wall heights as low as 6 metres. The sway of unbraced frames during a fire is resisted only by the flexural strength of the cantilever wall panels. When the sway of the frame has produced sufficient overturning moments to form a plastic hinge at the base of the cantilever walls, the frame loses its sway resistance and collapses outwards onto the neighbouring property.

10.3.2. Braced frames

If the frames are fully braced, the walls will collapse inward without buckling of the wall panels, even with slenderness ratios as high as 96. The bracing provided by the steel roof diaphragm prevents sway of the frame. The effects of the fire cause plastic hinges to form in the steel rafter. When the steel rafter collapses inwards, the attached wall panel is pulled inwards. This prevents outward collapse of the wall panels onto the neighbouring property and also prevents a buckling failure of the wall panels.

10.3.3. Partially braced frames

For the partially braced frames in this study, outward collapse can be prevented if the walls are not greater than 9 metres high and the slenderness ratio is not greater than 65. For the partially braced frames analysed in the previous chapter, sway of the frame is resisted by frame action and the flexural strength of the cantilever walls. If the height of the wall exceeds 9 metres and its slenderness ratio exceeds 65, the frame would sway during a fire and collapse onto the neighbouring property when the overturning moment exceeds the sway resistance of the frame. Outward collapse occurs when a plastic hinge forms at the top of the unheated column member, leading to the loss of sway resistance.

Walls shorter than 8 metres and slenderness ratios under 65 collapse inwards during a fire when plastic hinges form in the rafter, pulling the wall panels in.

10.4.Design recommendations

10.4.1. Building design

The design of wall panels in industrial buildings that feature column-free walls attached to steel frames should follow the slenderness limits stated in section 10.3, depending on the level of bracing available during a fire. Some bracing of the frame by diaphragm action is essential to ensure good behaviour of the frame during a fire. Buildings with aluminium roofs or light timber purlins or large skylights will not provide sufficient bracing. There is no advantage to fire protecting or over-designing the steel rafters because that will delay the collapse of the frame, possibly resulting in buckling of the wall panels.

10.4.2. Connection of the wall panels to the steel frames

The wall panels should be connected to the steel frames so that the outward collapse of the wall panels due to thermal bowing can be prevented. This is regardless whether or not the steel frames are fire protected. To restrain the outward collapse of the panels by the steel frame, strong and well designed connections between the panels and the frame are required. The connections may have to withstand very high pull-out forces while exposed to high temperatures.

If the steel frames are not connected to every concrete panel, an eaves tie is required to prevent the non-load bearing panels from deforming and collapsing outwards. The purpose of the eaves tie is to keep all the wall panels connected during a fire. The connections that connect the eaves ties to the panels require special attention to prevent outward collapse of the individual panels.

The current New Zealand Concrete Structures Standard and New Zealand Building Code do not provide any guidance on the design of the connections between the rafter and wall and between the eaves tie and the wall. The Building Code of Australia provides guidance on these connection details (refer to section 2.2.4) and could be used as a guideline for the construction of these tilt wall panels in New Zealand.

10.4.3. Base connections of the wall

The base connections must be detailed and designed to withstand the forces and moments due to thermal bowing of the walls. Even if the wall is able to sustain the large deflections and moments, it will still collapse if the connections at the base fail, or if the foundation system has insufficient overturning capacity.

10.5.Future research

It is recommended that future research should include:

- Analysis with real fire curves
- Analysis with different types of concrete
- Three dimensional analysis
- Fire resistance of the wall to rafter connections and wall to eaves tie connections.
- Analysis of base connections of cantilever walls to determine their ability to sustain the moments due to the thermal bowing deflections.
- Experimental verification of very slender reinforced concrete walls.

11. REFERENCES

1. ABAQUS Finite Element Analysis Programme, Hibbitt, Karlson and Sorenson Inc., 1988.

2. Anderberg, Y., Thelandersson, S. (1976) Stress and deformation characteristics of concrete at high temperatures, *Bulletin 54*, Division of Structural Mechanics and Concrete Construction, Lund Institute of Technology, Lund, Sweden.

3. Anderberg, Y., Magnusson, S.E., Thelandersson, S., Petterson, O., Wickström, U., (1978) Analytical design of fire exposed concrete structures, *Bulletin 65*, Division of Structural Mechanics and Concrete Construction, Lund Institute of Technology, Lund, Sweden.

4. Bažant, P.Z., Kaplan, M.F. (1996) *Concrete at High Temperatures: Material Properties and Mathematical Models,* Concrete Design and Construction Series, Longman Group Limited, U.K.

5. Blundell, R., Diamond, C., Browne, R.G. (1976) The properties of concrete subjected to elevated temperatures, *Technical Note No. 9*, CIRIA Underwater Engineering Group, London.

6. Brown, B.J. (1997) Some stability issues for tilt up precast panels under in-plane seismic loading, *SESOC Journal*, Vol. 10, No.1, 34-42.

7. Brown, B. (1999) Research needed on 'tilt-up' concrete walls, *Build* (November-December), 33-36.

8. Browne, R.D. (1972) Thermal movement of concrete, *Concrete*, Vol. 6, No.11, 51-53.

9. Buchanan, A.H. (1994) *Fire Engineering Design Guide*, Centre for Advanced Engineering, University of Canterbury, Christchurch, New Zealand.

10. Buchanan, A.H. (1999) *Structural Design for Fire*, School of Engineering, University of Canterbury, Christchurch, New Zealand.

11. Building Code of Australia 1996, Australian Building Codes Board.

12. Building Industry Authority (1992) *New Zealand Building Code Handbook and Approved Documents.* Building Industry Authority, Wellington.

13. Bull, D. (1998) Slenderness of concrete walls: NZS 3101: 1995 Requirements: Discussion paper by Des Bull, Holmes Consulting Group Christchurch, *SESOC Journal*, Vol. 11, No.1, 58.

14. Clifton, G. Charles (1996) Support of portal frame fire rated vertical spanning external concrete wall panels in severe fires, *SESOC Journal*, Vol. 9, No.2, 26-36.

15. Concrete Structures Standard (1995) NZS 3101: Part1: 1995. *The Design of Concrete Structures*, Standards New Zealand, Wellington.

16. Cooke, G.M.E. (1987a) Fire engineering of tall fire separating walls, *Fire Surveyor* Vol.16. No.3 13-29

17. Cooke, G.M.E. (1987b) Fire engineering of tall fire separating walls, *Fire Surveyor* Vol.16. No.4 19-29

18. Cooke, G.M.E., Morgan P.B.E. (1988) Thermal bowing in fire and how it affects building design, *Building Research Establishment Information Paper*, December.

19. Cooke G., Virdi K. And Jeyarupalingam N.(1996) The thermal bowing of brick walls exposed to fire on one side. *Proc Interflam '96*, Interscience, London, 915-919.

20. Cosgrove, B.W. (1996) Fire design of single storey industrial buildings, Fire Engineering Research Report No.96/3, School of Engineering, University of Canterbury, Christchurch, New Zealand.

21. Cruz, C.R., Gillen, M. (1980) Thermal expansion of Portland cement paste, mortar and concrete at high temperatures. *Fire and Materials,* Vol. 4, No. 2, pp. 66- 70.

22. EC1, (1994). Eurocode 1: *Basis of Design and Design Actions on Structures. Part 2-2: Actions on Structures Exposed to Fire. ENV 1991-2-2.* European Committee for Standardization, Brussels.

23. EC2, (1995). Eurocode 2: *Design of concrete structures. ENV 1992: Part1-2: General rules-Structural fire design,* European Committee for Standardization, Brussels.

24. EC3, (1995). Eurocode 3: *Design of steel structures. ENV 1993 Part1-2: General rules- Structural fire design,* European Committee for Standardization, Brussels.

25. Harmathy, T.Z. (1970) Thermal properties of concrete at elevated temperatures. *ASTM Journal of Materials*, Vol.5. No.1, pp.47-74.

26. Harmathy, T.Z. (1993) Fire Safety Design & Concrete, Concrete Design and Construction Series, Longman Group Limited, U.K.

27. Harmathy, T.Z., Allen L.W. (1973) Thermal properties of selected masonry unit concretes. *Journ. Amer. Concr. Inst.*, Vol.70. No.2, pp. 132-142.

28. Harmathy, T.Z., Stanzak, W.W. (1970) Elevated-temperature tensile and creep properties of some structural and prestressing steels. In *Fire Test Performance,* ASTM STP 464, American Society for Testing and Materials, Philadelphia A, pp. 186

29. Institution of Structural Engineers (1975) *Fire Resistance of Concrete Structures*. Report of a Joint Committee of the Institution of Structural Engineers and the Concrete Society, London.

30. Inwood, M. (1999) Review of the New Zealand Standard for Concrete Structures (NZS 3101) for high strength and lightweight concrete exposed to fire. University of Canterbury, Christchurch, New Zealand.

31. Khoury, G.A., Grainger, B.N., Sullivan, P.J.E, (1985a) Transient thermal strain of concrete: Literature review, conditions within specimen and behaviour of individual constituents, *Magazine of Concrete Research*, Vol.37. No. 132, pp.131-144.

32. Khoury, G.A., Grainger, B.N., Sullivan, P.J.E, (1985b) Strain of concrete during first heating to 600°C under load, *Magazine of Concrete Research*, Vol.37. No. 133, pp.195-215.

33. Khoury, G.A., Grainger, B.N., Sullivan, P.J.E, (1986) Strain of concrete during first cooling from 600°C under load, *Magazine of Concrete Research*, Vol.38. No. 134, pp. 3 -12.

34. Kirby, B.R., Preston, R.R. (1988) High temperature properties of hot-rolled structural steels for use in fire engineering design studies. *Fire Safety Journal*, 13, 27-37.

35. Kodur, V.K.R., Nwosu, D.I., Sultan, M.A., Franssen, J.-M. (1999) Application of the SAFIR computer program for evaluating fire resistance. *Proc. Third International Conference on Fire Research Engineering (Chicago, U.S.A.)* October 4-8. pp. 287-298

36. Malhotra, H.L., (1956) The effect of temperature on the compressive strength of concrete. *Magazine of Concrete Research*, Vol.8. No. 23, pp. 85-94.

37. Malhotra, H.L. (1984) Spalling of concrete in fires, *Technical Note No.118*, Construction Industrial Research and Information Association (CIRIA)

38. McMenamin, A. (1999) The Performance of Slender Precast Reinforced Cantilever Walls with Roof Level Lateral Displacement Restraint under Simulated In-plane Seismic Loading. Civil Engineering Research Report 99/4, Department of Civil Engineering, University of Canterbury, Christchurch, New Zealand.

39. Munukulta, V.R. (1989) Modelling Fire Performance of Concrete Walls, Research Report No. 89/5, Department of Civil Engineering, University of Canterbury, Christchurch, New Zealand.

40. New Zealand Concrete Society and the New Zealand National Society for Earthquake Engineering (1991) *Guidelines for the use of structural precast concrete in buildings.* Centre for Advanced Engineering, University of Canterbury, Christchurch, New Zealand.

41. Nwosu, D.I., Kodur, V.K.R., Franssen, J.-M., Hum J.K.(1999) *User manual for SAFIR: A computer program for analysis of structures at elevated temperature conditions.* Institute for Research in Construction, National Research Council of Canada.

42. O'Meagher, A.J. (1994) Behaviour of concrete walls, industrial buildings and composite columns in fire. PhD thesis, University of Melbourne.

43. O'Meagher, A.J., Bennetts, I.D. (1991) Modelling of concrete walls in fire, *Fire Safety Journal*, Vol. 17. 315-335.

44. O'Meagher, A.J., Bennetts, I.D. (1997) Single Storey Steel-framed Buildings: Support of External Walls in Fire-Technical Note No.1, *BHP Structural Steel Development Group*

45. O'Meagher, A.J., Bennetts, I.D., Dayawansa, P.H., Thomas, I.R., BHP Research Melbourne Laboratories (1992), Design of Single Storey Industrial Buildings for Fire Resistance, *Journal of Australian Institute of Steel Construction*, Vol. 26, No.2.

46. Park, R. and Paulay, T. (1975) *Reinforced Concrete Structures.* John Wiley and Sons.

47. Schneider, U. (1985), Behaviour of Concrete at High Temperatures, RILEM Committee 44- PHT.

48. Roark, R.J., Young, W.C. (1975) *Formulas for stress and strain.* Fifth edition. McGraw-Hill Book Company, U.S.A.

49. Restrepo, J.I., Crisafulli, F.J., Park, R. (1996) Earthquake resistance of structures: The design and construction of tilt-up reinforced concrete buildings, Research Report No. 96-11, Department of Civil Engineering, University of Canterbury, Christchurch, New Zealand.

50. *Tilt-up Technical Manual* (1991) Cement and Concrete Association of New Zealand, New Zealand.

51. Wade, C.A. (1992) Fire Resistance of New Zealand Concretes- Part 2, Building Research Association of New Zealand, BRANZ Study Report SR 40. Judgeford.

52. Wickström, U. (1979) *TASEF-2 A Computer Program for the Temperature Analysis of Structures Exposed to Fire,* Lund Institute of Technology, Sweden.

53. Wickström, U. (1986) A very simple method for estimating temperatures in fire exposed structures, In: *New Technology to Reduce Fire Losses and Costs*, Elsevier Applied Science, London, pp. 186-194.

54. Woodside, A., de Ruiter, J.J., Wade, C.A. (1991) Fire Resistance of New Zealand Concretes- Part 1, Building Research Association of New Zealand, BRANZ Study Report SR 34. Judgeford.

APPENDIX

Typical input file for wall analysis

*.DAT file for structural analysis

```
cantilever 10m high, 150mm x 56mm, steel ratio 0.67%,

    NPTTOT      50000
     NNODE  101
      NDIM    2
 NDIMMATER    1
   NDDLMAX    3
      FROM    1   TO  101 STEP    2 NDDL    3
      FROM    2   TO  100 STEP    2 NDDL    1

    STATIC
     NLOAD    1
   OBLIQUE    0
NOCOMEBACK         1
 ARCLENGTH      0.02
 LARGEUR11    1300
 LARGEUR12        50
   NORENUM
wall10m_EC1.str
 PRECISION     1.e-5
     LOADS
  FUNCTION        F1
 DISTRBEAM         1        0.      -200
 DISTRBEAM        50        0.      -200    1

      TIME
                10.     7200.
   ENDTIME
LARGEDISPL
     EPSTH
IMPRESSION
 TIMEPRINT       10.
PRINTREACT
PRNSIGMABM    1    2
   PRINTMN
```

*.STR file for structural analysis

```
cantilever 10m high, 150mm x 56mm, steel ratio 0.67%,

      NMAT    2
  ELEMENTS
      BEAM   50     1
        NG    2
    NFIBER  150

     NODES
      NODE    1   0.00000   0.00000
      NODE  101   0.00000  10.00000     1
 FIXATIONS
     BLOCK    1              F0         F0         F0

 NODOFBEAM
section150_EC1.tem
 TRANSLATE    1     1
 TRANSLATE    2     2

    1    1    2    3     1
   50   99  100  101     1     2
 MATERIALS
SILCONCEC2
    20.E+9         .15     30.E+6     2.7e+6
  STEELEC2
   210.E+9          .3    430.E+6
```

Typical input file for frame analysis

*.DAT file for structural analysis

```
    NPTTOT      80000
     NNODE    72
      NDIM     2
 NDIMMATER     1
   NDDLMAX     3
      FROM     1    TO    21 STEP     2 NDDL     3
      FROM     2    TO    20 STEP     2 NDDL     1
      FROM    22    TO    72 STEP     2 NDDL     3
      FROM    23    TO    71 STEP     2 NDDL     1

    STATIC
     NLOAD     1
   OBLIQUE     0
NOCOMEBACK        0.1
 ARCLENGTH       0.02
 LARGEUR11       1000
 LARGEUR12         50
   NORENUM
frameEC1_10mfull.str
 PRECISION      1.e-5
     LOADS
  FUNCTION         F1
 DISTRBEAM          1          0.     -10080
 DISTRBEAM         10          0.     -10080     1
 DISTRBEAM         11          0.      -4200
 DISTRBEAM         25          0.      -4200     1
 DISTRBEAM         26          0.       -715
 DISTRBEAM         35          0.       -715     1

      TIME
                10.       300.
                20.       600.
                30.      3600.
                40.      7200.
   ENDTIME
LARGEDISPL
     EPSTH
IMPRESSION
 TIMEPRINT       10.
PRINTREACT
PRNSIGMABM    16     2
   PRINTMN
```

*.STR file for structural analysis

```
NMAT    4
  ELEMENTS
      BEAM   35    3
        NG    2
    NFIBER 3500

     NODES
      NODE    1   0.00000   0.00000
      NODE   21   0.00000  10.00000    1
      NODE   22   0.00000  10.00000
      NODE   52  22.50000  10.00000    1
      NODE   53  15.00000   9.50000
      NODE   54  15.00000   9.00000
      NODE   72  15.00000   0.00000    1
 FIXATIONS
     BLOCK    1             F0         F0         F0
     BLOCK   52             F0                    F0
     BLOCK   72             F0         F0
      SAME   21   22       YES        YES

 NODOFBEAM
fullwallEC1.tem
 TRANSLATE    1    1
 TRANSLATE    2    2

ipe360EC1.tem
 TRANSLATE    1    3

he200BEC1.tem
 TRANSLATE    1    4

    1    1    2    3    1
   10   19   20   21    1    2
   11   22   23   24    2
   25   50   51   52    2    2
   26   42   53   54    3
   27   54   55   56    3
   35   70   71   72    3    2
 MATERIALS
SILCONCEC2
    20.E+9       .15    30.E+6    0.0e+6
  STEELEC2
   210.E+9        .3   430.E+6
  STEELEC3
   210.E+9        .3   430.E+6
  STEELEC3
   210.E+9        .3   320.E+6
```

FIRE ENGINEERING RESEARCH REPORTS

95/1	Full Residential Scale Backdraft	I B Bolliger
95/2	A Study of Full Scale Room Fire Experiments	P A Enright
95/3	Design of Load-bearing Light Steel Frame Walls for Fire Resistance	J T Gerlich
95/4	Full Scale Limited Ventilation Fire Experiments	D J Millar
95/5	An Analysis of Domestic Sprinkler Systems for Use in New Zealand	F Rahmanian
96/1	The Influence of Non-Uniform Electric Fields on Combustion Processes	M A Belsham
96/2	Mixing in Fire Induced Doorway Flows	J M Clements
96/3	Fire Design of Single Storey Industrial Buildings	B W Cosgrove
96/4	Modelling Smoke Flow Using Computational Fluid Dynamics	T N Kardos
96/5	Under-Ventilated Compartment Fires - A Precursor to Smoke Explosions	A R Parkes
96/6	An Investigation of the Effects of Sprinklers on Compartment Fires	M W Radford
97/1	Sprinkler Trade Off Clauses in the Approved Documents	G J Barnes
97/2	Risk Ranking of Buildings for Life Safety	J W Boyes
97/3	Improving the Waking Effectiveness of Fire Alarms in Residential Areas	T Grace
97/4	Study of Evacuation Movement through Different Building Components	P Holmberg
97/5	Domestic Fire Hazard in New Zealand	KDJ Irwin
97/6	An Appraisal of Existing Room-Corner Fire Models	D C Robertson
97/7	Fire Resistance of Light Timber Framed Walls and Floors	G C Thomas
97/8	Uncertainty Analysis of Zone Fire Models	A M Walker
97/9	New Zealand Building Regulations Five Years Later	T M Pastore
98/1	The Impact of Post-Earthquake Fire on the Built Urban Environment	R Botting
98/2	Full Scale Testing of Fire Suppression Agents on Unshielded Fires	M J Dunn
98/3	Full Scale Testing of Fire Suppression Agents on Shielded Fires	N Gravestock
98/4	Predicting Ignition Time Under Transient Heat Flux Using Results from Constant Flux Experiments	A Henderson
98/5	Comparison Studies of Zone and CFD Fire Simulations	A Lovatt
98/6	Bench Scale Testing of Light Timber Frame Walls	P Olsson
98/7	Exploratory Salt Water Experiments of Balcony Spill Plume Using Laser Induced Fluorescence Technique	E Y Yii
99/1	Fire Safety and Security in Schools	R A Carter
99/2	A Review of the Building Separation Requirements of the New Zealand Building Code Acceptable Solutions	J M Clarke
99/3	Effect of Safety Factors in Timed Human Egress Simulations	K M Crawford
99/4	Fire Response of HVAC Systems in Multistorey Buildings: An Examination of the NZBC Acceptable Solutions	M Dixon
99/5	The Effectiveness of the Domestic Smoke Alarm Signal	C Duncan

99/6	**Post-flashover Design Fires**	**R Feasey**
99/7	**An Analysis of Furniture Heat Release Rates by the Nordtest**	**J Firestone**
99/8	**Design for Escape from Fire**	**I J Garrett**
99/9	**Class A Foam Water Sprinkler Systems**	**D B Hipkins**
99/10	**Review of the New Zealand Standard for Concrete Structures (NZS 3101) for High Strength and Lightweight Concrete Exposed to Fire**	**M J Inwood**
99/12	**An Analytical Model for Vertical Flame Spread on Solids: An Initial Investigation**	**G A North**
99/13	**Should Bedroom Doors be Open or Closed While People are Sleeping? - A Probabilistic Risk Assessment**	**D L Palmer**
99/14	**Peoples Awareness of Fire**	**S J Rusbridge**
99/15	**Smoke Explosions**	**B J Sutherland**
99/16	**Reliability of Structural Fire Design**	**JKS Wong**
00/1	**Fire Spread on Exterior Walls**	**FNP Bong**
00/2	**Fire Resistance of Lightweight Framed Construction**	**PCR Collier**
00/3	**Fire Fighting Water: A Review of Fire Fighting Water Requirements (A New Zealand Perspective)**	**S Davis**
00/4	**The Combustion Behaviour of Upholstered Furniture Materials in New Zealand**	**H Denize**
00/5	**Full-Scale Compartment Fire Experiments on Upholstered Furniture**	**N Girgis**
00/6	**Fire Rated Seismic Joints**	**M James**
00/7	**Fire Design of Steel Members**	**K R Lewis**
00/8	**Stability of Precast Concrete Tilt Panels in Fire**	**L Lim**
00/9	**Heat Transfer Program for the Design of Structures Exposed to Fire**	**J Mason**
00/10	**An Analysis of Pre-Flashover Fire Experiments with Field Modelling Comparisons**	**C Nielsen**
00/11	**Fire Engineering Design Problems at Building Consent Stage**	**P Teo**
00/12	**A Comparison of Data Reduction Techniques for Zone Model Validation**	**S Weaver**
00/13	**Effect of Surface Area and Thickness on Fire Loads**	**H W Yii**

School of Engineering
University of Canterbury
Private Bag 4800, Christchurch, New Zealand

Phone 643 364-2250
Fax 643 364-2758